The Pennsylvania State University

The Graduate School

Department of Architectural Engineering

DEVELOPMENT OF A CLOSED-FORM EQUATION AND FRAGILITY CURVES FOR PERFORMANCE-BASED SEISMIC DESIGN OF GLASS CURTAIN WALL AND STOREFRONT SYSTEMS

A Thesis in

Architectural Engineering

by

William C. O'Brien Jr.

Submitted in Partial Fulfillment
of the Requirements
for the Degree of

Master of Science

May 2009

The thesis of William C. O'Brien Jr. was reviewed and approved* by the following:

Ali M. Memari
Associate Professor of Architectural Engineering
Thesis Advisor

Richard A. Behr
Charles and Elinor Matts Professor of Architectural Engineering

Gordon P. Warn
Assistant Professor of Civil Engineering

Chimay Anumba
Professor and Department Head of Architectural Engineering

*Signatures are on file in the Graduate School

ABSTRACT

This report provides research that will eventually lead to seismic design guidelines for glazing systems that will be utilized by professionals as a way to mitigate glass damage. Researchers at The Pennsylvania State University and University of Missouri have conducted many experimental studies on various curtain wall and storefront configurations, and based on the results from this extensive database a new closed-form equation and fragility curves were developed. Furthermore, conditions between the laboratory and field were investigated for practical application of the results.

To expand the set of existing experimental data, new testing on glass curtain walls with various glass-to-frame clearances was performed to study the effect that glass –to-frame clearances specifically have on the seismic performance of glass panels. Furthermore, sensor testing was conducted on the racking facility to measure if any significant flexibility existed.

Fragility curves were developed for twenty-four different glass configurations as a way to predict the seismic performance of glass in a probabilistic manner for gasket, cracking, and glass fallout damage states according to economic and life safety consequences. Then, a closed-form equation was formulated to predict the seismic cracking drift of a glass system. The equation uses the ASCE equation as its base, and then considers effects from glass type, glazing configuration type, substandard

clearances, frame system type, and aspect ratio through the application of defined factors. An analysis showed that the proposed equation increases the accuracy of failure prediction by 33% compared to the ASCE equation.

TABLE OF CONTENTS

LIST OF FIGURES

LIST OF TABLES

ACKNOWLEDGEMENTS

I would like to express my sincere gratitude to my advisor, Dr. Ali Memari, for providing me the great opportunity to perform research in the field of architectural glass systems. Without his constant advice, support, and guidance throughout my graduate school career, this thesis would not have been possible. I would also like to thank the members of my thesis committee, Dr. Richard Behr and Dr. Gordon Warn, for the time and knowledge they have provided me throughout this research and the development of this thesis.

In addition, I would like to thank the Applied Technology Council for funding the performance-based design related projects that became a portion of this research.

I would like to thank Paul Kremer, supervisor of the Building Envelope Research Laboratory, who assisted me in the construction and testing of the glass specimens. Furthermore, I am grateful for the knowledge he has provided me on various stages of my work that has been invaluable.

Lastly, I would like to express thanks to the laboratory assistants, Dan Clark, Joe Ridgeway, Mike Hopple, and Steve Tat, for their help in the fabrication and experimental testing of the glass specimens.

DEDICATION

I would like to thank all of my family, friends, and colleagues whose continuous support has made my graduate studies a reality. Especially to my mother, who pushed me academically and for her support on all of my life decisions over the years (and who doesn't forget to remind me from time to time that she received her master's before me). To my father, who has shown me the honor in hard work and the benefits of living life with a good sense of humor ("You shouldn't take life so seriously…you'll never get out alive" –Van Wilder). To my Grandma, who would do anything for me (like picking me up from sports practice a thousand times) and who taught me the advantages of living life with a glass that is half full. To my Grandfather, who introduced me to the "wonderful world" of engineering, and for his continuous support and endless supply of compelling stories. To my Grandmom O'Brien, who showed me the world when I was younger by taking me to cool places like Valley Forge. To Cheryl, Grandma and Grandpa "of South Bend", and to the rest of my extended family in Indiana who have given me a great Midwestern home away from home. To my sister and brother, who will be making college decisions soon enough, to keep in mind that a degree in business means that the weekends start on Thursday. To my close friends from home, UConn, and Penn State, who make getting through the workday a little easier. And finally to my girlfriend Becky, who dealt with my shortcomings through the development of this thesis more than anyone else.

Chapter 1

Introduction

1.1 Background and Statement of Problem

Disasters from earthquakes in the United States during the last three decades have resulted in unprecedented economic losses associated with building and infrastructure damage. While the buildings successfully resisted structural collapse, the resulting large amounts of property damage from nonstructural building components, such as architectural glass, has attracted the attention of the Federal Emergency Management Agency (FEMA). In response to the problem, FEMA spearheaded and developed with various other organizations a new building design method termed "Performance-Based Seismic Design" (PBSD) that would serve as a better way to predict how a building would be expected to perform in terms of capital loss and casualties in earthquake events for building owners, designers, insurers, and others. Now, in conjunction with the Applied Technology Council (ATC), the ATC-58 Project (ATC 2005) is under way to create the Next-Generation Performance-Based Seismic Design Criteria to develop specific guidelines for use by engineers and designers.

The ATC-58 Project has been refining the procedures involved with the PBSD of buildings. The main elements of PBSD are selecting the performance objectives for a building, developing a preliminary design, and then assessing performance capacity of

the design based on three measures of performance that include direct economic loss, indirect economic loss, and casualties. While the ATC-58 Project is developing guidelines that cover selecting performance objectives and the performance assessment of a building, the step of preliminary design will remain undeveloped as of yet.

Architectural glass exterior systems can be one of the largest systems on a building, and as part of the envelope, glazing is an important component contributing to the proper function of a building. Building envelopes, and specifically the wall systems portion on taller structures, are also economically significant and can cost over 20% of a building's construction budget (NIBS 2008). Currently there no seismic design approaches published for glazing systems that are extensive and assist engineers in proper selection of glazing details to more effectively resist earthquake damage. Considering the emphasis that PBSD places on the economic performance of a building, the exterior wall portion of a building envelope will have a significant role in the future PBSD of building projects. This report will provide research that will eventually lead to a Glass Curtain Wall and Storefront System Design Manual that professionals will be able to use in a performance-based or conventional design approach of glazing systems. Researchers at the Pennsylvania State University and University of Missouri have conducted large amounts of experimental studies on various curtain wall and storefront configurations, and based on the results from this extensive database, a new closed-form equation and fragility curves, which predict the performance of architectural glass, are developed.

1.2 Objectives

The ultimate goal of the research carried out is to provide work that leads to the development of a seismic design glazing manual for architectural glass systems. To accomplish this mission three objectives were emphasized: (1) developing fragility curves for use in a PBSD approach; (2) developing a closed-form equation as a way to predict the cracking capacity of various glass systems in terms of drift; and (3) investigating the different conditions between the laboratory and field. The first two objectives develop methods to predict the seismic performance and capacity of glass systems that can be utilized in design approaches. The third objective provides a way to apply and interpret design analysis results for glass systems on actual buildings.

A closed-form equation is developed because current or past seismic building codes do not offer ways to determine the cracking capacity of glazing systems. Equations present in different codes such as ASCE 7-05 (ASCE 2006) offer only design limitations that are based on edge clearances for seismic drift displacement and stresses of the glass pane with the goal of preventing glass fallout. The provisions were evaluated to interpret the glass failure response that is represented by the equations, and then the accuracy of these equations were determined by comparing the predicted failure values for certain glass systems with available experimental data. Then, based on the comparison results it was determined whether the equations should be used, modified, or disregarded in the formulation of the closed-form equation.

The probabilistic fragility functions are developed for glass configurations with various characteristics and detailing. Based on available past experimental glass testing and the results of new experimental tests, architectural glass configurations were selected for analysis which not only have sufficient experimental data to analyze but also contribute to the variety of glazing details represented in the research. Data for many of the glass configurations are provided from past studies (Behr 1996, Behr 1998, and Memari et al. 2003), while data for some of the glass configurations with varied glass-to-frame clearances were obtained through new experimental testing. To ensure conservatism in the data, sensor testing was also executed on the racking facility to determine whether flexibilities were present.

It is the hope that the developed fragility functions and closed-form equation will be incorporated within the context of design approaches for architectural glass in the future development of a Seismic Design Manual for Glazing Systems. In the meantime, though, professionals can utilize the proposed equation and fragility functions as tools to predict the seismic capacity of glass panels. In summary, to achieve the goal and objectives that were set the following research activities were carried out:

- Test glass configurations with varying glass-to-frame clearances to fill in current data gaps so that analytical research is more effective
- Conduct facility sensor testing to ensure data accuracy
- Develop fragility functions for various selected glass curtain wall and storefront configurations based on raw laboratory data and for defined damage failure limit states

- Develop closed-form equation which estimates glass panel seismic cracking capacity

- Provide users with procedures for translating individual glass panel performance results in the laboratory to the expected performance of a glass system on an actual building

Chapter 2

Literature Review

This chapter provides a literature review of research related to glazing systems, building code provisions, and the performance-based design approach. Section 2.1 gives an overview of architectural glass, which includes its application in curtain wall (CW) and storefront (SF) systems and different glazing configurations available. Section 2.2 examines requirements in current codes relating to the seismic capacity of glazing systems. Section 2.3 summarizes experimental studies that have been performed on the seismic performance of architectural glass. Section 2.4 reviews analytical research on glazing systems that have been published concerning the analysis of the seismic performance of architectural glass. Section 2.5 gives a background into PBSD, first-generation and next-generation. Finally, Section 2.6 provides conclusions based on the literature review.

2.1 Architectural Glass

Architectural glass can be used in many applications on a building, including use in various fenestration and atria systems, which are parts of the larger building envelope system. From the many different types of fenestration systems, glass CW and SF

window unit types will be investigated. These are the two glazing systems that will be analyzed for fragility curve and equation development.

2.1.1 Curtain Wall Systems

A curtain wall is defined as an exterior wall on a building, which does not support the roof or floor loads but is connected to the structural frame (NIBS 2008), and is an element of the larger building envelope system. While a CW encompasses systems that use various material cladding such as metal panels and stone, one of the most popular configurations is a metal frame assembly glazed with architectural glass. Glass CW systems have become a common building component as mass load bearing wall systems slowly transitioned and were replaced with cavity wall systems during the twentieth century and lightweight wall system options were needed. Figure **2.1** shows an example of the application of an aluminum architectural glass CW system on a building.

Curtain walls have many various functions, some of which are harder to achieve effectively than others. These wall systems have requirements which include structural load transfer and resistance, water infiltration protection, air infiltration control, condensation prevention, energy management, sound attenuation, safety, maintainability, constructability, durability, aesthetics, and economic viability (Schwartz 2001). On top of these considerations, though, a CW must be able to effectively resist

Figure 2.1: An example of an architectural glass CW system on a building (kawneer.com)

lateral loads transferred from the structural frame of the building during an earthquake event or the other functions will be compromised.

Architectural glass CW systems are grouped into two types, either stick-built or unitized. Stick-built systems use a series of horizontal transoms and vertical mullion frame members which are assembled and glazed on site, as seen in Figure **2.2** (a). Unitized systems are manufactured in modules in a factory and then erected on the building in sections, and are usually pieced together one floor height at a time (NIBS 2008). An example of the installation of a section of unitized CW can be seen in Figure 2.2 (b). Both types of curtain walls can be ordered according to standard manufacturer catalogs or can be custom designed to desired specifications. All of the glass CW and SF systems which will be analyzed in this report are considered stick-built type assemblies.

(a) **(b)**

Figure 2.2: Comparison between (a) stick-built and (b) unitized CW systems (www.livemodern.com, www.archsd.gov.hk)

2.1.2 Storefront Window Systems

An exterior storefront wall system is a type of window unit system that utilizes a frame assembly in which architectural glass is glazed. It is similar to a glass CW system in that both systems use two main components of framing and glazing. However, unlike CW systems, SF and window unit systems are not an exterior wall onto themselves (NIBS 2008), but rather integrated into it. Glass SF wall systems have widespread applications in mall facades, store facades, and other low-rise commercial buildings (Behr et al. 1995), an example of which is shown in Figure **2.3**.

Figure 2.3: An example of a glass SF window unit system application (kawneer.com)

Storefront and other window unit systems have many functions, which include thermal performance, moisture protection, aesthetics, acoustical performance, life safety, durability, constructability, and maintainability (NIBS 2008). Unlike CW systems, SF and window units are not solely responsible for transferring loads, such as wind, to the structural system of the building. Although, the architectural glass will be subjected to any loads that the exterior wall system experiences, and as a result will be expected to reasonably resist these loads for reasons such as life safety. The most important consideration when attempting to effectively achieve these functions successfully is the integration of the SF window units with the wall elements, so that all components act as one exterior wall system (NIBS 2008).

2.1.3 Glazing

The architectural glass, which is commonly glazed in CW or SF systems, is available in many different varieties and configurations. First of all, there are three strength level options due to surface pre-stressing manufacturing methods available. Annealed (AN) glass is the basic and most commonly used architectural glass type (NIBS 2008). It is not heat treated during fabrication and of the three options it has the least amount of strength. Heat-strengthened (HS) glass is heated and cooled in a process that allows surface compression to develop increasing the resistance of glass breakage. Fully-tempered (FT) glass undergoes a more complete heat and cooling process, which gives it the highest resistance to breakage out of all three glass types. The industry generally accepts that HS glass is twice as strong as AN, and FT four times stronger than AN (NIBS 2008). Furthermore, AN glass usually fails into large shards when damaged, while FT breaks into small "dice-like" fragments. HS fails in a manner somewhere in between either the failure behaviors, depending on the level of glass surface pre-compressive stresses.

The three different types of glass can also be used in a laminated configuration. A laminated glass unit consists of at least two panes of glass with an interlayer between the glass lites. The interlayers are generally composed of plasticized polyvinyl butyral (PVB), aliphatic urethane, or ionoplast rigid sheet permanently bonded with use of heat and pressure, or a liquid resin permanently cured with exposure to ultraviolet light, heat, or chemicals (GANA 2004). Polyester (PET) film can also be applied on

configurations. Some laminated glass units can have higher resistance to glass breakage compared with AN glass, and prevent the large shard failure behavior that AN glass exhibits. Furthermore, laminated glass has impact energy absorption characteristics, vibration attenuation characteristics, and can provide protection against ultraviolet rays (NIBS 2008). As a result, common applications of laminated glass include overhead glazing, specific acoustical projects, and blast or bullet-resistant needs.

Another glass configuration is an insulating glass unit (IGU), which is composed of two (or more) panes of glass and an enclosed air space in between them. The air space is created with continuous spacers that seal the gap, and the sealed space can be filled with gas. Certain IGU configurations contain glass panes that are of different types. For example, the inner pane might be AN glass and the outer pane a laminated HS glass panel. IGU's are popular in many building projects due to their thermal, energy, and acoustical performance qualities compared with single pane glass configurations (NIBS 2008), which are termed monolithic.

In addition, glass can be coated or tinted to achieve particular goals. A popular glass coating application is reflective or "low-emissivity," which alters the thermal performance in a beneficial manner (NIBS 2008). Also, glass that has been tinted alters the solar radiation behavior depending on the characteristics of the tint (GANA 2004). However, neither of these detailing options has been found to affect the seismic performance of glass.

The architectural glass in a CW or SF system can also be glazed in different ways. The purpose of glazing around the glass perimeter is to prevent water infiltration and help control the thermal performance of a building as much as possible. Nevertheless, the glazing can affect the movement of the glass within the CW frame when in-plane loading occurs. Generally, types of glazing are characterized as either dry or wet. Dry-glazing consists of rubber gaskets that compress onto the glass edges and are attached to the framing members. Wet-glazing is a liquid sealant or tape that is applied on top of a backer rod and allowed to cure. Both dry-glazing and wet-glazing have various advantages and disadvantages, and when a glazing type is selected for a glass wall system the designer considers the economics, constructability, performance, and life-cycle factors (NIBS 2008).

Glass panels are kept in place within the framing through the use of setting and side blocks. Generally, there are two setting blocks placed in between the glass and the bottom horizontal frame member which the glass panel "rests" on, and one side block in between the glass panel and vertical framing members to restrict movement. Figure **2.4** depicts the suggested location of these blocks by the GANA Glazing Manual (GANA 2004). As a result of the setting and edge blocks, there is a glass-to-frame clearance between the glass and framing, and a glass "bite," which is the distance between the edge of the glass and the lip of the framing. The glass-to-frame clearances and bite characteristics can vary among glass CW and SF configurations.

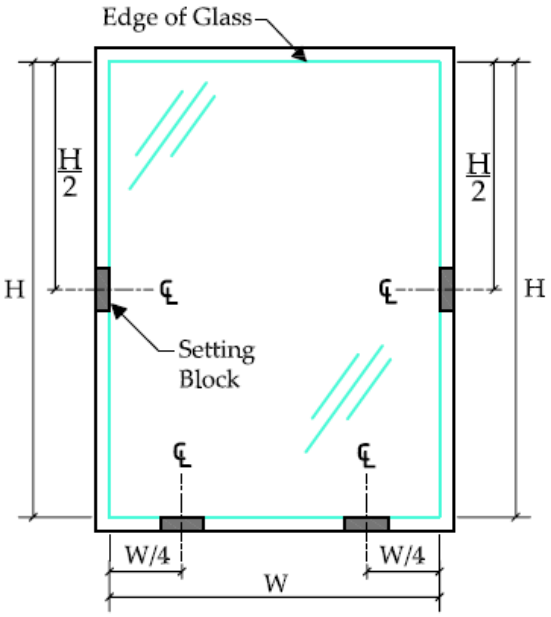

Figure 2.4: Suggested setting block locations as suggested by GANA 2004

2.2 Architectural Glass Provisions in Seismic Codes

Currently there are some provisions regarding architectural glass in seismic codes. The International Building Code (IBC) of 2006 (ICC 2006) references ASCE 7-05 (ASCE 2006) to provide drift limit requirements that glass systems must meet. Originally introduced in ASCE 7-02 (ASCE 2002) under sections 9.6.2.4.2 through 9.6.2.10.2 (Behr 2006), section 9.6.2.4.2 states that "glass in glazed curtain walls and storefronts shall be designed and installed in accordance with Sec. 9.6.2.10" (ASCE 2002). Section 9.6.2.10 provides Equation **2.1**, which needs to be satisfied by glass panels in CW or SF system:

$$\left.\begin{array}{l}\Delta_{\text{fallout}} \geq 1.25ID_p \\ \text{or} \quad \geq 0.5 \text{ in.}\end{array}\right\} \text{ whichever is greater} \qquad \textbf{2.1}$$

where I denotes the importance factor, Δ_{fallout} denotes the drift that causes glass fallout in the CW or SF system under consideration, and D_p denotes the drift that the glazing component must be designed to accommodate. D_p is defined as the relative displacement over the height of the component, and originates from the building structural analysis conducted for seismic loads under ASCE 7-02 with the consideration of displacement amplification factor. As stated in Section 9.6.2.10.2, Δ_{fallout} for a particular glass system must be determined by engineering analysis or laboratory testing according to the recommended dynamic test protocol as outlined in AAMA 501.6 (AAMA 2001b).

An exception from determining Δ_{fallout} as offered by ASCE 7-02 under Section 9.6.2.10.1 is designing a system with a sufficient glass-to-frame clearance that satisfies Equation **2.2**:

$$D_{clear} \geq 1.25D_p \qquad \textbf{2.2}$$

where D_{clear} denotes the drift that occurs relative to the height of the glass panel and represents expected initial glass-to-frame contact. D_{clear} can be determined by Equation **2.3** for glass specimens of rectangular dimensions within rectangular framing:

$$D_{clear} = 2c_1\left(1 + \frac{h_p c_2}{b_p c_1}\right) \qquad \textbf{2.3}$$

where h_p and b_p denote, respectively, the height and width of the rectangular glass panel, c_1 denotes the glass-to-frame clearance along the vertical glazing edges, and c_2 denotes the glass-to-frame clearance along the horizontal glazing edges.

2.3 Review of Experimental Research

The seismic performance of architectural glass has been investigated in the laboratory by a variety of institutions. Initial experiments determined that in-plane dynamic loading on a steel frame facility was a practical way to mimic seismic motions on a glass specimen, while following experiments refined the testing protocols and isolated the factors affecting the seismic performance of architectural glass.

The first experimental study published concerning the seismic performance of glass panels was conducted by Bouwkamp (1961) at the University of California. In this experiment, the in-plane static behavior of glass window panels was studied. The variables of the glass assemblies used included the size of the glass pane and configuration, panel attachment to structural frame, the material of the frame, glass-to-frame clearance, and type of putty. The testing facility was a steel frame where pinned connections existed at the four corners to allow the top steel horizontal to freely translate when lateral load was applied, which also occurred on the top horizontal. Glass panel sizes 4 ft by 2 ft (1.2 m x 0.6 m), 4 ft by 4 ft (1.2 m x 1.2 m), and 4 ft by 8 ft (1.2 m x 2.4 m) with glass thicknesses of 1/8 in. (3 mm), 3/16 in. (5 mm), and 1/4 in. (6 mm), respectively, were tested with two different panel attachment (to hinged loading frame) conditions:

panel attached all-around or panel attachment at top and bottom horizontal only. Furthermore, the three glass configurations were tested with different sash materials of aluminum, steel, or wood, different glass-to-frame clearances, which was either the minimum or maximum dimensional clearance possible, and putty that was either soft or hard. Not every combination possible was tested, but the authors set up testing groups of 12 different specimen combinations in a way that they believed could allow for the best variable effect analysis.

Failure of the glass panels was identified when either cracking or fallout of glass occurred, and was recorded as the drift displacement experienced by the top horizontal at time of failure. The authors observed that the drift value, which resulted in failure of the glass, was related to the point at which the glass came in contact with the framing. Glass contact was a consequence of the horizontal translation and rotation of the glass panel within the frame combined with framing deformation. Using this theory and dimensional analysis, Equation **2.4** was suggested as a way to predict the lateral drift that a glass panel would experience before contacting the framing for configurations with soft putty:

$$\Delta - \varphi h = 2c\,(1 + h/b) \qquad \textbf{2.4}$$

where Δ denotes total drift displacement between top and horizontal frame members, φh denotes rotational adjustment, c denotes glass-to-frame clearance, b denotes the nominal width of panel, and h denotes the nominal height of panel. For configurations with hard

putty, the authors added a reduction factor "*F*" to the equation, where *F* was empirically derived and based on the aspect ratio (b/h) of the glass.

Lim and King (1991) experimented on five different glass CW configurations, which included dry-glazed, patch fitting, two-sided silicone wet-glazed, four-sided silicone wet-glazed, and conventional windows. Similar to Bouwkamp, these tests studied the in-plane dynamic loading performance of glass. The test setup consisted of a testing facility constructed of vertical and horizontal steel members, to which the glazing framing was attached to, and connections that could be fixed or free depending on the test protocol. King and Lim's findings concentrated on the applicability of the racking testing procedures rather than the seismic behavior of the glass. The authors concluded that it was possible to determine the racking capacities of full-scale curtain walls accurately through appropriate controlled in-plane displacement loading in the laboratory. Also, the authors noted glass rotation and subsequent glass contact within the frame during increasing loading, similar to the observations of Bouwkamp (1961). They stated that to achieve the full potential capacity in the glass, the glass should move unrestricted within the glazing panel to prevent premature stresses and subsequent failure.

Behr et al. (1995) performed racking tests on a variety of full-scale SF window unit configurations. Two loading histories were developed, a Serviceability Test and an Ultimate Test (see Figure **2.5**), modeled from a former moderate-to-severe earthquake event. The Serviceability Test was designed to impose a serviceability limit state on the

glass, which was defined as glass edge damage, glass panel translation and rotation, and gasket seal damage. The Ultimate Test, which was twice the displacement amplitude but the same frequency as the Serviceability Test, was designed to impose an ultimate limit state on the glass, which was defined as minor and major glass fallout. The testing facility consisted of an upper and lower horizontal steel tube situated on roller assemblies. Displacement was applied to the bottom horizontal through a hydraulic arm, and the top horizontal was coupled to the bottom tube by means of a fulcrum and pivot arm, which let the top tube displace opposite of the bottom. Figure **2.6** shows the racking facility and testing setup, where three specimens were tested at once. The different types of glass tested included 1/4 in. (6 mm) AN monolithic, 1/4 in. (6 mm) FT monolithic, 1/4 in. (6 mm) AN laminated, 1 in. (25 mm) AN IGU, and 1 in. (25 mm) FT IGU. All of the glass specimens were 5 ft wide by 6 ft high (1.5 m x 1.8 m). The variables in the experiments concentrated on different glass configuration types and their effect on glass failure, which was either Serviceability or Ultimate.

Many glass panel observations were documented, which included edge damage, glass panel translation and rotation, gasket seal degradation (distortion, pull-out, push-in, and shifting), gasket seal degradation per edge, fallout damage locations, and displacement values for serviceability and ultimate limit failure states. For the serviceability limit state failure behavior, the authors concluded that all three AN glass configurations experienced significant glass edge damage, while the FT glass d

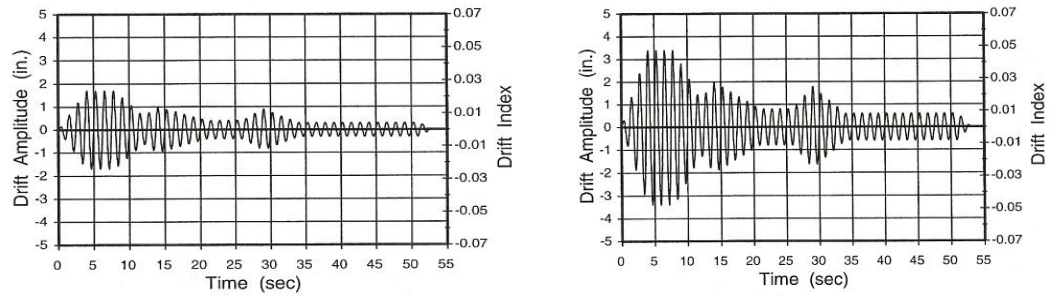

Figure 2.5: Drift time histories for, respectively, the Serviceability and Ultimate test (Behr et al. 1995)

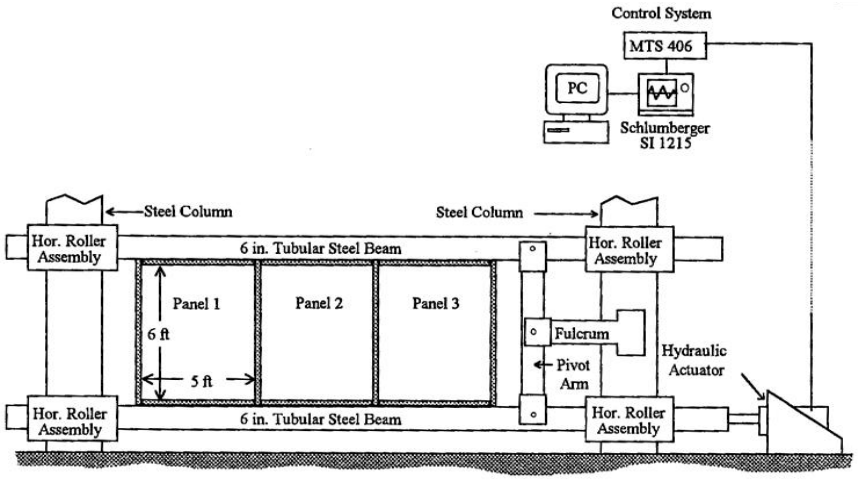

Figure 2.6: Facility setup for the storefront glass (Behr et al. 1995)

configurations better resisted this type of damage. Furthermore, most glass specimens experience considerable horizontal translation within the frame during the serviceability testing. For the ultimate limit state testing, the authors observed that only the 1/4 in. (6 mm) AN monolithic glass type experienced glass fallout.

Behr and Belarbi (1996) reported on more racking experiments including glass SF architectural glass, but in this study the specimens were tested according to a newly

proposed "crescendo test" protocol. The authors offered the crescendo test method as a way to better relate interstory drift experienced by a building and the limit states subsequently experienced by the CW systems, and as a possible standard seismic test method for architectural glass in the future. The proposed crescendo test consisted of a continuous series of alternating intervals of "ramp-up" and "consistent" displacements, with each interval composed of four sinusoidal cycles at a frequency of 0.8 Hz. Each "ramp-up" interval step increased by an amplitude of ±0.25 in. (6 mm), the time histories of which are shown in Figure **2.7**.

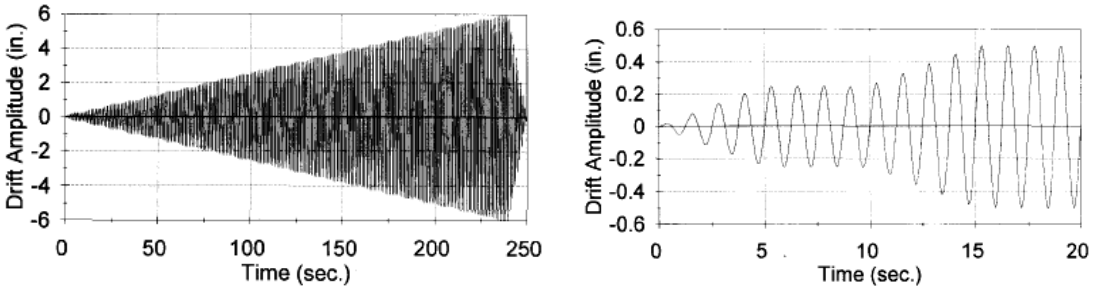

Figure 2.7: Time histories for the "crescendo test" with, respectively, the entire crescendo test and first twenty seconds of the crescendo test shown (Behr and Belarbi 1996)

The same racking test facility and set-up used in the previous SF tests was used (see Figure 2.6). Also, the same five various glass configurations were tested as the previous experiment, with 12 or 16 specimens tested for each configuration. For the failure modes, a "lower ultimate limit state" was defined as reached when a cracking pattern in the glass appeared that was significant enough to lead to major fallout. An "upper ultimate limit state" was defined as reached when major fallout of the glass

occurred. The conclusions from the authors regarding the performance of the different glass configurations were very similar to the previous SF experiments. Also, the failure drift values were consistent and the statistical standard deviation of the data was small, which suggested that the crescendo test is a good standard for measuring the seismic capacity of glass.

Behr (1998) went on to study the racking performance of various mid-rise glass CW configurations. Similar to past testing, in-plane dynamic loading was performed on the specimens and used the standard crescendo test method (see Figure 2.7). The same racking test facility used in the Behr et al. (1995) SF tests was used, except the setup was slightly different as each glass specimen was tested individually (see Figure **2.8**). The variables among different glass configurations included glass type, glazing details, and PET film application. All of the glass configurations were 5 ft wide by 6 ft high (1.5 m x 1.8 m) and used aluminum Kawneer 1600™ CW framing. A summary of the different glass configurations tested are listed in Table **2.1**. Through the course of the crescendo test the authors were looking to determine the following failure states for each glass specimen:

a. "serviceability drift limit" defined as the drift causing observable glass cracking
b. "ultimate drift limit" defined as the drift causing glass fallout (glass fallout fragment greater than 1 in.^{2})

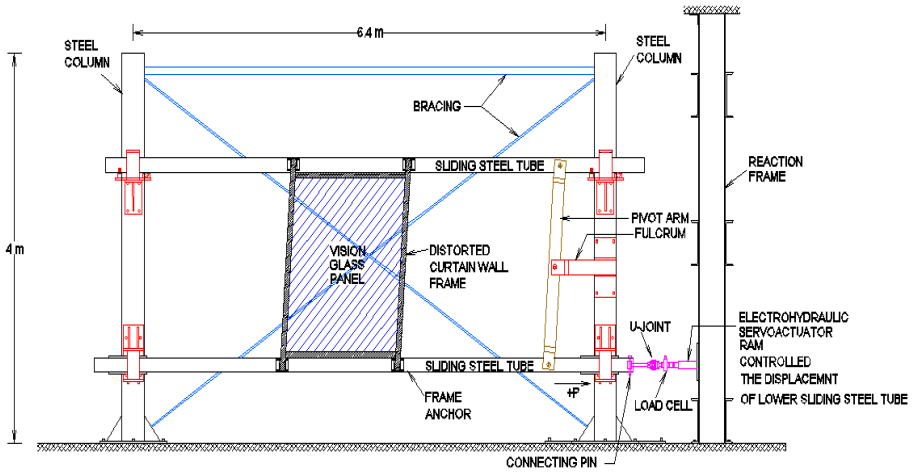

Figure 2.8: Racking facility and setup used for the mid-rise CW testing (Behr et al. 1995)

Table 2.1: Summary of the various glass mid-rise CW configurations

Glazing Type	Glass Thickness	Sealant
AN[1] monolithic	0.25 in. (6 mm)	Dry[6]
HS[2] monolithic	0.25 in. (6 mm)	Dry
HS monolithic	0.25 in. (6 mm)	Wet[7]
FT[3] monolithic	0.25 in. (6 mm)	Dry
AN laminated	0.25 in. (6 mm)	Dry
AN monolithic with 4 mil. (0.1 mm) PET[4] film	0.25 in. (6 mm)	Dry
HS monolithic spandrel	0.25 in. (6 mm)	Dry
HS monolithic spandrel	0.25 in. (6 mm)	Wet
HS laminated	0.375 in. (10 mm)	Dry
AN IGU[5]	1.0 in. (25 mm)	Dry
AN IGU	1.0 in. (25 mm)	Wet
HS IGU	1.0 in. (25 mm)	Dry

[1]AN = annealed, [2]HS = heat strengthened, [3]FT = fully tempered, [4]film is not anchored mechanically to the curtain wall frame, [5]IGU = insulating glass unit, [6]Dry = dry glazing gaskets used on curtain wall frame, [7]Wet = beaded structural silicone glazing used on vertical edges (with dry glazing used on horizontal edges)

Comparing the drift failure values for both limit states among the various glass configurations, the authors isolated the effect that each different glazing detail had on the lateral capacity of these CW systems. Conclusions reached included: (1) minor increases in serviceability and fallout failure drift limits occur across increasing glass surface pre-stress treatments from AN to HS to FT, (2) glass with PET film or lamination had significantly higher ultimate limit state capacities compared with standard AN glass specimens but no difference in capacities for cracking, and (3) compared with the SF systems, the mid-rise CW systems had overall lower cracking and fallout drift capacities due to the stiffer nature of the mid-rise systems.

Memari et al. (2003) performed research on mid-rise curtain wall configurations by dynamically racking different asymmetric insulating glass units (IGU). An asymmetric IGU consists of an AN inner pane and an outer laminated pane, with an argon gas filled space in between the two panes of glass. A summary of the different IGU CW configurations which were tested are listed in Table **2.2**. The racking facility located in the Building Envelope Research Laboratory at PSU was used to apply in-plane controlled displacements according to the crescendo test protocol. The cyclic loading test was run in a "step-wise" manner as opposed to a continuous crescendo fashion, as shown in the time history profile in Figure **2.9**. The failure limits documented for each glass specimen included the drift amplitude associated with first glass-to-frame contact, the serviceability drift limit for the inner and outer glass pane, the ultimate drift limit for the inner pane, pullout of the glass unit from the glazing

pocket, and the ultimate drift limit for the entire IGU. The limit state of glass pullout was defined as when the laminated pane came out of the framing pocket as a result of glass panel buckling or forces from pressure plate clamping. Also, since the laminate pane did not experience fallout until maximum loading (if at all), an alternative ultimate limit state termed "entire unit fallout" was recorded and defined as when the outer laminated pane along with the attached IGU spacer completely separated from the CW framing.

Table 2.2: Summary of various CW configurations containing asymmetric IGU's tested

ID	Inner Pane[1]	Outer Pane	LAM PVB interlayer[2]
A	0.25 in. (6 mm) AN	0.25 in. (6 mm) AN LAM[3]	0.030 in. (0.76 mm)
B	0.25 in. (6 mm) AN	0.25 in. (6 mm) AN LAM	0.060 in. (1.52 mm)
C	0.25 in. (6 mm) AN	0.5 in. (13 mm) AN LAM	0.030 in. (0.76 mm)
D	0.25 in. (6 mm) AN	0.25 in. (6 mm) HS LAM	0.060 in. (1.52 mm)
E	0.25 in. (6 mm) AN	0.5 in. (13 mm) HS LAM	0.060 in. (1.52 mm)
F	0.25 in. (6 mm) AN	0.5 in. (13 mm) FT LAM	0.060 in. (1.52 mm)
G[4]	Monolithic: 0.25 in. (6 mm) AN LAM		0.030 in. (0.76 mm)

[1]All IGU specimens were 59.5 in. wide x 72 in. high (1511 mm x 1829 mm), dry glazed, and used Kawneer 1600 framing, [2]PVB Saflex interlayer which resides between the two panes of glass which compose a laminated glass unit, [3]LAM = laminated, [4]Configuation G was the control for the experiment and was not an IGU configuration

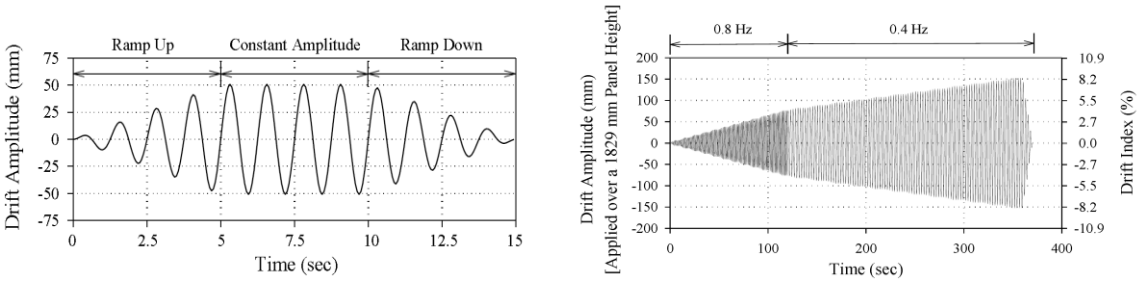

Figure 2.9: Typical crescendo racking step (Step 8, 2 in. (50 mm), 0.8 Hz) and the entire time history of the crescendo test (with the "ramp-down" intervals removed), respectively (Memari et al. 2003)

The authors concluded from the analysis of the racking results that the polyvinyl butyral (PVB) interlayer thickness, glass thickness, and glass type variables did not have significant effects on the serviceability (cracking) or ultimate (fallout) failure capacity for the AN inner glass panes, the serviceability of the outer AN laminated panes, or the entire unit fallout limit state. Overall, the authors concluded that asymmetric IGU configurations had larger serviceability capacities for the entire unit and also each AN inner and laminated outer pane individually compared with non-hybrid IGU's or single laminated glass units. Lastly, it appeared that no benefit to the fallout capacities existed with asymmetric IGU configurations.

Memari et al. (2004) evaluated the seismic capacity of architectural glass curtain walls fitted with anchored PET film as a pilot study. Three different film-to-frame anchoring options were tested: (I) SSG applied along the entire glass perimeter, (II) an aluminum bar anchoring the film along the top horizontal of the glass to the frame, and (III) two aluminum bars anchoring the film along both verticals of the glass to the frame.

Besides finding the limit state values, damage relating to the film and anchoring bars also would be observed. Due to the nature of pilot studies, the testing was limited.

Memari et al. (2006a) reported on the in-plane dynamic racking performance of architectural glass with rounded corners. In an effort to discover a technique which increases the cracking capacity of glass that is cost effective and simple to employ, the authors proposed the rounded-corner glass (RCG) concept. RCG modifies standard rectangular glass panes by rounding square corners and then finishing the corners and/or edges as illustrated by Figure **2.10** below. Based on the observations from testing, the authors suggest that drift capacities may ultimately be more critical from glass edge corner conditions rather than material strength. In general, it was stated that the RCG design concept was promising because of the overall increased seismic resistance.

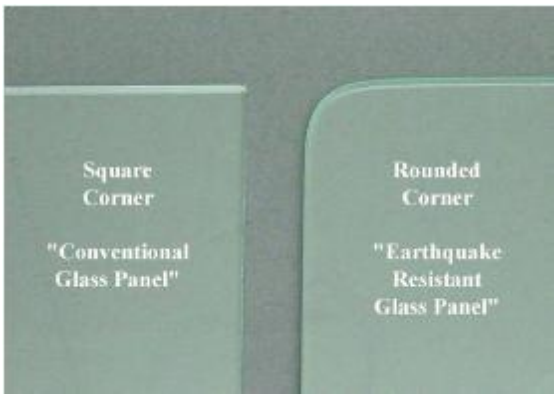

Figure 2.10: A square corner of a standard glass pane compared with the rounded corner of the modified glass panels (Memari et al. 2006a)

Memari et al. (2006b) studied the seismic performance of various glass curtain wall configurations with two-side structural silicone glazing. The objective of the experiment was to identify the failure limit states associated with glass in SSG assemblies. It was noted that load transfer between the glass and framing systems in SSG configurations must occur through the sealant, which means that the seismic response of SSG systems are most likely different from systems that are dry-glazed.

2.4 Review of Analytical Research

Analytical research projects have been conducted, which further contribute to the understanding of the seismic performance of architectural glass. These works include an investigation into the combined in-plane deformation and out-of-plane resistance of glass and subsequent equation development and also a static finite element analysis of glass under in-plane loads.

Sucuoglu and Vallabhan (1997) investigated the seismic response of glass by defining the in-plane deformation and out-of-plane resistance capacity of glass subjected to in-plane loading. For seismic capacity of the glass relating to in-plane deformation the authors continued Bouwkamp's (1961) work and performed a dimensional analysis to further develop an equation to predict glass capacity in terms of drift. The authors concluded that the in-plane deformation capacity of glass is determined by two separate responses by the glass panel when it is subjected to lateral loading. The first response behavior is rigid body motion, which occurs when the framing surrounding the glass

deforms and the glass pane translates within the frame until opposite diagonal corners come in contact with the framing as shown in Figure **2.11** (b). Then, the contact causes the glass panel to rotate and translate further until the opposite corners of the glass are up against within the corner of the framing as shown in Figure 2.13 (c). Rigid body movement and subsequent contact leads to glass cracking, and the drift capacity of the glass as a result of this response as validated by the authors offered initially by Bouwkamp (1961) is represented in the first term of Equation 2.1.

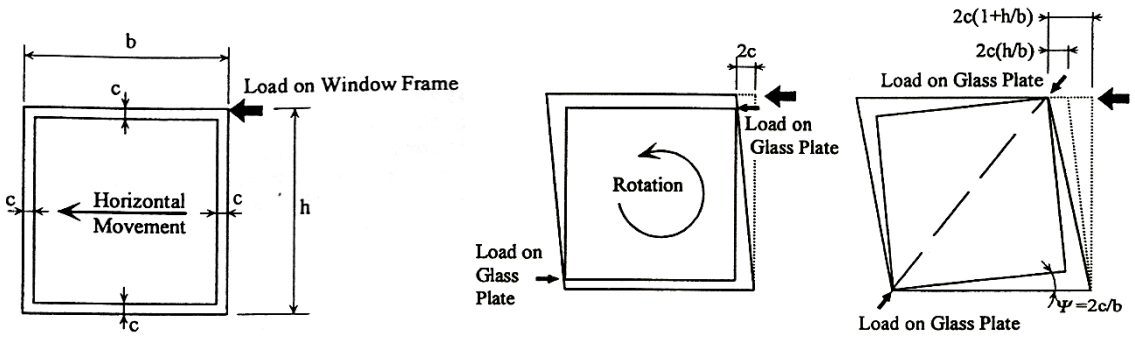

Figure 2.11: Summary of glass panel movement under lateral loading with (a) undeformed glass specimen, (b) loaded glass specimen depicting frame deformation and initial glass contact, and (c) loaded glass panel with opposite corners within glazing pockets (Sucuoglu and Vallabhan 1997)

The second glass response from seismic loading that contributes to the in-plane deformation capacity according to the authors is diagonal buckling, which occurs after rigid body motion and once opposite diagonal corners of the glass pane become flushed against the corners of the framing. At this point loading creates a diagonal compressive force across the pane of the glass. The authors claim that as a result of this compressive

force, the glass deflects diagonally out-of-plane as shown in Figure **2.12** and subsequently shortens and further rotates, which continues until the maximum allowable flexural tensile stress of the glass is reached and the specimen fails. The authors proposed Equation **2.5** as a way to estimate the in-plane seismic glass capacity, where the second term accounts for the capacity added from out-of-plane deformation:

$$\delta = 2c\left(1+\frac{h}{b}\right)+\frac{1}{b}\left(\frac{\sigma_{all}\,d^2}{\pi E t}\right)^2 \qquad \textbf{2.5}$$

where δ denotes drift capacity, c denotes glass-to-frame clearance, b denotes nominal width of panel, h denotes nominal height of panel, σ_{all} denotes allowable tensile stress, d denotes nominal diagonal distance across the glass through opposite corners, E denotes glass Young's modulus, and t is the thickness of the glass.

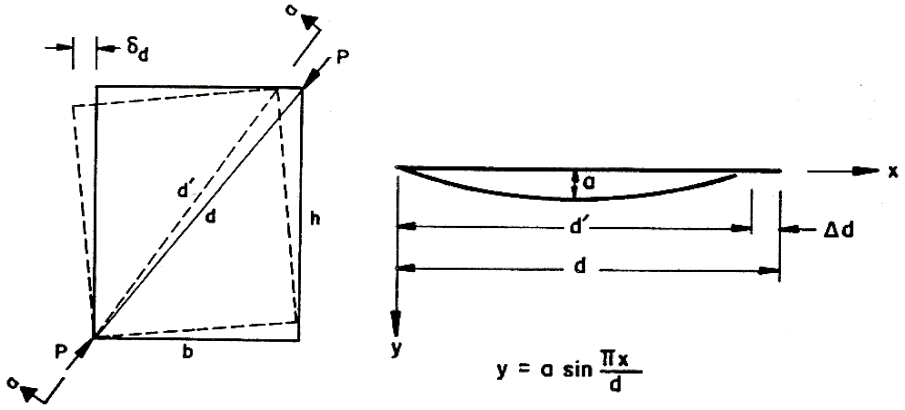

(a) (b)

Figure 2.12: Framing deformation leading to (a) the development of a diagonal compressive force with rotation and (b) out-of-plane deflection along section a-a (Sucuoglu and Vallabhan 1997)

Furthermore, Sucuoglu and Vallabhan discuss the out-of-plane vibration response of glass from seismic loading. They then develop charts based on slenderness ratio and floor acceleration variations to aid in an out-of-plane vibration analysis of glass SF systems. For CW configurations, it is stated that the tensile strength of the glass on buildings need to be larger than the maximum principal flexural stress that is predicted in an earthquake. Overall, the publication states that observations in past earthquake reconnaissance reports show that in-plane deformations are most likely the cause of glass failure, as opposed to glass panels experiencing failure from out-of-pane vibrations.

Memari et al. (2007) performed a pilot study to determine the feasibility of creating finite element modeling formulations of architectural glass curtain walls under in-plane dynamic loads. The objective of the analysis was to correlate strains measured at two locations on the glass panel during one experimental test with predicted strains from a finite element model (FEM) to determine if the onset of a cracking damage limit could be accurately estimated in the experimental mockup. For the finite element analysis many different finite elements were used to model the glass panel, aluminum frame, and glass-to-frame connection of the experimental mockup as shown in Figure **2.13**. For simplicity reasons, the authors stated the analysis would cover the behavior of the glass panel after initial glass-to-frame contact.

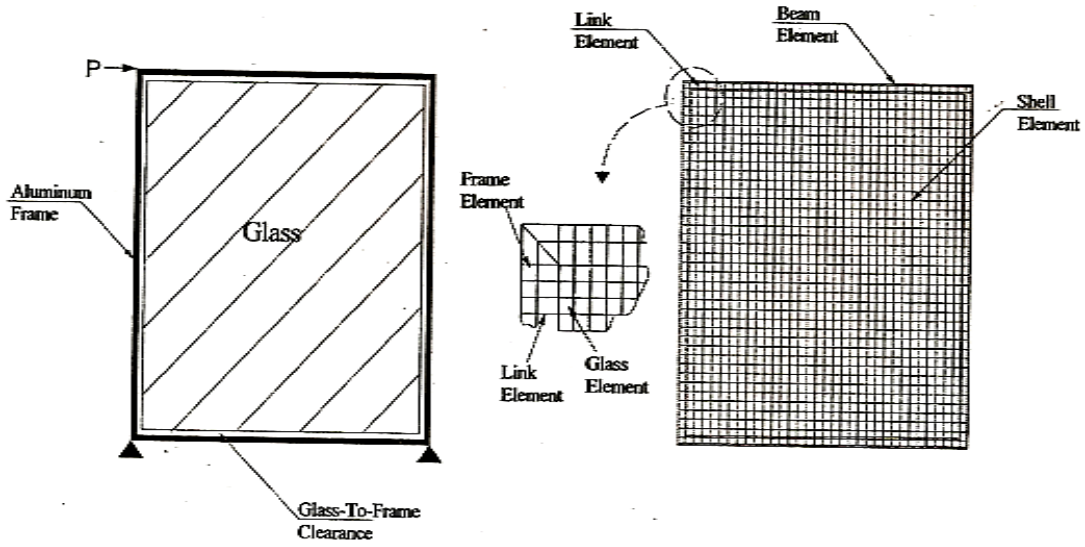

Figure 2.13: FEM schematic depicting the lateral load application and FEM meshing components (Memari et al. 2007).

The results from the measured strains in experimental test compared with the FEM showed some significant differences. When relating principal strain versus load, it was found that the measured strains in the top corner of the glass panel was larger than those measured in the bottom corner, and overall the two measured experimental strains were larger than those predicted by the FEM. Some matching correlation was reported at certain points in the experimental testing but ultimately the FEM departed significantly from the measured strains over the course of the loading. Reasons for these differences include simplified FEM assumptions. Despite these discrepancies, the authors state that finite element modeling could eventually be a viable tool in predicting the stress and failure behavior of glass panels with further research and modifications to the FEM.

2.5 Performance-Based Seismic Design

Performance-based seismic design (PBSD) is an alternative to current design methods that offers professionals a way to design buildings with respect to an expected probable performance of a structure for various types of future earthquake events. It ultimately allows a more reliable understanding and prediction of seismic risk associated with buildings. In its basic form, the performance-based design process involves actively analyzing the performance capability of a building to determine if the predicted performance meets the selected design objectives (ATC 2005). The primary steps involved with PBSD are: (1) selecting building performance objectives, (2) creating a preliminary design, (3) assessing the performance capability of the current design, and (4) determining whether the assessed performance satisfies the selected objectives. Figure **2.14** depicts a flow diagram of these fundamental steps. The PBSD process is finished when the selected objectives are met in an assessed design.

Performance-based seismic design was developed in response to the inadequate performance and related large amount of economic losses from buildings designed to standard seismic codes in earthquake events in the last three decades (EERI 2000). Seismic design procedures found in current building codes, such as IBC 2006 (ICC 2006), give requirements which rely on meeting minimum levels of standard for stiffness, strength, ductility, and dynamic response. The main purpose of these codes is to protect the life safety of the public by such methods as preventing structural collapse, and therefore is not based on the actual performance of the building. As a result,

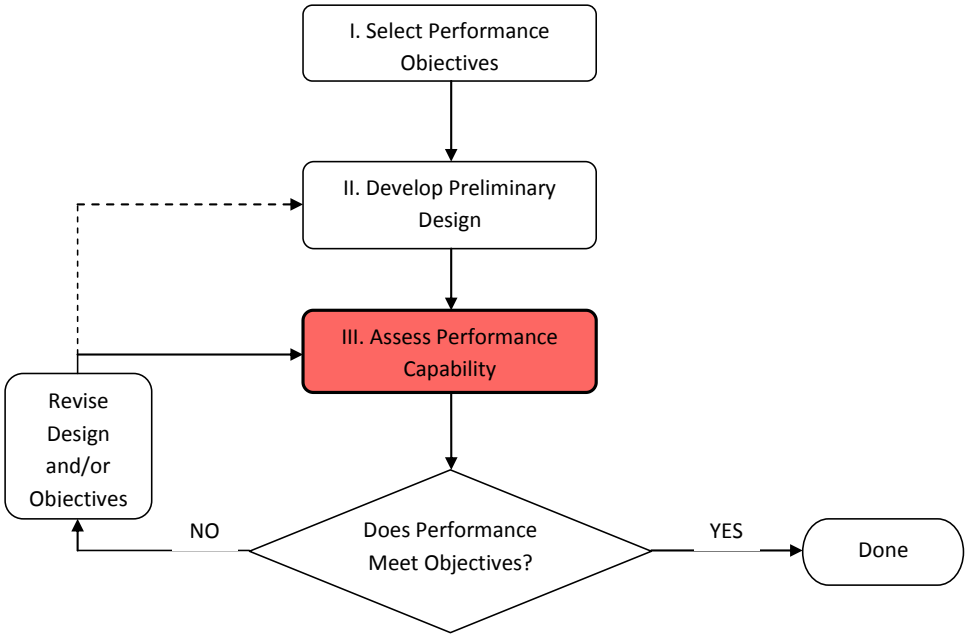

Figure 2.14: Fundamental flow diagram for Performance-Based Seismic Design

buildings which are currently still designed to earthquake resistant requirements in conventional codes will most likely sustain significant damage and result in large economic losses for the owner in a moderate seismic event, even if the goal of life safety is achieved (Hamburger 2006).

There are several advantages of PBSD compared to conventional design procedures. These advantages include the potential for buildings to better resist economic losses associated with earthquake damage, a higher chance that buildings will perform as expected, adoption of new materials or structural systems not yet addressed by codes, and designing to a desired performance with lower project costs (ATC 2008).

Furthermore, the potential exists for PBSD to be adopted to other disaster events, such as wind, blast and fire.

2.5.1 First-Generation

The first steps taken toward the development of PBSD was undertaken by the Federal Emergency Management Agency (FEMA), which states that one of its main goals is the prevention and mitigation of damage of the built environment from natural disasters (ATC 2006). Citing knowledge limitation that exist in the understanding of the performance of buildings in earthquake events, FEMA contracted with the Pacific Earthquake Engineering Research Center (PEER) to develop a plan, referred to as the FEMA-283 (EERC 1996) project, outlining the research needed to successfully develop PBSD for existing building retrofitting purposes. Updated with the FEMA-349 (EERI 2000) project outlines, these initial efforts on PBSD were termed "first-generation" because of their emphasis on existing structures and the inability to quantify the loss predictions in terms of parameters important to the decision making community, such as repair costs (Hamburger 2006).

The first-generation PBSD represents the current state of practice of performance-based methodology in field today. First-generation practices have made their way into national guidelines for the seismic evaluation, upgrade and retrofit of existing buildings (ATC 2008). Under these procedures, professionals select a desired performance level (fully functional, immediate occupancy, life safety, and collapse prevention) and match

it with an earthquake event that the performance level needs to achieve. The retrofit design is modeled and analyzed according to engineering criteria (i.e., deformations and stresses) to see if the selected performance level is met. In this respect the first-generation is performance-based, although measures such as economic loss are left to the independent judgment and personal experiences of engineers. As a result, the predicted performance of a building is considered subjective (ATC 2008).

2.5.2 Next-Generation

In efforts to develop PBSD procedures that address new building design, the "Action Plan for Performance-Based Seismic Design" was created under the FEMA-349 project (EERI 2000). To execute the plan, FEMA contracted with the Applied Technology Council (ATC) to create guidelines for the new design procedures. As a result, the ATC-58 project entitled "Development of Next-Generation Performance-Based Seismic Design Guidelines for New and Existing Buildings" was established (ATC 2005). The goal of the ATC-58 project is to develop PBSD procedures that can directly relate performance in terms of quantified risks (as opposed to subjective) that the decision-making community can relate readily with (ATC 2008). ATC-58 has been split into two major phases that are: (1) creating a building assessment guideline in terms of defined quantified risks, and (2) developing design guidelines with respect to PBSD. Currently, the first phase of the ATC-58 project is underway with the development of "Guidelines for Seismic Performance Assessment of Buildings," (ATC 2005).

As noted previously, the four primary steps of PBSD are selecting building performance objectives, creating a preliminary design, assessing the performance capability of the current design, and determining whether the assessed performance satisfies the select objectives (see Figure 2-9). These four main components of PBSD have remained intact in lieu of the development of next-generation protocols; however, the details and guidelines for some of these steps have become more developed than others. Since the development of PBSD has been an ongoing effort, the current stage of development for each primary step is investigated for clarity.

The selection of performance objectives is the first step for a project at the start of a performance-based design process. This task is intended to be executed by a committee of decision makers, which could include the building owner(s), designers, building officials, or other people given this responsibility, and may have to represent the needs of other groups, such as insurers or the public. A "performance objective" represents the accepted probability risk in an earthquake event, and any losses associated with the damage. New measures of performance are introduced in the ATC-58 *Guidelines*, which are separated into direct economic loss, indirect economic loss, and losses associated with casualties (injuries and/or death). Direct economic loss represents the costs of repair and/or replacement of building components from the damage, while indirect economic loss is defined by the costs incurred while the building is not functional and unoccupied (ATC 2005). Depending on the intended use for a building, any given performance measure could be more useful than other measures.

The ATC-58 *Guidelines* present measures of performances, or losses, of a building that are quantified through the use of cumulative probability functions. These probability functions, termed loss distributions or loss functions, plot a curve of a cumulative probability on the y-axis against damage values (sum of direct, indirect, and casualty) on the x-axis representing a capital loss range. A point on the curve represents the probability that for a given loss value among all possible loss values, the outcome will be equal to or less than the given loss value. The data distribution is based on the mean value (x) and standard deviation (σ) parameters, and can be distributed normally or lognormally. Figure **2.15** shows a cumulative probability function for a hypothetical building design for a selected given earthquake event. As an example, let's say that it is desired to know the probability that the damage losses for this building will not exceed $1.25 million for the given earthquake event. Using the loss function, it is determined that there is a 55% chance that the total damage to the building will not exceed $1.25 million for the selected earthquake. The loss function will alter according to the type and intensity of a given earthquake event and how susceptible to damage the structural and nonstructural components of a building are (ATC 2005).

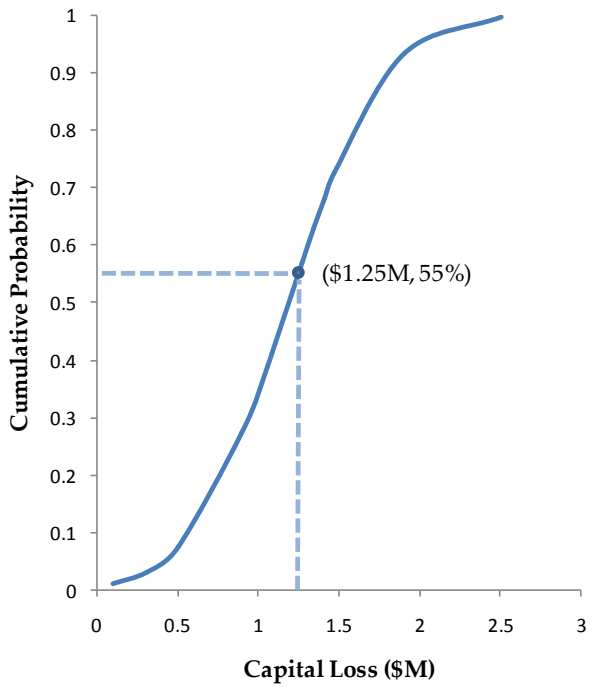

Figure 2.15: An example of a cumulative fragility function for a hypothetical building design and given earthquake

The types of values suggested by the ATC-58 *Guidelines* as a way to be used to quantify the performance of a building design or an existing building from the loss functions include median loss, average loss, probable maximum loss (PML), and bound loss. The median loss represents a damage loss value that has a 50% probability of being exceeded, and therefore a 50% probability of being conservative or exactly met. An average loss represents the capital loss that is expected in an earthquake event, and will vary from the median loss value if the loss distribution is lognormal due to the lopsided nature of lognormal distributions. A PML is a loss value where there is a 90% chance that the capital loss on a building will not exceed that value. A bound loss gives a lower

and upper loss value where there is an 80% chance that the capital loss in an earthquake event will be between those two values (ATC 2005). From these available various loss value parameters, decision-makers can select quantifiable performance objectives for a building during the first step of PBSD.

The next primary step in PBSD is development of a preliminary design. Ideally, this preliminary design should be developed with the performance objectives in mind. The closer the initial preliminary design is to creating a final building design that meets the objectives on a performance-based level, the greater the possibility of reducing the number of assessments and PBSD cycles required will be, consequently saving time and money. Currently, there is no literature with guidelines or procedures outlining this step.

The third stage in PBSD is to assess the preliminary building design. The ATC-58 *Guidelines* give the following five sub-steps for the assessment process (see Figure **2.16**): (1) Define building, (2) Characterize earthquake shaking (or ground motions); (sub-steps 1 and 2 can be done simultaneously), (3) Simulate building response, (4) Assess building damage, and (5) Compute building losses. Also, there are three suggested types of performance assessments (intensity-based, scenario-based, and time-based) all of which follow the five sub-steps outlined. In an intensity-based assessment, the damage is assessed according to a given intensity (e) of an earthquake. A scenario-based assessment estimates the damage losses from a specific earthquake at a defined location, where the magnitude and distance of the earthquake is determined

based on the relationship between the defined earthquake location and the known building site. For a time-based assessment, damage is assessed as an estimate of the probable damage that may happen from all potential earthquakes over a given period of time (ATC 2005).

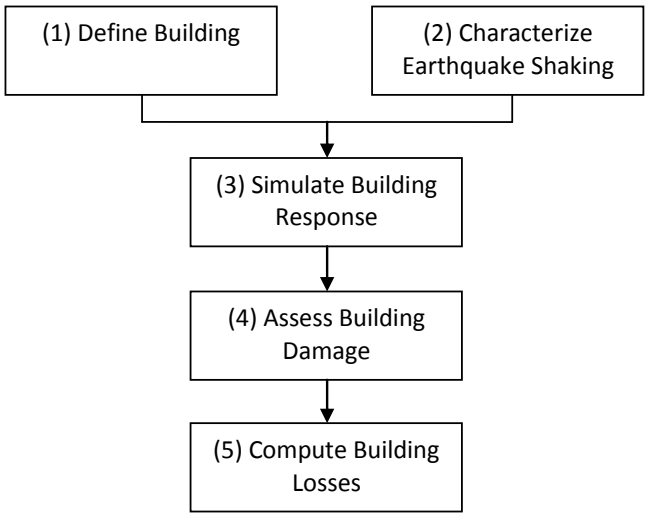

Figure 2.16: Flow Diagram for the performance assessment of a building as outlined in the *Guidelines*

The first sub-step of the performance assessment involves identifying the seismic hazard and ground motion intensity at the site location, the site conditions, the structural/nonstructural systems and components, and information on intended occupants and contents. Next, an earthquake event for the assessment needs to be defined, which will take the form as either a response spectrum for intensity-based, a median spectrum and related period-dependant dispersion value for scenario-based, or a mean seismic hazard curve (or median seismic curve with dispersion) for time-based assessment type. The third sub-step entails simulating the response of the building

through the use of simplistic or complex modeling (determined by designer) from the defined earthquake event characteristics. The fourth step, or the assessment of building damage, calculates the probability of damage to each structural and nonstructural building component based on the demands found in the structural analysis of Step 3. This is accomplished through the use of component-specific fragility functions, which produce expected damage losses on an individual component level based on the building responses (story drifts, floor accelerations, etc.) from the structural analysis. Lastly, the fifth step of computing building losses is finished through the use of a Monte Carlo statistical analysis of all factors which affect performance (earthquake intensity, structural response, estimated damage, and losses from damage), that results in mean estimates for direct economic loss, indirect economic loss, and casualties (ATC 2005).

2.5.2.1 Fragility Functions

As introduced by the ATC-58 *Guidelines*, fragility functions are used to calculate a probable loss for each building component during the building performance assessment stage (Step 4) of PBSD conditioned on the found structural responses (Step 3). Each component or system has a unique fragility curve for predefined damage limit states particular to the component or system. As a result, a different fragility function will be required for each building component/system and for each limit state associated with that particular assembly (Porter and Kiremidjian 2001). The predicted losses are calculated through the input of expected seismic structural responses, where this

demand of which is measured by story drifts, floor accelerations, component force, or component deformation.

Discrete damage states are defined for each building component based on the three performance loss measures (direct loss, indirect loss, and casualties). For example, a damage state may be defined when an initial damage failure benchmark is reached during drift displacements for a component, which leads to direct damage. Certain damage states may be related to one of the loss measures, but not any of the others. It is required that all three performance loss measures are represented in the set of one or more damage states identified for a building component (ATC 2005).

Fragility functions must be developed for a building component if they do not already exist. They can be developed from experimental test data, derived from modeled behavior, or created from expert opinions. The methods for properly developing fragilities are outlined in the Guidelines for Seismic Performance Assessment of Buildings (ATC 2005).

The fragility function is defined in the form of the following lognormal cumulative distribution function (Equation **2.6**) since the demand is always positive:

$$F_i(D) = \Phi\left(\frac{ln(D/\theta_i)}{\beta_i}\right) \qquad \textbf{2.6}$$

where D denotes the demand parameter, θ_i denotes the median of the probability distribution, β_i denotes the logarithmic standard deviation (or dispersion), subscript "i" represents the damage state of interest, $F_i(D)$ expresses the conditional probability that the component/system under consideration will sustain damage state "i" or a more

severe damage state, and Φ represents the standard normal cumulative distribution function. The conditional probability for damage state "*i*", P[*i*|D], is given by the difference between the conditional probability associated with damage state "*i*+1", $F_{i+1}(D)$, and that for damage state "*i*", $F_i(D)$ (ATC 2005).

The dispersion β is a measure of uncertainty associated with a particular building component or system. This uncertainty represents the disparity between the conditions of the actual construction with that of the tested laboratory specimen in addition to the differences in the actual loading an actual component/system may experience in a seismic event as compared to that of the laboratory loading conditions. Furthermore, the *Guidelines* state that for cases where a fragility function is generated from a limited experimental database, a two-part β parameter can be used, computed from Equation **2.7**:

$$\beta = \sqrt{\beta_r^2 + \beta_u^2} \qquad \textbf{2.7}$$

Accordingly, β_r expresses the random variability in the experimental data, which is statistically determined based on the variability within the laboratory data value results. On the other hand, β_u is a measure of the uncertainties associated with the actual physical construction details and loading conditions on the building as compared to the component testing conditions in the laboratory. Also, β_u can represent the uncertainty concerning the adequacy of the experimental database to properly reflect the variability of the specimens behavior. The ATC-58 *Guidelines* recommends a minimum value of 0.25 for β_u if: (a) five or fewer specimens were tested under the same loading protocol;

(b) different configurations are possible for the installation of the component on the building, but the specimens tested all had the same configuration; and (c) although the laboratory specimens were tested, for example, in only one direction, but the components on an actual building could experience different loading conditions. The *Guidelines* further recommend a value of 0.1 if such conditions are not applicable.

The fragility functions derived from laboratory data are based on two primary statistical parameters: the median value of demand (θ) and the dispersion (β) value. The median value of demand is the demand intensity at which a damage state is most likely to initiate, and is found by Equation **2.8**:

$$\theta = e^{\left(\frac{1}{M}\sum_{i=1}^{M}\ln d_i\right)} \qquad \textbf{2.8}$$

where M denotes the total number of specimens tested that at least experienced the initiation of the damage state, and d_i denotes the demand value in test "i" when the damage state was reached. The random dispersion value, β_r, which is input into Equation 24 to find β, is determined through Equation **2.9**:

$$\beta_r = \sqrt{\frac{1}{M-1}\sum_{i=1}^{M}\left(\ln\left(\frac{d_i}{\theta}\right)\right)^2} \qquad \textbf{2.9}$$

where M, d_i, and θ are denoted previously.

2.5.2.2 Fragility Analytical Review for Architectural Glass

In conjunction with the ATC-58 project, two separate analytical efforts were undertaken to develop fragility functions for architectural glass curtain walls. These initial works were produced based on available published glass CW laboratory data. The two reports represent the beginning groundwork in determining how fragility functions will be developed for architectural glass, the laboratory data that is applicable, and the types of damage states which should be identified.

Porter and Kiremidjian (2001) began exploring fragility development by reviewing previous published architectural glass experiments. It was noted that Behr (1998) had completed glass testing of interest, and that the damage states would be comprised of glass cracking and glass fallout. The authors went ahead and developed fragility functions for fourteen different glass configurations and a "mixed" fragility, which is a probabilistic mixture of all fragilities. It is noted that the fragilities can be used directly if glazing on a building has the same framing system, glass type, and sealant.

Porter (2006) further examined fragility curve development for curtain walls with the intention of creating fragility functions for configurations detailed with AN glass, square corners, glass dimensions of 12 ft (3.7 m) high by 10 ft (3.0 m) wide, and glass-to-frame clearances of 7/16 in. (11 mm). For this report, Porter identified three damage states of interest, which are: (1) glass cracking, (2) glass fallout, and (3) curtain wall framing damage. The author proceeded to review Bouwkamp (1961), ASCE 7-05

(2006), Behr (1998), Memari et al. (2006), and Sucuoglu and Vallabhan (1997). Overall, Porter stated that only specimens from the study of Behr and Worrell (1998) are similar to the characteristics of glass configurations in the field, but not enough so for direct empirical development of fragility functions from the laboratory data.

Consequently, Porter attempted to determine if fragility functions could be analytically derived. He started this process by comparing the cracking failure values from all reviewed experiments and compared the results to the expected cracking failure values from both the ASCE 7-05 equation (see Equation 2.3) and Sucuoglu and Vallabhan's equation (Equation 2.5). It was concluded that while Sucuoglu and Vallabhan's overestimated the cracking capacity of glass slightly, it seemed the best choice for estimating capacity. It was noted that the ASCE 7-05 equation did not account for varying glass strength. In general, it was concluded that neither equation accounts for uncertainty, and as a result a Monte Carlo simulation was carried out using the factors in Sucuoglu and Vallabhan's equation to produce a cracking damage state fragility. Then, Porter created a glass fallout fragility by direct correlation to the cracking fragility parameters by a ratio derived from the cracking and fallout failure value data relationships observed in the Behr (1998) and Memari et al. (2006) experimental tests. Lastly, Porter concluded that frame damage generally will not occur before structural collapse, so therefore this damage state should ultimately be disregarded in fragility development.

2.6 Summary and Discussion

Architectural glass curtain wall and storefront systems are an important component of a building envelope and are available in a wide variety of configuration types. Despite a significant economic cost, importance to a building's function, and widespread use, there are only a few drift limit equations required to be satisfied by architectural glass systems which are outlined in IBC 2006 (ICC 2006). Consequently, the lack of well-defined seismic design guidelines for glazing systems leaves professionals with a subjective and challenging dilemma of designing an architectural glass system that is properly capable of resisting earthquakes.

It is the intent of this thesis to perform analytical research based on seismic performance studies on architectural glass that leads to the development of seismic design approaches for glazing systems. The early studies of Bouwkamp (1961), Lim and King (1991), and Behr et al. (1995), while important in finding that in-plane dynamic loading is an acceptable method for determining the seismic capacity of glass panels, are too diverse in the test methods and configuration details for the failure data results to be useful in research analysis. However, the data from later experimental tests which used the same racking facility, similar crescendo loading protocols, and consistent glazing characteristics as utilized in this research. These studies include Behr and Belarbi's (1996) tests on SF configurations, Behr (1998) on mid-rise glass CW configurations, and Memari et al. (2003) on CW configurations with asymmetric IGU's. Memari et al. (2006b) on the seismic performance of glass with SSG was not be analyzed because the

seismic behavior of architectural glass that is wet-glazed is substantially different from dry-glazed assemblies.

Two analytical studies in the past have been carried out in an effort to model the failure behavior of architectural glass, and ultimately a suggested equation from Sucuoglu and Vallabhan (1997) is evaluated for accuracy. Sucuoglu and Vallabhan (1997) present an interesting observation pertaining to the out-of-plane deformation of glass, but it is predicted that these types of deformations contribute little to the drift capacity of the types of glass systems studied. Therefore, it was predicted that out-of-plane deformations modeled by the Sucuoglu and Vallabhan equation should not be used in the formulation of the closed-form equation, but an accuracy analysis determines whether this is the proper decision. One reason why out-of-plane deformations are not likely not develop before glass failure occurs is because the edges and surfaces of most glass panes are riddled with microscopic flaws. These flaws can be incurred during manufacturing and handling of the glass and are propagated by weathering elements and long-term loading after installation. The consequence of these defects is that stresses concentrate around them, eventually leading to premature fracture and resulting in an overall reduced strength for the glass pane (Schwartz 1984). As a result, it is unlikely that a glass pane will experience significant out-of-plane deformations before more localized edge failures during an earthquake event. Secondly, out-of-plane deformations of glass panels are more prone to occur in larger and thinner specimens as opposed to thicker and relatively smaller glass panes. The relatively

modest dimensions of glass panels (5 ft x 6 ft, 1.5 m x 1.8 m) experimentally tested and used in the research analysis diminish the chances of out-of-plane deformations occurring.

The second analytical work of Memari et al. (2007) to develop a FEM to estimate the seismic capacity showed potential. However, more research needs to be performed on this subject before this type of analysis of architectural glass is truly verifiable. As a result, finite element modeling will not be used in the analytical research in this report.

On the whole, PBSD is a fairly new design method that is still being developed. While the first-generation PBSD offered the engineering community an alternative approach to evaluating and retrofitting existing buildings that cut costs and gave a better understanding to the expected seismic performance of a structure, first-generation procedures had many limitations. The next-generation PBSD is more performance-based that can be used for new building projects.

Fragility functions were introduced by the ATC-58 project as a tool to quantify the probability of risk for individual building components and systems. Two analytical efforts were made with intentions of developing fragility functions for architectural glass wall systems. Porter and Kiremidjian (2001) carried out an analysis based on only limited CW and SF failure data that have been published. Furthermore, glass configuration results were combined in analysis, which should be avoided when two very different glass detailing options (i.e., dry-glazing vs. SSG) are combined into the same computation. Porter (2006) compiled a more extensive review and analysis for his

fragility development, but again was based on only a limited experimental database. A Monte Carlo simulation was combined with Sucuoglu and Vallabhan's (1997) equation to produce a single fragility function for a cracking limit state, but ideally there should be fragility functions for each different glass configuration. For the fallout limit state, Porter applied an empirically determined ratio from laboratory data and applied it to the cracking fragility parameters, which should also be avoided because it would be most appropriate if the fallout fragilities were based on actual glass fallout experimental data. Overall, while the two analytical projects to develop fragility functions for architectural glass were useful as a beginning step at fragility development, future analyses of glass CW and SF systems will need to be more comprehensive.

Chapter 3

Research Program and Plan

3.1 Overview

The main goal of this study was to perform analytical research on the seismic performance of architectural glass glazing systems that will be a basis for and allow the development of glazing design guidelines for these types of nonstructural building components. The research program entailed executing new architectural glass laboratory testing to gather needed in-plane dynamic loading performance information for glass configurations with substandard clearances, performing sensor testing on the racking facility to determine the accuracy of laboratory results, and conducting analytical research on the glass failure data to create two different design approaches. Then, investigations were carried out to provide methods on how to apply the performance knowledge from the laboratory to building glass systems in the field for practical applications.

The analytical research began with the development of fragility functions for each glass configuration and defined damage limit states. The past experimental failure data were reanalyzed to ensure that it is accurate, and represents the point in which the glass panel experienced the defined damage state. The analytical research continued with the development of a closed-form equation to predict the seismic performance of

various glass configurations for the cracking limit state. For the formulation of the equation, previous equations (ASCE 7-05, Sucuoglu and Vallabhan) that predict the seismic behavior of glass were evaluated using the known experimental data, and the accuracy of their predictions are determined. The result of the analysis guided the formulation of the new closed-form equation.

3.2 Selected Glass Configurations

There is a wide database of architectural glass experimental testing results that were performed by researchers at the Pennsylvania State University and University of Missouri that were analyzed in this study. Table **3.1** lists the selected CW and SF configurations that were analyzed for fragility development, and whose data was later used for the formulation of the new equation. Glass configurations studied in Behr et al. 1996, Behr 1998, and Memari et al. 2003 contributed to the selected configurations listed in Table 3.1. Furthermore, glass configurations studied in the past with varying aspect ratios, listed as (14) and (15) in Table 3.1, were included but had not been published. Lastly, configurations with substandard clearances are represented by glass configurations (10-13), the experimental study of which is carried out in this report.

Table 3.1: Summary of glass CW and SF configurations analyzed

ID	System	Glazing Type	Glass-to-Frame Clearance	Aspect Ratio
1	MR[1]	1/4 in. (6 mm) AN[3] monolithic	0.43 in. (11 mm)	6:5
2	MR	1 in. (25 mm) AN IGU[4]	0.43 in. (11 mm)	6:5
3	MR	1/4 in. (6 mm) inner AN / 1/4 in. (6 mm) outer AN LAM[5] (0.030 PVB[6]) IGU	0.43 in. (11 mm)	6:5
4	MR	1/4 in. (6 mm) inner AN / 1/4 in. (6 mm) outer AN LAM (0.060 PVB) IGU	0.43 in. (11 mm)	6:5
5	MR	1/4 in. (6 mm) inner AN / 1/2 in. (13 mm) outer AN LAM (0.030 PVB) IGU	0.43 in. (11 mm)	6:5
6	MR	1/4 in. (6 mm) AN LAM (0.030 PVB)	0.43 in. (11 mm)	6:5
7	SF[2]	1/4 in. (6 mm) AN monolithic	0.41 in. (10 mm)	6:5
8	SF	1 in. (25 mm) AN IGU	0.59 in. (15 mm)	6:5
9	SF	1/4 in. (6 mm) AN LAM (0.030 PVB)	0.41 in. (10 mm)	6:5
10	MR	1/4 in. (6 mm) AN monolithic	0 in. (0 mm)	6:5
11	MR	1/4 in. (6 mm) AN monolithic	0.13 in. (3 mm)	6:5
12	MR	1/4 in. (6 mm) AN monolithic	0.25 in. (6 mm)	6:5
13	MR	1 in. (25 mm) AN IGU	0.25 in. (6 mm)	6:5
14	MR	1/4 in. (6 mm) AN monolithic	0.43 in. (11 mm)	2:1
15	MR	1/4 in. (6 mm) AN monolithic	0.43 in. (11 mm)	1:2
16	MR	1/4 in. (6 mm) HS[7] monolithic	0.43 in. (11 mm)	6:5
17	MR	1 in. (25 mm) HS IGU	0.43 in. (11 mm)	6:5
18	MR	3/8 in. (10 mm) HS LAM (0.030 PVB)	0.43 in. (11 mm)	6:5
19	MR	1/4 in. (6 mm) inner AN / 1/4 in. (6 mm) outer HS LAM (0.060 PVB) IGU	0.43 in. (11 mm)	6:5
20	MR	1/4 in. (6 mm) inner AN / 1/2 in. (13 mm) outer HS LAM (0.060 PVB) IGU	0.43 in. (11 mm)	6:5
21	MR	1/4 in. (6 mm) FT[8] monolithic	0.43 in. (11 mm)	6:5
22	SF	1/4 in. (6 mm) FT monolithic	0.41 in. (10 mm)	6:5
23	SF	1 in. (25 mm) FT IGU	0.59 in. (15 mm)	6:5
24	MR	1/4 in. (6 mm) inner AN / 1/2 in. (13 mm) outer FT LAM (0.060 PVB) IGU	0.43 in. (11 mm)	6:5

[1]MR = mid-rise CW system with Kawneer 1600™ framing, [2]SF = storefront system with Kawneer TriFab II® 450 or 451 framing, AN = annealed, [4]IGU = insulating glass unit, [5]LAM = laminated glass unit, [6]PVB = polyvinyl butyral, [7]HS = heat-strengthened, [8]FT = fully-tempered

These configurations contain different glazing characteristics that are known to affect the seismic performance of glass, which include glass type (material strength), system type (CW or SF), aspect ratio, glass configuration (monolithic, Lami, or IGU), aspect ratio, and glass-to-frame clearances. All configurations have a square corner geometry, cut (or raw as termed by some glass manufacturers) corner and edge finish

conditions, and are dry-glazed. These twenty-four configuration types were chosen based on the amount of data available, the most common CW or SF systems used on buildings, and representation of a range of glazing options available. For referencing throughout the report, an identification label has been assigned to each assembly.

3.3 Curtain Walls with Various Glass-to-Frame Clearances Test Plan

The performance of glass subjected to lateral loading is known to be sensitive to its glass-to-frame clearance, but as of yet no studies have been performed which isolate this glazing detail. Past studies such as Bouwkamp (1961) and Sucuoglu and Vallabhan (1997) show how the glass-to-frame clearance dimension is related to the drift when a glass panel comes in contact with the metal framing due to panel translation during lateral loading. Glass contact is followed by further translation and rotation of a glass panel, which leads to the initiation of glass crushing and cracking in the corner regions of panels. This glass behavior has been observed in the studies by Behr (1998) and Memari et al. (2003) which recorded initial contact data to compare with cracking failure values. In all previous studies outlined in this report, the glass panels cyclically racked contained glass-to-frame clearances of approximately 0.5 in. (13 mm). Therefore, the magnitude of effect of different clearances on the experimental failure of glass panels is not known.

As a result, new laboratory testing was conducted on glass specimens with varying glass-to-frame clearances with the purpose of fulfilling two main objectives.

The first was to acquire an understanding of how glass-to-frame clearances affect the seismic performance of glass panels. The second goal was to provide a way to apply the modeled behavior of glass performance as a function of clearance to the past experiments so that the capacity of glass systems on buildings with nonstandard glass-to-frame clearances can be accurately predicted through fragilities and the closed-form equation.

To compare with the existing database of studied glass configurations with standard clearances, glass panels with clearances of 0 in. (0 mm), 0.125 in. (3 mm), and 0.25 in. (6 mm) were tested. The testing was performed on AN monolithic and AN-IGU glass type CW configurations. Two AN-Mono glass specimens with 0 in. (0 mm) and 0.125 in. (3 mm) clearances, three AN-Mono glass specimens with 0.25 in. (6 mm) clearances, and one AN-IGU glass specimen with a 0.25 in. (6 mm) clearance were tested.

3.4 Sensor Testing

To validate the accuracy and ensure conservatism of the experimental failure data that were used in the analytical research, the effect of flexibility in the racking facility itself was evaluated through the use of sensor testing. Various sensor racking tests were run on the racking facility in conjunction with the glass-to-frame clearance testing and other ongoing glass racking projects. These tests determined whether significant flexibility in the facility existed, and whether the flexibilities effected the

desired loading displacements experienced by the glass panels. Table **3.2** provides a list of glass configurations that sensor tests were performed on. The wide array of glass configurations allowed for comparisons among varying glazing details.

Table 3.2: Glass CW specimens tested with sensors

1	AN Monolithic – 0.43 in. (11 mm) clearance
2	AN Monolithic – 0.25 in. (6 mm) clearance
3	AN Monolithic – 0 in. (0 mm) clearance
4	AN IGU – 0.43 in. (11 mm) clearance
5	AN IGU – 0.25 in. (6 mm) clearance

Sensors were attached to important points on the racking facility and glass panels. Linear potentiometers backed by a spring-controlled vertical slide, which allowed free up and down movement of the sensors, were used to measure the horizontal displacement of the lower and upper steel tubes of the testing facility during testing. Also, a DC LVDT was attached to the actuator to measure any deflection of the actuator plate. Furthermore, a DC RVDT rotation sensor mounted on an x-y slide table measured the angle of rotation of the fulcrum arm. Lastly, three sensors were used to measure the rotational and translational movement of the glass pane within and relative to the framing, which was accomplished by connecting a DC RVDT rotation sensor to the center of the glass panel and having a horizontal and a vertical string potentiometer measure any linear translation from the same point on the pane of glass. Table **3.3** summarizes the sensors utilized and the purpose that each one served.

Table 3.3: Summary of sensor descriptions with items measured

Item Measured	Sensor Description
Actuator Plate Displacement	DC LVDT – spring loaded
Fulcrum Arm Rotation	DC RVDT – mounted on x-y plane
Lower Tube Displacement	Linear potentiometer – mounted on spring controlled slide
Upper Tube Displacement	Linear potentiometer – mounted on spring controlled slide
Glass Panel Rotation	DC RVDT – mounted on x-y plane
Glass Panel Horizontal Translation	String potentiometer – mounted on rotation sensor x-y plane with assembly that allows vertical slide
Glass Panel Vertical Translation	String potentiometer – mounted on rotation sensor x-y plane with assembly that allows horizontal slide

The results from these sensor tests were analyzed to determine whether flexibilities were present in the racking facility. The analysis involved identifying the displacements measured by the lower and upper tube sensors. In a given loading step, the lower and upper tubes of the racking facility will have eight peak displacements during the "constant interval" portion of the step. The average of the absolute value of these eight peaks were calculated to determine a displacement for each tube, and the displacements for both tubes were added for an actual displacement experienced by the glass specimen for any given racking step. A comparison between actual displacements with the expected (and past reported) displacements exposed if any flexibilities existed, and the results can be found in Section 4.1.1.

3.5 Fragility Function Development

Fragility functions were developed for all glass CW and SF configurations listed in Table 3.1. As previously mentioned, fragility functions are introduced by the ATC-58 *Guidelines* as a way to calculate a probable loss for building components during the building performance assessment stage (Step 4) of PBSD conditioned on computed structural responses (Step 3). Fragility functions for the CW and SF configurations are defined by a lognormal cumulative distribution function (see Equation 2.3), where the median value of the demand (θ_i) when damage is expected to initiate (at damage state "*i*") and the dispersion value (β) are the two main parameters that characterized the curves. These parameters were determined from the experimental failure data values for each CW or SF configuration and for any given damage state.

The demand parameter chosen for the development and calculation of fragilities for glass systems was drift ratio, as defined by Equation **3.1**:

$$Drift\ Ratio = \frac{\delta}{h} \qquad \textbf{3.1}$$

where δ is equal to the horizontal drift displacement that a glass panel is subject to and h is equal to height over which the horizontal drift displacement occurs, which will usually be the height of the glass panel. This type of demand was chosen as the most appropriate measure to use, because the failure values which were reported as drifts in the studies (Behr et al. 1996, Behr 1998, Memari et al. 2003, Memari et al. 2006) were readily converted into drift ratios. Also, drift ratio is one of the structural demand

parameters deemed acceptable for fragility use by the ATC-58 *Guidelines* (ATC 2005). Lastly, AAMA 501.4 (AAMA 2001a) and AAMA 501.6 (AAMA 2001b), or the two seismic test methods recommended for the seismic and wind evaluation of CW and SF systems by AMMA, are measured in interstory drift ratios.

The fragility functions developed for architectural glass systems can be used for two primary purposes. The first is for use within the context of a general PBSD approach of an entire existing building or building design with an exterior glass system. The second is for curve utilization during the design process of a glass CW or SF system to give a user the expected seismic performance of different glass configurations in a probabilistic manner. In this manner, the median damage failure values (θ) represent the expected seismic capacity of a given damage state for a glass configuration at 50% probability. Furthermore, the curves can be used to find likely failure demands as a function of other probability values. It should be noted that θ is different than the average failure drift ratio value for a given data set, because θ is based on a lognormal distribution while the straight average assumes a normal distribution of the failure data. The ATC-58 *Guidelines* uses a lognormal statistical analysis because it takes into account the skewed failure phenomena in some building components. For example, it may be more likely that a building component will fail far above the average failure value as opposed to failing below the average, and a lognormal distribution will more accurately model this performance behavior.

The *Fragility Function Calculator version 1.02* software as offered in conjunction with the ATC-58 Project was utilized to find the fragility parameters θ and β_r (Porter 2007). According to the ATC-58 *Guidelines* (ATC 2005), the fragility parameter calculator in the software can be used on many different types of data sets. Two data set types are represented in the experimental failure values, which are:

1) Actual Demand Failure Values: values of laboratory excitation such as drift displacements at which each of several specimens failed

2) Bounding Failure Values: maximum value of laboratory excitation each of many specimens experienced where some of the specimens failed and some did not fail

The following input information for the calculation of fragility parameters as required for the fragility calculator software as shown in Figure **3.1** was compiled: "Component ID", "Component Description", "Describe Specimen", "Describe Excitation", "Demand Parameter", "Damage Evidence", "Damage Measure", and laboratory failure demand values.

The fragility functions were then plotted using Excel software according to directions detailed in the Guidelines for Seismic Performance Assessment of Buildings 35% Draft (ATC 2005). The parameters used to define the curves were θ values found previously, and β values calculated by Equation 2.7 with β_r values also found previously.

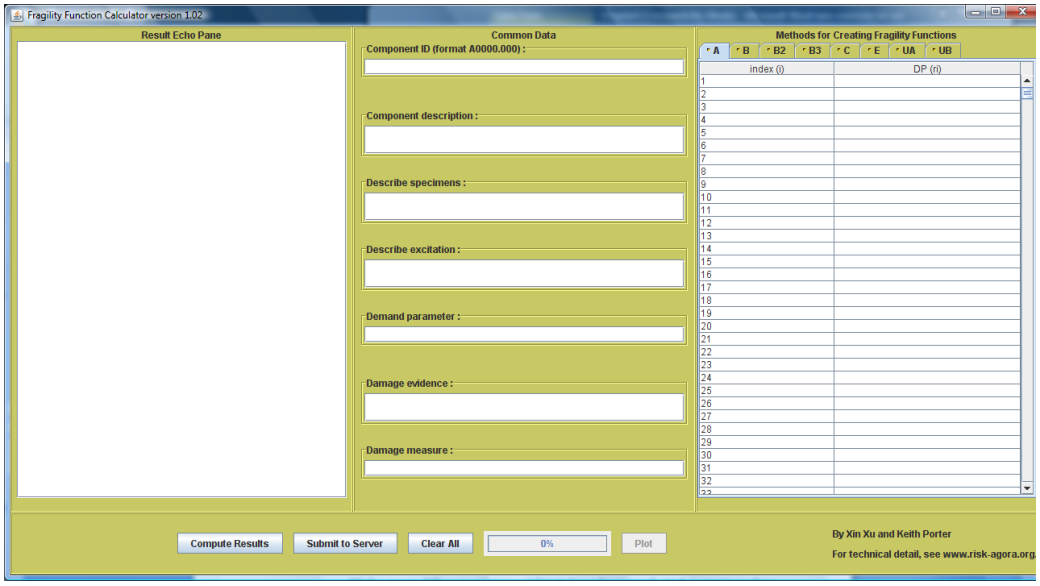

Figure 3.1: Snapshot detailing required input information from the *Fragility Function Calculator version 1.02*

3.5.1 Damage Limit States

Three damage limit states have been identified as appropriate for the fragility curve development, which are: (1) onset of glass cracking; (2) glass fallout as defined in AAMA 501.6 (AAMA 2001) as the event when a fragment of glass equal to or larger than 1 in.^{2} (645 mm^2) breaks away from the glass panel and falls out; and (3) gasket seal degradation. In Section 5.1, each of these damage limit states were thoroughly defined and investigated.

3.5.2 Cracking and Fallout Damage Limit State Data Adjustments

Experimental studies outlined in Chapter 2 defined the cracking limit state as the drift amplitude associated with the observation of a through-thickness crack in the vision area of the glass panel. However, it is known that these cracks in the vision area radiate from initial crushing and crack formation in the corners of a glass panel, which is hidden by aluminum framing and rubber gaskets. In an effort to provide fragility curves based on conservative data, the cracking damage failure values were adjusted to represent the onset of the cracking damage limit state. This was accomplished by reviewing "load vs. time" charts for past experimental testing, and reducing cracking limit state values for certain glass specimens where cracking onset damage evidence is apparent in the charts before the previously recorded vision cracking failure values.

To further ensure conservatism in the cracking and fallout damage limit values, the data were checked to see if the recorded failure values represent the displacement where the glass panel experienced fallout. Since many specimens were racked in a "stepwise" crescendo loading manner, it is possible that either failure limit state occurred on the "ramp-up" loading interval, which means that the peak displacements of the loading step were not reached. The "load vs. time" charts for the laboratory glass specimens were reviewed, and the failure values were reduced accordingly for glass specimens where evidence is present that fallout was reached on the ramp-up loading cycle.

3.5.3 Gasket Damage Limit State Data Acquisition

The failure drift values corresponding to gasket degradation were not documented at the time of testing during the laboratory experiments. However, racking test data sheets and recorded video footage were reviewed to compile the gasket degradation failure limit values for available glass configurations.

3.6 Analytical Development of a Closed-Form Equation

As a way to offer another design approach for seismic design guidelines of architectural glass, analytical calculations were performed on the compiled experimental failure data to produce a new closed-form equation which predicts the seismic capacity of glass panels. Based on the analytical approaches of Bouwkamp (1961), Sucuoglu and Vallabhan (1997), and adoption of ASCE 7-05 (ASCE 2006) in the codes reviewed in Chapter 2 for prediction of the seismic capacity of glass panels, a closed-form was the best option, as opposed to an open-form method such as FEM. Not enough research information is available for the development of an accurate open-form approach. Furthermore, the equation addresses the effects that different glazing characteristics have on the seismic performance of glass panels, and the scope of glazing characteristics accounted for are represented in the selected glass configurations analyzed (see Table 3.1).

The architectural glass seismic capacity equations suggested by ASCE 7-05 (ASCE 2006) and Sucuoglu and Vallabhan (1997) were compared with available initial contact and cracking damage state failure values observed in the experimental test results for all CW and SF configurations. The accuracy of the equations were determined through this comparison, and for the first time the level of error of these equations are presented in literature. Based on the results of this analysis that can be found in Section 6.3, it was determined whether either equation should be used, modified, or ignored for the formulation under development. Modifications were then proposed for the ASCE 7-05 (ASCE 2006) equation, where a factor was then added for each glazing detailing characteristic. Modification factors added to the base equation included a factor representing substandard glass-to-frame clearances, glass strength type (AN, HS, or FT), glass configuration type (Mono, Lami, or IGU), system type (CW or SF), aspect ratio, and connection detailing. The magnitude and formulation of each different factor found in Section 6.5 was based on trends extracted from the compiled experimental test results.

3.7 Field Application of Analytical Results Procedures

Procedures are presented in this report for professionals as a way to translate the seismic performance results and analysis of single glass panels to predict the seismic performance of entire glass CW or SF systems on an actual building. The development of a new closed-form equation allow users to predict the seismic capacity of glass for

design and proportioning of CW and SF systems, and factors in the equation allow users to account for varying configurations details. On the other hand, fragility curves allow users the prospect of predicting the performance of an entire glass CW and SF system according to various PBSD measures. Generally, the fragility data developed can be used directly if the considered glass system has the same general framing system glazing details, glass type, glass panel size, aspect ratio, thickness and glass-to-frame clearances of one of the configurations listed in Table 3.1. Otherwise, a fragility curve can be modified to reflect the differences between the field system and configuration tested in the laboratory. The procedures to accomplish this task were outlined for the differences in framing systems, glass-to-frame clearances, and aspect ratio, and can be found in Section 5.5. Lastly, other conditions which might alter the performance results from the laboratory to application on an entire glass system were investigated, the discussions of which can be seen in Chapter 7.

For the framing system details of CW and SF configurations, different aluminum framing systems were compared with the Kawneer framing systems used in the laboratory testing. An analysis determined how critical a different framing system is in affecting the seismic performance of architectural glass. The study provides ways for modifying fragility curves for their specific glass systems with different framing detailing if necessary, the magnitude of which was determined from the research and analysis conducted.

A section was developed outlining how users can determine the capacity of glass in systems with a nonstandard glass-to-frame clearance. Fragilities developed for configurations tested in this study can be directly used for AN monolithic configuration types with similar nonstandard clearances. Otherwise, an investigation was performed to develop alternative options available for configurations with substandard clearances not represented by any of the studies. On offered solution for altering fragilities is the process of "fragility mixing," which was introduced in Porter and Kiremidjian (2001) and presented in this study.

Also, another section was developed to detail how fragilities can be altered for glass configurations with aspect ratios that differed from the aspect ratios used in laboratory testing. Similar to the glass-to-frame clearance glazing detail, an investigation was performed to find ways that the curves can be altered so that the fragilities can be applicable to a wide range of glass aspect ratios found in the field.

Finally, procedures were developed outlining how to apply the results and capacity predictions for individual glass panels from both equation and fragility design approaches to a large architectural glass system on a building in the field. The different factors that alter the expected performance of a system on a building, such as connection detailing and continuity of the glazing over multiple stories, were addressed. Also, an example found in Section 7.2 was developed to illustrate how to relate interstory drift ratio values of individual glass panels to drift in inches or millimeters over an entire CW section.

Chapter 4

Experimental Study

This chapter presents the experimental study carried out and the results obtained for areas of the research plan laid out in Chapter 3. Section 4.1 examines the facility flexibility sensor testing, and includes the conclusions from the sensor results and resulting data adjustment. Section 4.2 initially discusses the test setup, specimens and the loading applied, and then summarizes the results of the varying glass-to-frame clearance testing. Section 4.3 states the overall results and conclusions reached during the study of facility flexibility, modification of the experimental data, and testing of glass configurations with substandard glass-to-frame clearances.

4.1 Facility Flexibility Sensor Testing

As mentioned previously, to assess the accuracy of the previous experimental data failure results using the BERL dynamic racking test facility, sensors were attached to the racking facility during certain specimen tests to determine whether flexibilities in the facility were present. The variety of glass specimens tested represented five different glass configurations and allowed for comparisons among various configuration details. A list of the CW specimens that were tested with sensors can be reviewed in Table 3.2,

and a summary list of sensors used with their functions can be reviewed in Table 3.3. Overall, an analysis that was performed on the compiled data determined that flexibilities did exist in the facility, as detailed in the following subsection. Furthermore, the flexibilities were significant enough to warrant a data adjustment of most past experimental testing to reflect the findings of the analysis. This data adjustment resulted in the reduction of failure values by an average of 17.6%.

4.1.1 Sensor Data Analysis

The analysis to find whether flexibilities exist in the racking facility consisted of comparing the actual displacement experienced by glass specimens with the expected controlled displacement that a glass panel is supposed to be subjected to. The expected displacement is equal to the controlled applied displacement to the bottom steel tube of the racking facility by a hydraulic actuator, the values of which are measured by a LVDT embedded in the actuator. The actual displacements experienced by glass specimens, though, has to be determined by analyzing the measured displacements by linear potentiometer sensors that were attached to the lower and upper steel tubes of the facility, as detailed in Section 3.4. To complete this task, the displacements measured by the linear potentiometer sensors were extracted by reviewing recorded "displacement vs. time" charts, as shown in Figure **4.1a**. In a given racking load step as seen in Figure

4.1b, the lower and upper steel tubes will each see eight peak displacements during the constant interval portion of a loading step. The recorded "displacement vs. time" charts give the actual displacements that a given steel tube experienced during the load intervals measured by the sensors. An average of the absolute values of each of these eight peaks was calculated from the charts to find the horizontal displacement of the lower or upper steel tube. Then, the displacements for the lower and upper tubes were combined to give an actual displacement that the attached glass specimen experienced during a given load step.

A comparison between the actual displacements with the expected displacements for glass specimens which received sensor testing (see Table 3.2) showed that the actual displacements were lower than the expected displacements. Since the actual displacements were lower than the expected, this was an indicator that flexibilities existed in the facility. Specifically, two separate flexibilities were identified.

The first flexibility in the racking facility was found to exist between the actuator and the lower tube. In this instance, flexibility occurred between the point where the actuator applies a controlled load to the lower steel tube and the distance the lower tube horizontally translates. However, this flexibility was found to be relatively minor, having an effect of less than 1% between the expected and actual displacement values.

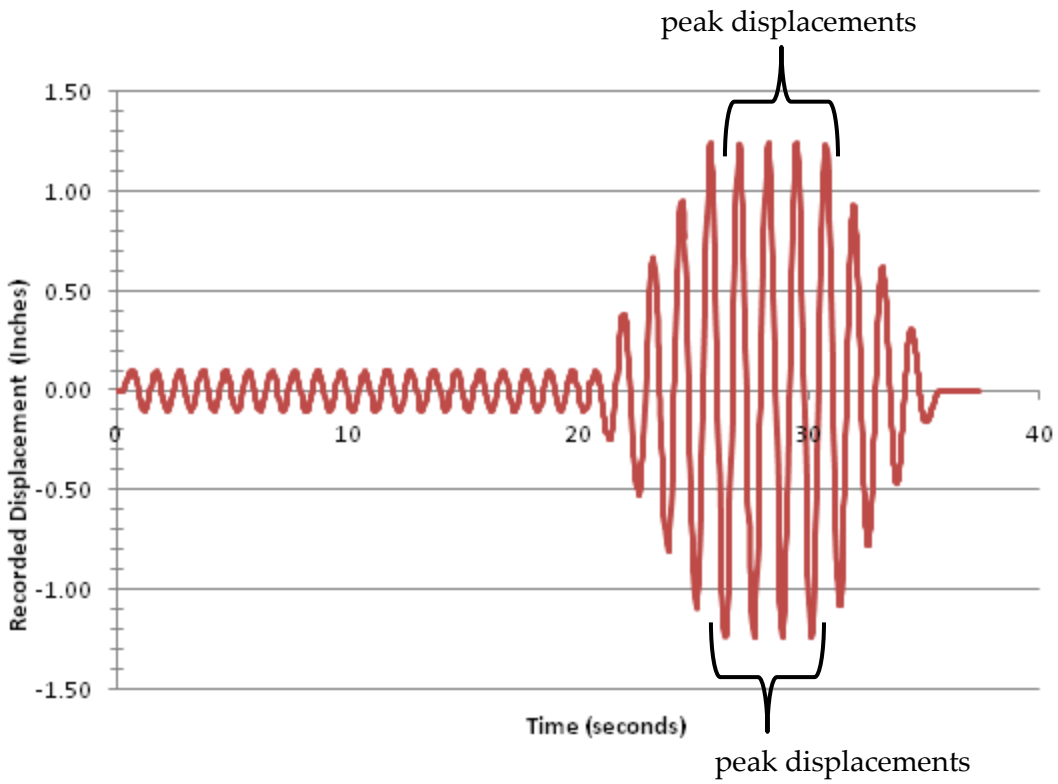

(a)

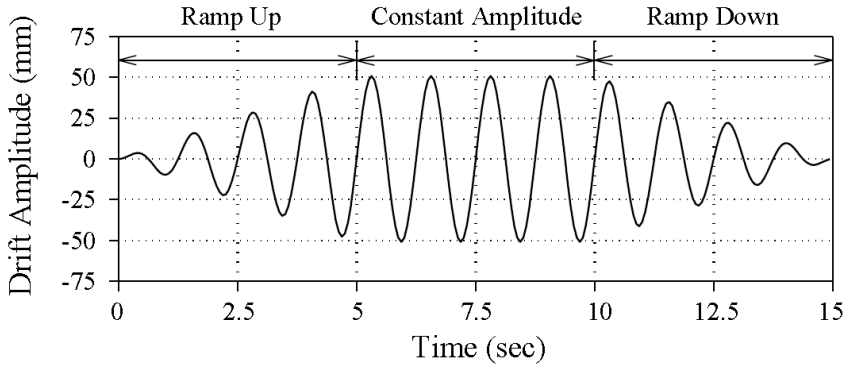

(b)

Figure 4.1: Depiction of (a) a sample recorded displacement vs. time chart during the sensor tests and (b) typical load step that a glass panel is subject to with the three intervals labeled (Memari et al. 2003)

The second flexibility was detected when differences between the displacement values of the upper and lower tubes were found. This condition is depicted in Figure **4.2**, where the steel tubes on the racking facility are shown in a displaced condition for a given load cycle during the sensor testing. It is assumed that the lower tube displaced a length equal to Δ_{lower}, while the upper tube displaced a length equal to Δ_{upper}. If there was no flexibility, then the glass panel would have experienced the expected displacement, a condition where Δ_{lower} would have been equivalent to Δ_{upper}. However, a flexibility in the fulcrum arm behavior and from hole tolerances lessened the displacement of Δ_{upper}, such that the upper steel tube displaced less than the lower steel tube. As a result, the actual displacement of the glass panel was less than the expected displacement, which was assumed to be doubled the measured displacement at the actuator on the lower steel tube.

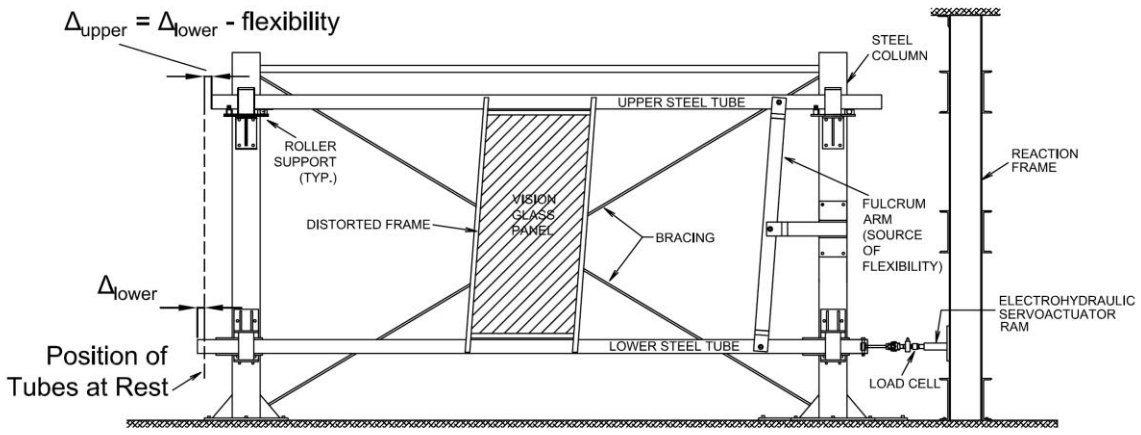

Figure 4.2: Depiction of the facility in a displaced condition where the effect of the flexibility in the fulcrum arm on the displacement of the upper and lower steel tubes is shown

The effect of both flexibilities combined was significant. Overall, the glass specimens experienced an actual displacement that was 23.3% less than the displacement that was expected. This calculation was found by dividing the summed differences between the expected and actual displacements for all loading steps of all specimens tested by the summation of expected displacements. The calculation was based on the information of about forty load steps in all, where the glass specimens were subjected to maximum displacements of either 2.25 in. (57 mm) or 2.5 in. (64 mm) before glass fallout occurred and testing was stopped. It was observed that the flexibility had a greater effect in terms of percent difference on lower load steps than load steps with greater displacements. Since overall the effect of the flexibility was significant, the failure data should be adjusted accordingly such that the failure values are reduced to represent the overestimation of capacity of the specimens.

4.1.2 Failure Data Adjustment

Overall, the effect of the flexibilities was consistent for any given load step for the different glass configurations that were tested, which means that a general adjustment method can be applied to the failure data. The consistency was determined based on statistical regressions that were performed on the data of each specimen. Specifically, a regression analysis was conducted between the actual and expected displacements data values to see if these two variables were statistically correlated. The results of the analysis showed that a nearly perfect linear relationship existed for each configuration

between the two data points. These relationships were found to be extremely linear because the R-squared values, which were around 0.99, are near the 1.0 value that indicates a perfect linear relationship between the two variables. The linear nature of the differences between expected and actual displacement values means that the effect of the flexibilities across the different loading steps and for various glass configurations were consistent in magnitude.

Since the flexibilities identified in the racking facility were consistent, the linear equations that resulted from the regression analysis were used as the standard method of adjustment for the failure limit values because the equations directly relate the actual displacements with the expected displacements. The data from the new experimental testing and from previous experiments were adjusted, although there is a possibility that the flexibility grew over time due to factors such as enlarging holes. However, stiffening of the steel members supporting the fulcrum arm on the facility has since eliminated most of the flexibilities. Therefore, the flexibility was most likely present during the past testing, and to be conservative the past failure values were reduced in the same manner as the failure values for the new laboratory testing.

Due to the similar nature of the regressions for the four glass configurations with 0.25 in. (6 mm) and standard 0.43 (11 mm) glass-to-frame clearances, the data were combined to develop one linear regression that would be utilized as the adjustment factor for all past experimental glass specimens with those clearances. The glass configuration with the 0 in. (0 mm) clearance would then be adjusted based off of the

linear regression for that particular configuration. A summary of these findings can be seen in Figure **4.3**, which has a chart of the two separate linear relationships.

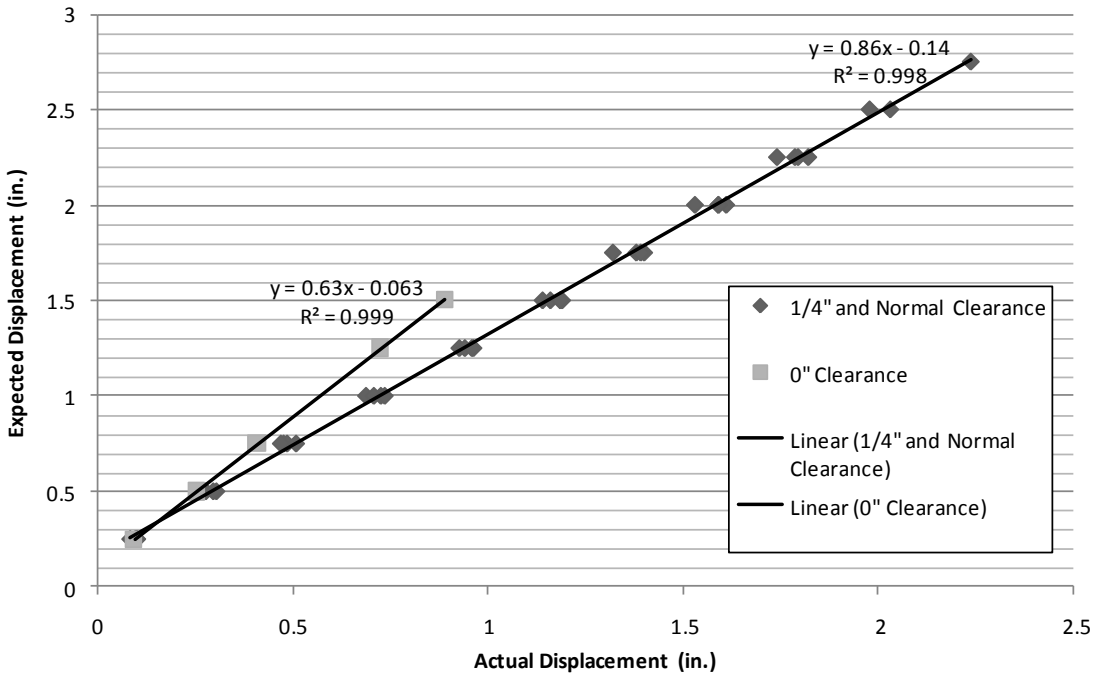

Figure 4.3: The two linear relationships and properties determined based from the actual displacement versus expected displacement values

In summary, the mid-rise CW configurations with 0.25 in. (6 mm) or 0.43 in. (11 mm) glass-to-frame clearances, were adjusted according the linear regression represented by Equation **4.1**:

$$\Delta_{actual} = 0.86\Delta_{actuator} - 0.14 \qquad \textbf{4.1}$$

where $\Delta_{actuator}$ denotes the expected displacement value as measured from the actuator for the original failure limit state, and Δ_{actual} the resulting actual displacement value that a glass panel most likely experienced a failure limit state at. Specifically, Equation 4.1

was applied to glass configurations (1-6, 12-21, 24). Equation **4.2** represents the linear regression for the CW configuration (10) with a 0 in. (0 mm) glass-to-frame clearance, and was only applied to that configuration:

$$\Delta_{actual} = 0.63\Delta_{actuator} - 0.063 \qquad \textbf{4.2}$$

where $\Delta_{actuator}$ and Δ_{actual} were denoted previously.

For glass configuration (11) with a 0.13 in. (3 mm) glass-to-frame clearance, the failure values were adjusted based on interpolation between Equation 4.1 and 4.2. The SF configurations did not receive adjustment because these specimens were tested three at a time as opposed to individually as CW configurations, and therefore the extent of the facility flexibility (if one was present) is unknown. Finally, for the remainder of this report it can be assumed that any failure data presented has received an adjustment accounting for facility flexibility.

4.2 Varying Glass-to-Frame Clearance Testing

The specimens tested with varying substandard clearances were built to similar specifications as the other glass configurations from past studies listed in Table 3.1 so that the performance results of the glass panels with substandard clearances could be readily compared with glass configurations with standard clearances. The specimens were dry-glazed within mid-rise CW Kawneer 1600™ aluminum framing, with the

glazing details shown in Figure **4.4**. The glass panels were secured within the framing using pressure plates, that were installed using self drilling screws located 9 in. (229 mm) on center and a torque limiting drill attachment to torque the screws to 95 -100 in. • lbs (10.7 - 11.3 N • m) as recommended in the Kawneer 1600™ system installation instructions (1998). Furthermore, all of the glass specimens were 5 ft wide by 6 ft high (1.5 m x 1.8 m). To ensure that the specified varying glass-to-frame clearance for each specimen was accurately achieved, a caliper was used to measure the clearances around the glass panel when the specimens were being built.

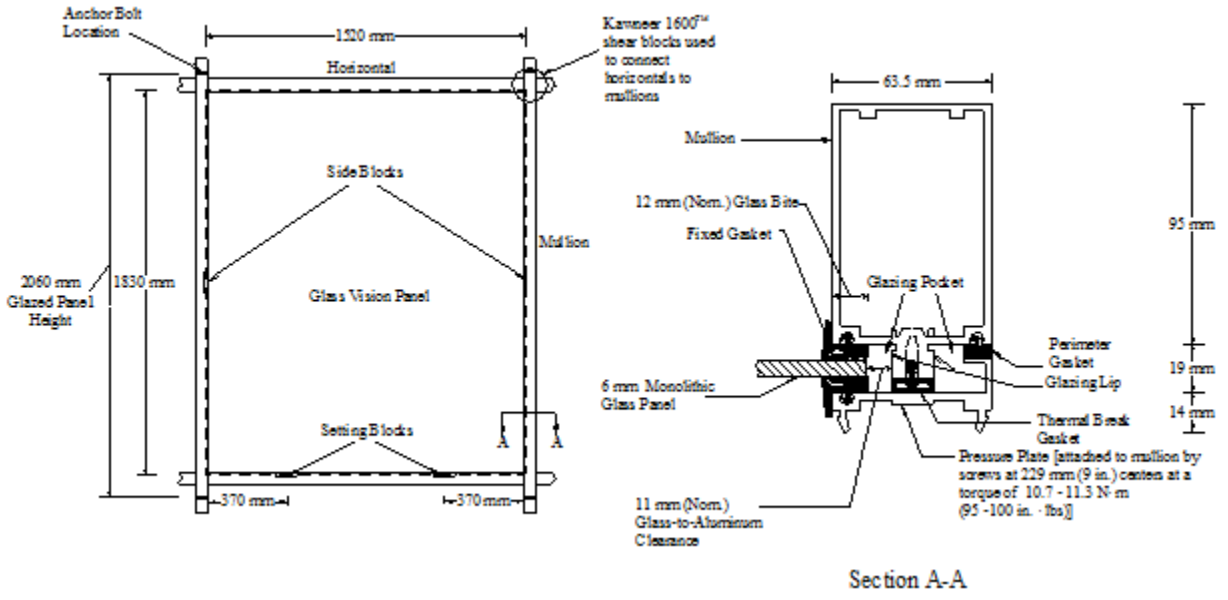

Figure 4.4: General glazing details for the Kawneer 1600™ mid-rise CW system (Memari et al. 2003)

To obtain the proper failure states of the glass specimens, in-plane cyclic racking tests were performed on the racking facility depicted in Figure 2.8 in the Building Envelope Research Laboratory (BERL) at the Pennsylvania State University. The glass

panels were tested individually, where each specimen was connected to the facility through pi-shaped anchors (see Section 5.3.1) that attached the mullions at all four corners of the specimen to the lower and upper steel tubes of the racking facility. The sliding steel tubes of the facility, which are interconnected with a fulcrum arm mechanism, transmit the racking displacements to the glass panels. Similar to past studies, the bottom steel tube is displaced in a computer-controlled fashion by means of a MTS 244.22 electrohydraulic servoactuator, where the displacements of the actuator are computer-controlled by a MTS 458.20 system. The actuator has a stroke capacity of ±3.0 in. (±76 mm), but through the fulcrum and pivot arm connection to both steel tubes the glass specimen can be subjected up to ±6.0 in. (±152 mm) (Behr 1998). A displacement transducer within the actuator measures and reports the racking displacements during testing which are recorded on a computer.

The specimens were tested using the "crescendo test method" in a step-wise fashion as detailed in Memari et al. 2003. The crescendo test method, originally introduced in Behr and Belarbi (1996) and adopted in AAMA 501.6 (AAMA 2001b), was conducted in a step-wise manner such that cracking and fallout drift limits could be properly recorded. The step-wise testing method consisted of a series of alternating "ramp up," "constant amplitude," and "ramp-down" intervals, each comprised of four sinusoidal cycles. The loading steps were applied in increasing 0.25 in. (6 mm) increments. However, after glass cracking was observed, the crescendo test was performed in a continuous manner until fallout occurred. Figure **4.5**a depicts a sample

loading step used in the dynamic crescendo testing, and Figure 4.4b shows a continuous drift time history of concentrated load step with the "ramp-down" intervals of each loading step not included. The displacements in the loading steps were applied at a frequency of 0.8 Hz for load increments with amplitudes between 0 and 3 in. (0 and 76.2 mm) and 0.4 Hz for amplitudes between 3 and 6 in. (76.2 and 152 mm).

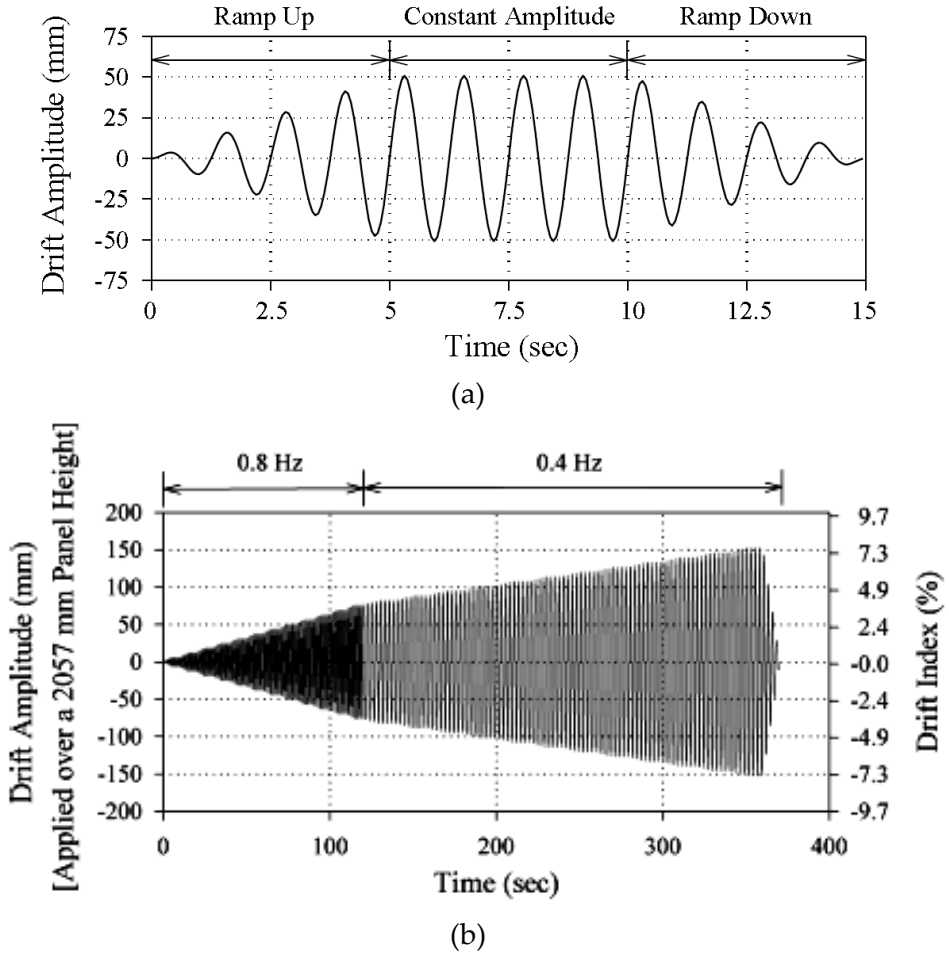

Figure 4.5: Depiction of (a) sample loading step (Step 8) from the racking tests and (b) entire crescendo test history of combined load steps with "ramp-down" intervals removed (Memari et al. 2003)

The number of specimens tested for each different glass configuration with given substandard clearance is summarized in Table **4.1**. During the racking tests the drifts associated with two failure limit states were recorded: (1) the drift causing observable glass cracking; and (2) the drift corresponding to glass fallout, where glass fallout was considered reached when a glass fragment larger than one square inch (625 mm^2) broke away from the panel as recognized in AAMA 501.6 (AAMA 2001b). Specific failure values for any given specimen can be found in Appendix A.2. Figure **4.6** depicts an example of an AN-Mono glass specimen after glass fallout had been experienced.

Table 4.1: Summary of glass configurations and number of specimens tested

ID	# Specimens Tested	Glazing Type	Clearance
10	2	1/4 in. (6 mm) AN-Mono	0 in. (0 mm)
11	2	1/4 in. (6 mm) AN-Mono	0.125 in. (3 mm)
12	3	1/4 in. (6 mm) AN-Mono	0.25 in. (6 mm)
13	1	1 in. (25 mm) AN-IGU	0.25 in. (6 mm)

The results from the experimental testing proved that the glass-to-frame clearance dimension is critical to the failure capacity of a glass panel. The findings are summarized in Figure **4.7**, where the average cracking and fallout damage states for the AN-mono configurations with 0 in. (0 mm), 0.13 in. (3 mm), and 0.25 in. (6 mm) are compared with the failure values from the AN-Mono configuration with a standard clearance of 0.44 in. (13 mm). Furthermore, the cracking and fallout failure values of the AN-IGU glass configuration with a 0.25 in. (6 mm) clearance is compared with the AN-

Figure 4.6: Depiction of an AN-Mono glass specimen attached to the racking facility after glass fallout was reached

IGU glass configuration with a standard 0.44 in. (13 mm) clearance. For the AN-Mono glass types, the graph indicates that from the configuration with a standard clearance, the failure values of both damage states generally decrease as the clearances among configurations decrease. However, for the cracking limit state, it appears that the experimental cracking results for the 0.25 in. (6 mm) clearance glass configuration was slightly higher compared with the cracking failure value from the configuration with a standard clearance. It is assumed that if more experimental testing is performed on glass specimens with a 0.25 in. (6 mm) clearance, the average cracking experimental capacity would likely fall below the observed cracking capacity for the configuration

with a standard clearance. For the AN-IGU glass types, the cracking and fallout displacements significantly decreased with the lower glass-to-frame clearance.

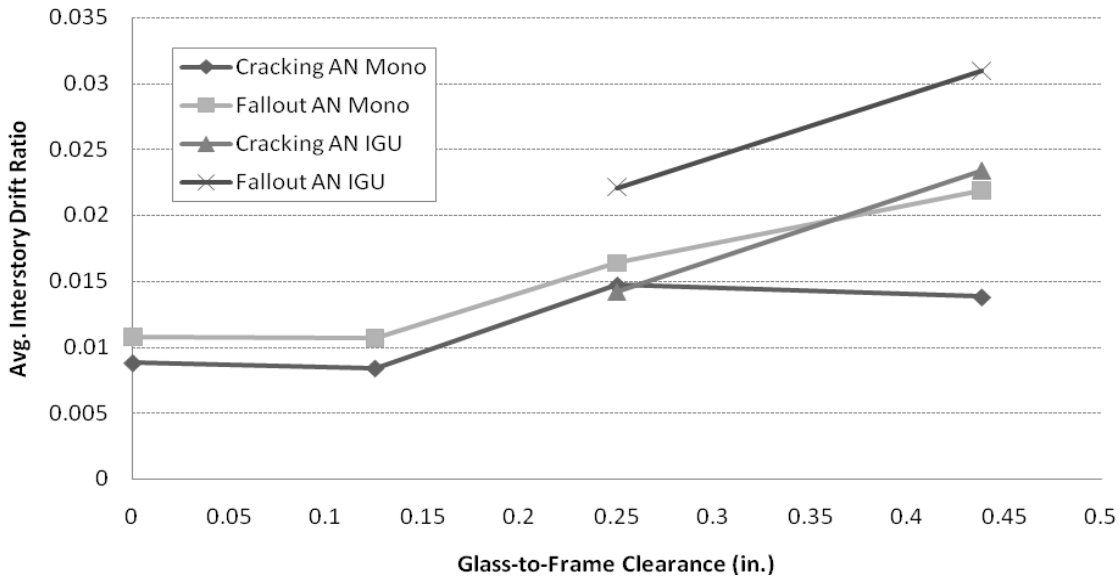

Figure 4.7: Comparison of cracking and fallout damage states for AN-Mono and AN-IGU configurations with 0 in. (0 mm), 0.125 in. (3 mm), 0.25 in. (6 mm), and 0.43 in. (13 mm) glass-to-frame clearances

Viewing slots that were milled in the corners of the framing (shown in Figure **4.8**) allowed observance of a glass behavior phenomenon that has been attributed to increasing the failure capacity of glass configurations with especially low clearances. Gasket pressure plates that are attached to the glass framing normally cover the edges of glass panels. However, the viewing slots allowed inspection of the conditions of the glass corner regions of specimens throughout the experiments. As an example of panels with greater than expected experimental capacity, the cracking and fallout values for the

glass configuration with a 0 in. (0 mm) clearance are slightly greater than for the similar configuration with a 0.13 in. (3 mm) clearance, which seems counterintuitive. However, during testing it was witnessed through the viewing slots that without a gap between the glass corners and aluminum framing for the configuration with a 0 in. (0 mm) clearance, the common occurrence of impact between the glass corners and framing corners from horizontal racking displacements did not take place. Instead, the glass corners gradually chipped and then crushed as the loading steps increased. The consequence was a gradual natural glass corner rounding action as shown in Figure **4.9**, which depicts the progressive corner rounding behavior in documented photographs. For clarity, illustrative representations of the corner conditions of the glass specimens are shown in Figure **4.10**.

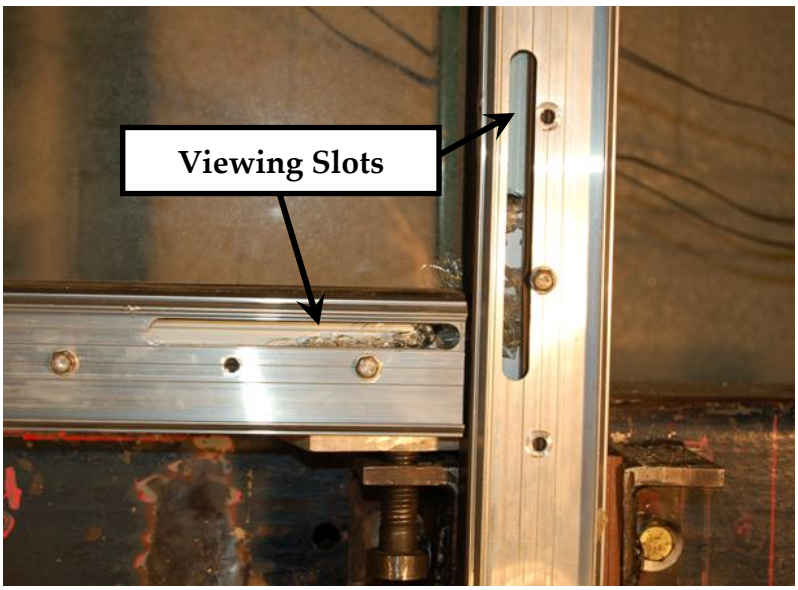

Figure 4.8: Depiction of viewing slots milled into the gasket pressure plates to allow observation of corner regions of glass panels during testing

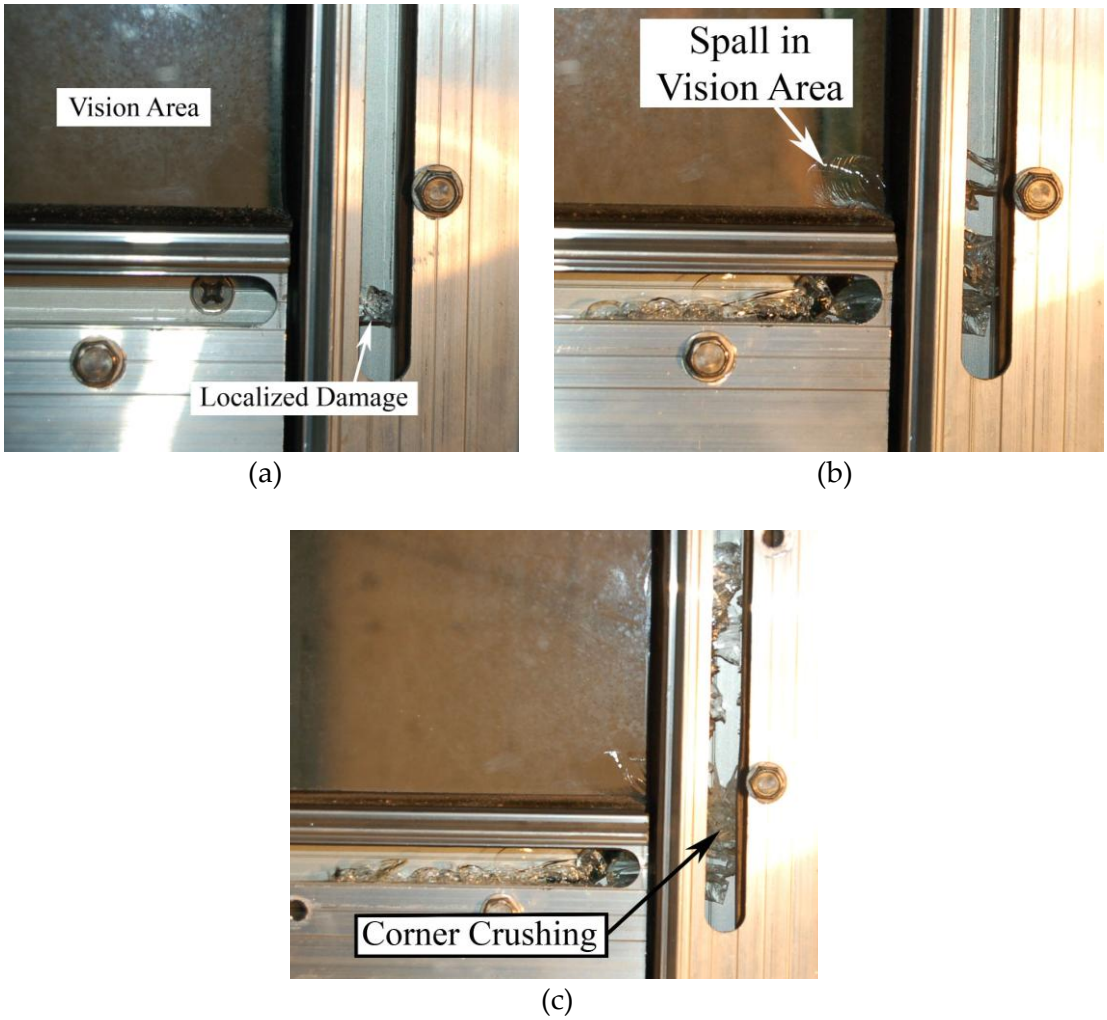

Figure 4.9: Pictures (a), (b), and (c) depict the natural rounding corner action of the glass corners observed during increasing loading steps

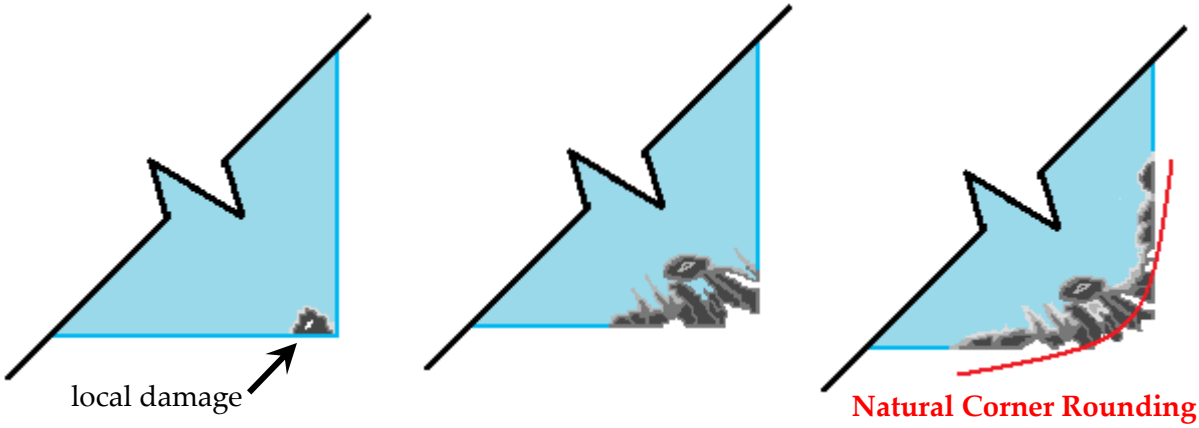

Figure 4.10: Illustration of the progression of natural corner rounding action for pictures (a), (b), and (c) as seen in Figure

The degree to which natural corner rounding action impacts failure capacity, and how the influence changes over increasing clearances is unknown. Specifically, natural corner rounding is seen to significantly increase the fallout capacity of glass configurations with 0 in. (0 mm) clearances. As for the initial cracking and crushing limit state of the same configuration, the natural rounding action increased the capacity to some degree because small amounts of chipping and localized damage did not constitute as reaching the cracking and crushing failure. For configurations with clearances greater than 0 in. (0 mm), natural corner rounding action most likely increased the failure values by some unknown magnitude. The effect of natural corner rounding action likely diminishes as the clearances increase.

4.3 Summary and Conclusions

To improve the accuracy of the data, sensor testing was performed on the racking facility and showed that flexibilities were present in the BERL dynamic racking test facility. An analysis of displacements measured by linear potentiometers on the upper and lower steel tubes of the racking facility showed that the upper steel tube was not translating as far as the lower tube due to flexibility in the fulcrum arm mechanism of the facility (see Figure 4.2). This flexibility combined with another minor flexibility between the actuator and the lower steel tube led to a reduced displacement experienced by the glass specimens. Overall, the actual displacements were 23.3% less than the expected displacements as measured at the actuator.

The flexibilities were significant enough to warrant adjustment of applicable past experimental data. A statistical regression analysis found a very high correlation between the actual and expected displacements of all loading steps among the varying glass specimens that received sensor testing. Therefore, the linear nature of the flexibilities proved that the reduced displacements were consistent, and resulted in adjusting the failure data according to the linear equations (see Equations 4.1 and 4.2). The glass SF configurations (7-9) as listed in Table 3.1 did not receive an adjustment because these specimens were tested three at a time as opposed to individually as CW configurations, and therefore the extent of the facility flexibility (if one was present) is unknown.

Overall, the experimental failure data for CW systems received an average reduction of 17.6% from Equations 4.1 and 4.2, which represents the effect of test facility flexibility on the actual glass specimen displacements when failure occurred. These corrections were important in reducing the unconservative error in failure data values from previous studies due to frame flexibility. Specifically, the cracking failure values and fallout failure values for the CW specimens were reduced by an average of 21.0% and 14.2%, respectively. These average reductions differed because the flexibility in the facility had a greater effect (in terms of percent difference) on the lower displacement loading steps as compared to subsequent loading steps with greater displacements. Since the fallout drifts were equal to or greater than the cracking failure drifts for glass specimens, the needed adjustment for fallout data due to facility flexibility was not as high as compared with the cracking data. Of course, the required adjustment for any given drift from any load step interval was consistent for all failure values, whether the damage state was cracking or fallout.

In this chapter, it was also confirmed through new testing of glass configurations with various substandard glass-to-frame clearances that the dimension of the clearance is critical to the failure capacity of a glass panel, as seen in Figure 4.7. It was generally found that the failure values decreased as the clearance of a configuration lessened. However, the failure values were greater than expected for configurations with the lowest substandard clearances due to an observed natural corner rounding action as depicted in Figures 4.9 and 4.10.

The natural corner rounding action phenomenon observed through viewing slots during testing of low glass-to-frame clearance specimens is characterized by a slow progression of chipping, spalling, and eventually crushing in the corner regions of glass panels. The slow degradation process occurs because the low glass-to-frame clearance eliminates the distance a glass panel has available to impact the metal framing, thus reducing the force of impact as compared with glass configurations with more standard 0.43 in. (11 mm) clearances. This condition is highlighted by glass configuration (10) with a clearance of 0 in. (0 mm) which had cracking and fallout failure drifts nearly the same as the similar glass configuration (11) with a 0.13 in. (3 mm) clearance. The effect of natural corner rounding action on failure values most likely diminishes as a clearance increases.

Chapter 5

Analytical Development of Fragility Functions

In this chapter fragility functions are developed, and fragility curve modification procedures are presented for glass systems with different glazing features. Section 5.1 defines the three identified damage limit states used for fragility development, Section 5.2 examines the data adjustments performed to prepare the data for fragility analysis, Section 5.3 details the acquisition of gasket degradation data from past studies, Section 5.4 examines the development of the fragility functions, and Section 5.5 lays out the developed fragility modification procedures. Section 5.6 details a summary and conclusions reached from the research carried out in this chapter.

5.1 Failure Limit States

Three glazing system damage limit states are defined for fragility development, the first of which is the onset of glass cracking. This damage is characterized by initial glass crushing or through-thickness panel cracking in the vision or non-vision area. Figure **5.1** depicts an example of a glass panel that has experienced a through-thickness crack in the vision area, which originated from corner crushing and cracking. Initial glass cracking and crushing is considered a serviceability failure, which will likely

require glass replacement, but does not compromise life safety. However, cracking and crushing do result in a breach of the building envelope, which could lead to air leakage, water infiltration, and other indirect damages that could impose high costs to building owners and occupants.

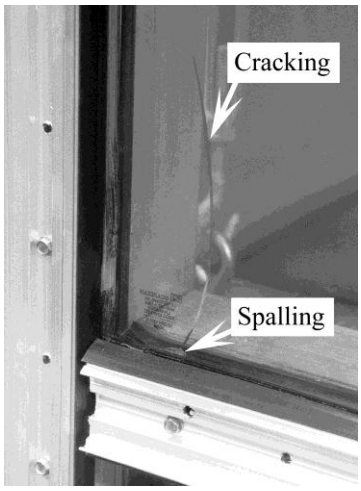

Figure 5.1: An example of a through-thickness crack in a glass panel (Memari et al. 2003)

The second glazing system damage limit state that has been identified for fragility development is glass fallout. This failure is defined in AAMA 501.6 (AAMA 2001) as being reached as the in-plane drift demand that causes a fragment of glass larger than 1 in.^{2} (645 mm^2) to break away from a glass panel and physically fall off. Glass fallout is considered an ultimate type failure because it poses a potential life safety hazard. Furthermore, similar to the cracking damage, there are many negative indirect economic consequences that result from a breached building envelope. Also, major fallout can make a building nonfunctional while posing security issues at the same time.

The third and last damage limit state recognized for fragility development is degradation of the glazing system perimeter gasket seal. There are four different ways that a gasket can be damaged and failure reached: (1) distortion, which is distinguished by a twisted or bulged gasket; (2) pull-out, which is defined by a gasket that has been entirely pulled out of a glazing pocket; (3) push-in, which is characterized by a portion of gasket that has been pushed into a glazing pocket; and (4) shifting, which is defined by a section of gasket that has longitudinally translated along the pocket and has left an unsealed gap. (Behr et al. 1995) Gasket degradation is considered a serviceability type damage state because it does not pose any life safety risks, but allows the possibility of air and water infiltration following the failure leading to indirect economic losses.

5.2 Failure Limit State Data Adjustments

5.2.1 Redefining Cracking Limit State

Previous experiments defined the cracking limit state as when the first through-thickness crack in a glass panel was observed specifically in the vision area of the specimen (Behr and Belarbi 1996, Behr 1998, Memari et al. 2003). The vision area of the glass is considered the area of the panel that can be seen once the glass is installed within the framing, and does not include the edge areas of the glass covered by gaskets and pressure plates. However, a following study (Memari 2006a) which tracked the

origin of through-thickness vision cracks in glass by the use of viewing slots (an example as shown in Figure 4.8) found that glass crushing was occurring in the corner regions of the glass panel before the observed cracking. Furthermore, sometimes cracks formed in the non-vision areas at earlier drifts than the vision cracks. As a result of this finding, it was deemed appropriate to reduce the previous cracking data to ensure that the fragility functions are based from conservative cracking failure data. The redefined limit state is defined as the onset of glass vision cracking as characterized by initial glass corner crushing or through-thickness cracks.

The mechanism used to properly adjust the previous cracking failure values involved evaluating recorded "load vs. time" charts, that are available each loading step of each tested specimen. These charts were useful because when a glass specimen experiences cracking or crushing during testing, the load being measured fluctuates in a way which can be identified. As an example, Figure **5.2** compares two load vs. time charts of subsequent load steps for a glass specimen. The first graph (a) is an example of a step where no failure occurred, while the second graph (b) depicts evidence of cracking and crushing that subsequently occurred in the next load step. This evidence is characterized by fluctuating measured loads or apparent spikes in the load measurements.

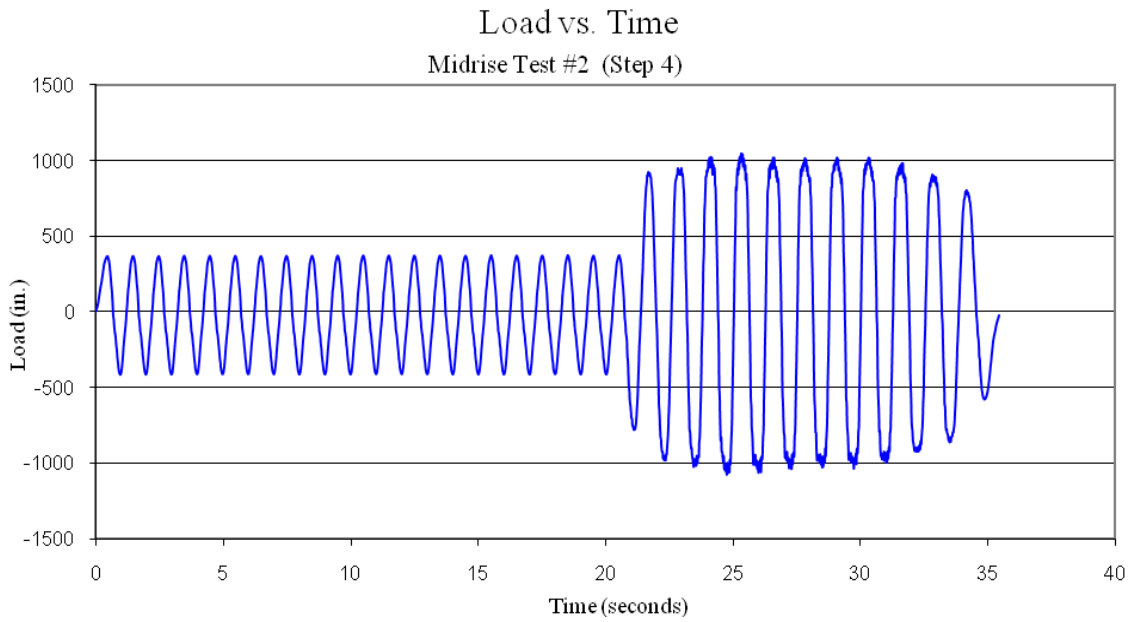

(a)

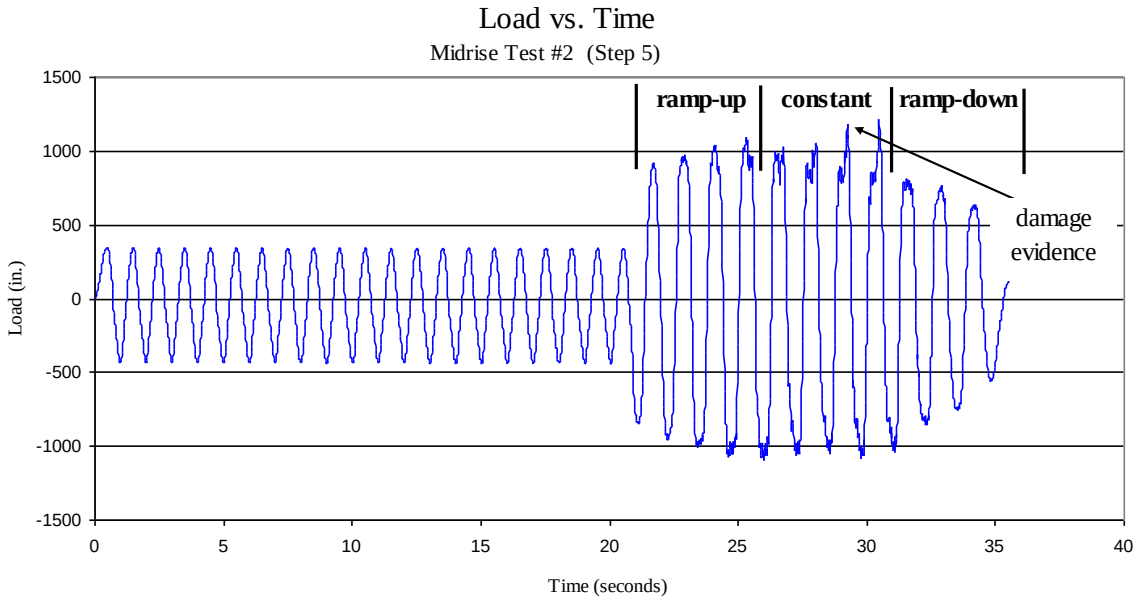

(b)

Figure 5.2: Comparison of load vs. time charts from subsequent loads step for a glass specimen where (a) has no failure evidence but (b) depicts initial cracking/crushing

The adjustment reduced the average cracking failure values overall, but not to an extent that remarkably modified the initially observed experimental cracking capacity. Approximately 12.5% of glass specimens with cracking failure data (does not include glass configurations (23) and (24)) received a data adjustment of this kind. The average cracking failure decreased from a drift of 2.76 in. (70 mm) to 2.72 in. (69 mm), an overall reduction of about 1.5%. There was no trend in the glass specimens that received a data adjustment, but rather the data were affected in an apparent random manner. It should be noted that this adjustment was applied to the failure data before any adjustments for facility flexibility. Also, the data for the SF configurations were not adjusted due to lack of load vs. time charts. Furthermore, HS and FT glass type configurations did not receive any data adjustment due to the more sudden nature of failure behavior of HS and FT glass. These glass types do not gradually crush and crack as AN glass does; rather, sometimes HS and especially FT glass quickly cracks in a dice pattern, which negates a need for the adjustment.

5.2.2 Load Interval Failure Check

In consideration of the step-wise loading nature of glass specimens in increasing 0.25 in. (6 mm) intervals, there is a possibility that a glass panel's failure capacity is between the intervals. To address this issue, and in the process further ensure the conservatism of the data for fragility development, load vs. time charts were analyzed again in another manner. The charts were checked for each specimen to see whether a

damage state might have been reached during the "ramp-up" interval of a loading step, or before the "constant" interval of a load step that contains the maximum displacement amplitudes (see Figure 2.9). If a failure is reached in the "ramp-up" interval, then the actual drift that a specimen failed at is less than step-wise interval. In these cases, the recorded failure drifts are replaced with the actual reduced failure values. As an example, Figure **5.3** shows a load vs. time chart of a loading step of a specimen that experienced fallout on the "ramp-up" interval, and as a result the failure drift was adjusted.

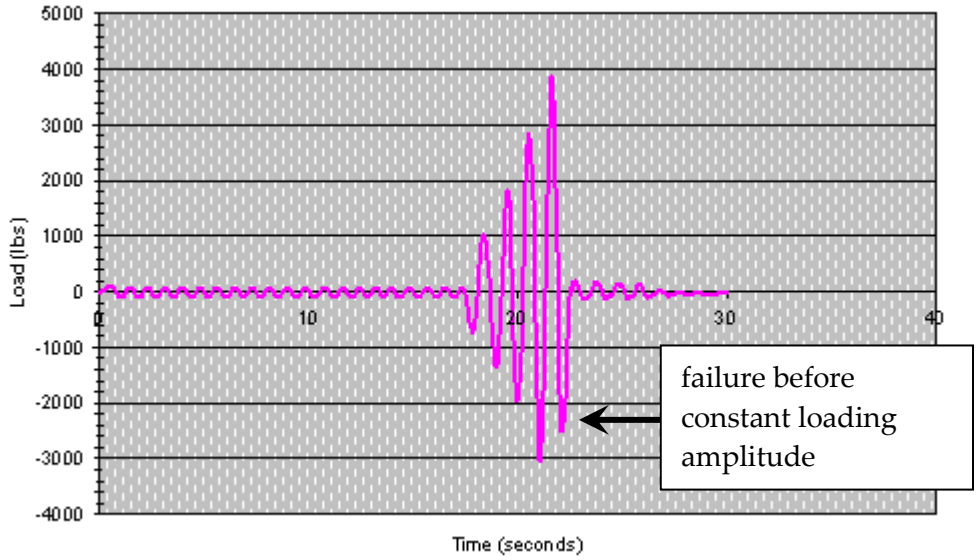

Figure 5.3: A load vs. time chart for a specimen that experienced fallout on the "ramp-up" loading interval

In all, fourteen specimens out of around 175 specimens received adjustments of this type. Consequently, the overall impact of the adjustment was minimal, where the failure data was reduced by 0.5%. The most impacted glazing type was FT-Mono, or

glass configuration (21) as listed in Table 3.1, where the failure values for five of the six specimens tested for that configuration were adjusted.

5.3 Gasket Damage Limit State Data Acquisition

The gasket damage limit state was not recorded and collected during the experimental testing like the other limit states. However, testing video footage supplemented with recorded notes was used to extract gasket degradation failure data. The combination of these two resources were available for glass configurations (3-5) and (7-9). The video analysis consisted of reviewing the loading steps, and visually identifying when one of the four possible gasket failure modes has been reached. For some of the specimens, none of the gasket failure options were seen before glass cracking occurred. In these instances, the cracking drift value was used as the gasket failure value as well, because at this point glass shards tear apart the rubber gaskets. This action leads to gasket degradation and would require gasket replacement. A summary of the gasket failure data collected can be found in Appendix A.1.

5.4 Fragility Functions

Fragility functions were developed for all twenty-four of the CW and SF configurations as a way to provide a tool to calculate the probable loss associated with the exterior glass systems according to the three defined damage states. To prepare the data for fragility analysis, the failure data values that were in the form of drifts in inches (and millimeters) were converted into drift ratios as defined by Equation 3.1. This task involved dividing the drifts by the height over which the displacement occurred. In the case of the experimental studies, the height over displacement equals the height of the glass panel in addition to 9 in. (229 mm), which was the vertical distance between the glass and anchors. For example, for 6 ft x 5 ft (1.5 m x 1.8 m) glass specimens, the failure displacements were divided by 6 ft (1.5 m) plus 9 in. (229 mm), or 81 in. (2057 mm). The converted drift ratio values can be seen in Appendix A.1.

Then, the *Fragility Function Calculator version 1.02* software provided by the ATC for use in the ATC-58 Project was used to calculate the two primary parameters, θ and β_r, which define the curve of each fragility function (see Equation 2.6). Figure 3.2 illustrates the input screen that is used by the software. Besides the failure data, information about each glass configuration and failure limit state for a fragility function was compiled, of which the subjects included: Component ID, Component Description, Describe Specimen, Describe Excitation, Demand Parameter, Damage Evidence, and Damage Measure, as organized in Appendix A.2. Furthermore, when the failure data was input into the software, the correct analysis method had to be selected as a function of the

failure characteristics of the data. For all but three fragility functions, the type "A" analysis method termed "Actual Demand Data" was used, which represents a data set where all of the specimens of a particular limit state experienced failure. The other three fragilities used the type "B" analysis method termed "Bounding Demand Data," which represents a data set where some of the specimens tested did not experience failure.

The software analysis of a data set returns an output of various parameters. The variable M denotes the total number of test specimens involved, θ denotes the median interstory drift ratio value or expected damage limit state capacity, β_r denotes the random dispersion value, and a statement of whether the fragility function passes the Lilliefor's goodness-of-fit test at the 5% significance level for a lognormal distribution. An example of the output software frame from the cracking limit state data of glass configuration (2) can be found in Figure **5.4**, and the outputs for all glass configurations can be referenced in Appendix A.3.

With the random dispersion (β_r) value calculated, the next step involved determining the dispersion (β) values so that fragility curves could be developed. As reviewed in Section 2.5.2.1, β is a measure of uncertainty in the demand values, and is found by calculating the square root of the squares of variables β_r and β_u (see Equation 2.7). The random dispersion value β_r is statistically calculated from the failure data values, while β_u takes on value determined by experimental conditions. For this research, β_u equals 0.25 according to the ATC-58 Guidelines (ATC 2005) because the following conditions were met: (1) for an actual building in the field, the CW or SF could

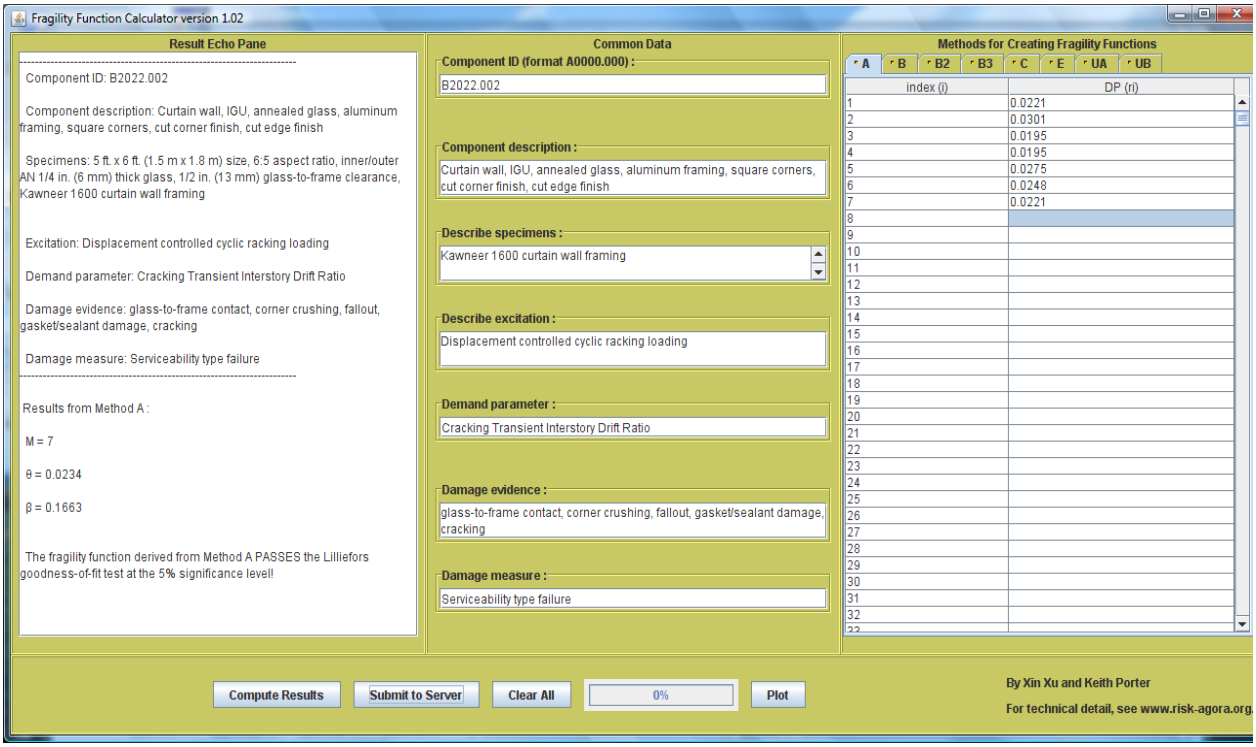

Figure 5.4: An example of an output screen for the *Fragility Function Calculator version 1.02*

be installed in a number of ways; however, all test specimens were racked on the facility with the same anchoring setup; and (2) all specimens received the same loading protocol. Subsequently, a dispersion value was calculated for each fragility using Equation **5.1** :

$$\beta = \sqrt{\beta_r^2 + 0.25^2} \qquad \textbf{5.1}$$

where the variables were denoted previously. For comparison purposes, the median interstory drift ratio (θ) and dispersion value (β) that defines each fragility function are summarized in Table **5.1.**

Table 5.1: Summary of median drift ratio and dispersion values for the gasket, cracking, and fallout limit states of each glass configuration

	Gasket		*Cracking*		*Fallout*	
ID	Θ	β	Θ	β	Θ	β
1			0.0138	0.262	0.0219	0.315
2			0.0234	0.300	0.0310	0.295
3	0.0270	0.320	0.0276	0.298	0.0303	0.290
4	0.0262	0.317	0.0266	0.322	0.0299	0.346
5	0.0260	0.272	0.0268	0.289	0.0339	0.268
6			0.0156	0.343	0.0561	0.311
7	0.0303	0.492	0.0413	0.284	0.0510	0.290
8	0.0423	0.303	0.0590	0.258	0.0665	0.253
9	0.0290	0.514	0.0567	0.289	0.0800	0.990
10			0.0088	0.252	0.0108	0.251
11			0.0084	0.261	0.0107	0.359
12			0.0147	0.252	0.0164	0.262
13			0.0142	0.250	0.0221	0.250
14			0.0181	0.262	0.0212	0.250
15			0.0220	0.277	0.0257	0.271
16			0.0239	0.236	0.0248	0.279
17			0.0263	0.298	0.0267	0.297
18			0.0219	0.288	0.0300	0.990
19			0.0260	0.272	0.0337	0.274
20			0.0281	0.325	0.0324	0.268
21			0.0236	0.377	0.0236	0.377
22					0.0492	0.265
23					0.0631	0.293
24			0.0331	0.273	0.0346	0.284

After the parameters of a fragility function were calculated, the curves were plotted using Excel software. A detailed discussion on how to plot a fragility curve using the Excel software is found in the *Guidelines for Seismic Performance Assessment of Buildings 35% Draft* (ATC 2005). An example of a plotted fragility curve for the cracking

damage state of glass configuration (2) can be seen in Figure **5.5.** The plots of the fragility functions for all glass configurations and limit states can be seen in Appendix A.4.

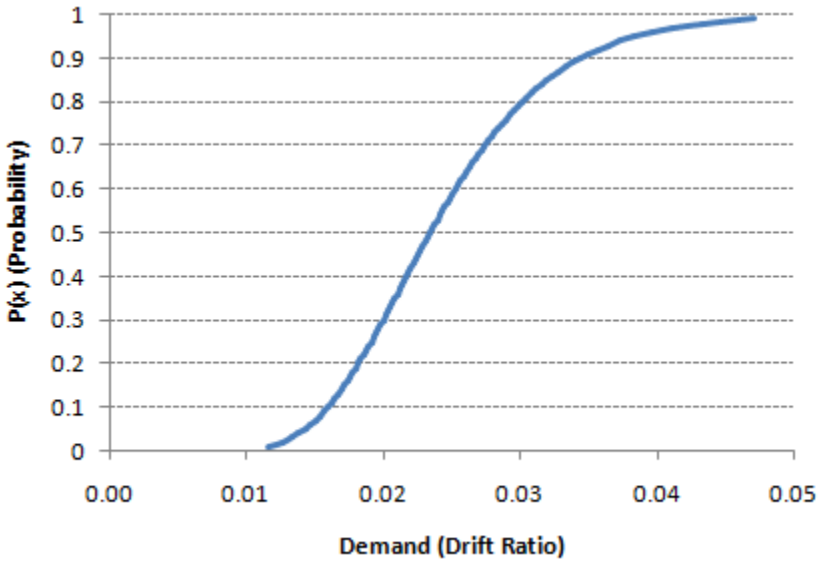

Figure 5.5: An example of a plotted fragility curve for the cracking damage state of glass configuration (2)

5.5 Fragility Modification Procedures

The fragility functions and related fragility data presented in Section 5.1.4 can be used directly if the glass system under consideration has the same glazing details and characteristics, which include framing detailing, glass-to-frame clearance, system type, configuration type, glass type, glass panel dimensions, glass panel thickness, and glazing (dry vs. wet) type. Otherwise, procedures are offered for users to modify the

developed fragilities in this report to reflect their unique glass configuration details. If a given glass panel has a height that differs from the height of a glass panel for which a fragility function was developed for, then an adjustment is needed for the fragility drift ratio demand values through the use of a modification multiplier so that the drift ratio values reflect the dimensions of the considered glass panel. Furthermore, fragility modification methods are given for glass configurations that vary in framing, glass-to-frame clearance, and aspect ratio characteristics as compared to the laboratory specimens upon which the fragility functions were based.

5.5.1 Glass Panel Dimensions

Two hypothetical glass panels with similar system configuration details including aspect ratios but different panel dimensions will have different seismic failure capacities, at least in terms of drift ratio (θ). This condition is true because ultimately the glass-to-frame clearance and aspect ratio determines the maximum displacement drift (δ) that a glass panel can withstand before failing. While varying glazing details such as glass type alters the damage capacity as well, two panels which both have the same configuration details such as the ones mentioned previously will have their drift capacity altered to the same degree. As a result, in this scenario the two glass panels will have the same drift displacement capacity, a condition that is supported by the new closed-form equation developed in Chapter 6 that would calculate the same drift

capacity ($\Delta_{failure}$) for both glass panels. However, when this drift capacity is converted in terms of interstory drift ratio, the glass panel that has a smaller height will have a greater drift ratio capacity than the larger glass panel. This is due to the fact that the drift failure value for smaller glass panel is equivalent to the failure value of the larger glass panel, but is divided by a height that is smaller in value when the drift is converted into drift ratio.

This principle is supported by the following example. Consider glass panel (1) and glass panel (2), as shown in Figure **5.6.** It is assumed that both are mid-rise CW systems with comparable Kawneer 1600™ framing, have an AN-Mono glass configuration, a 6:5 glass aspect ratio, and a glass-to-frame clearance of x in. (x·25.4 mm). Furthermore, it is assumed that glass panel (1) has a height (h_1) and width ($b1$) that is less than the height (h_2) and width (b_2) of glass panel (2).

To begin, the following relationships are known where (1) is defined from Equation 3.1 and (2) is determined from the known information in Figure 5.6:

$$(1) \quad Drift\ Ratio = \theta = \frac{\delta}{h} \qquad (2) \quad \frac{h_1}{b_1} = \frac{h_2}{b_2} = 1.2$$

To find the drift ratio cracking capacity (θ_{crack}) of either glass panel, first the cracking capacity in terms of drift (Δ_{crack}) is found using the code ASCE 7-05 equation (ASCE 2005, see Equation 2.3).

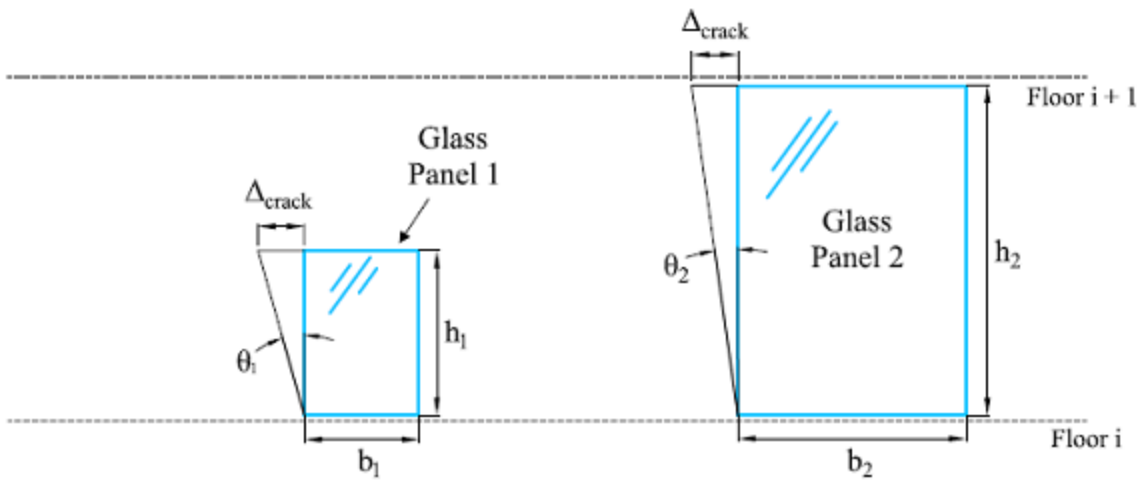

Clearance:	x	x
Glass Type:	AN	AN
Configuration Type:	Mono	Mono
Aspect Ratio:	6:5	6:5
System:	CW	CW

Figure 5.6: Assumed characteristics of glass panel (1) and glass panel (2)

So,

$$\Delta^1_{crack} = 2x\left(1 + \frac{6x}{5x}\right) = 4.4x$$

$$\Delta^2_{crack} = 2x\left(1 + \frac{6x}{5x}\right) = 4.4x$$

$$\therefore\ \Delta^1_{crack} = \Delta^2_{crack} = 4.4x$$

Using the ASCE equation, it is found that glass panel (1) and glass panel (2) each have the same predicted cracking capacity in terms of displacement drift. To find the capacity of each glass panel in terms of drift ratio, the drift capacity values are applied to

the drift ratio definition (see known (1) stated previously) for each glass panel as follows:

$$\theta^1_{crack} = \frac{\Delta^1_{crack}}{h_1} = \frac{4.4x}{h_1} \qquad \theta^2_{crack} = \frac{\Delta^2_{crack}}{h_2} = \frac{4.4x}{h_2}$$

However, it is known that:

$$h_1 < h_2$$

$$\therefore \ \theta^1_{crack} > \theta^2_{crack}$$

With the knowledge that the dimensions of a glass panel have a direct effect on its capacity in terms of drift ratio, it can be subsequently deduced that the developed fragilities only reflect the capacity of glass panels that have similar dimensions as the glass configurations that each fragility represents. Otherwise, if a user's glass panel is smaller than the glass panel that a fragility function was developed for, the fragility needs to be modified to reflect the increased drift ratio capacity that the smaller panel has. The same is true for larger glass panels, except that the fragility needs to be adjusted to reflect the decreased glass drift ratio capacity. Therefore, a method has been developed so that a user can adjust the drift ratio values of a fragility function to reflect the capacity of a glass panel that has different dimensions than those listed in Appendix A.1. It should be noted that while this method applies to glass panels, which have different dimensions, the same aspect ratio is assumed to be the same as the glass

configuration of the fragility. If the aspect ratio varies as well, then further fragility adjustments will be needed as suggested by methods in Section 5.1.5.4.

The method for modifying a fragility for a glass panel with different dimensions is simple; a user multiplies the median value of demand (θ) of the original fragility by a derived modification factor (r) to create a new median demand value that is representative of the user glass panel capacity. For the derivation of the r factor, consider two glass panels shown in Figure **5.7**, a user glass panel (x) and a similar glass panel (*exp.*) which represents any given glass configuration listed in Table 3.1 that was experimentally researched. It is assumed that both systems have comparable framing, have similar glass configuration and glass types, the same aspect ratio, and the same glass-to-frame clearance. However, it is also assumed that glass panel (x) has a height (h_x) and width (b_x) that is not equivalent to the height (h_{exp}) and width (b_{exp}) of the experimental glass panel.

To begin, the following relationships are known where (1) and (2) are based on the given information previously, and (3) is based on the derivation previously (see Figure 5.6) since the two panels have similar clearances, aspect ratios, and all other glazing characteristics besides similar glass dimensions.

$$(1) \quad h_x \neq h_{exp} \qquad (2) \quad \frac{h_x}{b_x} = \frac{h_{exp}}{b_{exp}} \qquad (3) \quad \Delta_{failure}^{capacity} = \delta_x = \delta_{exp}$$

where for known (3) the variable $\Delta_{failure}$ denotes the drift that causes failure for a glass panel, δ_x the failure capacity of a given user glass panel x, and δ_{exp} the failure capacity of an experimentally tested glass configuration.

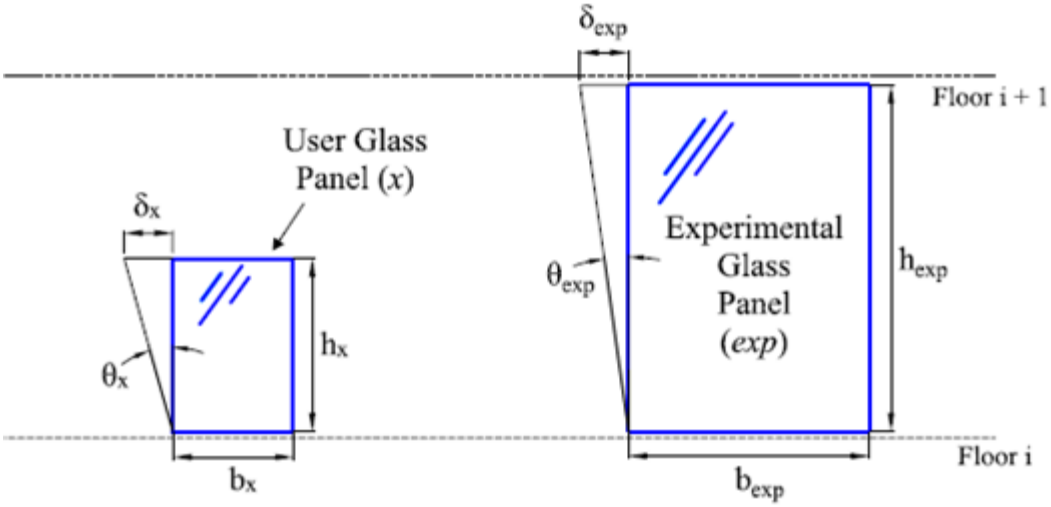

Figure 5.7: Assumed characteristics of the user glass panel (x) and considered experimental glass panel (exp)

Now, let us define the drift ratio capacity (θ) for each glass panel:

$$\theta_x = \frac{\delta_x}{h_x} = \frac{\Delta_{failure}^{capacity}}{h_x} \qquad \theta_{exp} = \frac{\delta_{exp}}{h_{exp}} = \frac{\Delta_{failure}^{capacity}}{h_{exp}}$$

,

It is desired to relate θ_x with θ_{exp}. With the knowledge of known (1), the following is true:

$$\theta_x \neq \theta_{exp}$$

Therefore, let us define the following relationship between the heights of the glass panels with Equation **5.2**:

$$r = \frac{h_{exp}}{h_x} \qquad \textbf{5.2}$$

where r denotes a ratio value relating the heights of a user panel (x) and an experimental panel (exp), and h_x and h_{exp} were denoted previously.

So, rearranging Equation 5.2 we have:

$$h_x = \frac{h_{exp}}{r}$$

Then,

$$\theta_x = \frac{\delta_x}{h_x} = \frac{\Delta_{failure}^{capacity}}{\frac{h_{exp}}{r}} = \left(\frac{\Delta_{failure}^{capacity}}{h_{exp}}\right) \cdot r = \theta_{exp} \cdot r$$

$$\therefore \quad \theta_x = \theta_{exp} \cdot r$$

With the r factor derived in the previous example, it can then be defined in terms for general use. As stated previously, to alter a fragility curve so that the predicted performance of a given glass panel is modified to account for different glass dimensions the r factors needs to be applied to the median value of demand (θ). Equation **5.3** defines the calculation to be used by a user to modify the median value of demand:

$$\theta_i = \theta_j \cdot r \qquad \textbf{5.3}$$

where θ_i denotes the median value of demand for the user glass panel, θ_j denotes the median value of demand of the fragility to be modified, and r denotes the modification factor values as defined by Equation **5.4**:

$$r = \frac{h_j}{h_i} \qquad \textbf{5.4}$$

where h_j denotes the height of the glass panel of the glass configuration that the fragility represents and h_i denotes the height of the user glass panel. With the new median value of demand θ, a user can develop a new fragility function through the use of the Performance Assessment Calculation Tool (PACT) assuming the dispersion value β has not changed. The *Guidelines for Seismic Performance Assessment of Buildings* (ATC 2005) details how a user can input a new fragility function into the PACT software.

As an example of the application of this modification method, assume that a user has a glass panel 4 ft high by 3.33 ft wide (1.2 m x 1.0 m) and desires a cracking failure state fragility function for a building analysis. The glass panel is a 0.25 in. (6 mm) AN-Mono, has a 0.43 in. (11 mm) glass-to-frame clearance, dry-glazed, and has mid-rise CW Kawneer 1600™ framing. It has the same glazing and configuration characteristics as glass configuration (1) for this report, except that the glass dimensions are different (but the 6:5 aspect ratio is the same). To modify the fragility of glass configuration (1), Equations 5.2 and 5.3 are used to find a new median value of demand for the user glass panel as follows:

$$r = \frac{6\ ft}{4\ ft} = 1.5$$

$$\theta_i = \theta_j \cdot r = (0.0138)(1.5) = 0.0207$$

Using the new median value of demand and dispersion value, a fragility curve was developed with the PACT software for the user glass panel. Figure **5.8** shows a snapshot of the newly developed fragility curve in red (darker for black and white), the

curve for glass configuration (1) in yellow (lighter for black and white) for comparison purposes, and the input data below the plots.

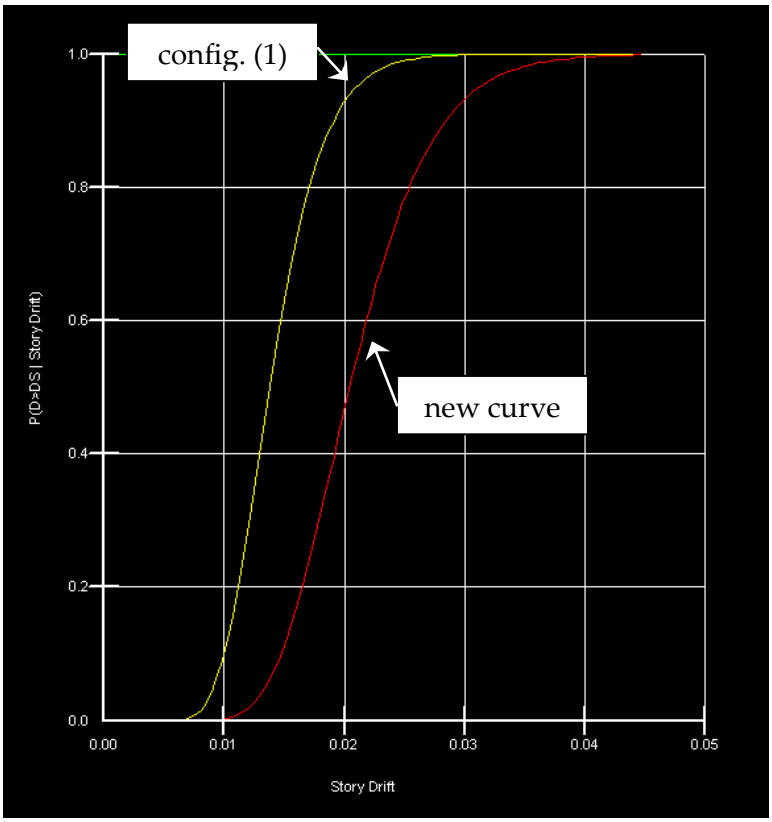

	Description	Median	β		
DS-1	Glass Configuraion (1) - 6ft x 5ft	0.0138	0.262	Edit	Delete
DS-2	User Glass Panel - 4ft x 3.33ft	0.0207	0.262	Edit	Delete

Figure 5.8: Fragility curves plotted using PACT for glass configuration (1) (yellow) and the user glass panel (red)

5.5.2 Framing

There are many different framing options available on the market currently, and it is likely that properties of the framing vary from one manufacturer to the next. The

glass CW configurations in the laboratory were tested with the Kawneer 1600™ Curtain Wall system and the SF configurations were tested with the Kawneer TriFab II® 451 Storefront system. While some framing types manufactured by other companies can be similar the Kawneer framing systems used experimentally, the details that could differ include the width, depth, and gasket detailing (dry vs. wet), while combined with varying structural properties including moment of inertia could possibly affect the racking seismic response of the system.

An analysis was performed to determine the effect of a varying framing system. First of all, it was determined that the physical factors of a framing system that would have the greatest effect on the seismic behavior of a glass system are width, area, and moment of inertia of the mullions. Then, a comparison was made between two glass configurations that have all of the same details except a framing system which varies in width, area, and moment of inertia as illustrated in Figure **5.9**. In the first depiction (a) the two glass systems are shown at rest, where the framing system of glass configuration Type 1 has cross-section properties of area = A, width = W, and moment of inertia = I, while glass configuration Type 2 has framing cross-sectional properties of area = 0.75A, width = 0.6W, and moment of inertia = 0.33I. In the second illustration, a lateral load is applied to the top transoms (horizontal) of each configuration. It was determined that even though the flexural stiffness will differ between the framing systems, the displacement Δ resulting from the lateral loading will be nearly the same for Type 1 and Type 2. This is due to the fact that the structural stiffness of a building is much greater

than that of any framing stiffness, and therefore as long as the connection types and the mullions are continuous the two different configurations will displace the same amount.

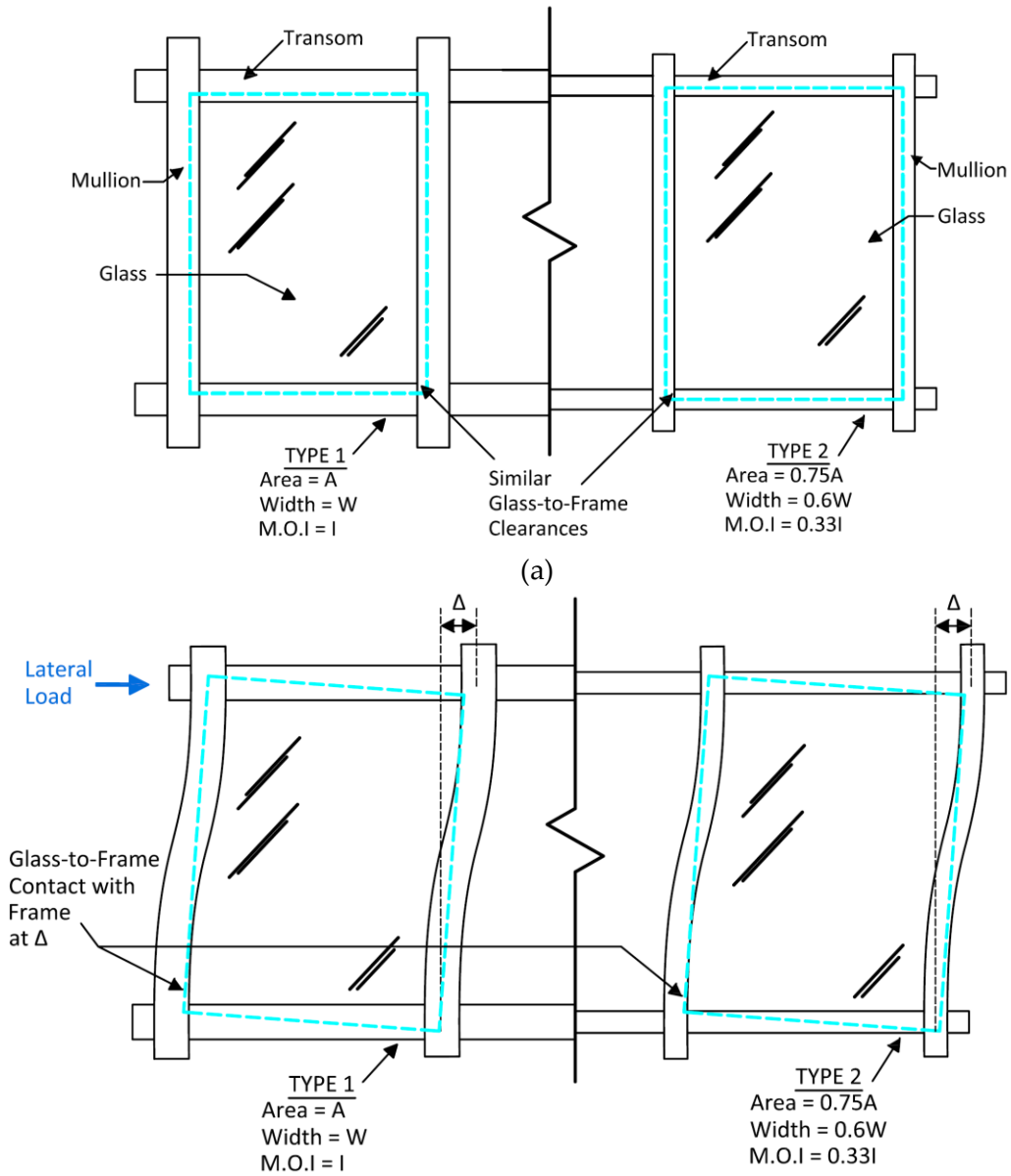

Figure 5.9: Comparison of two glass configurations with different framing system properties at rest (a) and after a lateral load is applied (b)

As a result of the conclusion that differences in the framing system from one manufacturer to the next will not have an impact on the seismic response displacement of glass configurations, these fragilities can be applied to glass configurations that have a different framing manufacturer than Kawneer. It is noted that other framing detail characteristics determined by designers such as glass-to-frame clearances have an important effect. Furthermore, while it is concluded that the varying manufacturer does not an effect on the seismic performance of glass, the connection details of the framing system should be comparable. For example, some framing systems that are comparable to the Kawneer 1600™ are Vistawall CW-250 and YKK AP America YCW 750 OG, all three of which are compared in Figure **5.10.**

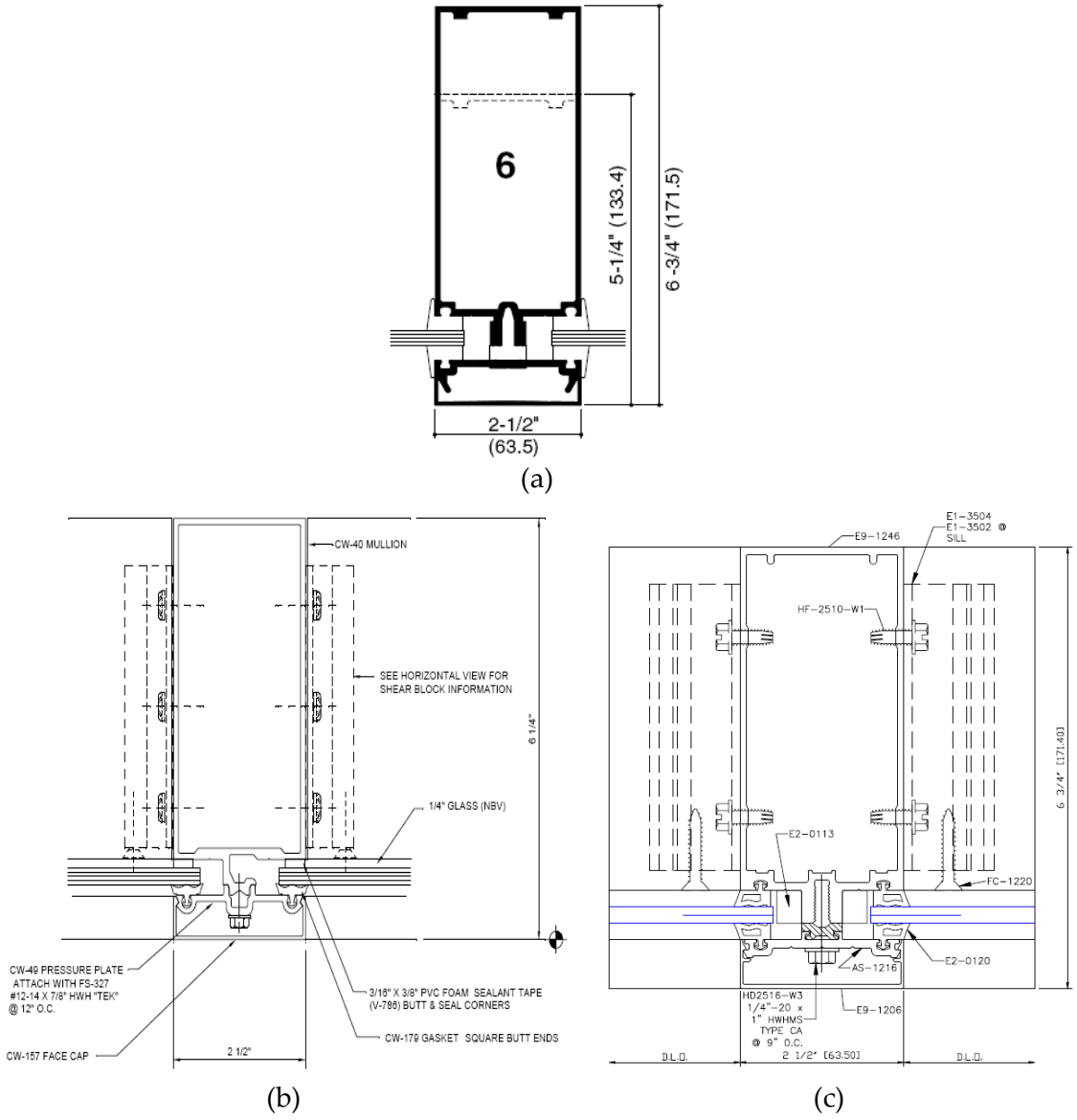

Figure 5.10: Comparison of cross-sectional details of (a) Kawneer 1600™, (b) Vistawall CW-250, and (c) YKK AP America YCW 750 OG curtain wall framing systems

5.5.3 Glass-to-Frame Clearance

It is known that a glass-to-frame clearance has an effect on the seismic behavior and capacity of glass CW and SF systems, as it was proven by the new experimental testing discussed in Section 4.2. In light of this information, users can directly apply fragility functions to their analysis if the considered glass configuration matches one of the twenty-four configurations that fragilities are provided for. Otherwise, if the considered glass configuration is similar in all other details and characteristics of one of the system listed in Table 3.1 except that the glass-to-frame clearance is different, then the following options including fragility modification procedures are offered as a solution to this condition.

One option is to use a more conservative fragility function borrowed from a glass configuration with a more conservative glass-to-frame clearance. For considered configurations with a glass-to-frame clearance larger than 0.43 in. (11 mm), a fragility function from a similar configuration with a standard clearance could be used in a conservative fashion because glass seismic capacity increases as the glass-to-frame clearance increases. For configurations with a sub-standard clearance without a fragility function available, the next conservative option could be used. For example, if a user has an AN-Mono configuration with all of the same characteristics as configuration (1) except that the clearance is 0.1875 in. (5 mm), then the fragility for AN-Mono configuration (11) with a clearance of 0.125 in. (3 mm) could be used conservatively.

A second option would involve deriving a new fragility curve for a given glass configuration from existing fragility functions of glass configurations that share characteristics of the configuration under consideration. This method is termed a "fragility mixture," and is described in the article *Assembly-Based Vulnerability of Buildings and its Uses in Seismic Performance Evaluation and Risk-Management Decision-Making* by Porter and Kiremidjian (2001). Of the two fragility mixture methods available, the one that assumes the relationship between a considered glass configuration with respect to the existing fragilities is not known will be used. Therefore, the analysis will involve a discrete uniform distribution.

The following steps need to be taken for a user to produce a new fragility using the fragility mixture method: (1) select appropriate fragility functions from the existing set available; i.e., from glass configurations listed in Table 3.1. The properly selected existing fragilities will be from configurations that share the largest number of similar details and characteristics with the CW or SF configuration under consideration. In most cases, only two existing fragilities are sufficient to derive a new fragility. Once proper curves have been identified for analysis, then: (2) the user performs a statistical "mixture" of the fragilities that results in the development of a new curve. This accomplished through the following mathematic procedure:

let N = number of existing fragility functions selected, and if

$$i = [Nu_1]$$

then Equation **5.5** produces the median demand value of the new fragility curve:

$$\theta = \sigma_i \Phi^{-1}(u_2) + \mu_1 \quad \textbf{5.5}$$

where i is the index for one of the N types of fragilities selected randomly, u_1 and u_2 are independent samples of a uniform (0,1) random variate, Φ^{-1} is the inverse of the standard normal cumulative distribution (Φ), σ_i is the standard deviation value at which damage occurred for i, μ_i is the mean intensity value at which damage was experienced for i, and θ is the calculated median value of demand at which the damage state is likely to occur (Porter and Kiremidjian 2001). The dispersion β is then determined in a similar manner as for a traditional fragility function where it is defined by Equation 2.7 and the two separate β_r and β_u components. However, β_r is found using Equation 2.9 except that the d_i values are equivalent to the median value of demand (θ) of the existing fragilities individually, and θ in Equation 2.9 is input as the median value of demand determined from Equation 5.2. An example of a fragility mixture can be reviewed in following Section 5.5.5.

The variables θ and β determined using the method outlined above are the parameters that define the newly derived fragility for a glass configuration under consideration. This process allows the fragilities that have already been developed to be applicable to a wide range of different glass configurations possible, and in this case to user configurations with glass-to-frame clearances that were not experimentally tested. Although, the degree of accuracy of the derived fragility is ultimately a function of how closely related the glass configurations from which selected existing fragilities were used are to the user glass configuration under consideration.

5.5.4 Aspect Ratio

The experimental testing of glass panels with aspect ratios of 2:1 and 1:2, which had dimensions of 8 ft x 4 ft (2.4 m x 1.2 m) and 4 ft x 8 ft (1.2 m x 2.4 m), respectively, proved that the aspect ratio has an effect on the seismic capacity of glass systems. Similar to the conditions of glass systems with varying glass-to-frame clearances, users can use the fragility functions directly if they have a glass configuration with a matching aspect ratio listed in Table 3.1. Otherwise, a user can (1) use a more conservative fragility or (2) perform a fragility mixture as outlined in the previous section to develop a new fragility that is representative of the seismic behavior of the considered glass configuration with a different aspect ratio than 2:1, 6:5, and 1:2.

If a user decides to use an existing fragility function in a conservative fashion, then the following is guidance regarding how to choose a conservative fragility properly. For the cracking limit state, among the AN-monolithic glass configurations with varying aspect ratios of 2:1, 6:5, and 1:2, the configuration with the lowest cracking capacity is the system with a 6:5 glass panel. This condition can be seen in Figure **5.11**, which contains a graph comparing the cracking and fallout experimental capacities of these configurations. As a result, using the fragility from glass configuration (1) with a 6:5 aspect ratio is considered conservative. As an example, assume a user has an AN-Mono glass system with the same details as configuration (1), except the aspect ratio of

the glass panel is 3:2. The user desires a fragility curve for the cracking limit state, except none exist for this particular configuration. Although, the user could use the cracking limit state fragility for glass configuration (1) with the knowledge that it is a slightly conservative model of the probabilistic seismic capacity of the glass configuration with a 3:2 aspect ratio.

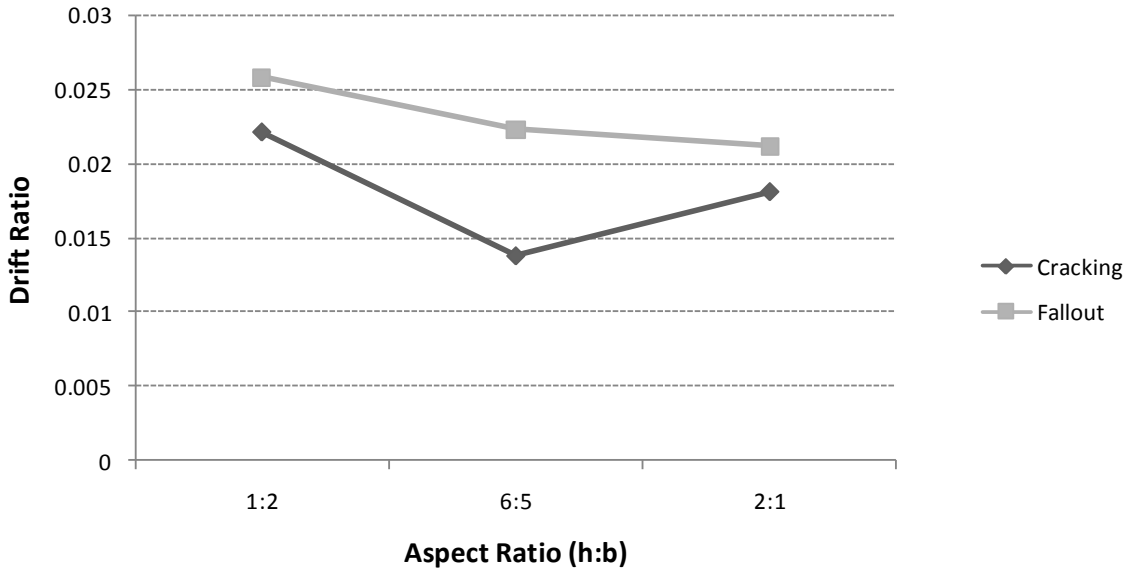

Figure 5.11: Average drift ratio capacities for the cracking and fallout limit states for the AN-Mono configurations with varying aspect ratios

The same logic can be applied to the fallout limit state for glass configurations with varying glass ratios, except that unlike the cracking limit state the fallout capacity decreases consistently as the aspect ratio decreases. Therefore, the most conservative fragility available is the curve for glass configuration (15) with a 1:2 aspect ratio. This condition is charted in Figure 5.11 as well.

The other option besides using an existing fragility conservatively is deriving a new fragility as outlined in the fragility mixture method in the previous section. An example of a fragility mixture is outlined in the following subsection.

5.5.5 Fragility Modification Example

As an example, assume that a user desires a cracking fragility function for an AN-laminated glass unit CW system with the same characteristics as configuration (6) except the dimensions of the glass panel are 6 ft high x 12 ft wide (1.8 m x 3.7 m), which results in a 1:2 aspect ratio. Unfortunately, no configuration like this has been tested, and therefore no fragility for it has been developed either. However, a new fragility can be derived using the fragility mixture method.

First, the following fragilities are selected as appropriate for mixing, because they share details similar to the considered glass configuration:

I) Configuration (6): AN-laminated with a 6:5 aspect ratio

II) Configuration (14): AN-Mono with a 1:2 aspect ratio

Then, the data from both of these configurations are mixed according to Equation 5.2. The results of this mixture are summarized below, and the new parameters that define the derived fragility represent the estimated probabilistic cracking seismic capacity for the considered glass configuration.

Configuration	*Cracking*	
	Θ	β
(6): AN-Lami w/6:5	0.0156	0.343
(15): AN-Mono w/1:2	0.0220	0.277
Custom: AN-Lami w/1:2	**0.0185**	**0.349**

5.6 Results and Conclusions

The developed fragility functions can be utilized in the Performance Assessment Calculation Tool (PACT) for PBSD or individually in a design approach for architectural glass systems by a user. The median value of demand (θ) and the dispersion (β) parameters as computed by the *Fragility Function Calculator version 1.02* software are seen in Appendix A.3, and a summary of the parameter values that define each fragility curve are seen in Table 5.1. The plotted fragility curves are seen in Appendix A.4, and were plotted manually through Excel.

When defining the damage limit states of gasket degradation, initial glass cracking and crushing, and glass fallout for fragility development, it was known that the experimental data could reflect more conservatism. Specifically, two experimental data adjustments were carried out. The first was to adjust the past cracking failure data such that it represented the drift where initial glass cracking and crushing first occurred anywhere on the glass panel, as opposed to the originally defined limit state as the drift where the first through-thickness crack was observed in the vision-area of the glass

panel. The second data adjustment checked for failure in the "constant load" interval of a loading step, or otherwise adjusted the observed drift to the maximum displacement experienced before failure. It was found that more data points were adjusted for the redefinition of the cracking limit state, as opposed to the load interval failure check adjustment. In all, the failure values were reduced by an average of 1.5% for the first data adjustment, compared with an average reduction of 0.5% as a result of the second data adjustment. Finally, the nature of the first adjustment was random, while the second adjustment mainly affected FT-Mono glass, or glass configuration (21) as listed in Table 3.1.

While gasket degradation failure information has been presented in other studies (Behr et al. 1995), gasket failure data was collected for the first time for glass configurations (3-5, 7-9) as listed in Table 3.1. For these glass configurations, gasket failure was found to occur at an average drift 24% less than the average drift causing the initial glass cracking and glass edge crushing limit state. Fortunately, replacing a damaged dry-gasket seal is less labor intensive and less expensive than is replacing a damaged glass panel or framing member. However, if left unrepaired, a damaged gasket seal can lead to water and air infiltration that could result in significant indirect damage to a building.

The physical nature of most of the curves seen in Appendix A.4 is very similar from one glass configuration to the next. The curves are characterized by having more vertical elongation toward the center of the curve, or the median value of demand θ,

than towards the extremes where the curve becomes more horizontally elongated. The exception is for the fallout damage states of certain glass configurations (such as (9) as listed in Table 3.1), where some glass specimens of the particular configuration did not experienced failure during testing. These curves were analyzed using the "B"-type method termed "Bounding Demand Data", which produces curves that are more vertically elongated for probability values 0-0.7, and then more horizontally elongated after 0.7.

While the physical nature of most of the curves is similar, the probability of failure as a function of a given demand input varies from one curve to the next. The probability of failure varies according to the damage state, and then varies according the failure performance of a given glass configuration experimentally. This condition is illustrated in Table 5.1, where the median value of demand θ for any given damage state varies across different glass configurations. It is interesting to note that assuming an interstory drift ratio of 0.002 is likely to cause non-structural damage as stated in Naeim (2001), the median value of demands θ (i.e., the expected drift ratio to cause failure) of fifteen glazing configurations as listed in Table 3.1 exceed this benchmark. This means that more than half of the glass configurations would be expected to withstand damage from a moderate earthquake, using the general nonstructural damage demand as stated by Naeim (2001).

The fragility functions developed in this report can be used directly if the glass system under consideration has the same glazing details and characteristics as the

fragility, which include framing detailing, glass-to-frame clearance, system type, configuration type, glass type, glass panel dimensions, glass panel thickness, and glazing (dry vs. wet) type. Otherwise, if a glass panel has a different height (but similar aspect ratio) than the experimental glass height that a fragility function represents, an *r* modification factor (see Equation 5.4) needs to be applied to the drift ratio fragility values. If the framing differs but is relatively comparable, it is assumed that the seismic performance of the glass will not be affected.

If the glass-to-frame clearance or aspect ratio differs, two options are available for users. The first is that a fragility of a similar glass configuration with a conservative clearance or aspect ratio can be used. The second option is that a new fragility can be developed by performing a probabilistic mixture of known fragilities from configurations with similar details to the user configuration. This mixture is defined by Equation 5.5 and procedures detailed in Section 5.5.3.

Chapter 6

Development of a Closed-Form Equation

In this chapter a new closed-form equation is formulated to predict the cracking capacity of glass systems. Section 6.1 details the methodology of the equation formulation, Section 6.2 the analysis and comparison of existing equations, Section 6.3 the formulation of the base of the closed-form equation, Section 6.4 the approach taken when modifying the base equation for various glazing variables, Section 6.5 the development of factors for application to the closed-form equation, and Section 6.6 a summary of the proposed closed-form equation.

6.1 Closed-Form Equation Development

The purpose of the new closed-form equation is to predict the drift that causes cracking failure while considering various glazing and configuration details of a glass system that the ASCE 7-05 equation currently does not address. Specifically, the closed-form equation takes into account the glass type (AN, HS, FT), glass configuration (Mono, Lami, sym. IGU, asym. IGU), glass system (CW or SF), substandard glass-to-frame clearances, aspect ratio, and is designed to consider mullion-to-structure connection type in the future.

The method to develop the closed-form equation starts by determining whether the Bouwkamp (1960), Sucuoglu and Vallabhan (1997), or ASCE 7-05 (ASCE 2006) equations should be used, modified, or disregarded in the formulation of the new equation. Comparison of the Bouwkamp and ASCE equations shows that the same glass failure behavior is represented in both. The experimental cracking failure results for the different glass configurations listed in Table 3.1 are compared with the predicted cracking values from the ASCE and the Sucuoglu and Vallabhan equations, where it is determined that the ASCE equation is more accurate. With the ASCE equation left as the best option for possible formulation, an investigation is performed to determine how accurately the equation models the experimental initial contact and cracking glass failure behavior. The analysis shows the geometric relationship that the equation uses to predict glass failure is sound, and ultimately the ASCE equation should be used as the base in the formulation of the new closed-form equation.

For the formulation of the selected base equation to account for various glazing details, the large set of available experimental failure values (see Appendix A.2) is analyzed to find trends in the data that are caused by each of the glazing variables that are known to affect glass capacity. It is known from the studies that glass type, glass configuration, system type, clearance, and connection detailing of a glazing system will affect the experimental outcome of the failure values. The data are analyzed such that each variable is controlled for, and then trends are extracted from the experimental data with the given variable isolated. Finally, these trends and patterns are modeled in the

closed-form equation through the application of a factor (Φ) to the base-equation for each variable.

The following methodology is used for factor development:

- Factors for glass type and configuration type are developed in parallel
- Factors for substandard clearance, system, and aspect ratio are developed using the base equation (ASCE) with applied values from the Φ_{type} and Φ_{config} factors
- The substandard clearance and aspect ratio factors are defined by linear equations which reflect the open range of values that a clearance or aspect ratio can have on any given glass configuration

With the application of the factors to the base equation, the proposed new closed-form equation takes on the structure as defined in Equation **6.1**:

$$\Delta_{crack} = \Phi_{type}\Phi_{config}\Phi_{clearance}\Phi_{system}\Phi_{connection}\left[2c_1 + \Phi_{aspect}\left(2c_2\left(\frac{h}{b}\right)\right)\right] \quad \textbf{6.1}$$

where Δ_{crack} denotes the predicted cracking drift for a given glass panel, Φ_{type} a factor accounting for glass type (AN, HS, FT), Φ_{config} a factor accounting for glass panel configuration (Mono, Lami, sym. IGU, asym. IGU), $\Phi_{clearance}$ a factor correcting for the affects of a substandard glass-to-frame clearance, Φ_{system} a factor accounting for framing system type (CW or SF), $\Phi_{connection}$ a factor accounting for the framing-to-structure connection of a glass system, Φ_{aspect} a factor correcting for the affects of the aspect ratio of a glass panel, and c_1, c_2, h, and b are defined previously.

Throughout this section, some analyses utilize demands in the form of drift ratio as opposed to displacements in inches or millimeters. The notation θ is used to signify drift ratio and Δ is used to signify drift; Refer to Equation 3.1 for the drift ratio definition. The first reason that drift ratios are used is because the experimental failure drifts cannot be directly compared with the predicted drifts from the closed-form equation. This condition exists because in the laboratory the height over which the displacement occurs is equivalent to the height of the glass panel plus 9 in. (229 mm) due to the framing setup to the racking facility, while for the equation it is assumed that the height over which the displacement occurs is the height of the glass panel. Therefore, by using drift ratio values the experimental and equation values can be directly related.

The second reason that drifts are converted to drift ratios is because the glass configurations listed in Table 3.1 have varied panel dimensions. Therefore, drift ratios provide a medium to properly compare the experimental failure results and predicted cracking capacity among the different glass configuraitons. For example, glass configuration (14) experimentally failed at an average drift of 1.73 in. (44 mm), while glass configuration (15) failed at an average drift of 1.06 in. (27 mm). This comparison makes it seem that (14) has a greater cracking capacity. However, since (14) and (15) have dimensions of 8 ft x 4 ft (2.4 m x 1.2 m) and 4 ft x 8 ft (1.2 m x 2.4 m), respectively, the drift ratios that the configurations failed at are 0.0181 and 0.0220, respectively.

Therefore, configuration (15) actually has the greater cracking capacity in terms of drift ratio.

6.2 Existing Equation Comparison and Analysis

6.2.1 Bouwkamp (1960) Equation

Bouwkamp concluded with his studies that the displacement of a glass panel within the framing members when subjected to lateral loading occurs in two separate phases (Bouwkamp 1960). During the first phase, the framing deforms and the glass panel translates horizontally within the frame until the vertical frame members makes initial contact with the glass panel at opposite corners. Figure 2.2b illustrates the end of this phase, while Figure 2.2a shows the configuration at rest for comparison. This displacement is defined as follows in Equation **6.2:**

$$\Delta_1 = 2c \qquad \textbf{6.2}$$

where c denotes the glass-to-frame clearance. After the first response event, the second phase is characterized by further translation and rotation of the glass panel within the frame until opposite corners of the glass panel are situated within the corners of the framing. Once this point is reached, compressive forces develop diagonally across the glass pane, as shown in Figure 2.2c. The additional second displacement corresponding with the second glass response event is represented by Equation **6.3**:

$$\Delta_2 = 2c\left(\frac{h}{b}\right) \qquad \textbf{6.3}$$

where *h* and *b* denotes the nominal height and width, respectively, of the glass panel.

Bouwkamp states that for "soft mastic metal-sash window panels," which is comparable to the dry-glazed aluminum mid-rise CW glass configurations studied in this research, the glass failed locally in the loaded corners and was characterized by crushing. Overall, for the soft mastic metal-sash glass panel configurations, Bouwkamp states that the "drift limitations" for this general cracking failure can be represented by the combination of the two displacement events, as defined by Equation 2.4. In the soft putty metal-sash window testing, Bouwkamp noted that the rotation of the frame (denoted as the variable ϕ, see Equation 2.4 defined previously) was zero for his experiments with these types of glass systems.

6.2.2 ASCE Equation

As mentioned previously, the ASCE 7-05 (ASCE 2006) equation specifies drift requirements, which glass systems must meet under seismic conditions. An exception to determining the relative displacement that causes a glass fallout failure is using sufficient glass-to-frame clearances represented by term D_{clear}, which is defined by Equation 2.3. The term D_{clear} is defined as the "relative horizontal (drift) displacement, measured over the height of the glass panel under consideration, which causes initial glass-to-frame contact" (ASCE 7-05). This definition is further explained by Behr (2006)

where it is stated that the term represents specifically initial glass-to-frame contact simultaneously at the two opposite corners of a glass panel.

6.2.3 Bouwkamp versus ASCE Equation

Ultimately, the ASCE equation is a slightly revised version of the Bouwkamp equation that represents the drift limit right before glass panel cracking and crushing is expected to occur. While ASCE 7-05 states that the equation is to be used within the context of preventing glass fallout in an glazing system, the ASCE equation represented by the term D_{clear} is stated to represent "glass with sufficient clearances from its frame such that physical contact between the glass and frame will not occur" (Behr 2006), and specifically is defined as "the relative horizontal displacement between top and bottom of the glass panel under consideration causing initial glass-to-frame contact at the opposing corners along a main diagonal of a rectangular glass panel" (Behr 2006). Therefore, while the ASCE equation represents simultaneous opposite diagonal contact and is used in the context of preventing glass fallout, it ultimately predicts the drift at the point right before a glass panel will most likely experience glass cracking in a seismic event. This is due to the fact that after the second glass panel response of glass diagonal contact with the framing in opposing corners (see Figure 2.2c) is reached, glass cracking and crushing soon results as observed in Bouwkamp (1960). Therefore, for this research it is assumed that the equation represents the limit of contact before the cracking failure of a glass panel occurs, and is a conservative prediction of the previously defined initial

cracking and crushing limit state because of the consequences of damage when the drift represented by D_{clear} (i.e., the ASCE equation) of a glass panel is experienced.

The Bouwkamp equation also differentiates from the ASCE equation by the addition of the rotational adjustment term ϕh. Bouwkamp added this adjustment to account for the rotation of the framing intersections, which could occur on buildings in the field, a condition that is illustrated in Figure **6.1**. When ϕ equals zero, such as the conditions represented in the laboratory, Bouwkamp's equation only represents the combination of the displacements from the two separate glass response phases and can be considered a conservative prediction of the cracking limit state.

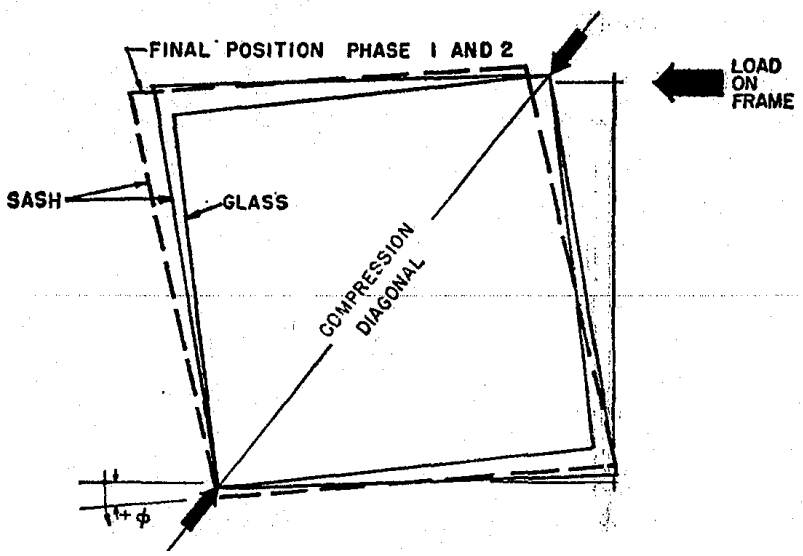

Figure 6.1: Movement of glass panel with positive frame rotation ϕ (Bouwkamp 1961)

Another difference is that the ASCE equation differentiates between the horizontal and vertical clearances, while Bouwkamp's equation assumes a consistent clearance on all sides of a glass panel. Also, the ASCE equation uses the height and

width of the glass panel for dimensions of the *h* and *b* variables, while Bouwkamp's *h* and *b* variables equal the dimensions of the glass panel in addition to the clearance values. Despite these differences, the fundamentals which led to the development of Bouwkamp's equation have remained intact through its refinement in the form of the ASCE equation. Accordingly, the equality of the original Bouwkamp equation and the current ASCE 7-05 equation can be assumed when it comes to the experimental data (where $c_1 = c_2$) that is studied in this research, as seen in Equation **6.4**:

$$2c\left(1+\frac{h}{b}\right) \equiv 2c_1\left(1+\frac{h_p c_2}{b_p c_1}\right) \qquad \textbf{6.4}$$

6.2.4 Analytical Comparison of the Experimental Results versus ASCE and Sucuoglu and Vallabhan Predicted Values

The purpose of this analysis is to determine the accuracy of the glass panel failure behavior predicted by the equations, by comparing the percent differences in the values of the ASCE (and Bouwkamp) equation and the Sucuoglu and Vallabhan equations with respect to the experimental results. The percent difference represents the inaccuracy of the predicted cracking failure for any given glass configuration relative to the experimental cracking failure results assuming that the experimental values are the accepted cracking capacity values as represented in Equation **6.5**:

$$\%\ Diff. = \frac{\theta_{predicted} - \theta_{experimental}}{\theta_{experimental}} \qquad \textbf{6.5}$$

where $\theta_{predicted}$ denotes the drift ratio as found using the given equation (ASCE or Sucuoglu and Vallabhan) and $\theta_{experimental}$ denotes the experimental failure drift ratio value. The accuracy of the equation is calculated for each glass configuration, and then a percent difference average is calculated based on the absolute percentage values of all glass configurations for either equation as seen in Table **6.1**.

The results in Table 6.1 show that overall the ASCE equation has a 26.3% inaccuracy, while the Sucuoglu and Vallabhan equation has a 28.2% inaccuracy with respect to experimental values. The ASCE equation inaccuracy is bounded by underestimating the cracking failure of glass configuration (10) by 100.0%, and overestimating the capacity of glass configuration (1) by 93.7%. Similarly, for the Sucuoglu and Vallabhan equation, the bounds of inaccuracy is composed of underestimating the cracking capacity of glass configuration (10) by 89.8%, and overestimating the capacity of glass configuration (1) by 100.2%.

While the inaccuracy of either the ASCE or Sucuoglu and Vallabhan equation are close in value, ultimately the ASCE equation is more accurate. As noted in Section 2.4, the Sucuoglu and Vallabhan equation adds cracking capacity to account for perceived out-of-plane glass panel deformation. It appears that the increased inaccuracy that the Sucuoglu and Vallabhan exhibits in the analysis is a result of the out-of-plane deformation that the equation models. Section 2.6 discusses why it is not likely that these out-of-plane deformations occur in most glass panels when seismically loaded,

Table 6.1: Percent error comparison for ASCE and Sucuoglu and Vallabhan cracking capacity estimations with experimental results

ID	$\theta^{crack}_{experimental}$	ASCE		Sucuoglu & Vallabhan	
		$\theta^{crack}_{predicted}$	% Diff.	$\theta^{crack}_{predicted}$	% Diff.
1	0.0138	0.0267	93.7%	0.0276	100.2%
2	0.0237	0.0267	13.0%	0.0276	16.8%
3	0.0279	0.0267	-4.2%	0.0270	-3.4%
4	0.0270	0.0267	-1.0%	0.0269	-0.3%
5	0.0270	0.0267	-1.0%	0.0269	-0.4%
6	0.0161	0.0267	66.5%	0.0276	72.0%
7	0.0417	0.0253	-39.2%	0.0259	-37.7%
8	0.0592	0.0372	-37.2%	0.0363	-38.7%
9	0.0573	0.0253	-55.7%	0.0259	-54.7%
10	0.0088	0.0000	-100.0%	0.0009	-89.8%
11	0.0085	0.0076	-10.6%	0.0085	0.1%
12	0.0147	0.0153	4.1%	0.0162	10.2%
13	0.0142	0.0153	7.7%	0.0162	14.1%
14	0.0181	0.0273	51.0%	0.0284	57.0%
15	0.0220	0.0273	24.1%	0.0284	29.0%
16	0.0241	0.0267	10.8%	0.0284	17.6%
17	0.0266	0.0267	0.6%	0.0272	2.2%
18	0.0221	0.0267	20.7%	0.0278	25.7%
19	0.0261	0.0267	2.3%	0.0271	3.9%
20	0.0285	0.0267	-6.2%	0.0271	-5.1%
21	0.0244	0.0267	9.8%	0.0298	22.3%
22		0.0253		0.0281	
23		0.0372		0.0368	
24	0.0332	0.0267	-19.5%	0.0274	-17.6%
Abs. AVERAGE			26.3%		28.2%

which is supported by the former analysis. Therefore, the Sucuoglu and Vallabhan equation will not be considered for formulation of the new closed-form equation.

6.3 Base Equation Development

With only the ASCE 7-05 (ASCE 2006) equation left for consideration, the equation was further investigated to determine whether it could be used in the formulation of the new closed-form equation. It was found in the previous analysis that the ASCE equation generally predicts glass cracking failure with 26.3% inaccuracy. However, it is desirable to determine if the equation models the glass response behavior characterized by the two separate glass response events to lateral loading as depicted in Figure 2.2. If the ASCE equation is found to model the rigid body motion of glass to within a reasonable degree of accuracy, then its definition will be used in the formulation of the new closed-form equation.

The analysis to determine the accuracy of the ASCE equation for predicting the two glass response events is performed by comparing the experimental test results of the various glass configurations with the initial contact and cracking displacement estimations that is represented by the first term and the entire equation, respectively. To begin with, the comparison is visually shown in Table **6.2**, where two columns denote the predicted displacements in terms of drift ratio (θ) of the two identified glass

responses. In this table, Column B signifies the prediction of initial contact, or glass response Event 1 as illustrated in Figure 2.2b, and Column D signifies the prediction of cracking, or glass response Event 2 as shown in Figure 2.2c. The experimental drift ratios for initial glass contact and cracking for each glass configuration are then inserted into the table according to whether the failure occurred before the ASCE predicted occurrence of Event 1, between Events 1 and 2, or after Event 2. It should be noted that experimental initial glass contact information is available for only some glass configurations.

A difference in the modeling trends between initial contact and cracking is seen in Table 6.2, where the ASCE equation overestimates the experimental initial contact for the most part while the times that experimental cracking is underestimated or overestimated is evenly distributed. Only glass configuration (4) experienced initial glass contact after the prediction of contact by Event 1 (Column B). On the other hand, experimental cracking failure (Column C) occurred before the predicted cracking drift ratio (Column D) for half of the glass configurations. The general glass configurations that fit this trend were CW system types with monolithic or laminated units, with a standard glass-to-frame clearance of 0.43 in. (11 mm). The other eleven glass configurations that experienced experimental cracking (Column E) beyond the predicted cracking drift ratio (Column D) were characterized as configurations with substandard glass clearances, configurations with asymmetric IGU's, or SF systems.

Table 6.2: ASCE equation predicted glass response versus experimental results

		A	B	C	D	E
ID	**System**	*Experimental Results* (θ)	**Event 1 Initial Contact[1]** $2c_1$	*Experimental Results* (θ)	**Event 2 Glass Cracking[1]** $2c_1(1 + hc_2/bc_1)$	*Experimental Results* (θ)
1	CW	*0.0036*	**0.0122**	0.0138	**0.0267**	
2	CW	*0.0080*	**0.0122**	0.0237	**0.0267**	
3	CW	*0.0084*	**0.0122**		**0.0267**	0.0279
4	CW		**0.0122**	*0.0142*	**0.0267**	0.0270
5	CW	*0.0067*	**0.0122**		**0.0267**	0.0270
6	CW		**0.0122**	0.0161	**0.0267**	
7	SF		**0.0087**		**0.0253**	0.0417
8	SF		**0.0122**		**0.0372**	0.0592
9	SF		**0.0087**		**0.0253**	0.0573
10	CW		**0.0000**		**0.0000**	0.0088
11	CW		**0.0035**		**0.0076**	0.0085
12	CW		**0.0069**	0.0147	**0.0153**	
13	CW		**0.0069**	0.0142	**0.0153**	
14	CW		**0.0091**	0.0202	**0.0273**	
15	CW		**0.0182**	0.0181	**0.0273**	
16	CW	*0.0102*	**0.0122**	0.0241	**0.0267**	
17	CW	*0.0084*	**0.0122**	0.0266	**0.0267**	
18	CW	*0.0098*	**0.0122**	0.0221	**0.0267**	
19	CW	*0.0093*	**0.0122**	0.0261	**0.0267**	
20	CW	*0.0057*	**0.0122**		**0.0267**	0.0285
21	CW	*0.0111*	**0.0122**	0.0244	**0.0267**	
22	SF		**0.0087**		**0.0253**	
23	SF		**0.0122**		**0.0372**	
24	CW	*0.0071*	**0.0122**		**0.0267**	0.0332

[1]The results normalized by being given in drift ratios where the predicted drift from the term is divided by the height of the configuration's glass panel

KEY	
	average experimental initial contact failure drift ratio
	average experimental cracking failure drift ratio

To numerically determine the modeling accuracy of the ASCE equation for both glass response events, the percent difference between the experimental and predicted values is calculated by Equation 6.5. For completeness, the percent difference is calculated for each glass configuration and according to the two glass response limit states of initial contact and cracking. Then, to find the general accuracy an absolute overall average was calculated for each glass response. Table **6.3** summarizes the results of the analysis.

The analysis results in Table 6.3 show that the equation has a greater inaccuracy modeling initial contact with a 62.5% difference compared with an average difference of 26.3% when the equation models cracking. The first reason for the high initial contact inaccuracy is that there are two configurations with very high and high percent difference values (config. 1: 241.3%, config. 20: 113.8%), and with the results from these outliers not considered in the averages the percent difference falls to 39.5%. The second reason for the high inaccuracy is attributed to the first term in the ASCE equation ($2c_1$) modeling the displacement before initial contact between the frame and glass panel occurs, where glass-to-mullion contact ideally occurs simultaneously at opposing corners from the symmetrical horizontal translation of the glass and deformation of the vertical framing members (Bouwkamp 1961). Experimentally, however, initial glass contact was observed when any of the sensors at glass corners signaled glass contact. The experimental contact from nonsymmetrical glass translation could occur earlier than when opposing glass corner regions simultaneously experience initial contact with

Table 6.3: Percent error for the ASCE equation based on the experimental results for the two separate glass responses

	% Diff.	
ID	Initial Contact	Cracking
1	241.3%	93.7%
2	52.2%	13.0%
3	44.2%	-4.2%
4	-16.7%	-1.0%
5	82.5%	-1.0%
6		66.5%
7		-39.2%
8		-37.2%
9		-55.7%
10		-100.0%
11		-10.6%
12		4.1%
13		7.7%
14		51.0%
15		24.1%
16	19.2%	10.8%
17	44.2%	0.6%
18	24.6%	20.7%
19	30.5%	2.3%
20	113.8%	-6.2%
21	9.7%	9.8%
22		
23		
24	71.0%	-19.5%
Abs. AVG.	**62.5%**	**26.3%**

framing members. Therefore, a large inaccuracy for this glass response event is seemingly difficult to avoid due to the actual experimental conditions and glass response to lateral loading.

It is proposed that the new closed-form equation uses the base equation from ASCE 7-05 because the analysis shows that the geometric relationship which models glass cracking underlying the equation is sound. As the comparison with test results in Table 6.3 shows, the equation can predict glass cracking within approximately 26% error overall for the 24 glass configurations considered, which is quite good considering the random nature of glass cracking and variety of glazing frame properties. Given the soundness of the form of the equation to model the glass responses of lateral loading mimicking seismic events, the modifications that are proposed here will further improve the equation's ability to predict the cracking capacity for CW configurations with different glazing and configuration details and different glass types.

Since the previous analysis shows that the glass events of initial frame contact and the cracking limit state can be modeled reasonably well with respect to experimental results (considering the limitations for initial contact), it is proposed that the terms representing the two glass response events be separated for the new closed-form equation, as shown in Equation **6.6**:

$$\Delta = 2c_1 + 2c_2\left(\frac{h}{b}\right) \qquad \textbf{6.6}$$

where the variables are as previously defined. Equation 6.6 represents the new base equation, which will be modified using different factors to account for the different glazing and glass configuration details. The factors include the following: (1) glass type, (2) glass configuration, (3) glass panel aspect ratio, (4) substandard glass-to-frame clearance, and (5) frame-to-structure connection. Furthermore, the second justification for separating the terms is that the modification factors can be applied to one part or the whole equation, which has the potential to make the closed-form equation more effective by targeting certain factors to specific variables.

6.4 Base Equation Modification Approach

With the base of the closed-form equation developed, an approach is taken in the formulation of the closed-form equation where the set of available experimental failure values (see Appendix A.2) are analyzed to find trends in the data caused by the various glazing and configurations variables that are known to affect glass capacity. Overall, a large set of failure data is available (see Appendix A.2) from experimental studies that looked at a wide variety of glass configurations. By analyzing these data in a particular fashion, a certain variable such as glass type can be controlled for. When an analysis isolates the effect that a certain variable has on the outcome in the failure values, trends or patterns can be extracted from the data. Then, these trends can be modeled and applied to the equation in the form of factors. Trends in the experimental failure data

have been identified for the variables of glass type, glass configuration, glass system type, and aspect ratio.

A trend identified in the experimental data for the glazing variable of glass type shows that the experimental capacity of glass panels generally increases as the material strength goes from AN to HS to FT. This trend is presented in Figure **6.2**, where the experimental glass cracking failure drift ratios for the four glass configuration types are plotted according to glass type. In this analysis (and following trend analyses), the experimental capacity of any given glass configuration listed in Table 3.1 was calculated by averaging the failure values of all the glass specimens tested for that configuration, where the specific specimen values can be referenced in Appendix A.2. For each glass configuration, the data points across glass types are connected by lines to illustrate the relationships. Furthermore, the predicted cracking drift ratio from the ASCE (or base) equation is shown by the dotted red line. This predicted value is the same for all four configurations, and across the three glass types. From this reference line, it can be seen how the base ASCE equation needs to be modified to account for the varying experimental failure values. Limitations in the data include the fact that FT glass types in laminated or symmetrical IGU configurations were not tested.

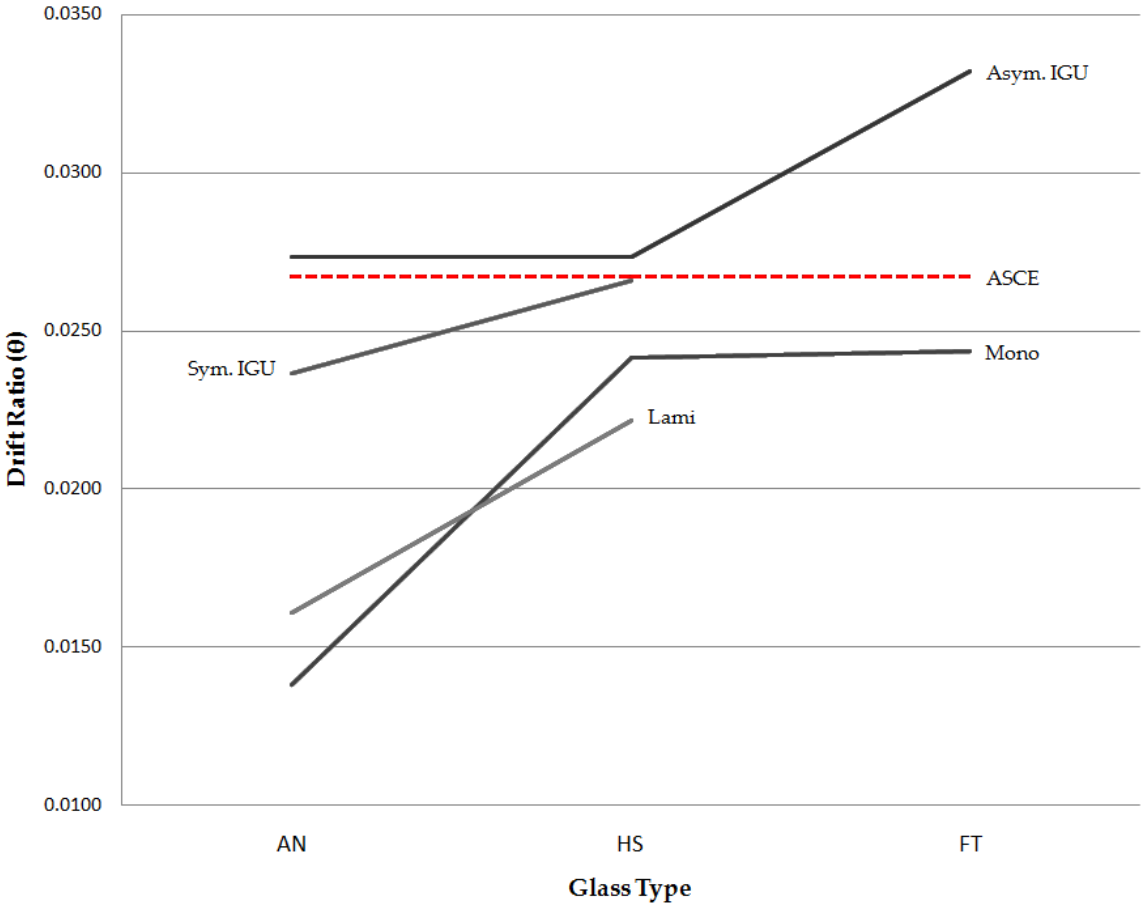

Figure 6.2: Plotted experimental glass cracking failure drift ratios for various glass panel configuration types according to glass material type compared with the predicted cracking drift ratio failure from the ASCE equation

For glass configuration types, a trend was observed where IGU configurations (symm. or asym.) generally have greater experimental cracking values than laminated or monolithic configuration types. This trend is seen in Figure 6.2 as well, where the lines representing experimental values for both IGU's are clearly above the lines for laminated and monolithic configuration types across all three glass types. Again, it can

be seen that the predicted values by the base equation need to be altered to account for the different capacities seen by the varying four configuration types.

When the experimental data for the AN monolithic configurations with substandard clearances is plotted with the similar AN-Mono configuration with a standard clearance (Figure 6.3), a general trend is seen where the experimental capacity gradually decreases as the clearance decreases. If the predicted capacity from the ASCE equation is plotted for comparison, another trend emerges where the ASCE equation goes from significantly overestimating the capacity for the configuration with the standard clearance to significantly underestimating the experimental drift ratios of configurations with the lowest clearances. This condition is shown in Figure **6.3**, where chart (a) plots the actual data points, and (b) shows the trend using best of fit lines for both sets of experimental and ASCE data.

A trend for SF configurations is extracted when the experimental failure values for those systems are compared with the results of similar CW configurations. Generally, it is seen that SF systems have significantly greater experimental capacity than comparable CW systems. This scenario is shown in Figure **6.4.**

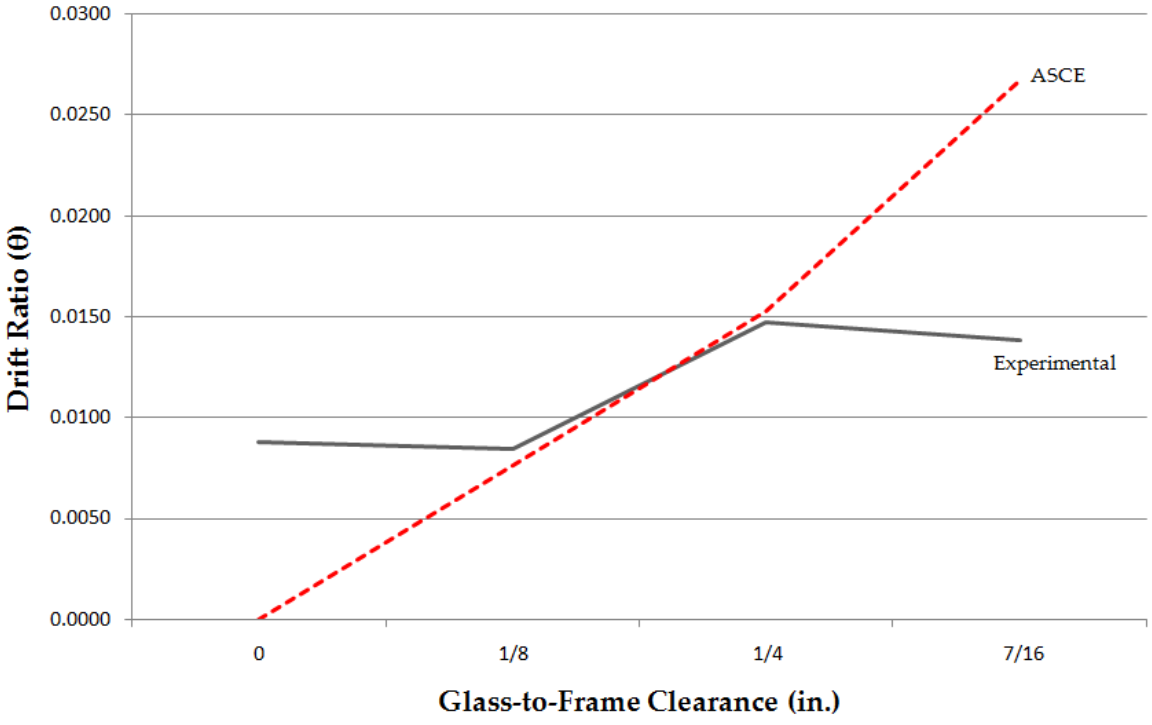

(a)

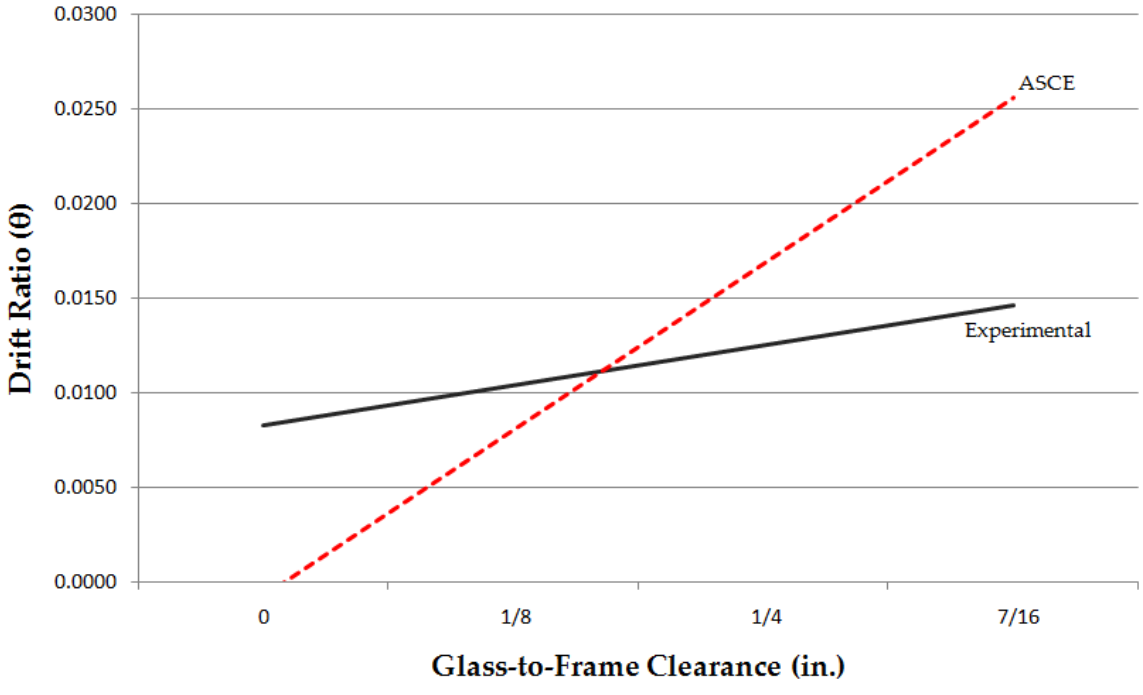

(b)

Figure 6.3: Depiction of (a) glass cracking experimental versus predicted ASCE values and (b) best of fit lines of the two data sets for AN-Mono configurations with substandard glass-to-frame clearances

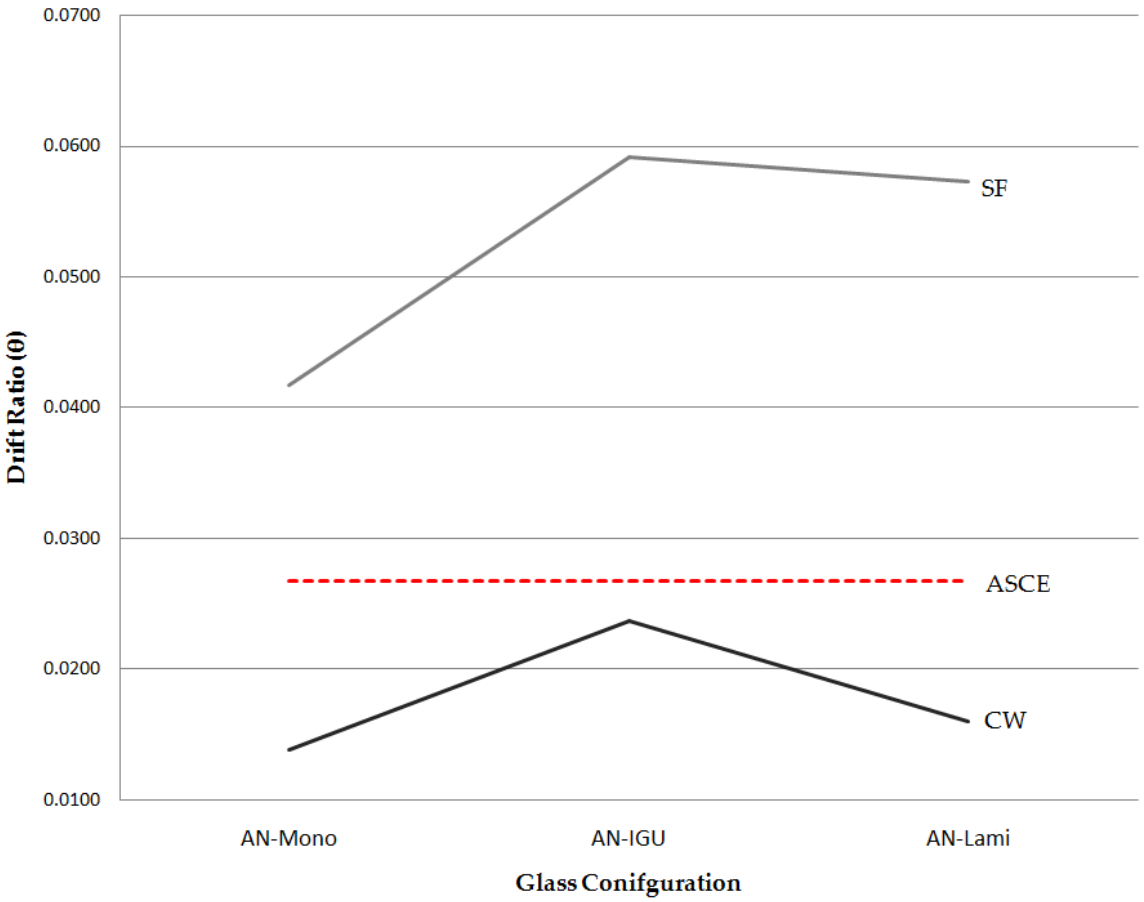

Figure 6.4: Plots of SF experimental glass cracking data for AN-Mono, AN-IGU, and AN-Lami glass configurations compared with data for comparable CW configurations and the predicted SF cracking failure values from ASCE equation

Lastly, a trend in the data was identified concerning the effect that the aspect ratio of a glass panel has on the experimental capacity of glass CW systems. The glass cracking failure data from two tests on AN-Mono glass configurations with 2:1 and 1:2 glass panel aspect ratios were compared with the similar configuration with a standard 6:5 aspect ratio. The experimental data shows that the capacity increases for a

configuration as the glass aspect ratio of a configuration increases or decreases from 6:5. This condition is shown in Figure **6.5**, where the ASCE predicted values are also given. It can be seen that the ASCE equation does not adequately model the effect that a varying aspect ratio has on the failure performance of glass panels, because there is not enough change in the predicted values to reflect the changes in the experimental results from the assumed effects from a varying aspect ratio. The limitation with the trends is that failure data is available on glass configuration with only three different aspect ratios. However, an accurate factor to correct the equation for a varying aspect ratio can still be developed for the equation based on the available data, and then follow-up studies can verify the results that are reached in this research.

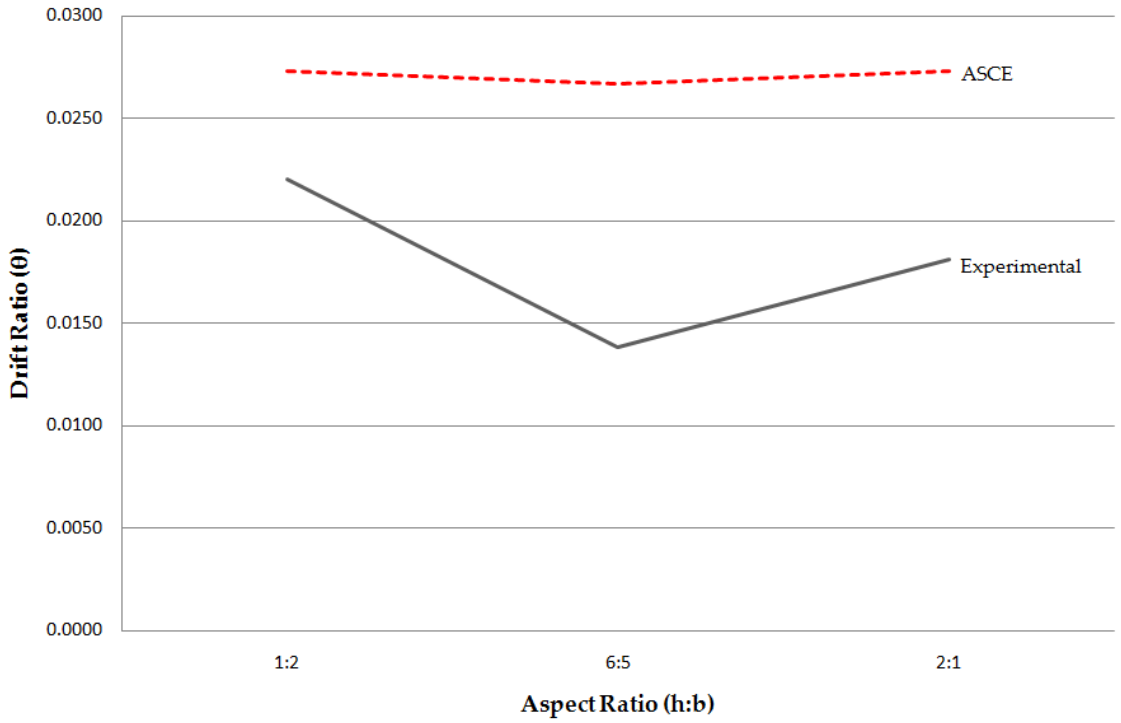

Figure 6.5: Plotted experimental and predicted cracking drift ratios for AN-Mono configurations with 1:2, 6:5, and 2:1 aspect ratios

6.5 Factor Development

Factors serve the purpose of modifying the base equation to account for the effects that varying glazing and configuration details have on the cracking capacity of glass panels. The magnitude and formulation of the factors are based directly on the identified trends in the experimental data. Since multiple factors will be developed, it is known that the application of a given factor may affect not only the base equation but the value of other factors as well. This condition can be viewed in Equation 6.1, where five factors modify the entire base equation, and in the process affect other factors. As a

result, a method is devised where the factors are formulated in an orderly fashion, so that the development of later factors take into account the numeric effects that previously developed factors have on the base equation.

The method to develop the sequencing of factor formulation is characterized by beginning with factors that represent the composition of a glass panel, and then developing factors that represent glass configuration components that envelop the glass panel. With this methodology, the development starts with the factors accounting for glass type (Φ_{type}) and configuration type (Φ_{config}) of a glass panel. The factors are developed in parallel, such that the formulation of each of these factors does not consider the development of the other factor. Moving on from the glass panel, a factor to adjust the equation for configurations with substandard glass-to-frame clearances ($\Phi_{clearance}$) is developed. Proceeding from the glass-to-frame clearance, a factor is developed to consider the system surrounding a glass panel (Φ_{system}), which adjusts the equation specifically for SF systems. The exception to the factor development methodology is the factor developed for a varying glass aspect ratio (Φ_{aspect}), because this factor is applied to only the second term of the base equation (see Equation 6.1) and does not directly affect the other factors. Figure **6.7** visually depicts the sequencing of factor development as applied to the base closed-form equation, whose own development is illustrated in Figure **6.6**. It should be noted that the values determined for the factors Φ_{system}, $\Phi_{clearance}$, and Φ_{aspect} are based on the comparison between the experimental results

with the predicted cracking values from the base equation and applied factor values for glass type and configuration.

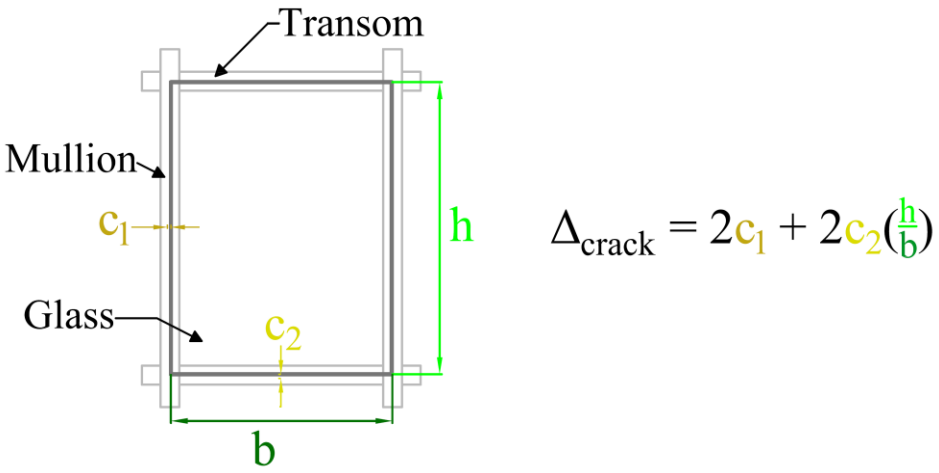

Figure 6.6: Glazing variables considered in the base of the closed-form equation

In the proposed closed-form equation (see Equation 6.1), a factor takes on one of two forms. Whether a factor takes on one form or the other is a function of the glazing characteristic that the factor represents, and if the glazing characteristic has a perceived overall effect on both terms in the base equation or just one of the terms. The first type of factor is mathematically represented by the placement of a multiplier in front of the second term of the equation, as defined by Equation **6.7**:

$$\Delta = 2c_1 + X \cdot 2c_2\left(\frac{h}{b}\right) \qquad \textbf{6.7}$$

where X denotes a multiplier in the form of a fractional value with the purpose of modifying the predicted glass cracking capacity of a glass panel. While the Φ_{aspect} factor is proposed to take the form of an "X" type factor, the others are applied to the

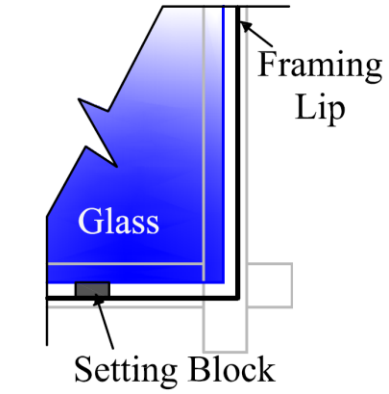

$$\Delta_{crack} = \Phi_{type}\Phi_{config}\left[2c_1 + 2c_2\left(\frac{h}{b}\right)\right]$$

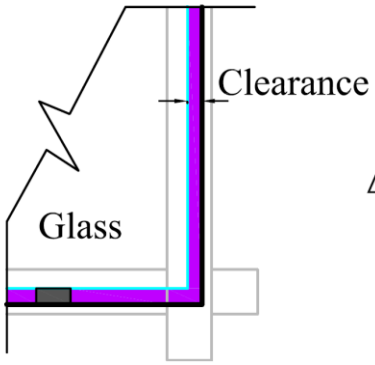

$$\Delta_{crack} = \Phi_{type}\Phi_{config}\Phi_{clearance}\left[2c_1 + 2c_2\left(\frac{h}{b}\right)\right]$$

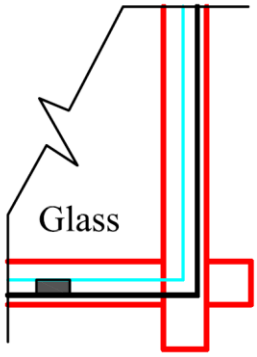

$$\Delta_{crack} = \Phi_{type}\Phi_{config}\Phi_{clearance}\Phi_{system}\left[2c_1 + 2c_2\left(\frac{h}{b}\right)\right]$$

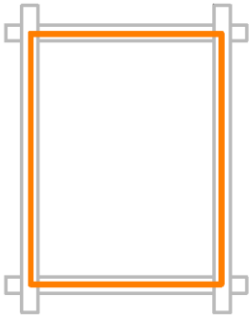

$$\Delta_{crack} = \Phi_{type}\Phi_{config}\Phi_{clearance}\Phi_{system}\left[2c_1 + \Phi_{aspect}\left(2c_2\left(\frac{h}{b}\right)\right)\right]$$

Figure 6.7: Illustration depicting the order of factor development and glazing characteristic that the factor accounts for

whole equation because of their effects on the entire seismic behavior response of a glass system. This second factor can take the form as represented in Equation **6.8**:

$$\Delta = Y\left[2c_1 + X \cdot 2c_2\left(\frac{h}{b}\right)\right] \qquad \textbf{6.8}$$

where Y denotes a factor that modifies the prediction of glass cracking displacement values for all terms in the equation.

6.5.1 Parallel Factor Development of: Φ_{type} and Φ_{config}

In the process to develop factors to model the effect that glass type and configuration type have on the glass cracking failure performance of glass systems, many formulation options were investigated. Ultimately, it was deemed best to move forward with separate Φ_{type} and Φ_{config} factors developed in parallel because this formulation approach best aligned with the overall equation formulation approach of modeling trends in the experimental data to account for each glazing variable separately. However, a method that developed a combined factor $\Phi_{type\text{-}config}$ to model glass type and configuration in an integrated fashion was explored. While the integrated factor offers benefits compared to the separate factor method in terms of an increase in degree of modeling accuracy by considering the performance effects of a given glass panel configuration type as a function of panel's glass material type, in the end this factor development method does not align with the overall approach used in the formulation of the closed-form equation which aims to model the effect of various

glazing variables. This is because the integrated approach simply offers a correction factor, rather than a method that models the sensitivity of effect that glass type or configuration type has on the capacity of glass panels. For reference, the developed integrated factor approach can be seen in Appendix B.

6.5.1.1 Factor Development of: Φ_{type}

A factor to be applied to the closed-form equation that models the effect of varying glass type (Φ_{type}) on glass panel failure performance is developed here. The experimental data show that the experimental failure values generally increase as a glass panel type goes from AN to HS to FT, as seen in Figure 6.2. To control for the effects that glass type has on the failure values, only the data from CW glass configurations with standard glass-to-frame clearances of 0.43 in. (11 mm) and glass panel dimensions of 5 ft wide by 6 ft high (1.5 m x 1.8 m) is considered. Glass configurations that fit this criteria are configurations (1-6, 16-21, and 24) as listed in Table 3.1.

Factor values of Φ_{type} are developed for a discrete set of glass types, which are AN, HS, and FT. The magnitude of the value of each glass type is determined by quantifying the effect that a particular glass type has on the experimental results among the four different configuration types. Then, this quantified effect is divided by the predicted capacity from the base ASCE equation, such that the final value adjusts the base equation to reflect the modeled experimental effect of a given glass type.

The factor value for a given glass type is defined by Equation **6.9**:

$$\Phi_{type}^{x} = \frac{\theta_{exp}^{x_{ave}}}{\theta_{ASCE}} \qquad \textbf{6.9}$$

where Φ_{type} denotes the factor value for a given glass type x [x = AN, HS, or FT], $\theta_{x\text{-}avg}$ the average experimental drift ratio of the four configurations with glass type x as defined by Equation **6.10**, and θ_{ASCE} the cracking drift ratio as presumed to be predicted by the base ASCE equation.

$$\theta_{exp}^{x_{avg}} = \frac{\theta_{exp}^{x_{mono}} + \theta_{exp}^{x_{lami}} + \theta_{exp}^{x_{sym-IGU}} + \theta_{exp}^{x_{asym-IGU}}}{4} \qquad \textbf{6.10}$$

The determined factor values using Equations 6.9 and 6.10 are presented in Table **6.4.** The trend noticed in the experimental data where experimental capacity increased from AN to HS to FT glass types is reflected in these factor values. Before the accuracy of the application of these factor values to the base equation can be determined, the Φ_{config} factor modeling the effects of configuration type needs to be developed.

Table 6.4: Developed Φ_{type} factor values for glass cracking limit state predictions

	$\boldsymbol{\Phi}_{type}$
AN	0.76
HS	0.94
FT	0.99

It should be noted that experimental data for laminated and symmetric IGU's configuration types with FT glass are not available. It is important that failure values

representing the performance of glass type from each configuration be present in the calculations of factor values for consistency purposes. This is because if one of the factor values is calculated using average experimental values for a given glass type from only the results of two configurations, then those data points are given more weight. This leads to an imbalance when that particular factor value is used in the context of other factor values that were determined from data points that are relatively less critical from a purely statistical standpoint. Therefore, when calculating the factor value for the FT glass type it was assumed that the FT-Lami and FT-IGU systems had an experimental glass cracking capacity equal to similar configurations with HS glass. This is a conservative assumption that ultimately allows a consistent development for all glass type factor values. However, follow-up testing on these configurations with FT glass could find experimental values which can be used to refine the Φ_{type} value for FT glass types.

6.5.1.2 Factor Development of: Φ_{config}

The next factor developed to be applied to the closed-form equation models the failure performance effect that a varying glass panel configuration type (Φ_{config}) has on glass systems. As noted in Section 6.4, the experimental data generally shows that symmetric and asymmetric IGU configurations had greater experimental capacities than did monolithic and laminated configuration types, as seen in Figure 6.2. To control for

the effects that glass configuration type has on the failure results, only the data from CW glass configurations with standard glass-to-frame clearances of 0.43 in. (11 mm) and glass panel dimensions of 5 ft wide by 6 ft high (1.5 m x 1.8 m) are considered. Therefore, data from configurations (1-6, 16-21, and 24) as listed in Table 3.1 are used in the Φ_{config} factor development.

Values for the Φ_{config} factor are developed for a discrete set of configuration options, which are Mono, Lami, sym. IGU, and asym. IGU. Similar to the Φ_{type} factor, the magnitude of the value of each configuration type is determined by quantifying the effect that a particular configuration type has on the experimental results among the three different glass types. Then, this quantified effect is divided by the predicted drift ratio from the ASCE equation, such that the final value adjusts the base equation to reflect the modeled experimental effect of a given configuration type.

The factor value for a given glass type is defined by Equation **6.11**:

$$\Phi^{x}_{config} = \frac{\theta^{x_{ave}}_{exp}}{\theta_{ASCE}} \qquad \textbf{6.11}$$

where Φ_{type} denotes the factor value for a given configuration type x [x = Mono, Lami, sym. IGU, or asym. IGU], $\theta_{x\text{-}avg}$ the average experimental drift ratio of the three glass types with configuration type x as defined by Equation **6.12**, and θ_{ASCE} the cracking drift ratio as predicted by the base ASCE equation.

$$\theta^{x_{avg}}_{exp} = \frac{\theta^{x_{AN}}_{exp} + \theta^{x_{HS}}_{exp} + \theta^{x_{FT}}_{exp}}{3} \qquad \textbf{6.12}$$

The calculated Φ_{config} factor values using Equations 6.11 and 6.12 are presented in Table **6.5.** The trend identified previously in the experimental data where experimental capacity for both IGU configuration types is greater than the values for monolithic and laminated types is mirrored in these factor values. Since the experimental data for laminated and symmetric IGU's configuration types with FT glass is not available as noted before, when calculating the factor value for the Lami and sym. IGU configuration types it was assumed that the FT-Lami and FT-IGU systems had an experimental capacity equal to similar configurations with HS glass.

Table 6.5: Developed Φ_{config} factor values

	$\boldsymbol{\Phi}_{config}$
Mono	0.78
Lami	0.75
Sym. IGU	0.96
Asym. IGU	1.10

6.5.1.3 Accuracy Analysis of Φ_{type} and Φ_{config} Factors

The accuracy of the application of the Φ_{type} and Φ_{config} factors to the base closed-form equation is determined here to see if the factors improve the accuracy of the modified equation before the other factors are developed. The accuracy is determined by finding the percent difference of the predicted drift ratios of a given glass system

with respect to the experimental results. The predicted drift ratio is calculated from the developed closed-form equation up to this point, which is represented by Equation **6.13** and where Δ_{crack} is normalized into a drift ratio by dividing by the height of the glass panel (72 in.).

$$\Delta_{crack} = \Phi_{type}\Phi_{config}\left[2c_1 + \left(2c_2\left(\frac{h}{b}\right)\right)\right] \qquad \textbf{6.13}$$

The analysis and results are summarized in Table **6.6**. In the table, Column A denotes a given glass system, Column B the applicable analyzed glass configuration(s) as listed in Table 3.1, Column C the predicted drift ratio from the base (ASCE) equation, Column D and E the appropriate values for Φ_{type} and Φ_{config}, respectively, Column F the predicted drift ratio from Equation 6.13 compared with the experimental drift ratio, and Column G the percent difference between either predicted drift ratios from Equation 6.13 or ASCE with respect to the experimental results. The percent difference is found using Equation **6.14.** For the glass systems where more than one glass configuration listed in Table 3.1 applies, the data were averaged among applicable glass configurations.

$$\%\ Diff. = \frac{\theta_{predicted} - \theta_{experimental}}{\theta_{experimental}} \qquad \textbf{6.14}$$

Table 6.6: Accuracy of closed-form equation with the application of Φ_{type} and Φ_{config} factors compared with accuracy of the unmodified ASCE equation

A	B	C	D	E	F		G	
System	ID	θ_{base}	Φ_{type}	Φ_{config}	Cracking		% Difference	
					θ_{pred}	θ_{exp}	Eq. 6.13	ASCE
AN-Mono	1	0.0267	0.76	0.78	0.0159	0.0138	14.8%	93.7%
AN- IGU (sym.)	2	0.0267	0.76	0.96	0.0195	0.0237	-17.6%	13.0%
AN-IGU (asym.)	3-5	0.0267	0.76	1.10	0.0224	0.0273	-18.2%	-2.1%
AN-Lami	6	0.0267	0.76	0.75	0.0152	0.0161	-5.1%	66.5%
HS-Mono	16	0.0267	0.94	0.78	0.0196	0.0241	-18.8%	10.8%
HS-IGU (sym.)	17	0.0267	0.94	0.96	0.0241	0.0266	-9.2%	0.6%
HS-Lami	18	0.0267	0.94	0.75	0.0188	0.0221	-14.9%	20.7%
HS-IGU (asym.)	19, 20	0.0267	0.94	1.10	0.0276	0.0273	1.1%	-2.2%
FT-Mono	21	0.0267	0.99	0.78	0.0206	0.0244	-15.2%	9.8%
FT-IGU (asym.)	24	0.0267	0.99	1.10	0.0291	0.0332	-12.3%	-19.5%
ABS. AVG							**12.7%**	**23.9%**

The analysis shows that with the application of the Φ_{type} and Φ_{config} factors, the closed-form equation predicts the experimental failure performance of glass systems with a relatively high degree of accuracy. The application of the factors which model the effects of glass type and configuration type decreases the percent difference of the equation predicted values relative to the experimental values from 23.9% to 12.7%. In some cases, the percent difference for certain glass systems such as AN-IGU increases from the ASCE equation to the modified closed-form equation. However, these increases are small relative to the decreases in percent difference that some systems exhibit. For example, for the AN-Mono glass system, the percent difference between the predicted and experimental values decreased from 93.7% to 14.8% from the ASCE equation to the modified equation. Since the analysis shows that the factors provide

models of the effects of glass type and configuration type that significantly improve the accuracy of the base equation, the formulation of the closed-form equation will move forward using these defined factors.

6.5.2 Factor Development of: $\Phi_{clearance}$

Moving forward with the factor development methodology (see Figure 6.7), the next factor formulated to modify the closed-form equation models the performance effects that substandard glass-to-frame clearances have on glass systems. As detailed in Section 6.4, the data show that the experimental capacity of systems with substandard clearances gradually decreases as the clearance decreases as well. However, the decreasing capacity in the trend is less than what would be expected, which is reflected by the ASCE equation significantly underestimating the experimental failure capacity of systems with the lowest clearances (see Figure 6.3b).

This trend does not change when comparing the experimental results with the predicted drift ratios of the modified base (ASCE) equation with application of the Φ_{type} and Φ_{config} factors (see Equation 6.13). This condition is shown in Figure **6.8**, which compares the drift ratios predicted from the closed-form equation and experimental values with relation to the glass-to-frame clearance of a glazing system. This chart

shows that the trend is similar to the trend in the analysis shown in Figure 6.3b that employs the original ASCE equation.

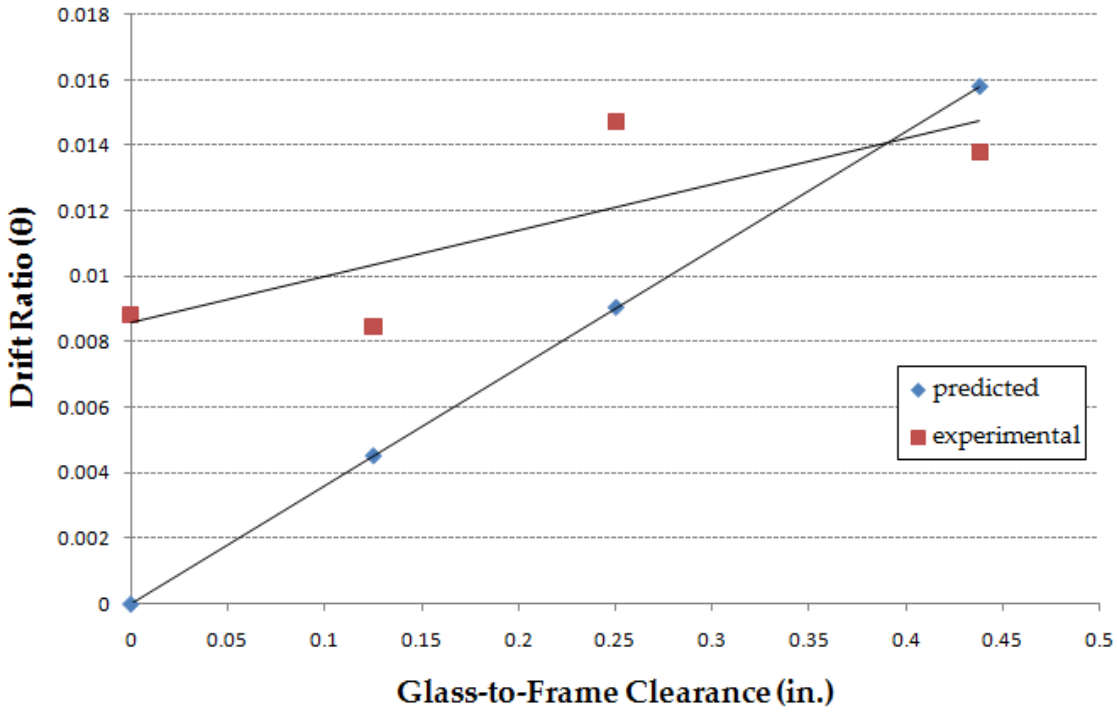

Figure 6.8: Plotted predicted and experimental drift ratios with corresponding best-of-fit lines

The data used in Figure 6.8 for the glass configurations with substandard clearances is summarized in Table **6.7**. In the table, Column A denotes the predicted drift ratio from the base equation, Column B the glass type factor value, Column C the configuration type factor value, and Column D compares the predicted drift ratio from the modified base equation with the experimental failure values. The data from glass configuration (13) as listed in Table 3.1 is not included in the analysis shown in Figure 6.8 and throughout the formulation of the factor, because only one specimen of this type

was tested and therefore the degree of experimental accuracy does not match that of the other glass configurations (10-12) with substandard clearances.

Table 6.7: Comparison of glass cracking drift ratios as predicted from the equation and experimentally observed for glass configurations with substandard clearances

	A	B	C	D	
	$2c_1 + 2c_2\left(\frac{h}{b}\right)^*$	Φ_{type}	Φ_{config}	Cracking Failure	
				$\theta_{predicted}$	$\theta_{experimental}$
10	0.0000	0.76	0.78	**0.0000**	**0.0088**
11	0.0076	0.76	0.78	**0.0045**	**0.0085**
12	0.0152	0.76	0.78	**0.0091**	**0.0147**
13	0.0152	0.76	0.96	**0.0111**	**0.0142**

*The results are normalized and given in drift ratios where the predicted drift from the term is divided by the height of the configuration's glass panel

As proposed in the methodology for factor development, the $\Phi_{clearance}$ factor is developed such that it modifies the entire base equation as a "*Y*" type factor (see Equation 6.8). This is because clearance variables c_1 and c_2 are present in both base equation terms. The closed-form equation with the addition of the $\Phi_{clearance}$ factor is then defined by Equation **6.15**, and is formulated accordingly.

$$\Delta_{crack} = \Phi_{type}\Phi_{config}\Phi_{clearance}\left[2c_1 + \left(2c_2\left(\frac{h}{b}\right)\right)\right] \qquad \textbf{6.15}$$

Since the base equation contains variables that consider glass-to-frame clearance (c_1 and c_2), the clearance factor ($\Phi_{clearance}$) cannot directly modify the equation by applying the quantified effect that a decrease in clearance is assumed to have on the experimental results. Instead, it needs to be formulated to correct the underestimated capacity predicted by the equation based on the trends in the experimental results. Furthermore,

the $\Phi_{clearance}$ factor is formulated such that it can be used to find a modification value for a range of substandard clearance values. Unlike the Φ_{type} and Φ_{config} factors, there is not a discrete set of points that values need to be developed for. As a result, the factor is developed in the form of an equation that addresses a range of possible input (clearance) values.

The first step taken in the formulation of the $\Phi_{clearance}$ factor is to find initial factor values for the glass configurations as calculated by Equation **6.16**. This equation was found by adding the underestimated experimental drift of a glass configuration with a given substandard clearance to the predicted drift, and then equating this sum to Equation 6.15, and solving the unknown value of $\Phi_{clearance}$. It should be noted that the variables were normalized into drift ratios for the calculations, but are denoted in drifts for illustrative purposes.

$$\Delta_{crack} + \Delta_{sub-clearance} = \Phi_{type}\Phi_{config}\Phi_{clearance}\left[2c_1 + \left(2c_2\left(\frac{h}{b}\right)\right)\right]$$

$$\rightarrow \Phi_{clearance} = \frac{\Delta_{crack} + \Delta_{sub-clearance}}{\Phi_{type}\Phi_{config}\left[2c_1 + \left(2c_2\left(\frac{h}{b}\right)\right)\right]} \qquad \textbf{6.16}$$

where Δ_{crack} denotes the predicted capacity from Equation 6.13 for a given glass configuration, and $\Delta_{sub\text{-}clearance}$ denotes the experimental drift capacity underestimated by the predicted drift for a glass configuration for a system with a given substandard clearance as determined from Equation **6.17**.

$$\Delta_{sub-clearance} = \Delta^{pred}_{sub-clearance} - \Delta^{exp}_{sub-clearance} \quad \textbf{6.17}$$

where $\Delta_{subclearance\text{-}pred}$ denotes the predicted decrease in drift from Equation 6.13 because of a decrease to a given substandard clearance x from a standard clearance as found by Equation **6.18**, and $\Delta_{subclearance\text{-}exp}$ denotes the actual decrease in experimental drift that is assumed to be caused from decreasing the clearance of a glass configuration from the standard clearance to a given substandard clearance x as shown in Equation **6.19**.

$$\Delta^{pred}_{sub-clearance} = \Delta^{pred}_{standard} - \Delta^{pred}_{x} \quad \textbf{6.18}$$

where $\Delta_{pred\text{-}standard}$ denotes the predicted cracking drift for a glass configuration with a standard 0.43 in. (11 mm) clearance, and $\Delta_{pred\text{-}x}$ denotes the predicted drift for a similar configuration with a substandard clearance x.

$$\Delta^{exp}_{sub-clearance} = \Delta^{exp}_{standard} - \Delta^{exp}_{x} \quad \textbf{6.19}$$

where $\Delta_{exp\text{-}standard}$ denotes the experimental cracking drift for a glass configuration with a standard 0.43 in. (11 mm) clearance, and $\Delta_{exp\text{-}x}$ denotes the experimental drift for a similar configuration with a substandard clearance x.

Using Equation 6.16, the initial $\Phi_{clearance}$ factor values were found for glass configurations (1), (11), and (12) as shown in Table **6.8**.

Table 6.8: Calculated initial factor values from Equation 6.16 for glass configurations (1), (11), and (12)

ID	Clearance (in.)	Initial $\Phi_{clearance}$
1	0.4375	1.02
12	0.25	1.81
11	0.125	2.34

The data from certain glass configurations with a substandard clearance are excluded from the analysis and the remaining factor formulation, while the data from glass configuration (1) with a standard clearance is included. Specifically, the data from glass configuration (13) is excluded for reasons described previously. Also, the data from glass configuration (10) with a glass-to-frame clearance of 0 in. (0 mm) is left out of the analysis because the glass configuration presents a special case that is addressed later on. Lastly, the data from AN-Mono glass configuration (1) with a standard 0.43 in. (11 mm) glass-to-frame clearance was included because it provides data points that relate the values between the other substandard clearances to the results of a configuration with a 0.43 (11 mm) standard clearance.

It should be noted that it seems counterintuitive that glass configurations with a lower clearance have greater $\Phi_{clearance}$ initial factor values than configurations with greater clearances. However, it should be kept in mind that in essence the $\Phi_{clearance}$ factor is a corrective modifier, which means that configurations with lesser clearances need more correction than configurations that have clearances closer to the standard 0.43 in. (11 mm) clearance. This is because the equation underestimates the experimental

capacity of configurations with lower clearance to a greater degree, as described in the experimental trends previously.

With the initial factor values determined, the second step in the formulation of the $\Phi_{clearance}$ factor definition is to perform a regression analysis that relates the initial factor values with a clearance dimension. The purpose of this analysis is to determine whether these two variables are highly correlated, or whether the nature of the initial factor values is random with respect to the glass-to-frame clearance. The regression analysis is shown in Figure **6.9**.

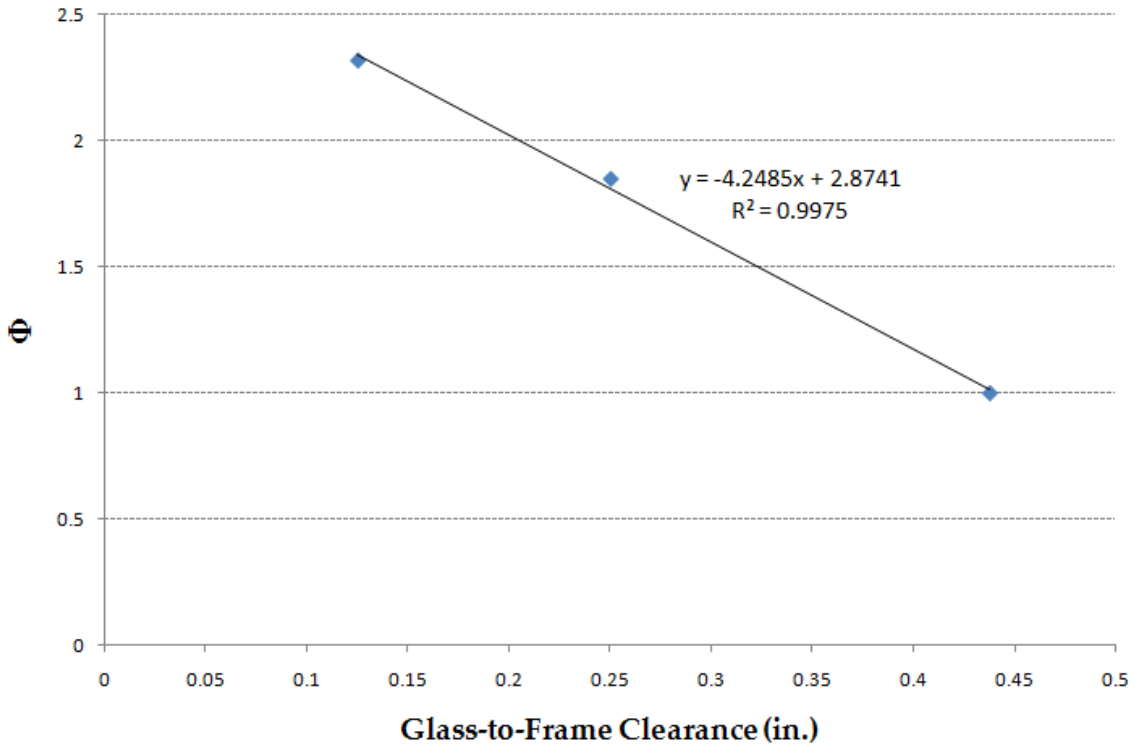

Figure 6.9: Linear regression analysis relating the glass-to-frame clearance and initial factor values for AN-Mono glass configurations (1, 11, and 12) with various glass-to-frame clearances

The results in Figure 6.9 show that a highly linear relationship is found to exist between the glass-to-frame clearance values and the initial (or needed) factor values for glass configurations (1, 11, and 12). This is proven by the coefficient of determination value, or R^2, which has a value around 0.998 for this linear regression. When $R^2 = 1.0$ it indicates that a perfect linear relationship exists between two variables. The value specifically represents the percentage of variations between two parameters (represented on the x and y axes of a chart) that can be accounted by a linear relationship (Dickey et al. 1998). In our case, a R^2 value of 0.998 can be interpreted that nearly 100% of the variation existing in the differences between the clearance dimension of a glass panel and the initial factor values can be explained by the calculated linear relationship.

Since the linear relationship relates a glass clearance so highly with a value that represents a multiplier needed to adjust the predicted drift ratio to reflect the experimental failure values, the $\Phi_{clearance}$ factor is formulated based on the linear equation from the regression analysis. For this factor development method, the variable x of the linear equation is equal to the glass-to-frame clearance, and the function variable y is the equal to the value for the $\Phi_{clearance}$ factor of a given glass configuration with clearance x (in.). This linear equation developed in the regression is $y = -4.2485x + 2.8741$.

The third and last step in the formulation of the $\Phi_{clearance}$ factor is to slightly adjust the linear equation for the final definition. This adjustment consists of first rounding the numeric values. Then, the intercept of the equation is adjusted slightly such that a factor

value of 1.0 is obtained for an input standard clearance value of 0.43 in. (11 mm). With the application of these adjustments to the linear equation found in the regression analysis, Equation **6.20** defines the final formulation of the $\Phi_{clearance}$ factor:

$$1.0 \leq \Phi_{clearance} = -4.25x + 2.86 \qquad \textbf{6.20}$$

where x is equivalent to the glass-to-frame clearance of a given configuration. A limitation is added in the definition where it is defined that the $\Phi_{clearance}$ factor should not take on a value less than 1.0. While this condition would not occur unless a clearance value more than the standard 0.43 in. (11 mm) value was input, this limitation ensures that users realize the factor is only intended to be used on glass configurations with substandard clearances.

An exception to the $\Phi_{clearance}$ factor to address is a system with a glass-to-frame clearance less than 0.125 in. (6 mm). It was mentioned earlier that the equation predicts a glass capacity of 0 in (0 mm) for glass configuration (10) with a glass-to-frame clearance of 0 in. (0 mm), which negates any effect that a factor would have. However, referring back to Table 6.7, it can be seen the experimental cracking drift ratio failure for glass configuration (10) is 0.0088, which is nearly equivalent to the experimental drift ratio of 0.0085 for glass configuration (11) with a 0.125 in. (6 mm) clearance. It is conceivable that similar configurations with clearances between 0 in. (0 mm) and 0.125 in. (6 mm) have drift ratio capacities near to (10) and (11). As a result, it is proposed that for glass configurations with a glass-to-frame clearance below 0.125 in. (3 mm), the capacity of the glass configuration is calculated using a 0.125 in. (3 mm) clearance

dimension value for the closed-form equation and $\Phi_{clearance}$ factor. The exception eliminates the potential of compromising the accuracy of the $\Phi_{clearance}$ factor by formulating the factor considering the especially unique seismic response behavior of glass systems with clearance near 0 in. (0 mm).

For a sampling of the different values that $\Phi_{clearance}$ has for various glass-to-frame clearances, a range of clearance dimensions was input into Equation 6.20 and the values were organized into Table **6.9**:

Table 6.9: Sample $\Phi_{clearance}$ factor values

Clearance (in.)	$\boldsymbol{\Phi_{clearance}}$
0.5	1.0
0.4375	1.0
0.25	1.80
0.125	2.33
0	2.33

To determine the accuracy of the closed-form equation with the application of the $\Phi_{clearance}$ factor for the glass configurations with a substandard clearance, a new analysis comparing the predicted drift ratios (Equation 6.15) with the experimental failure drift ratios presented in Table **6.10**. For comparison purposes, the percent difference for the equation that does not correct for a substandard clearance and only additionally considers glass type and configuration type (Equation 6.13) is shown next to next to Equation 6.15 as well. The percent differences calculated for both equations in

the last column was found by using Equation 6.14. Glass configuration (1) with a standard clearance of 0.43 in. (11 mm) is included for reference purposes.

Table 6.10: Comparison of predicted glass cracking capacity in drift ratios as compared with the experimental results with the addition of the $\Phi_{clearance}$ factor.

	$\frac{2c_1}{h} + 2c_2\left(\frac{h}{b}\right)^*$	Φ_{type}	Φ_{config}	$\Phi_{clearance}$	Cracking Failure		% Difference	
					θ_{pred}	θ_{exp}	Eq. 6.15	Eq. 6.13
1	**0.0267**	0.76	0.78	1.0	**0.0159**	0.0138	**14.8%**	14.8%
10	**0.0000**	0.76	0.78	2.33	**0.0106**[1]	0.0088	**19.9%**	100%
11	**0.0076**	0.76	0.78	2.33	**0.0106**	0.0085	**24.8%**	-46.7%
12	**0.0152**	0.76	0.78	1.80	**0.0163**	0.0147	**10.8%**	-38.3%
13	**0.0152**	0.76	0.96	1.80	**0.0201**	0.0142	**41.5%**	-21.8%

*The results are normalized and given in drift ratios where the predicted drift from the term is divided by the height of the configuration's glass panel

[1]According to the new defined exception to the equation, glass configurations with glass-to-frame clearances < 1/8 in. (3 mm) will assume clearances of 1/8 in. (3 mm) for variables c_1 and c_2 in the equation

The addition of the $\Phi_{clearance}$ factor to the closed-form equation increases the accuracy of the estimated capacity of glass configurations with substandard glass-to-frame clearances compared to Equation 6.13, which includes only the effect of glass type and configuration type. While the closed-form equation with the addition of the $\Phi_{clearance}$ factor predicts the experimental capacity of glass configurations (10-13) with substandard clearances with a remaining degree of inaccuracy, this is caused by inaccuracies inherit in the factors modeling glass type and configuration type, and a larger degree of experimental error in configurations such as (13) which only had one specimen of its type tested. As a result, the analysis shows that the $\Phi_{clearance}$ factor effectively adjusts the closed-form equation given the limitations. Also, this factor assumes that the clearances are uniform around the glass perimeter, because the factor

was developed on experimental tests of glass specimens where the clearances were uniform on all four sides of the glass panel.

6.5.3 Factor Development of: Φ_{system}

Continuing on with the factor development methodology (see Figure 6.7), the next factor formulated to modify the closed-form equation models the effects that SF type systems have on the failure performance of glass systems compared with CW type systems. Due to the different framing and glazing detailing of SF systems and how the systems are generally anchored to structural members compared with mid-rise CW systems, SF systems exhibit their own glass response behavior. It is desired to develop a less complex Φ_{system} factor because the SF experimental results as a whole are not precise enough to warrant specific values for various configurations such as the other factors. The SF drift failure data did not get reduced when flexibilities were discovered in the racking facility because no sensor testing was executed on SF specimens. As a result, the magnitude of the effect of facility flexibilities on the experimental data is unknown; however, more than likely, the flexibility existed during the SF experimental testing. Furthermore, the two data adjustments (initial cracking and crushing limit state redefining and constant amplitude failure check) were not performed on the SF configurations due to the lack of available "time vs. loading" charts. Between these two known discrepancies, it is probably the case that if the same SF configurations were tested again the failure drifts would be lower, but by a degree of magnitude which is

unknown. With renewed testing, however, the developed factor value will be able to be adjusted to reflect future experimental test results.

To find the current degree of accuracy of the closed-form equation for SF systems, a comparison is carried out between the predicted and experimental drift ratios. This comparison can be seen in Table **6.11** for SF configurations (7-9) of Table 3.1. In the table, Column A denotes the predicted drift ratio from the base equation, Column B the glass type factor value, Column C the configuration type factor value, and Column D compares the predicted drift ratio from the modified base equation (Equation 6.13) with the experimental failure values. The other two SF glass configurations (22 and 23) are not included because experimental cracking failure data is not available for those systems.

Table 6.11: Comparison of glass cracking drift ratios as predicted from the equation and experimentally observed for SF glass configurations (7-9)

	A	B	C	D	
	$2c_1 + 2c_2\left(\frac{h}{b}\right)^*$	Φ_{type}	Φ_{config}	Cracking Failure	
				$\theta_{predicted}$	$\theta_{experimental}$
7	0.0253	0.76	0.78	**0.0150**	**0.0417**
8	0.0372	0.76	0.98	**0.0277**	**0.0592**
9	0.0253	0.76	0.75	**0.0144**	**0.0573**

*The results are normalized and given in drift ratios where the predicted drift from the term is divided by the height of the configuration's glass panel

The table shows that there are significant differences between the predicted and experimental drift ratios for the SF configurations that a Φ_{system} factor needs to address. Overall, the closed-form equation underestimates the cracking capacity of SF glass

configurations (7-9) by an average of 64.0%, which was found by dividing the average predicted drift ratio by the average experimental drift ratio for the three SF configurations. This means that unlike the previously developed factors which alter the predicted cracking capacity of a given glass system in a moderate fashion, having a SF system compared to a CW system significantly changes the seismic glass panel failure performance. As a result, SF configurations need a factor that reflects this general significant increase in cracking capacity.

It is determined that the factor will take the form of a "*Y*" type factor (see Equation 6.8). It takes this form because the effect of a varying system (CW vs. SF) affects both seismic response behavior events of the glass panel during loading, and therefore both terms of the base equation (Equation 6.6) as well. With the addition of Φ_{system} factor, the closed-form equation is revised in the form of Equation **6.21**:

$$\Delta_{crack} = \Phi_{type}\Phi_{config}\Phi_{clearance}\Phi_{system}\left[2c_1 + \left(2c_2\left(\frac{h}{b}\right)\right)\right] \qquad \textbf{6.21}$$

To formulate the Φ_{system} factor and the magnitude of the values, an analysis is conducted that relates the predicted and experimental drift ratios for SF configurations (7-9). Table **6.12** summarizes the comparison, where Column A lists the predicted cracking drift ratio from previous Equation 6.15, Column B the experimental drift ratio, and Column C a ratio found by dividing the experimental values by the predicted values of Column A. Column C represents a hypothetical Φ_{system} value, which if used in

Equation 6.21 the predicted values would equal the experimental drift ratios for SF configurations.

Table 6.12: Comparison of predicted and experimental glass cracking drift ratio values with calculated needed factor values for application to the equation to equate the two values

ID	A	B	C
	$\theta_{predicted}$	$\theta_{experimental}$	$\frac{\theta_{experimental}}{\theta_{predicted}}$
7	0.0150	0.0417	2.78
8	0.0277	0.0592	2.14
9	0.0144	0.0573	3.98

Table 6.12 shows that the values for Column C vary across the SF configurations (7-9). The hypothetical factor values are all significant and on the order of between 2.14 and 3.98, which means that the experimental results are double to quadruple the current capacities estimated by the closed-form equation. While the values vary from one SF configuration to another, it is desired to have one Φ_{system} value that is used for SF configurations and another value (1.0) for CW systems to make the equation more user-friendly.

To be consistent with the trends in experimental data observed in Table 6.11 and depicted in Figure 6.4, the value of Φ_{system} should model that SF systems have a higher cracking capacity as compared with CW systems. The magnitude of Φ_{system} can be determined through the following steps: (1) find the lowest factor as the starting value, (2) assume facility flexibility by applying the data adjustment equation used on CW

specimens (see Equation 4.1) to the SF cracking experimental data, finding the percentage reduction as a result of the equation, and applying the same reduction to the factor value, and (3) round the value to a simple number. The other two data adjustments, which included one adjustment for the redefined initial cracking/crushing limit state and another adjustment that checked to ensure failure at the "constant amplitude" loading step, are not going to be considered in the Φ_{system} factor development. This is because the effect of these adjustments was not consistent like the facility flexibility data adjustment, and was glass specimen specific. Therefore, attempting to account for these adjustments in the SF Φ_{system} factor values would be misguided. Furthermore, the general 2.5% reduction for these two adjustments (see Section 5.1.2) was minor compared with the estimated 17.8% reduction in failure values for the SF failure values due to facility flexibility as found from Equation 4.1.

Using the defined procedure, the following calculations were performed:

(1): smallest of: [2.78, 2.14, 3.98] = 2.14

(2): The reductions as a result of the flexibility analysis for the SF data yielded an average reduction of 17.8% as calculated using Equation 4.1. Applying this reduction to the lowest factor value, the calculation yields a value of: 2.14 – 0.178(2.14) = 1.759

(3) To simplify the factor, it is rounded so that Φ_{system} for SF configurations is 1.75.

The results of such calculations are presented in Table **6.13** that summarizes the two separate values of Φ_{system}.

Table 6.13: Values of the Φ_{system} factor

System Type	Φ_{system}
CW	1.0
SF	1.75

With the magnitude of the Φ_{system} factor values determined for SF systems, a new comparison is made to find the accuracy of the revised closed-form Equation 6.21 with the Φ_{system} factor. Table **6.14** presents the analysis results for SF glass configurations (7-9, 22, 23) as listed in Table 3.1, where the predicted cracking drift ratios are compared with the experimental failure results. The percent difference between the predicted and experimental results are calculated in the last column was found by using Equation 6.14, where the percent difference is compared for the equation which models for SF systems and the closed-form equation that only models glass type and configuration (Equation 6.13).

The percent difference values for the predicted values from closed-form equation that considers SF configurations (Equation 6.21) are less than the percent difference values for Equation 6.13. While the percent differences still seem high, this buffer was designed in the value of the Φ_{system} factor because the experimental results for SF configurations have a larger uncertainty than the mid-rise CW configurations. It should be noted that because SF configurations (7, 9, and 22) have average glass-to-frame clearances of 0.41 in. (10 mm) which is below the considered standard clearance of 0.43 in. (11 mm), the $\Phi_{clearance}$ factor value for these configurations was slightly above 1.0.

Table 6.14: Comparison of predicted drift ratios with the experimental results with the addition of the Φ_{system} factor to the closed-form equation with SF configurations highlighted

	$2c_1 + 2c_2\left(\frac{h}{b}\right)^*$	Φ_{type}	Φ_{config}	$\Phi_{clearance}$	Φ_{system}	Cracking Failure		% Difference	
						θ_{pred}	θ_{exp}	Eq. 6.21	Eq. 6.13
7	0.0253	0.76	0.78	1.13	1.75	**0.0297**	**0.0417**	-28.7%	-64.0%
8	0.0372	0.76	0.98	1.0	1.75	**0.0484**	**0.0592**	-18.2%	-53.3%
9	0.0253	0.76	0.75	1.13	1.75	**0.0286**	**0.0573**	-50.1%	-74.8%
22	0.0253	0.99	0.78	1.13	1.75	**0.0387**	**n/a**	n/a	n/a
23	0.0372	0.99	0.98	1.0	1.75	**0.0631**	**n/a**	n/a	n/a

*The results are normalized and given in drift ratios where the predicted drift from the term is divided by the height of the configuration's glass panel

Overall, the Φ_{system} factor models for the general increase of cracking capacity that was observed experimentally for the SF configurations.

6.5.4 Factor Development of: Φ_{aspect}

The last factor to be fully developed is Φ_{aspect}, which is the exception from the method of development for the other factors because it is applied in a different fashion to the closed-form equation. The factor takes into account the aspect ratio of a glass panel, which is the height divided by the width (h:b). All of the glass configurations analyzed so far have had a glass aspect ratio of 6:5, with a glass panel height of 6 ft (1.8 m) and width of 5 ft (1.5 m). However, glass configurations (14) and (15) listed in Table 3.1 have aspect ratios of 2:1 and 1:2, respectively, and the experimental results of these

two configurations show that the Φ_{aspect} factor is generally needed to model the effects that a varying aspect ratio has on the failure performance of glass panels.

To determine how the inaccurate the equation is in predicting the cracking failure of glass configurations with varying aspect ratios, the predicted drift ratios from Equation 6.13 that only additionally considers glass type and configuration type is compared with the experimental results for glass configurations (14) and (15), as shown in Table **6.15**. In the table, Column A denotes the predicted drift ratio from the base equation, Column B the glass type factor value, Column C the configuration type factor value, and Column D compares the predicted drift ratio from the modified base equation (Equation 6.13) with the experimental failure values.

Table 6.15: Comparison of predicted glass cracking drift ratios with the experimental results for configurations with varying aspect ratios

	A	B	C	D	
	$2c_1 + 2c_2\left(\frac{h}{b}\right)^*$	Φ_{type}	Φ_{config}	Cracking Failure	
				$\theta_{predicted}$	$\theta_{experimental}$
14	0.0273	0.76	0.78	**0.0162**	**0.0181**
15	0.0273	0.76	0.78	**0.0162**	**0.0220**

*The results are normalized and given in drift ratios where the predicted drift from the term is divided by the height of the configuration's glass panel

The results in Table 6.15 show that the predicted cracking capacity underestimates the experimental failure results. Even though the closed-form equation has variables h and b in the second term, which takes into account the dimensions of a glass panel, it is apparent that a Φ_{aspect} factor is necessary to account for the effects of a

varied aspect ratio. In an attempt to find trends in the data between a glass panel's aspect ratio and experimental failure value, graphs are created comparing experimental drift ratios with the current predicted drift ratios. This comparison was performed for the data of glass configurations (1), (14), and (15) with aspect ratios 6:5, 2:1, and 1:2, respectively, as seen in Figure **6.10**. The first figure (a) presents the data in terms of drift ratios, while the second figure (b) presents the data in terms of drift in inches. It should be noted that the experimental drift displacement values in (b) were reduced to represent the displacement as experienced by only the glass panel during testing, and not the entire glass configuration, which is slightly larger due to the extended 9 in. height over which the displacement occurs in the BERL dynamic racking test facility.

A commonality between both figures is that the closed-form equation underestimates the experimental failure values of the glass configurations with varied aspect ratios of 1:2 and 2:1. Therefore, a Φ_{aspect} factor will be developed such that it increases predicted cracking capacity of glass configurations with varying aspect ratios. Ultimately both figures represent the same comparison between the predicted and experimental glass failure behavior, but in Figure 6.10b it can be seen that without putting the data in terms of drift ratio it appears that glass configuration (15) with aspect ratio 1:2 has the same cracking capacity as glass configuration (1) with a 6:5 aspect ratio, which is not the case. Furthermore, the current horizontal relationship between the predicted cracking capacities among the three configurations as seen in Figure 6.10a can realistically be seen when the data are put in the context of drift ratios.

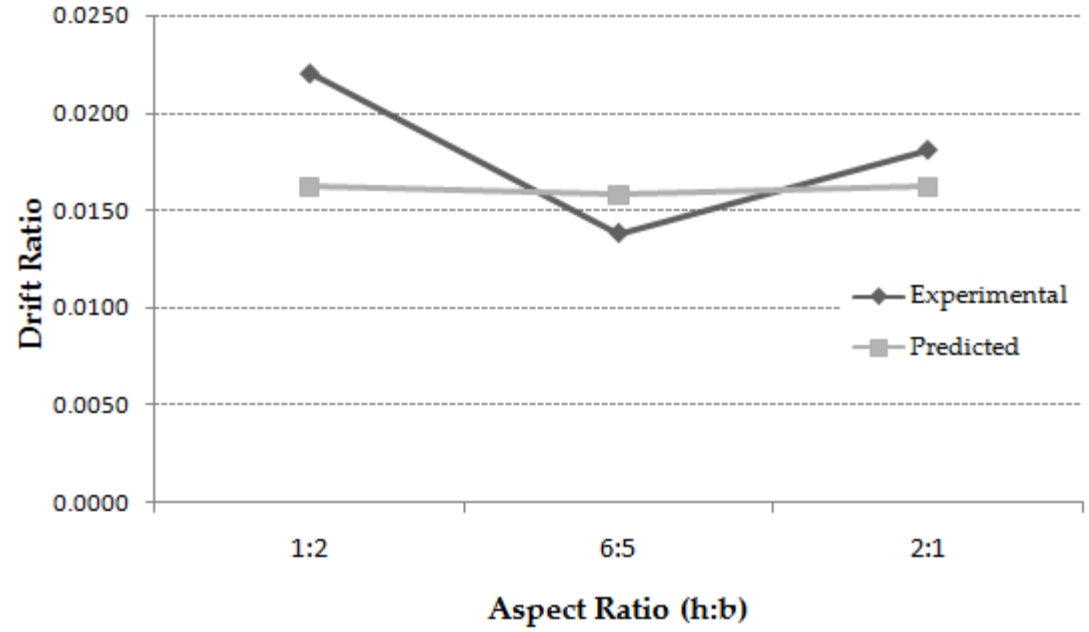

(a)

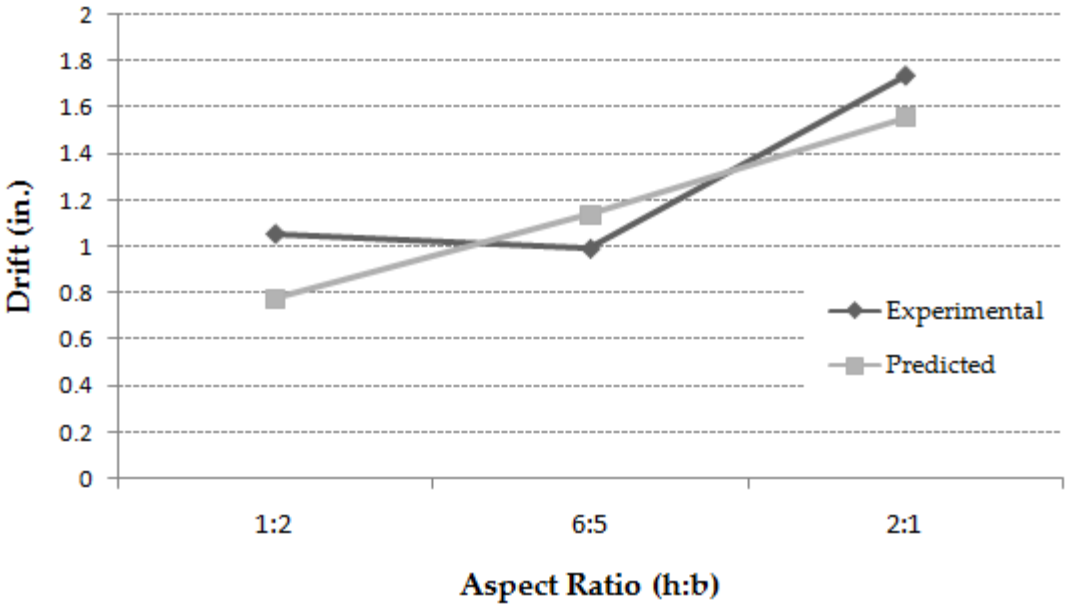

(b)

Figure 6.10: Comparison between experimental failure values and predicted glass cracking values with corresponding aspect ratio for a given AN-Mono glass configuration where (a) presents the data in drift ratio and (b) presents the data in terms of drift (in.)

The formulation and magnitude of the Φ_{aspect} factor will be based on the relationship that an aspect ratio of a glass panel has on the experimental failure performance of glass panels. Since the base equation considers the aspect ratio of a glass panel through the dimension variables *h* and *b*, the factor is formulated such that is compares the increase in experimental drift assumed to be caused by an aspect ratio with the change in predict drift attributed to a varying aspect ratio. In this respect, the Φ_{aspect} factor is similar to $\Phi_{clearance}$ because it corrects the equation instead of directly applying an experimental trend such as the Φ_{type} and Φ_{config} factors do. Furthermore, by controlling the other glazing variables and isolating the effect that aspect ratio has on the experimental failure values, the Φ_{aspect} factor can be applied to a system with any given glass type or configuration type. The limitations for developing this factor are characterized by the fact that only two data points are available for glass configurations with an aspect ratio other than 6:5, with one point associated with an aspect ratio greater and smaller than 6:5. Therefore, a linear relationship is assumed between the cracking capacities of configurations (14) and (15) with respect to the capacity of glass configuration (1) with a 6:5 aspect ratio. Experimental testing in follow-up studies can add more data points and refine the relationship.

In Figure 6.10a, data relationships are characterized by two different slopes of lines connected by points in the experimental data series; the first originates at glass configuration (1) with a 6:5 aspect ratio and extends to the experimental drift ratio for glass configuration (14) with a 2:1 aspect ratio, and the other originates at glass

configuration (1) but extends in the opposite direction to the experimental drift ratio for glass configuration (15) with a 1:2 aspect ratio. These linear relationships have absolute slope values of 0.01025 and 0.00614, respectively. The slope values were calculated by assuming Δy to be the change in drift ratio values, and Δx to be the difference between two aspect ratio values, where an aspect ratio value was determined by dividing the height by the width. For example, the aspect ratio value for glass configuration (1) with an aspect ratio of 6:5 is 1.2. Since the slopes of these two linear relationships are not similar, the Φ_{aspect} factor will consist of two separate definitions. The first definition will address situations where aspect ratios are greater than 6:5, and the second definition will address aspect ratios that are less than 6:5.

The Φ_{aspect} factor is developed to take the form of an "*X*" type factor (see Equation 6.7) so that it is only applied to the second term of the base equation. This is justified because the glass dimension variables *h* and *b* are only represented in the second term. As a result, it makes sense to apply the factor which accounts for a varying glass aspect ratio to the part of the equation that represents glass dimensions. With the addition of Φ_{aspect}, the closed-form equation is then defined by Equation **6.22**:

$$\Delta_{cracking} = \Phi_{type}\Phi_{config}\Phi_{clearance}\Phi_{system}\left[2c_1 + \Phi_{aspect}\left(2c_2\left(\frac{h}{b}\right)\right)\right] \qquad \textbf{6.22}$$

To calculate proper Φ_{aspect} factor values for use in Equation 6.22, three main steps are taken, where the first (1) is to find initial (ideal) Φ_{aspect} values for glass configurations (14) and (15) for use in the closed-form equation in the form of an adjustment value that is

only applied to the second term of the equation. This is accomplished by adding the extra capacity assumed to be caused by the aspect ratio of a glass panel minus any portion of this drift accounted for by the current predicted drift ratios because of a varying aspect ratio, and then equating this value to Equation 6.22 while keeping the value of Φ_{aspect} unknown, and solving for the unknown factor value. To find the initial factor values, the following calculations were performed resulting in Equation **6.23**. It should be noted that the variables were normalized into drift ratios for the calculations, but are denoted in drifts for illustrative purposes.

$$\Delta_{crack} + \Delta_{aspect} = \Phi_{type}\Phi_{config}\left[2c_1 + \Phi_{aspect}\left(2c_2\left(\frac{h}{b}\right)\right)\right]$$

$$\rightarrow \Phi_{aspect} = \frac{\Delta_{crack} + \Delta_{aspect} - \Phi_{type}\Phi_{config} \cdot 2c_1}{\Phi_{type}\Phi_{config} \cdot 2c_2\left(\frac{h}{b}\right)} \qquad \textbf{6.23}$$

where Δ_{crack} denotes the predicted capacity from Equation 6.13 for a given glass configuration, and Δ_{aspect} denotes the experimental drift increase as caused by a given glass panel aspect ratio relative to a similar configuration with a standard 6:5 aspect ratio that is not accounted for by predicted drifts, as determined from Equation **6.24**.

$$\Delta_{aspect} = \Delta_{aspect}^{exp} - \Delta_{aspect}^{pred} \qquad \textbf{6.24}$$

where $\Delta_{aspect\text{-}exp}$ denotes the increase in experimental drift that is assumed to be caused by a given glass panel aspect ratio x relative to a similar configuration with a standard 6:5 aspect as shown in Equation **6.25**, and $\Delta_{aspect\text{-}pred}$ denotes the predicted decrease in drift

from Equation 6.13 associated with a change in a standard aspect ratio to a given aspect ratio x for a glass configuration as found by Equation **6.26:**

$$\Delta_{aspect}^{exp} = \Delta_{x}^{exp} - \Delta_{6:5}^{exp} \qquad \textbf{6.25}$$

where $\Delta_{exp\text{-}x}$ denotes the experimental cracking drift for a glass configuration with a given aspect ratio x, and $\Delta_{exp\text{-}6:5}$ denotes the experimental drift for a similar configuration with a substandard 6:5 aspect ratio.

$$\Delta_{aspect}^{pred} = \Delta_{x}^{pred} - \Delta_{6:5}^{pred} \qquad \textbf{6.26}$$

where $\Delta_{pred\text{-}x}$ denotes the predicted cracking drift for a glass configuration with a given aspect ratio x, and $\Delta_{pred\text{-}6:5}$ denotes the predicted drift for a similar configuration with a standard 6:5 aspect ratio.

Using Equation 6.23, the initial Φ_{aspect} factor values for glass configurations (1), (14), and (15) are calculated and presented in Table **6.16:**

Table 6.16: Calculated initial factor values

ID	Aspect Ratio	Initial Φ_{aspect}
15	0.5	2.46
1	1.2	1.00
14	2.0	1.36

Then, the second step in the factor formulation is to (2) develop two separate linear relationships between the aspect ratio value and initial factor values found in Step (1) for configurations (14) and (15) with respect to the glass configuration (1) data, where a factor value of 1.0 is assumed for glass configurations (1). The linear relationships

produce equations that will relate any given aspect ratio value with a value representing the difference between the predicted drift ratio and expected capacity based on the experimental results of glass configurations (1), (14) and (15). The first relationship shown in Figure **6.11a** was created for instances where the aspect ratio of a given glass configurations is less than 6:5 (1.2), and was based on the data point sets from configurations (15) and (1). The other relationship in Figure 6.11b was created for the for instances where the aspect ratio of a given glass configuration is more than 6:5 (1.2), and was based on the data point sets from configurations (14) and (1).

Finally, the last step (3) is to define Φ_{aspect} factor values based on the linear equations found in Step (2) with rounded values. Using the linear relationships seen in Figure 6.11a and 6.11b, the values were rounded so that the Φ_{aspect} factor is defined by Equation **6.27**:

$$\Phi_{aspect} = \begin{cases} if\ aspect\ ratio \leq 6{:}5, then{:}\ \Phi = -2.09\left(\frac{h}{b}\right) + 3.5 \\ if\ aspect\ ratio > 6{:}5, then{:}\ \Phi = 0.45\left(\frac{h}{b}\right) + 0.46 \end{cases} \qquad \textbf{6.27}$$

where h and b are the height and width of the glass panel, respectively. As an example of factor values which result from the Φ_{aspect} factor definition, a sample set of aspect ratios is input into Equation 6.27 and the found values are organized into Table **6.17**:

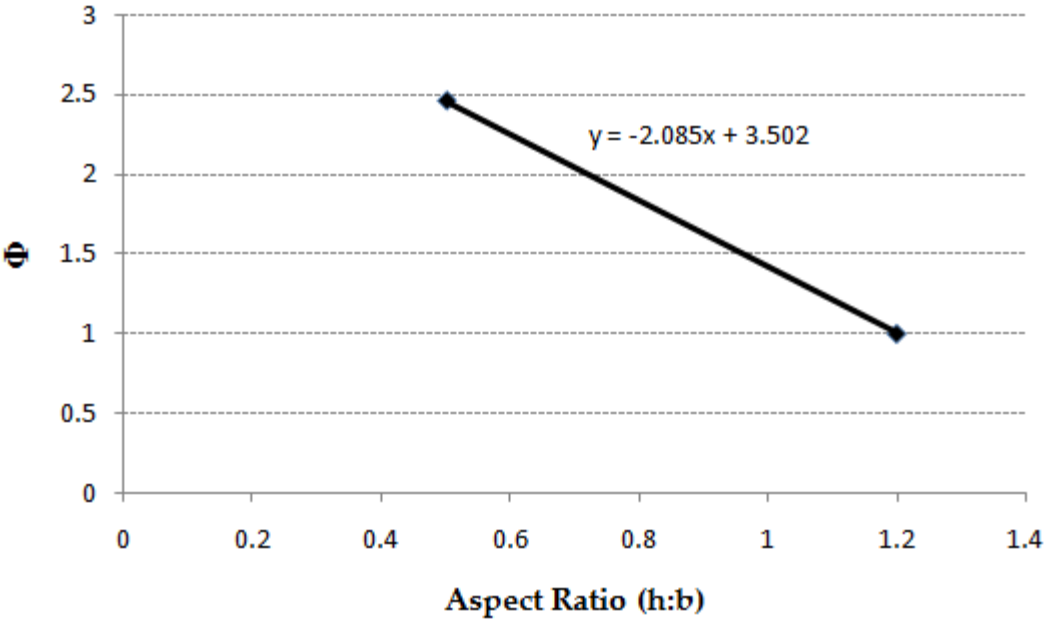

(a)

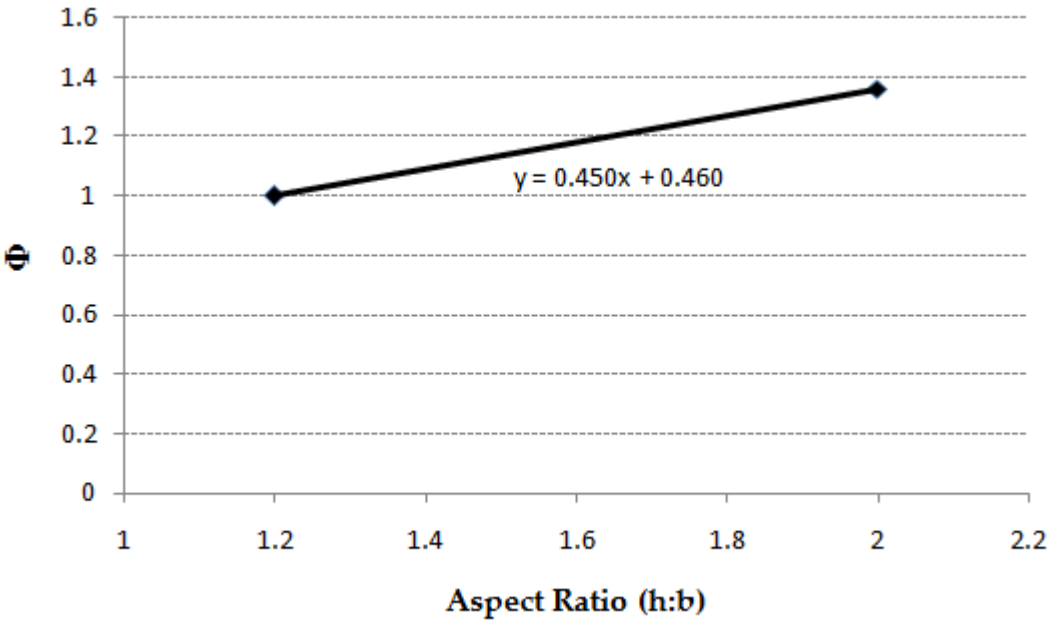

(b)

Figure 6.11: Developed linear equations for factor development based on data in Table 6.16 for (a) configurations (1) and (15) that account for aspect ratios less than standard (6:5) and for (b) configurations (1) and (14) that account for aspect ratios greater than standard (6:5)

Table 6.17: Sample values for the Φ_{aspect} factor for various aspect ratios

Aspect Ratio	Φ_{aspect}
1:2 (0.5)	2.46
3:4 (0.75)	1.93
6:5 (1.2)	1.0
3:2 (1.5)	1.14
2:1 (2.0)	1.36

To determine if the developed Φ_{aspect} factor accurately models the effects on capacity a given aspect ratio has on glass systems, the comparison analysis performed at the beginning of this subsection was repeated. Applying the developed Φ_{aspect} factor value found from Equation 6.27 to the revised closed-form Equation 6.22, the revised predicted drift ratios are compared with the experimental failure values in Table **6.18**. Furthermore, the predicted cracking drift ratio from Equation 6.13 that does not correct for a varying aspect ratio is compared with the experimental results as well. The results for glass configurations (1) as listed in Table 3.1 with a standard aspect ratio of 6:5 is shown for reference purposes.

Table 6.18: Comparison of predicted drift ratios from Equation 6.21 with the addition of the Φ_{aspect} factor and Equation 6.13 with the experimental cracking results for glass configurations (1), (14), and (15)

	$2c_1 + 2c_2\left(\frac{h}{b}\right)^*$	Φ_{type}	Φ_{config}	Φ_{aspect}	Cracking Failure		% Difference	
					θ_{pred}	θ_{exp}	Eq. 6.21	Eq. 6.13
1	0.0267	0.76	0.78	1.0	**0.0159**	**0.0138**	**14.8%**	14.8%
14	0.0273	0.76	0.78	1.36	**0.0201**	**0.0181**	**11.0%**	-10.4%
15	0.0273	0.76	0.78	2.46	**0.0241**	**0.0220**	**9.4%**	-26.4%

*The results are normalized and given in drift ratios where the predicted drift from the term is divided by the height of the configuration's glass panel

With the addition of the Φ_{aspect} factor, the inaccuracy of the closed-form equation shrinks for glass configurations (14) and (15) with varying aspect ratios from an average of 18.4% to 10.2%. These numbers were obtained by averaging the percent differences for configurations (14) and (15). Furthermore, the factor only models the effects that a given aspect ratio has on the experimental performance of a glass panel. Most of the inaccuracy remaining in the predicted values for glass configurations (14) and (15) is a result from the inaccuracies inherent in the applied factors that account for glass type and configuration type. As a result, the Φ_{aspect} factor is deemed a suitable method for modifying the base equation to account for the effects of varied glass aspect ratio.

In follow-up studies, it might be desirable to recalibrate the Φ_{aspect} factor so that it has a reference aspect ratio of 1:1 (1.0). This could be accomplished by performing laboratory tests on AN-Mono glass configurations with an aspect ratio of 1:1. Then, the data results could be added to the previous testing and new linear relations could be developed if necessary.

6.5.5 Factor Development: $\Phi_{connection}$

To account for the effects that a varied framing-to-structure connection has on the cracking seismic capacity of glass configurations in the closed-form equation, another factor is needed. In the test setup used, the frame-to-facility connection was extremely rigid and had negligible rotation, on which a more detailed discussion can be found in Section 5.3.1. However, connections in the field may have semi-rigid characteristics, where the magnitude of flexibility may vary from one type of connection to the next. Until laboratory testing is performed on various common connection types, the values of $\Phi_{connection}$ cannot be determined. It is assumed that the factor will add capacity to glass configurations, since the less rigid a connection is, the more rotation is allowed and subsequently the glass configuration will be able to withstand larger displacements before failure.

Since the factor $\Phi_{connection}$ represents a glass system detail that affects the entire glass configuration, it will take the form of a "Y" factor type. With the addition of the factor, the equation is then defined by Equation **6.28**:

$$\Delta_{crack} = \Phi_{type}\Phi_{config}\Phi_{clearance}\Phi_{system}\Phi_{connection}\left[2c_1 + \Phi_{aspect}\left(2c_2\left(\frac{h}{b}\right)\right)\right] \quad \textbf{6.28}$$

For now, the factor $\Phi_{connection}$ will be kept equal to 1.0, which is considered conservative. However, as different types of common mullion-to-structure connections get tested in the laboratory in possible future studies, better estimates of the effect of various connections will be obtained.

For the development of the $\Phi_{connection}$ factor, some of the common types of connections used currently in construction are identified here. The information was gathered from interviews with glass CW professionals (Chrisman 2009, Harmon 2009). It was found that the most common types of mullion-to-structure connections are cast-in-place edge of slab channels with a bolted anchor clip assembly, cast-in-place edge of slab embed plates with welded anchor clips, or cast-in-place top of slab channels with a bolted anchor clip assembly. Figure **6.12** illustrates a typical edge of slab cast-in-place Halfen® channel embed with bolted anchor clip assembly, where in this case the clip is multi-adjustable. Two profile details of this type of mullion-to-structure connection can be seen in Figure **6.13**, where (a) has a profile view as from the side and (b) has a profile view as from the top. For the top of slab cast-in-place channels with bolted anchor clip assembly mullion-to-structure connections, Figure **6.14** depicts a profile view of the connection from the side.

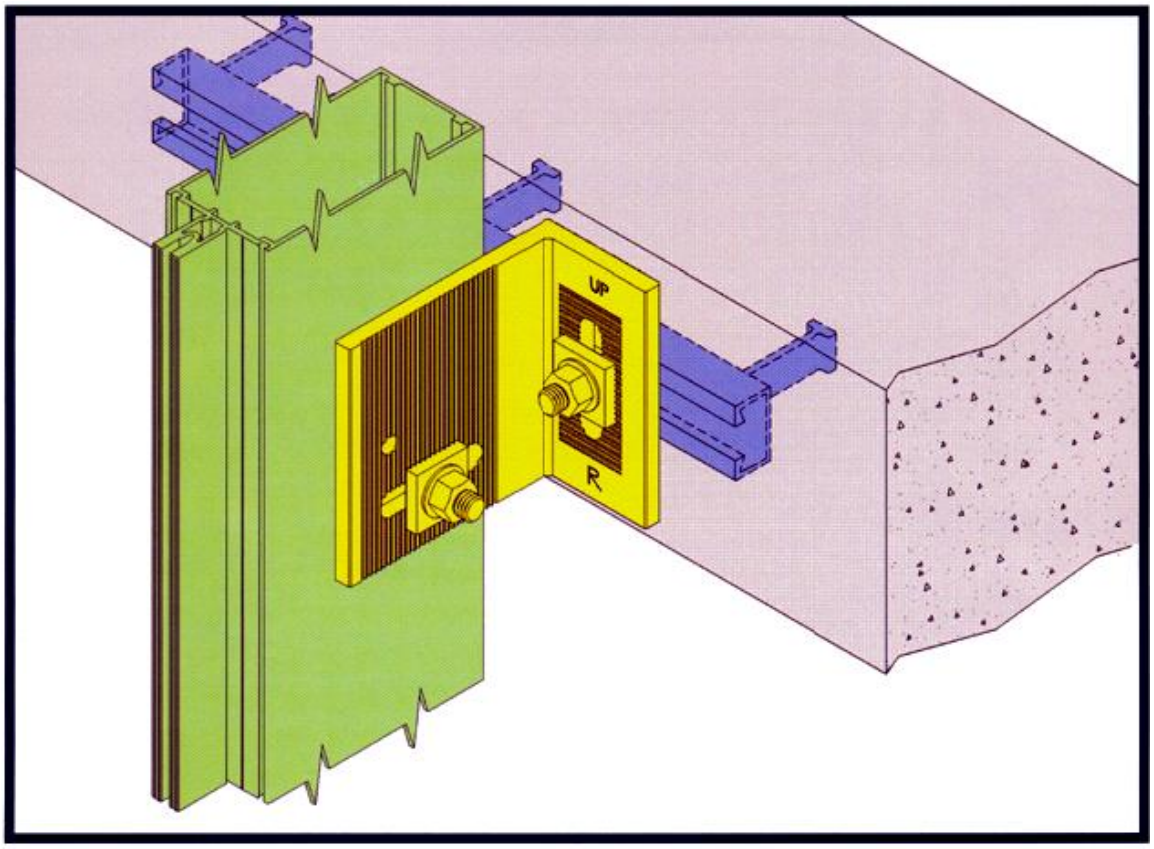

Figure 6.12: View of typical cast-in-place channel embed (edge of slab) with bolted anchor clip assembly where the clip is multi-adjustable (www.halfenusa.com)

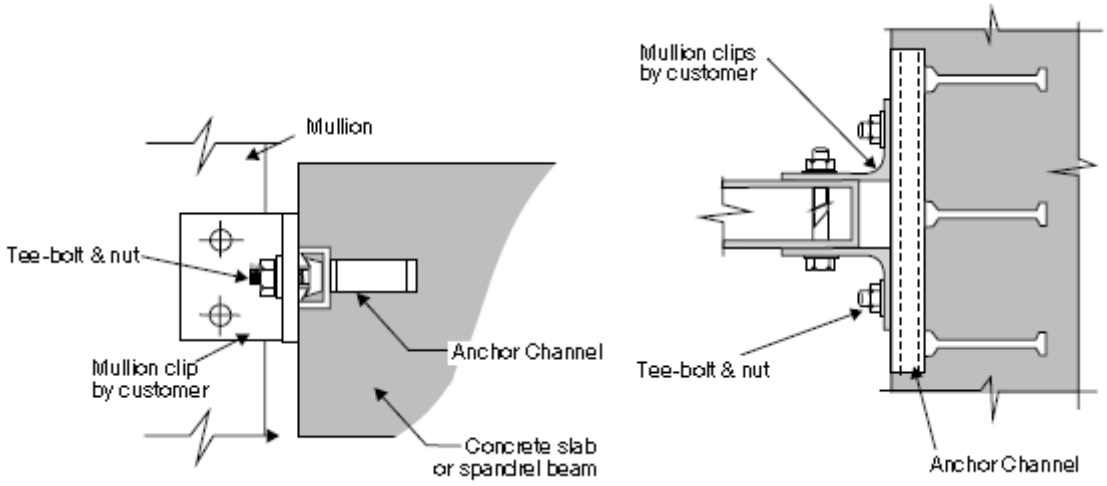

Figure 6.13: Profile view of a typical edge of slab cast-in-place channel embed with bolted anchor clip assembly from (a) the side and (b) overhead (www.halfenusa.com)

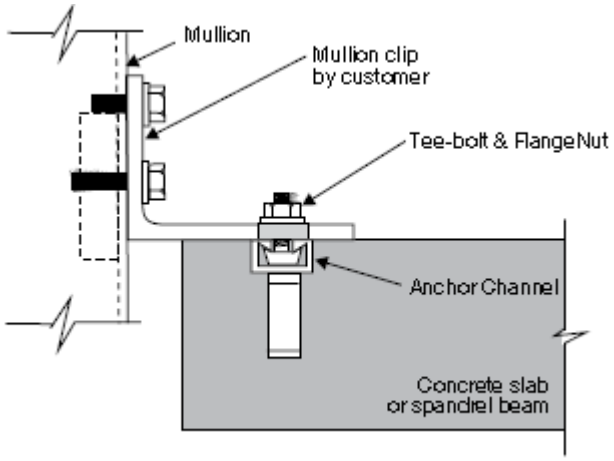

Figure 6.14: Profile view of a typical top of slab cast-in-place channel embed with bolted anchor clip assembly from the side (www.halfenusa.com)

Equally less common mullion-to-structure connections include welded clips to the steel deck edge and drilled wedge anchors. These types of connections are normally only utilized when other limitations eliminate the possibility of using the other

connections described previously. This is due to the increased costs associated with the labor and skills required to install the connections.

6.6 Closed-Form Equation Summary

The developed closed-form equation predicts the drift that causes cracking failure while considering various glazing and configuration details of a glass system through the application of factors. Specifically, the equation takes into account the glass type (AN, HS, FT), glass configuration (Mono, Lami, sym. IGU, asym. IGU), glass system (CW or SF), substandard glass-to-frame clearances, aspect ratio, and is designed to consider mullion-to-structure connection type in the future. The equation as defined in Equation 6.1 is shown below, and the definitions of all factors are summarized in Table **6.19**.

$$\Delta_{crack} = \Phi_{type-config}\Phi_{clearance}\Phi_{system}\Phi_{connection}\left[2c_1 + \Phi_{aspect}\left(2c_2\left(\frac{h}{b}\right)\right)\right]$$

Table 6.19: Summary of definitions for the factors in the closed-form equation

<table>
<tr><th>Factor</th><th>Definition</th></tr>
<tr><td>Φ_{type}</td><td>
<table>
<tr><th></th><th>Φ</th></tr>
<tr><td>AN</td><td>0.76</td></tr>
<tr><td>HS</td><td>0.94</td></tr>
<tr><td>FT</td><td>0.99</td></tr>
</table>
</td></tr>
<tr><td>Φ_{config}</td><td>
<table>
<tr><th></th><th>Φ</th></tr>
<tr><td>Mono</td><td>0.78</td></tr>
<tr><td>Lami</td><td>0.75</td></tr>
<tr><td>Sym. IGU</td><td>0.96</td></tr>
<tr><td>Asym. IGU</td><td>1.10</td></tr>
</table>
</td></tr>
<tr><td>$\Phi_{clearance}$</td><td>$$1.0 \leq \Phi_{clearance} = -4.25x + 2.86$$
where x denotes glass-to-frame clearance (in.)</td></tr>
<tr><td>Φ_{system}</td><td>
<table>
<tr><th></th><th>Φ</th></tr>
<tr><td>CW</td><td>1.0</td></tr>
<tr><td>SF</td><td>1.75</td></tr>
</table>
</td></tr>
<tr><td>Φ_{aspect}</td><td>$$\Phi_{aspect} = \begin{cases} if\ aspect\ ratio \leq 6{:}5, then{:}\ \Phi = -2.09\left(\frac{h}{b}\right) + 3.5 \\ if\ aspect\ ratio > 6{:}5, then{:}\ \Phi = 0.45\left(\frac{h}{b}\right) + 0.46 \end{cases}$$
where h and b denote the height and width of a glass panel, respectively</td></tr>
<tr><td>$\Phi_{connection}$</td><td>1.0</td></tr>
</table>

6.6.1 Final Comparison with ASCE Equation

The accuracy of the final formulated closed-form equation is calculated and compared with the accuracy of the ASCE equation. The accuracy is determined by finding the percent difference of the predicted drift ratios of a given glass system with respect to the experimental results, as determined from Equation 6.14. The analysis and results are summarized in Table **6.20**.

Overall, the average of the absolute percent differences decreases from 26.3% for the ASCE equation to 17.5% for the formulated equation. From these figures, it can be concluded that the closed-form equation improves the accuracy of the predicted capacities of glass systems by a relative 33% compared to the ASCE equation. It is also noted that the proposed equation tends to be more conservative than the ASCE equation, which is concluded from the fact that 13 out of 22 glass configurations have percent differences that are negative for the proposed equation (Equation 6.1).

Moreover, the closed-form equation is more consistent in the degree of inaccuracy of any given glass configuration compared with the ASCE equation. This is illustrated by the high percent difference values of the ASCE equation, such as 93.7% for glass configuration (1), which are not present for the formulated closed-form equation. This condition can be seen in Figure **6.15** where the percent differences for the proposed

Table 6.20: Calculated percent difference between predicted glass cracking drift ratios from the formulated closed-form and ASCE equations and experimental cracking drift ratios for all glass configurations

	θ_{ASCE}	Φ_{type}	Φ_{config}	$\Phi_{clear.}$	$\Phi_{sys.}$	Φ_{aspect}	Cracking Failure		% Difference	
							θ_{pred}	θ_{exp}	Eq. 6.1	ASCE
1	0.0267	0.76	0.78	1.0	1.0	1.0	**0.0159**	**0.0138**	14.8%	93.7%
2	0.0267	0.76	0.96	1.0	1.0	1.0	**0.0195**	**0.0237**	-17.6%	13.0%
3	0.0267	0.76	1.10	1.0	1.0	1.0	**0.0224**	**0.0279**	-19.9%	-4.2%
4	0.0267	0.76	1.10	1.0	1.0	1.0	**0.0224**	**0.0270**	-17.3%	-1.0%
5	0.0267	0.76	1.10	1.0	1.0	1.0	**0.0224**	**0.0270**	-17.3%	-1.0%
6	0.0267	0.76	0.75	1.0	1.0	1.0	**0.0152**	**0.0161**	-5.1%	66.5%
7	0.0253	0.76	0.78	1.13	1.75	1.0	**0.0297**	**0.0417**	-28.7%	-39.2%
8	0.0372	0.76	0.98	1.0	1.75	1.0	**0.0484**	**0.0592**	-18.2%	-37.2%
9	0.0253	0.76	0.75	1.13	1.75	1.0	**0.0286**	**0.0573**	-50.1%	-55.8%
10	0.0000	0.76	0.78	2.33	1.0	1.0	**0.0106**	**0.0088**	19.9%	-100.0%
11	0.0076	0.76	0.78	2.33	1.0	1.0	**0.0106**	**0.0085**	24.8%	-9.7%
12	0.0153	0.76	0.78	1.80	1.0	1.0	**0.0163**	**0.0147**	10.8%	3.9%
13	0.0153	0.76	0.96	1.80	1.0	1.0	**0.0201**	**0.0142**	41.5%	7.7%
14	0.0273	0.76	0.78	1.0	1.0	1.36	**0.0201**	**0.0181**	11.0%	51.1%
15	0.0273	0.76	0.78	1.0	1.0	2.46	**0.0241**	**0.0220**	9.4%	24.1%
16	0.0267	0.94	0.78	1.0	1.0	1.0	**0.0196**	**0.0241**	-18.8%	10.8%
17	0.0267	0.94	0.96	1.0	1.0	1.0	**0.0241**	**0.0266**	-9.2%	0.6%
18	0.0267	0.94	0.75	1.0	1.0	1.0	**0.0188**	**0.0221**	-14.9%	20.7%
19	0.0267	0.94	1.10	1.0	1.0	1.0	**0.0276**	**0.0261**	5.8%	2.3%
20	0.0267	0.94	1.10	1.0	1.0	1.0	**0.0276**	**0.0285**	-3.0%	-6.2%
21	0.0267	0.99	0.78	1.0	1.0	1.0	**0.0206**	**0.0244**	-15.2%	9.8%
22	0.0253	0.99	0.78	1.13	1.75	1.0	**0.0387**	**n/a**	n/a	n/a
23	0.0372	0.99	0.98	1.0	1.75	1.0	**0.0631**	**n/a**	n/a	n/a
24	0.0267	0.99	1.10	1.0	1.0	1.0	**0.0291**	**0.0332**	-12.3%	-19.5%
ABS. AVG									**17.5%**	26.3%

equation and ASCE equation are compared graphically for each glass configuration as listed in Table 3.1.

Finally, the cracking experimental failure drift ratios and the predicted cracking drift ratios for the proposed and ASCE equations are graphically compared for each glass configuration in Figure **6.16**. Referring to the graph, it can be seen how the ASCE predicted cracking drift ratios have been modified through the application of the factors in the form of the proposed equation relative to the experimental results. In the graph, glass configurations (3-5) as listed in Table 3.1 were combined into one data point, because the only glazing characteristics that differs between these three configurations is glass thickness and PVB interlayer thickness, and ultimately the three configurations together represent the performance of AN asymmetric IGU type glazing systems. In this process, the experimental cracking values for the configurations were averaged, although both equations predict the same cracking capacities across the three configurations and did not need to be averaged. The same process was applied to glass configurations (19) and (20), because those two glass configurations together represent HS asymmetric IGU type glazing systems.

Overall, the graph shows that the predicted cracking drift ratios from the proposed equation more closely mirrors the experimental cracking results and trends seen across the different glass configurations than the predicted cracking drift ratios from the ASCE equation. For glass configurations (1-6), which generally represent CW systems with AN glass of varying glass panel configurations, the proposed equation reflects the greater experimental capacities of the IGU configurations (2-5) compared with the Mono and Lami configurations of (1) and (6), respectively. However, the

predicted drift ratios from the ASCE equation do not change across these same configurations. Then, the proposed equation better reflects the increase in experimental cracking capacity of SF glass configurations (7-9) compared with the ASCE equation. For glass configurations (10-13) with substandard glass-to-frame clearances, the proposed equation eliminates the large cracking capacity inaccuracy of the ASCE equation for glass configuration (10) with a 0 in. (0 mm) glass-to-frame clearance. For glass configurations (14) and (15) with varying glass panel aspect ratios, the graph shows that the proposed equation follows the trend seen with the experimental cracking results with a slight degree of difference, while the ASCE equation generally significantly overestimates the cracking capacity of those systems. Finally, for glass configurations (16-24) that represent systems with HS and FT type glass (with (22) and (23) not included because of lack of experimental cracking data), it can be seen that the predicted cracking values from the proposed equation generally follows the increases and decreases of the cracking experimental results for those systems. However, the ASCE equation has the same predicted cracking drift ratio for all of those glass configurations.

A shortcoming of the proposed equation is that for select glass configurations the ASCE equation has a predicted drift ratio that is closer to the experimental results than the predicted cracking drift ratio from the proposed equation. This is the case for AN asym. IGU configurations, glass configurations (11-13) with substandard clearances, and a couple seemingly random glass configurations with HS or FT glass types. Although,

this condition is not unforeseen, because the ASCE equation which does not change its predicted values for glass configurations (1-6), (16-21), and (24) is expected to have values that is very close to the experimental results for at least one glass configuration. It happens that this condition exists for a few data points as seen in Figure 6.16 for glass configurations (1-6), (16-21), and (24). Then, for glass configurations (11-13), the inaccuracy in the proposed equation is a result of limitations with the glass type factor values, specifically with the value for AN that overestimates the capacity of AN-Mono glass configurations by 14.8%. If this factor value is refined through further laboratory testing and becomes more accurate, then the predicted values for all glass configurations with AN glass (i.e., glass configurations (11-13) with substandard clearances) will become more accurate as well. Also, for glass configuration (13), there was only one glass specimen of this glass configuration that was tested. It is assumed that more testing of this glass configuration will yield a greater glass cracking experimental capacity, at which point the predicted cracking drift ratio from the proposed equation would become more accurate. Overall, though, despite that for a few glass configurations (or data points) the ASCE equation is more accurate than the proposed equation, ultimately the proposed closed-form equation offers predicted cracking drift ratios that correspond to the experimental cracking results and trends across the varying glass configurations in Figure 6.16.

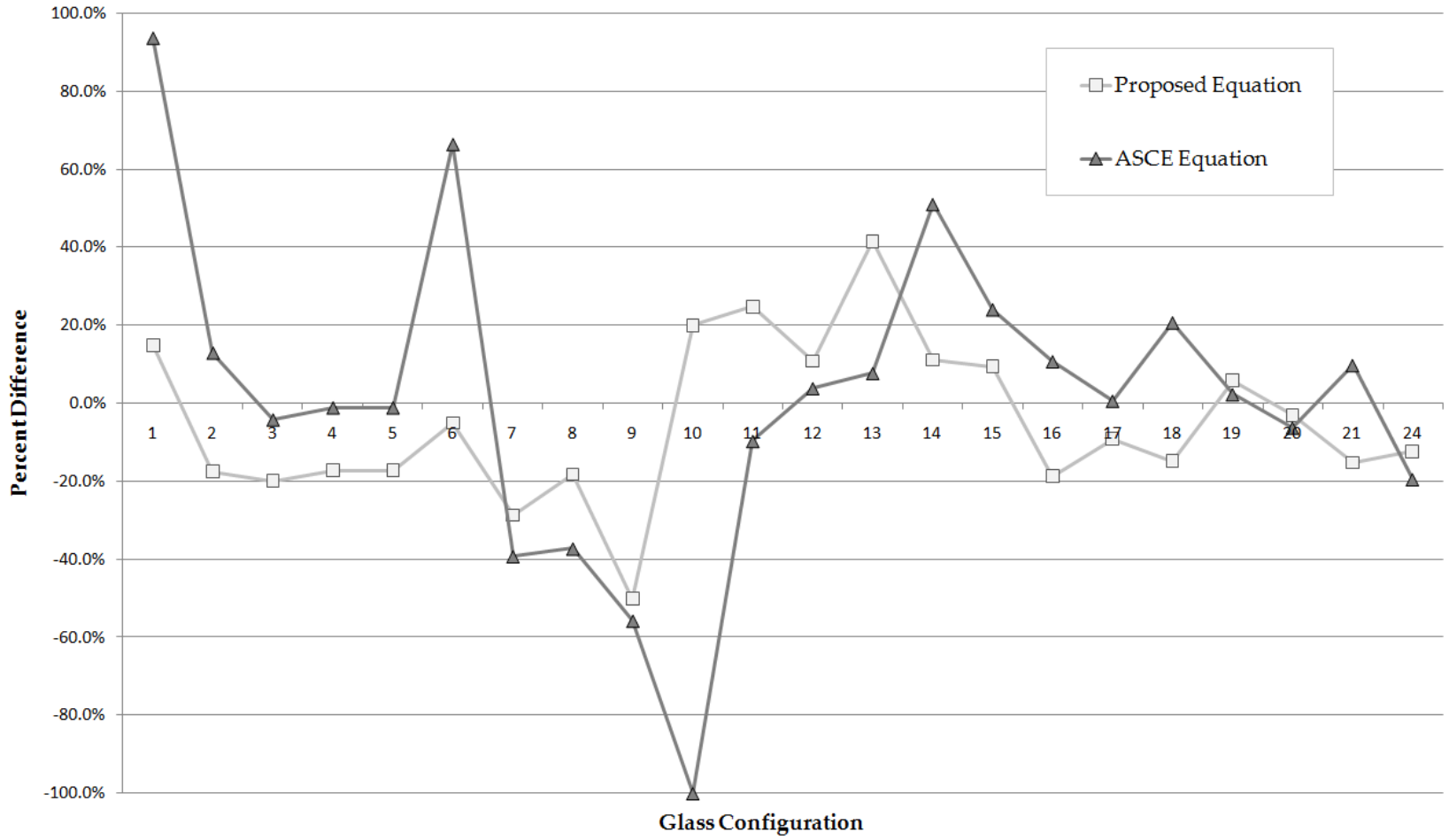

Figure 6.15: Comparison of the percent differences between the proposed equation and ASCE equation for each glass configuration as listed in Table 3.1

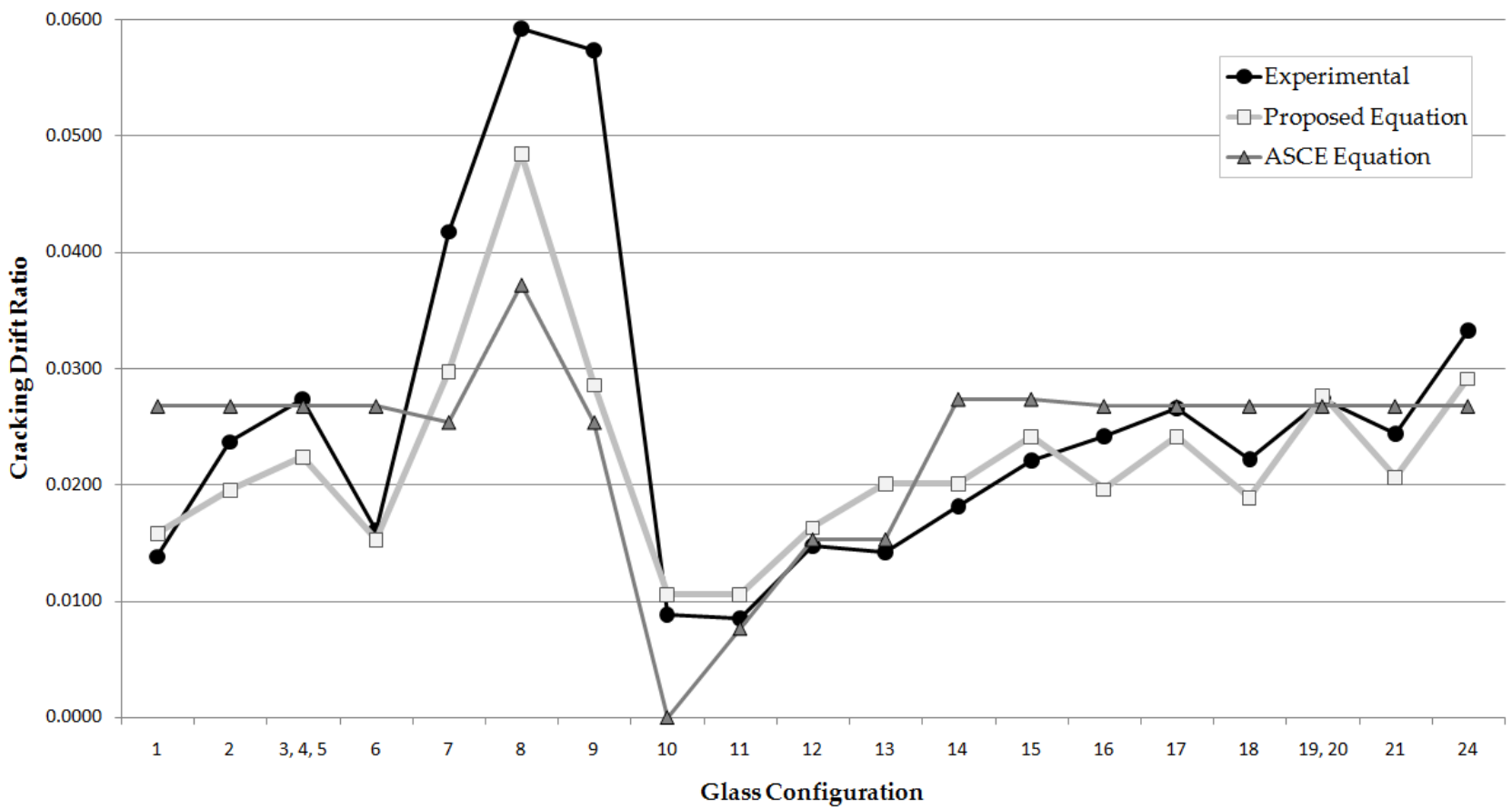

Figure 6.16: Graphical comparison of the predicted cracking drift ratio from the proposed equation, predicted cracking drift ratio from the ASCE equation, and the experimental failure drift ratio for the glass configurations

6.6.2 Random Specimen Accuracy Analysis

Another method that can be used to assess the accuracy of the proposed closed-form equation is to evaluate the accuracy of the equation with the experimental results for randomly selected individual glass specimens. The accuracy is reflected in the percent difference values found between the experimental failure values and the predicted drift ratio from the equation. Then, another percent difference calculated for the same data points with the ASCE equation can be compared with the percent differences for the closed-form equation.

For the sampling, ten specimens were randomly chosen from the compiled experimental data. The calculated percent differences for the selected specimens are summarized in Table **6.21**, where Column A denotes the specimen's configuration type as listed in Table 3.1, Column B the original specimen numbering (see Appendix A.1), Column C the experimental failure drift ratio, Column D the predicted drift ratio from the formulated (Equation 6.1) closed-form equation and ASCE equation, respectively, and Column E the calculated percent differences of the predicted values with respect to the experimental drift ratios for both equations as found by Equation 6.14.

Table 6.21: Calculated percent differences between predicted (closed-form and ASCE) drift ratios and experimental failure values for ten random glass specimens

A	B	C	D		E	
Group ID	**Original Specimen ID**	θ_{exp}	θ_{pred}		**% Difference**	
			Eq. 6.1	**ASCE**	**Eq. 6.1**	**ASCE**
1	1-5	0.0142	0.0159	0.0267	12.1%	88.3%
5	C-3	0.0275	0.0224	0.0267	-18.5%	-2.9%
6	SR 41	0.0142	0.0152	0.0267	7.2%	88.3%
6	Config G and UMR	0.0195	0.0152	0.0267	-22.0%	37.0%
9	2-1	0.0494	0.0286	0.0253	-42.1%	-48.8%
12	3/28/2008	0.0142	0.0163	0.0153	14.8%	7.9%
15	Dec 2006	0.0239	0.0241	0.0273	0.7%	14.1%
17	UMR -3	0.0248	0.0241	0.0267	-2.8%	7.7%
19	D-4	0.0275	0.0276	0.0267	0.5%	-2.7%
20	E-2	0.0301	0.0276	0.0267	-8.3%	-11.3%
ABS. AVG					**12.9%**	**30.9%**

The results of the analysis in Table 6.21 show that the proposed closed-form equation was significantly more accurate than the ASCE equation for this random sample. The absolute average of the percent differences for the ten specimens was 12.9% for Equation 6.1, while it was 30.9% for the ASCE equation. These numbers reflect the findings in the previous accuracy analysis for the data of all glass configurations (see Table 6.20) where the percent difference was found to be 17.5% and 26.3% for Equation 6.1 and the ASCE equation, respectively. Considering the outcome of both of the analyses, it can be concluded that the proposed closed-form equation improves the ability to predict the cracking failure drift limit of glass panels.

6.6.3 Example

As an example involving the closed-form equation, assume that a user desires to predict the drift that a proposed glass panel in a building can sustain before experiencing the cracking limit state. The glass panel is an 8 ft high by 4 ft wide (2.4 m x 1.2 m) asymmetric IGU, with an inner 0.25 in. (6 mm) AN-Mono pane, and an outer Lami unit with 0.25 in. (6 mm) HS lites in between a 0.060 in. (1.5 mm) PVB interlayer. The system utilizes a framing system comparable to the mid-rise CW Kawneer 1600™ framing system, and has a 0.25 in. (6 mm) glass-to-frame clearance.

Before the glass cracking drift limit equation can be utilized, the factor values need to be determined. The procedures and calculations used to find these values are seen in Table **6.22**. Then, the determined factor values are input into the closed-form equation (Equation 6.1) along with applicable design-specific values, such that predicted cracking capacity in terms of drift is found for the user glass panel as follows:

$$\Delta_{crack} = (0.94)(1.1)(1.80)(1.0)(1.0)\left[2(0.25\ in.) + (1.36)\left(2(0.25\ in.)\left(\frac{8\ ft}{4\ ft}\right)\right)\right]$$

$$= 3.46\ in.\ (88\ mm)$$

Table 6.22: Calculated factor values for example above

<table>
<tr><th>Factor</th><th>Determined Values</th></tr>
<tr><td>Φ_{type}</td><td>
<table>
<tr><th></th><th>Φ</th></tr>
<tr><td>AN</td><td>0.76</td></tr>
<tr><td>HS</td><td>0.94</td></tr>
<tr><td>FT</td><td>0.99</td></tr>
</table>
Φ_{type} = 0.94
</td></tr>
<tr><td>Φ_{config}</td><td>
<table>
<tr><th></th><th>Φ</th></tr>
<tr><td>Mono</td><td>0.78</td></tr>
<tr><td>Lami</td><td>0.75</td></tr>
<tr><td>Sym. IGU</td><td>0.96</td></tr>
<tr><td>Asym. IGU</td><td>1.10</td></tr>
</table>
Φ_{config} = 1.10
</td></tr>
<tr><td>$\Phi_{clearance}$</td><td>$\Phi_{clearance}$ = -4.25(0.25) + 2.86 = 1.80</td></tr>
<tr><td>Φ_{system}</td><td>
<table>
<tr><th></th><th>Φ</th></tr>
<tr><td>CW</td><td>1.0</td></tr>
<tr><td>SF</td><td>1.75</td></tr>
</table>
Φ_{system} = 1.0
</td></tr>
<tr><td>Φ_{aspect}</td><td>Φ_{aspect} = 0.45(8 ft / 4 ft) + 0.46 = 1.36</td></tr>
<tr><td>$\Phi_{connection}$</td><td>1.0</td></tr>
</table>

The proposed closed-form estimates that the given configuration has a cracking drift capacity of 3.46 in. (88 mm). This is in comparison to the ASCE equation that estimates the cracking drift capacity of the same configuration to be 1.50 in. (38 mm).

6.6.4 Results and Conclusions

The closed-form equation uses the ASCE 7-05 equation as its base, and then was formulated with the application of various factors to modify the equation for glazing characteristics that the ASCE equation does not consider. While a pilot study by Memari et al. (2007) showed that a finite element model predicting the seismic performance of architectural glass in an open-form approach has potential, further research needs to be performed on FEM of architectural glass systems before a practical design model can be developed. It was found that the ASCE equation predicted the experimental cracking failure with a 26.3% inaccuracy, but because the underlying geometric model of the equation is sound it was used in the formulation of the proposed equation. The terms representing two glass responses were separated (see Equation 6.6) so that factors could be targeted to certain variables.

Factors were developed in a methodical order, and were based on trends extracted from the experimental data caused by isolating the various glazing variables that are known to effect glass capacity failure values (see Appendix A.2). First the Φ_{type} and Φ_{config} factors were created in parallel to account for glass type and configuration type, respectively. An alternative method where glass type and configuration type were developed in an integrated fashion in a $\Phi_{type\text{-}config}$ factor was found not to align with the overall equation development approach, but is detailed in Appendix B for reference purposes. Then, $\Phi_{clearance}$, Φ_{system}, and Φ_{aspect} factors were developed to account for substandard clearances, type of system, and varying aspect ratios, respectively, relative

to predicted values offered by the equation with application of the Φ_{type} and Φ_{config} factors such that glass type and configuration type effects were controlled for. Since the base equation has variables that account for clearance and dimensions of a glass panel, the $\Phi_{clearance}$ and Φ_{aspect} factors specifically were formulated based on the experimental failure capacity caused by the respective glazing variable that were not already accounted for by the equation. While the magnitude of effect of each of the factors varies from one glass configuration to another, in general the predicted cracking drift is most sensitive to the base of the closed-form equation (see Equation 6.6).

Overall, the proposed equation with applied factors as defined in Table 6.19 is relatively easy to use. For the base of the equation, only glass-to-frame clearance and panel dimensions need to be input. Then for values of the Φ_{type}, Φ_{config}, and Φ_{system} factors, a user only has to select a correct factor value, because they are based on discrete sets of variables. Then, for the $\Phi_{clearance}$ and Φ_{aspect} factors, if the clearance or aspect ratio is not standard the value of this characteristic is input into the equation to produce a factor value, otherwise the factor is equal to 1.0. Since the calculations can be performed using a standard calculator, the proposed closed-form equation has been formulated such that it is simple to utilize.

The proposed closed-form equation has been shown to significantly improve the predicted cracking capacity of glass systems as compared to the ASCE equation, and therefore has the potential to be a useful architectural glass design tool for professionals. In the overall comparison analysis, the closed-form equation was shown in shrink the

percent difference (Equation 6.14) between the experimental and predicted values from 26.3% from the ASCE equation to 17.5%, which is a significant improvement. Also, a comparison between the percent differences of the proposed and ASCE equations in Figure 6.15 showed that the proposed equation is more consistent and eliminates large inaccuracies for any given glass configuration. Furthermore, a graphical comparison in Figure 6.16 between the predicted cracking drift ratios of the proposed and ASCE equations and experimental cracking results for the glass configurations as listed in Table 3.1 showed that ultimately the proposed closed-form equation offers predicted cracking drift ratios that more closely correspond to the experimental cracking results and trends across the varying glass configurations compared to the ASCE equation. Then, an accuracy analysis of randomly selected glass specimens showed similar results, where the predicted values from the proposed equation and the ASCE equation were 12.9% and 30.9%, respectively, off from the experimental results of the glass specimens. The remaining inaccuracies are mostly a result from modeling limitations with the $\Phi_{clearance}$ and Φ_{aspect} factors, that were described in detail in Section 6.4.

To illustrate the effects that differences in the accuracy between the ASCE and proposed equation exhibit, consider the following example. Assume a building has a 20,000 sq. ft. AN-IGU glazing system with details similar to glass configuration (2) as listed in Table 3.1. If an earthquake produces an interstory drift ratio for all building stories equal to the experimental capacity (0.0237) of glass configuration (2), the ASCE equation would underestimate the number of glass panels expected to crack by 40%

relative to the predicted drift ratio from the closed-form equation. This difference is found through the use of the fragility functions, where the predicted cracking drift ratio of 0.0267 and 0.0195 for the ASCE equation and the proposed equation, respectively, was input to obtain the probability of failure. Then, if it is assumed that is costs \$40/ft^2 to repair cracked AN-IGU panels, it is calculated that \$320,000 in repair costs would be unaccounted for in a design analysis using the predicted capacity from the ASCE equation as opposed to the closed-form equation.

The proposed closed-form equation has applications for many different types of CW and SF systems. However, follow-up studies and analysis on available data can extend the reach of the equation to glass systems with other glazing characteristics. Specifically, it would be desired to modify the equation so that it considers wet-glazed (i.e., structural silicone glazing) systems, unitized systems, and the effects of other commonly employed mullions-to-structure connections.

Chapter 7

Laboratory Versus Field Conditions Investigation for Practical Application

This chapter details an investigation into how some of the conditions on an actual building in the field compares with the laboratory testing conditions for the CW and SF glass systems, and how some differences could affect the applicability of the experimental findings. Section 7.1 examines how connection detailing differentiates between the experimental studies and glass system applications in the field. Section 7.2 details the practical application of the experimental results for individually tested glass panels to entire exterior glass systems on an actual building. Section 7.3 reviews the results and conclusions reached in the investigations performed in this chapter.

7.1 Connection Detailing

On actual buildings, the glass system mullion-to-structure connections (or anchors) are varied from one system to another. Therefore, the likely flexibility due to the connections of a given framing system during seismic loading will vary as well. The flexibility resulting from an anchor can affect the amount of drift that is transferred from the structural system of a building to the framing of a glass system in a seismic event. Consequently, the connections for the glass specimens tested in the laboratory will be explored for comparison with field connections and their seismic response behavior.

Experimentally, the vertical mullions of glass CW specimens were attached at all four corners to the racking facility's top and bottom steel tubes through the use of pi-shaped steel anchor connections. Examples of these connection details can be viewed in Figure **7.1**. The connection details used 1/2 in. (12 mm) diameter (13 threads per inch) Grade 8 bolts to attach the anchors to the 6 in. (152 mm) steel tubes of the racking facility. Furthermore, reinforcement plates were welded around the edges of the connection detail. Bolts were used in conjunction with bearing and reinforcement plates as seen in Figure 7.1 to restrict the rotation of both of the horizontal aluminum CW framing members, and were hand tightened only. These bolts simulated glass panels above and below the tested glass panel, since on an actual building adjacent glass panels would restrict horizontal rotation in a seismic event. Furthermore, 3/8 in. (10 mm) Grade 8 bolts were used to attach the vertical mullions to the steel anchors, which was accomplished by passing the bolt through the center of the anchor. Finally, any gaps between the frame and the corner pi-anchors were shimmed with wood. All of these details produce a fairly rigid mullion-to-facility connection for the tested glass specimens, resulting in negligible connection rotation and rotational flexibility.

In contrast to the laboratory conditions where the steel anchors were rigid, CW framing-to-structure connections on actual buildings may allow for more flexibility. Figure **7.2** depicts examples of CW anchors found in the field. In general, these connection details on actual buildings are not rigid. As a result, as a building structural frame deforms in a seismic event, the continuous mullions at connection points would

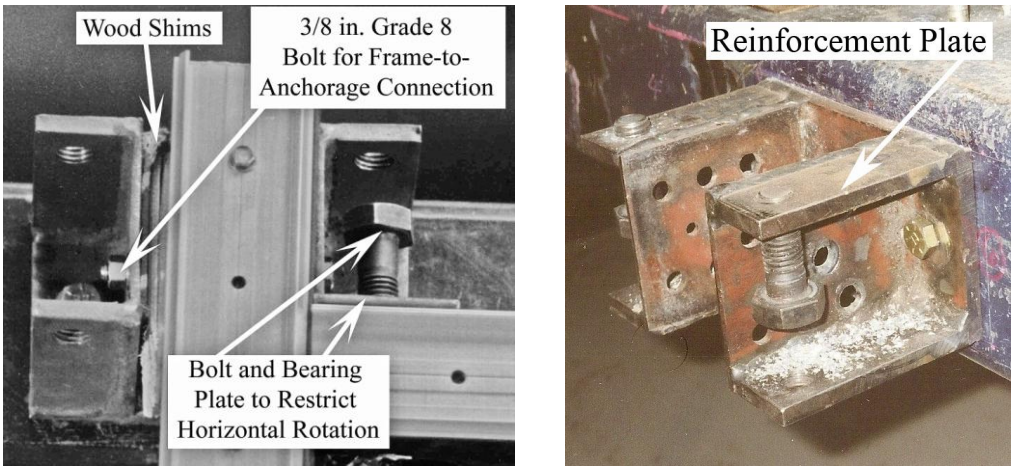

(a) (b)

Figure 7.1: Pictures of mullion-to-facility connection details where (a) is a view of the connection details with a mid-rise CW mullion in place and (b) is a view of the anchor without CW specimen

be expected to display rotation and possibly translation depending on the type of anchor present. This action could be compounded by vertical slots for thermal movement allowance in the connections, which would affect the vertical translation and rotation of the framing system.

A flexible or semi-rigid connection in the field results in a higher drift capacity for glass CW systems. To demonstrate schematically how a semi-rigid connection would lead to higher drift capacities, Figure **7.3** illustrates three conditions: (a) a glass panel within a framing system with no lateral loading; (b) assumed rigid body movement of a glass panel while its framing deforms from applied lateral loads where rigid mullion-to-structure are present containing minimal rotational movement; and (c) assumed rigid body movement of a glass panel with frame deformation due to lateral loading with mullion-to-structure connections that exhibit rotational capability from any

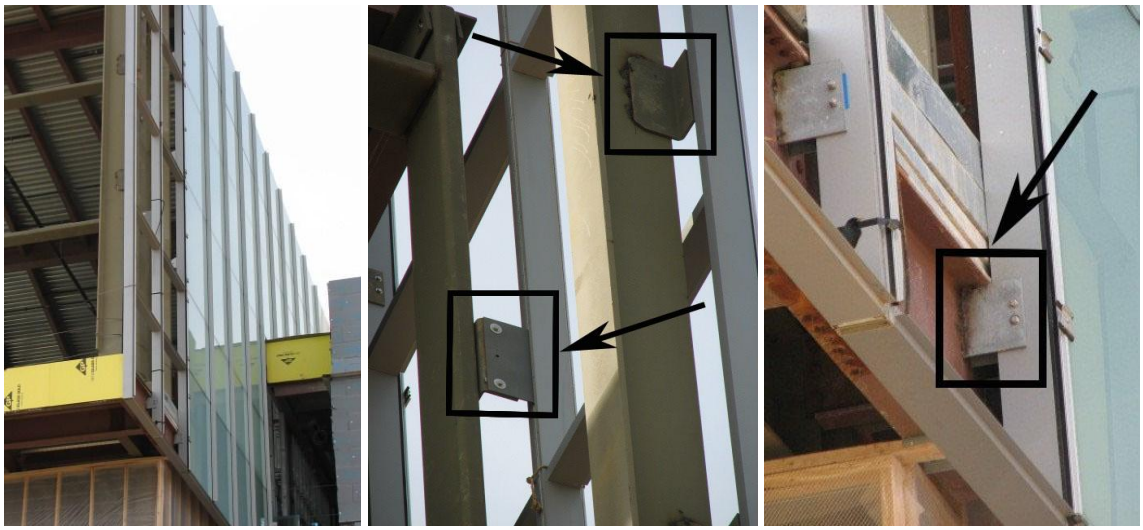

(a) (b) (c)

Figure 7.2: Examples of highlighted mullion-to-structure connections on an actual building in State College (Pennsylvania)

means (reduced anchor stiffness, slotted holes, etc.). It can be seen in illustration (b) that when a rigid connection is present, the glass panel will contact the framing earlier than when semi-rigid connections are present such as in illustration (c). This is a result from the fact that when semi-rigid connections are present, the displacement experienced by the structural system is not fully transferred to the CW framing system. In contrast, rigid connections allow for a near 1:1 ratio of displacement transfer between the structure and the CW system during a seismic event.

In many cases, the rotations and translations will be generally small enough that the CW will only experience a slightly smaller displacement than the story drift that the structural frame of the building experiences. Although, depending on the connection detailing, some systems may see much less displacement than the structural system of a building of which the magnitude is unknown. In all, it can be assumed that a large

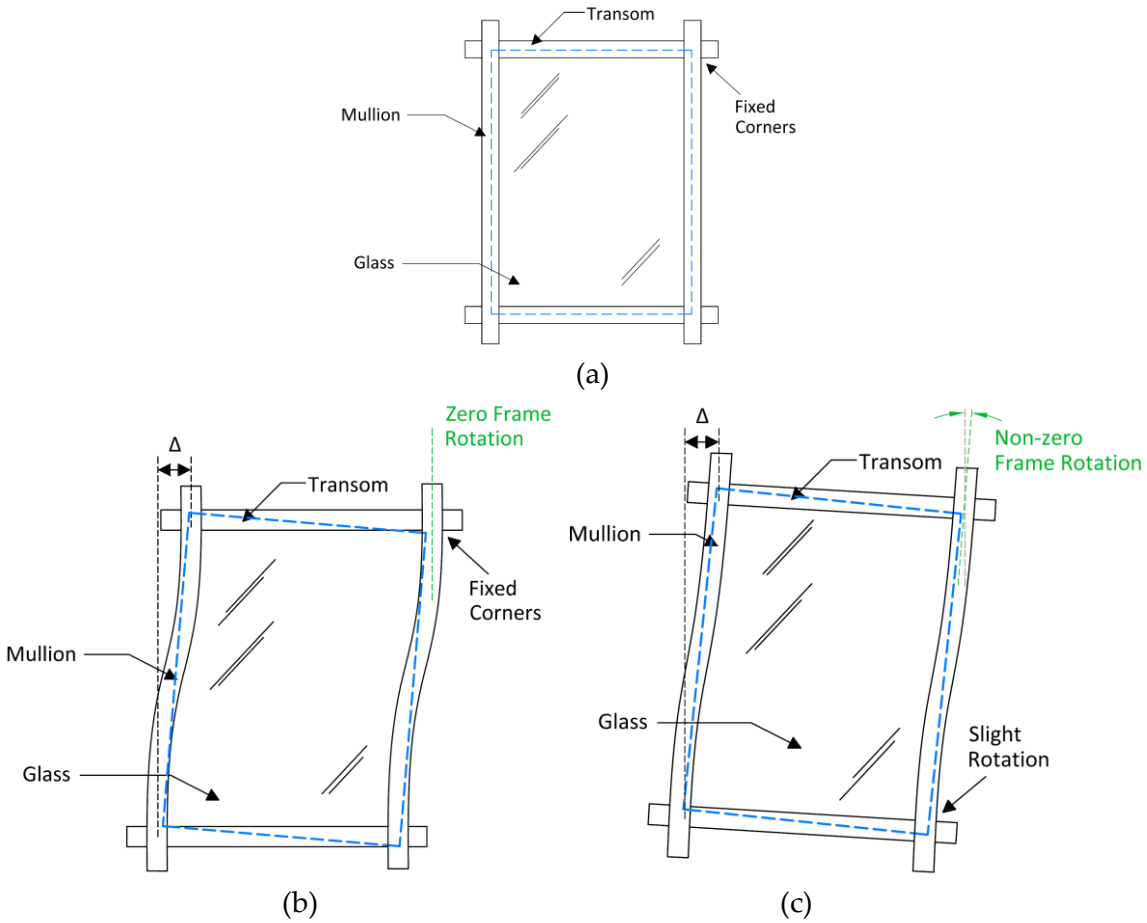

Figure 7.3: Illustrated corner flexibility conditions for (a) glass panel at rest, (b) glass panel response to lateral load with rigid connection detailing, and (c) glass panel response to lateral load with semirigid connection detailing exhibiting rotational flexibility

percentage of CW systems on buildings will not experience 100% of the story drift that the structural system will go through in a seismic event. Since the steel anchors on the racking facility were rigid, the glass panels were tested as if 100% of the story drift that a structure (represented by the steel tubes) experienced was transferred to the CW framing. Consequently, the fragility functions and closed-form equation presented in

this thesis are inherently conservative by some degree, because they are based on data of glass failure which occurred where a 1:1 displacement ratio between CW and structure was present. Follow-up studies can study the effects that common mullion-to-structure connections on actual buildings have on the failure performance of glass panels.

7.2 Entire Glass Systems

In this research, the fragility functions and developed closed-form equation both provide information for one glass panel within an aluminum framing system. In general, though, a glass panel is part of a larger exterior glass CW system, which contains multiple glass and spandrel panels. The exterior glass CW system can span great lengths and extend across several stories. Furthermore, one might find that on certain systems there may be several separate glass panels vertically within one story. This section seeks to provide information on how to apply the predicted failure drifts from the equation or the probabilistic failure from the fragilities, which account for one glass panel, within the context of large entire glass exterior CW systems.

When applying the experimental results to glass panels on actual buildings, the most important relationship to keep in mind is how the drift ratios of building, stories, glass panels, sections of CW systems, or any other involved components are related in terms of height and displacements. As defined previously in Equation 3.1, a drift ratio is equal to the horizontal drift displacement (δ) that a building component is subjected to

divided by the height (h) over which the horizontal displacement occurs. Building on this definition, consider a glass panel configuration as if in the laboratory, the same glass panel within the context of a CW system on an actual building, and then the entire interstory section of CW that the glass panel is located in on the building as represented in Figure **7.4.** The height of the glass panel in the laboratory is defined as h and the applied lateral displacement as δ, the height of the glass panel in the CW as h' and subjected lateral displacement as δ', and the height of the interstory section of CW as H and displacement of section of CW with height H as Δ. These three separate components can be related through drift ratio as expressed by Equation **7.1**, assuming that δ equals δ'**:**

$$\text{Drift Ratio} = \Theta = \frac{\delta}{h} = \frac{\delta'}{h'} = \frac{\Delta}{H} \qquad \textbf{7.1}$$

The relationship seen in Equation 7.1 provides a way to relate demands from the two design approaches to entire glass systems. For the fragility functions, the equation shows that the probabilistic failure drift ratio from fragilities can be applied directly to individual glass panels on actual CW systems as long as conditions laid out in the previous section are met. For the closed-form equation, though, the predicted capacity is given in terms of drift. In terms of Equation 7.1, the predicted drift from the equation is represented by the variable δ'. To relate the predicted drift (δ') to the drift of the building story (Δ) or certain section of CW, the term will need to be converted into a drift ratio since it is directly related to the drift ratio of the interstory CW section that the

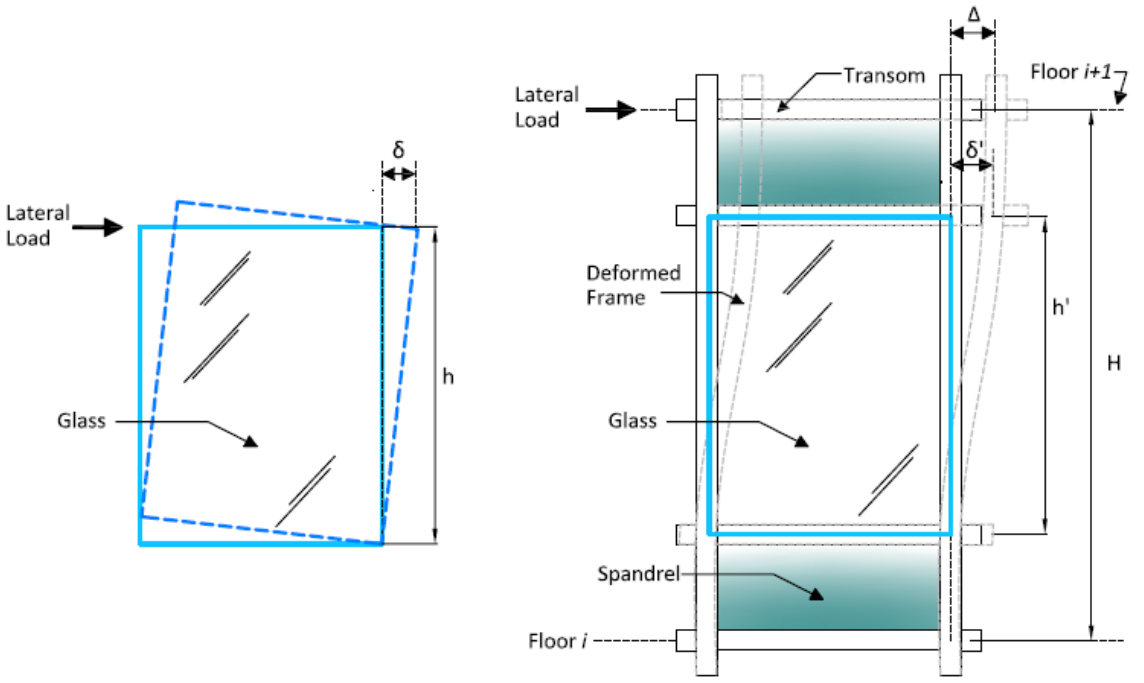

Figure 7.4: Parameters and relationship between (a) a glass configurations in the lab, and (b) a similar glass panel within an interstory section of CW on an actual building

glass panel is located within. For example, to find the equivalent story drift (Δ) of the section of interstory that would cause cracking for a given glass panel as predicted by the closed-form equation, the following computation could be made:

$$\Delta_{failure} = H \cdot \left(\frac{\delta'}{h'}\right)$$

It is assumed when using the relationships that the spandrel panels are comparably flexible to the vision glass panels. If the spandrel panels are rigid (i.e., precast concrete), then all of the interstory drift must be accommodated by the glass panel (Behr 2009).

To further illustrate how to relate a glass panel to an entire glass system for fragilities and the closed-form equation, an example is developed that uses an interstory section of CW on a building. Figure **7.5** shows the interstory section of CW with a story height or 12 ft (3.7 m) where within this height are four glass panels. All of the glass panels have a height of 3 ft (0.9 m) and width of 2.5 ft (0.8 m), resulting in an aspect ratio of 6:5. Furthermore, the glass panels utilize an asymmetric IGU composed of an inner AN monolithic 1/4 in. (6 mm) lite and an outer AN laminated unit with two 1/8 in. (3 mm) thick lites with a 0.030 in. (0.8 mm) PVB layer in between. Lastly, the mid-rise CW framing is comparable to aluminum Kawneer 1600™ framing, there is a glass-to-frame clearance of 0.43 in. (11 mm), and the glass is dry-glazed. In all, the glass configuration is similar to glass configuration (3) listed in Table 3.1.

Assume a user needs to acquire the relative horizontal displacement between Floor (*i*) and Floor (*i + 1*) that will cause initial glass cracking and crushing in the glass panel highlighted in the black box of Figure 7.5. To begin, the closed-form equation can be utilized to predict the drift causing a glass panel cracking failure. With the factor values calculated at $\Phi_{type} = 0.76$, $\Phi_{config} = 1.1$, $\Phi_{clearance} = 1.0$, $\Phi_{system} = 1.0$, and $\Phi_{aspect} = 1.0$, the closed-form equation estimates a failure drift of 1.61 in. (41 mm) over the height of the glass panel. Applying the predicted failure value to Equation 7.1, the interstory building

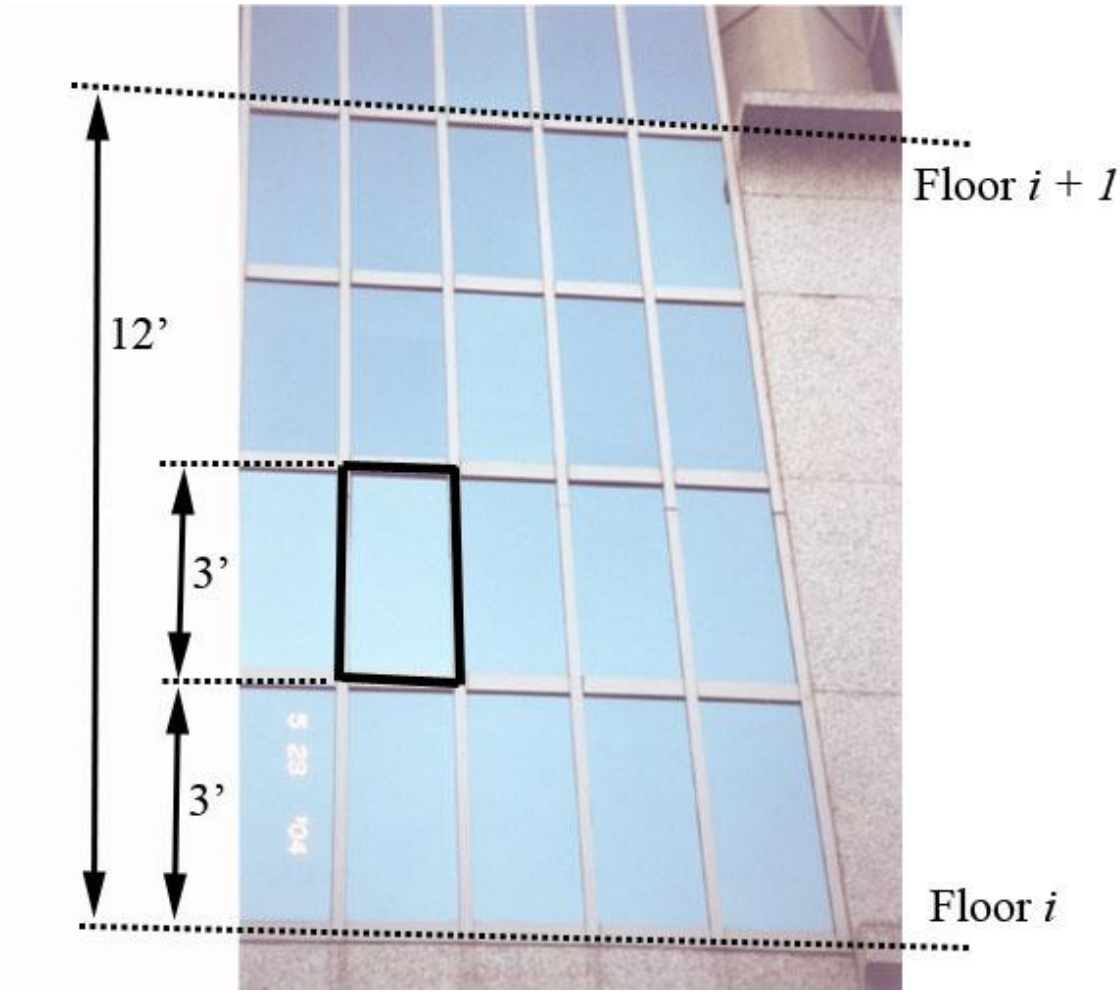

Figure 7.5: A section of an interstory CW on an actual building with given dimensions

displacement (Δ) estimated to cause cracking in the glass panel can be determined with the following calculations:

$$\Delta_{crack} = H \cdot \left(\frac{\delta'}{h'}\right) = (12' \cdot 12'') \left(\frac{1.61''}{3' \cdot 12''}\right) = 6.44\ in.\ (164\ mm)$$

Assume now that a user desires to find the estimated interstory drift ratios that would cause cracking with a 20%, 50%, and 80% probability for the highlighted glass panel in Figure 7.5 using the same glass panel characteristics previously. To start, the

fragility functions can be used to find drift ratios for the glass panel as a function of the probability. Using the fragility curve developed for cracking limit state of glass configuration (3), estimated drift ratios are found. However, since the given glass panel has a different height as glass configuration (3), the *r* factor (the height of the experimental glass panel divided by the height of the given glass panel) needs to be applied to the results. The calculation to determine the value of *r* is seen below and the application of the factor to the drift ratios are summarized in Table **7.1.**

$$r = \frac{h_j}{h_i} = \frac{6\ ft.}{3\ ft.} = 2.0$$

Table 7.1: Adjusted predicted cracking drift ratios according to different probabilities of failure for a given glass panel

P(x) (failure)	θ_{crack}	$\theta_{crack} \cdot r$
20% (0.2)	0.0182	0.0364
50% (0.5)	0.0234	0.0468
80% (0.8)	0.0301	0.0602

With the drift ratios estimated to cause cracking for three different probabilities found as seen in the last column of Table 7.1, the drift ratios most likely to cause cracking in the panel for the story can be determined. In Equation 7.1, it can be seen that the drift ratio of a given glass panel is equivalent to the drift ratio of the interstory CW section in which the glass panel is located within. Therefore, the drift ratios for the building story that is likely to cause cracking for the given glass panel with a 20%, 50%, and 80% probability are 0.0364, 0.0468, and 0.0602, respectively. These cracking failure

drift ratios seem large, but are inflated due to the shortness of the glass panel considered. In Section 5.5.1, it was shown how smaller glass panels can have significantly greater capacity in terms of drift ratio compared with glass panels greater in size and in height.

7.3 Results and Conclusions

In general, the performance of glass on actual exterior systems on buildings as compared to the laboratory is a function of several parameters. Two of these parameters, connection detailing and applying the predicted results for one glass panel within the context an entire CW system or section, were addressed in detail. The other factors that may affect the seismic response of glass panels include weathering of the glass and rubber gaskets, and the continuity of the vertical framing members. The magnitude of weathering effects on seismic glass performance is not fully understood. Therefore, for the fragility functions and the closed-form equation standard new construction conditions are assumed. Also, continuous vertical mullion conditions are assumed to be on the actual building, where the mullions span the height of the considered section or interstory of building uninterrupted.

Connection detailing was investigated because it was deemed that different common mullion-to-structure connections on an actual building could alter the seismic performance of a glass panel from the experimental findings. The flexibility resulting

from a semi-rigid anchor in the field can affect the amount of drift that is transferred from the structural system of a building to the framing of a glass system in a seismic event, increasing the capacity as a function of the degree of rotational flexibility. Since the connections in the laboratory are rigid, the analyses performed on the experimental data are inherently conservative. Follow-up studies that measure the effect on seismic performance that common mullion-to-structure connections (see Figures 6.13 and 6.14) have on glass panels could provide data that are used as the basis of formulation of modification factors for use by the fragility functions and the closed-form equation. If these studies show that the type of connection has a large effect on the seismic capacity of glass panels, an important step in the design of architectural glazing systems in future guidelines may be the selection of proper connection details.

Next, entire exterior glass systems were investigated and compared with glass panels as an individual unit, as they were tested in the laboratory. It is shown how the demand predicted by the closed-form equation or fragility function for one individual glass panel can be translated to an entire interstory or system through conversion with the drift ratio definition (see Equation 7.1). When using the definition, it is important for a user to keep in mind the differences between drift and drift ratio when interpreting the capacity of different building components.

Chapter 8

Summary and Conclusions

8.1 Summary

8.1.1 Objective and Scope

The ultimate goal of this research is to provide preliminary work that leads to the development of seismic design guidelines for architectural glass systems. Several tasks were performed to achieve this goal, which include: (1) developing fragility curves for use in a PBSD approach as a way to evaluate the performance of glass systems in terms of probabilistic economic and life safety consequences; (2) developing a closed-form equation as a way to predict the cracking capacity of various glass systems in terms of drift; and (3) investigating the different conditions between the laboratory and field for practical applications. The first two tasks involve developing tools that can be utilized to find the seismic capacity and performance of glass systems, while the third task provides a way to apply design analysis results to glass systems on actual buildings.

The probabilistic fragility functions were developed for twenty-four different glass configurations as listed in Table 3.1. Data for twenty of the glass configurations were provided from past studies (Behr 1996, Behr 1998, and Memari et al. 2003), while data for four of the glass configurations with varied glass-to-frame clearances were

obtained through new laboratory tests carried out in this research. To ensure maximum accuracy in previously reported data, sensor testing was also executed on the racking facility to determine whether flexibilities are present in the racking facility structure itself. Furthermore, before the fragility curves were developed the following tasks were performed:

- Definition of failure limit states
- Adjustment of data for refined definition of initial cracking/crushing limit state
- Checking data for premature failure during load intervals for each specimen
- Acquiring gasket seal degradation failure data from experimental videos

To create fragility curves, an Excel workbook was utilized to plot the functions based on the input of median value of demand (θ) and the dispersion (β) parameter values. The median value of demand (θ) and random dispersion value (β_r) were found by using the *Fragility Function Calculator version 1.02* software provided by the ATC (Porter 2006), where the dispersion value (β) was calculated according to Equation 2.7. The data input into the software was in the form of interstory drift ratio, where the experimental drift values are converted as according to Equation 3.1.

The new closed-form equation was developed to predict the in-plane drift that causes glass cracking failure in consideration of various glazing and configuration details in addition to glass-to-frame clearance and glass panel dimensions. Specifically, the closed-form equation takes into account the glass type (AN, HS, FT), glass

configuration (Mono, Lami, sym. IGU, asym. IGU), glass system (CW or SF), substandard glass-to-frame clearances, aspect ratio, and is also developed to consider mullion-to-structure connection type in the future. To determine whether either the ASCE 7-05 (ASCE 2006) or Sucuoglu and Vallabhan (1997) equation can be used in formulation of the closed-form equation, an analysis was performed that determined the accuracy of the equations. Then with the base equation established, separate factors were developed based on trends extracted from the available experimental data with certain variables controlled for in the analyses.

8.1.2 Sensor Facility Testing

The sensor analysis performed on the racking facility in the laboratory showed that flexibilities were present, especially in the fulcrum arm mechanism. As a result of the reduced actual displacements experienced by specimens compared to the expected computer-controlled displacements, the failure data was adjusted according to Equations 4.1 and 4.2. In all, the glass cracking and glass fallout experimental failure data for CW systems received an average reduction of 17.6%.

8.1.3 Varying Glass-to-Frame Clearance Testing

The experimental results validated that the glass-to-frame clearance is critical to the seismic performance of a glass panel. While the glass cracking and glass fallout

failure values generally decreased as the clearance of a particular glazing configuration decreased, the failure values were greater than expected for configurations with the lowest (i.e., near zero) glass-to-frame clearances. This condition may be explained by a natural glass corner rounding action that was observed for specimens with substandard glass-to-frame clearances, which was observed through the use of viewing slots milled in corner regions of the curtain wall pressure plates (see Figure 4.8).

8.1.4 Fragility Functions

The developed fragility functions for gasket failure, glass cracking, and glass fallout damage states for twenty-four glass configurations (see Appendix A.4) can be utilized in the Performance Assessment Calculation Tool (PACT) for PBSD or individually in the seismic design of architectural glass systems. Two adjustments were carried out on the experimental data before fragility analysis to ensure conservatism, where the first was a result of the redefinition of the glass cracking limit state and the second was due to a load interval failure check. The fragility functions can be used directly if the glass system under consideration has the same glazing details and characteristics. Otherwise, if a glass panel has a different height than the experimental glass height that a fragility represents, an r modification factor (see Equation 5.4) needs to be applied to the fragility drift ratios. If the glass-to-frame clearance or aspect ratio differs, a user can utilize a fragility function of a similar configuration with a conservative clearance or aspect ratio, or a new fragility function can be developed by

performing a probabilistic mixture of known fragility functions as described in Section 5.5.3.

8.1.5 Closed-Form Equation

The closed-form equation for glass cracking is formulated with the ASCE 7-05 equation that models the geometric response of a glass panel to lateral loading as its base, with the application of additional factors to account for glass type, configuration type, substandard clearance, system type, aspect ratio, and connection detailing as seen in Equation 6.1. Factors defined in Table 6.19 were developed in a methodical order as described in Section 6.5, and were based on trends extracted from the experimental data caused by isolating the various glazing and system variables that are known to affect glass failure values (see Appendix A.2). Overall, the closed-form equation was shown to decrease the percent difference (Equation 6.14) between the experimental and predicted values from 26.3% for the ASCE equation to 17.5%.

8.1.6 Laboratory Versus Field Conditions for Practical Applications

It was investigated how semi-rigid mullion-to-structure connections on an actual building could increase the seismic capacity of glass panels if rotational flexibilities are present at the wall to main structure anchorage points. Furthermore, it was shown how the demand predicted by the closed-form equation or fragility function for one

individual glass panel can be translated to represent the capacity of an entire interstory or section of CW system through conversion with the drift ratio definition (see Equation 7.1).

8.2 Conclusions and Recommendation for Future Research

The main goal of the study is to provide work that furthers the possibility of the development of seismic design guidelines for architectural glass systems. The closed-form equation developed estimates the cracking capacity of a glazed panel in terms of drift for several different common architectural glass systems. Furthermore, developed fragility curves can be used to estimate the performance of several common glass systems in a probabilistic manner for gasket degradation, initial glass cracking, and glass fallout damage states in terms of economic and life safety consequences.

The fragility functions and closed-form equation are based on experimental data that have been adjusted to ensure accuracy and conservatism in the failure data. Furthermore, the closed-form equation and the fragilities assume the most conservative connection detailing (i.e. rigid) between the exterior glass wall system and the building structure. However, follow-up studies can provide a means to adjust the closed-form equation and fragilities for common mullion-to-structure connections that can be semi-rigid and increase the seismic failure capacity of glass panels.

The conclusions stated in sections at the end of each chapter are summarized here, along with some additional overall conclusions with regard to the research. From

the development of the fragility functions and the experimental investigation of glass configurations with substandard glass-to-frame clearances it is concluded that:

- More than half of the glazing configurations analyzed in this report as listed in Table 3.1 would be expected to experience no glass cracking or glass fallout damage in a moderate earthquake.

- For the first time, users can predict the percentage of glass panels expected to fail in an entire exterior glass system for a given demand.

- The data adjustment for the loading interval failure check revealed that the experimental capacity of FT-Mono glass types was about 14.6% lower than initially observed.

- The reduction of failure values because of flexibilities found in the racking facility revealed that the failure of glass panels is more critical to seismic loading than initially observed.

- The development of fragility modification procedures for varying glass panel dimensions revealed that the interstory drift ratio capacity of glazing systems can be increased by reducing the size of glass panels.

- As the glass-to-frame clearance lessens, the glass cracking and glass fallout failure capacity of a glass panel decreases but not as much as might be expected intuitively.

- The natural corner rounding action exhibited by glass specimens with the lowest glass-to-frame clearances is attributed to adding seismic failure capacity to the glass cracking and glass fallout damage states of those systems.

- If glass panels for a building project are oversized leading to a glazed glass-to-frame clearance unknowingly lower than designed for, the seismic capacity of the system is not as low as originally expected.

- Below 0.125 in. (3 mm), a glass-to-frame clearance is no longer a critical glazing detail that alters the seismic performance of a glass panel for at least AN glass types.

- In the design of a glass system, differences in framing members among similar systems (i.e. CW or SF) are not critical to the seismic capacity of glass panels.

- Gasket failure generally occurs at a drift demand approximately 25% lower than the drift demand expected to cause glass cracking.

For the development of the closed-form glass cracking prediction equation, specifically, it is concluded that:

- By additionally considering various glazing details, the proposed equation increases the accuracy of the predicted seismic cracking capacity of glass systems by 33% (average of absolute percent errors) compared to the ASCE equation.

- The improvement in accuracy in the proposed equation can make the difference of hundreds of thousands of dollars in estimations of repair costs for glass systems.

- The base portion of the closed-form equation is generally the most critical component of the equation as compared to the affect from the applied factors.

- The gains in seismic cracking capacity when going from AN to HS glass is much greater than going from HS to FT glass.

- When considering glass configuration type, trends in the data showed that IGU systems have higher glass cracking capacity than monolithic or laminated units.

- Trends in the experimental data normalized into drift ratios showed that glass systems with aspect ratios less than and greater than the standard 6:5 have greater cracking capacity.

- Inaccuracies present in the proposed glass cracking prediction equation are mostly attributed to errors inherent in the Φ_{type} and Φ_{config} factors that model the effects from glass type and configuration type.

- The proposed equation can be easily used with the minimum requirements of a handheld calculator.

For the practical application of the fragility curves and closed-form equation, specifically, it is concluded that:

- Rotational flexibility from semi-rigid mullion-to-structure connections on actual buildings is predicted to add seismic capacity to glass systems.

- Since both design approaches (fragility function and closed-form glass cracking prediction equation) assume rigid connection detailing, the predicted performance of glass systems on actual buildings are likely conservative.

- For exterior systems on buildings which have continuous vertical framing members and components minimally degraded from the weather, the laboratory results, fragilities, and proposed equation can be easily applied.

It is recommended that follow-up studies aim to generally expand the types of glass configurations analyzed for fragility function development and be incorporated into the closed-form equation. Specifically, follow-up studies could study the effect of wet-glazing compared to dry-glazed systems, unitized compared to stick-built systems, and the effects of commonly employed mullion-to-structure connections. Furthermore, testing on FT-Lami and FT-IGU (symmetrical) glass configurations would fill gaps in the studies concerning the correlation between glass type and configuration type.

It would be beneficial to conduct follow-up testing that includes additional glass specimens with varying clearances, SF systems, and varying aspect ratios so that the pool of experimental data for theses glass configuration types can be enlarged. The data could further refine the values of the $\Phi_{clearance}$, Φ_{system}, and Φ_{aspect} factors. Also, follow-up testing that creates a set of independent experimental results for glass configurations with various glazing details could be used to measure the accuracy of the proposed closed-form equation, and then calibrate the factor values if needed.

For practical application of laboratory data to actual glass system purposes, it would be beneficial to study glass configurations subjected to various degrees of degradation due to weathering as a function of time in service on actual building in

various climates. Therefore, experimental results that are used to model the performance effects of weathering could modify the fragility functions and the predictive glass cracking equation for existing glass systems on buildings. Furthermore, for practical applications, a study could be performed to find the seismic performance of glass panels when anti-walk blocks on the vertical members are absent. Therefore, if it is known that glass panels on an actual system are missing anti-walk blocks from installation mistakes, the ramifications of this condition with regard to seismic glass response could be estimated.

Finally, it would be beneficial if additional analytical research was performed to develop a closed-form equation that predicts the fallout capacity of various glass configurations. An equation to predict glass fallout would help designers and professionals better understand the seismic demands that could lead to life safety issues associated with different glazing systems. Furthermore, an equation would be available for designers for either the cracking or fallout limit states of glass.

References

American Architectural Manufacturers Association (AAMA), 2001a. *Recommended Static Test Method for Evaluating Curtain Wall and Storefront Systems Subjected to Seismic and Wind Induced Interstory Drifts*, Publication No. AAMA 501.4-01, Schaumburg, IL.

American Architectural Manufacturers Association (AAMA), 2001b. *Recommended Dynamic Test Method for Determining the Seismic Drift Causing Glass Fallout From a Wall System*, Publication No. AAMA 501.6-01, Schaumburg, IL.

American Society of Civil Engineers (ASCE), 2002. *Minimum Design Loads for Buildings and Other Structures*, ASCE 7-02, ASCE, Reston, VA.

American Society of Civil Engineers (ASCE), 2006. *Minimum Design Loads for Buildings and Other Structures*, ASCE 7-05, ASCE, Reston, VA.

Applied Technologies Council (ATC), 2005. *Guidelines for Seismic Performance Assessment of Buildings 35% Complete Draft*, Prepared for the Department of Homeland Security, Washington, D.C.

Applied Technologies Council (ATC), 2006. *Next-Generation Performance-Based Seismic Design Guidelines: Program Plan for New and Existing Buildings*, FEMA 445 Report, prepared by ATC for Federal Emergency Management Agency (FEMA), Washington, D.C.

Applied Technologies Council (ATC), 2008. *Development of Next-Generation Performance-based Seismic Design Procedures For New and Existing Buildings: The ATC-58 Project in Brief*, www.atcouncil.org, July, 2008.

Behr, R. A., Belarbi, A. and Brown, A. T., 1995. "Seismic Performance of Architectural Glass in a Storefront Wall System," *Earthquake Spectra*, Volume 11, No. 3, pp. 367-391.

Behr, R. A. and Belarbi, A., 1996. "Seismic Test Methods for Architectural Glazing Systems," *Earthquake Spectra*, Volume 12, No. 1, pp. 129-143.

Behr, R. A., 1998. "Seismic Performance of Architectural Glass in Mid-Rise Curtain Wall," *Journal of Architectural Engineering*, Vol. 4, No. 3, pp. 94-98.

Behr, R. A., 2006. "Design of Architectural Glazing to Resist Earthquakes," *Journal of Architectural Engineering*, ASCE, Vol. 12, No. 3, pp. 122-128.

Behr, R. A. Written discussion of thesis material. The Pennsylvania State University, State College, PA. 18 March 2009.

Bouwkamp, J. G., 1961. "Behavior of Window Panel Under In-Plane Forces," *Bulletin of the Seismological Society of America*, Vol. 51, No. 1, pp. 85-109.

Chrisman, George. Email Contact. Walters and Wolf, Inc., San Francisco, CA. 7 January 2009.

Earthquake Engineering Research Center, 1996. *Performance Based Seismic Design of Buildings*, FEMA 283 Report, prepared by EERC for Federal Emergency Management Agency (FEMA), Washington, D.C.

Earthquake Engineering Research Institute (EERI), 2000. *Action Plan for Performance-based Seismic Design*, FEMA 349 Report, prepared by EERI for Federal Emergency Management Agency (FEMA), Washington, D.C.

Glass Association of North America (GANA), 2004. *Glazing Manual*, 2004 Edition, GANA, Topeka, KS.

Hamburger, R. O., 2006. "The ATC-58 Project: Development of Next-Generation Performance-Based Earthquake Engineering Design Criteria for Buildings," *Structures Congress 2006*, ASCE, St. Louis, MO.

Harmon, Inc. Telephone Interview with Glazing Specialist (name unknown). Eden Prairie, MN. 7 January 2009.

International Code Council (ICC), 2006. *International Building Code (IBC) 2006*, ICC, Falls Church, VA.

Lim, K. Y. S. and King, A. B., 1991. *The Behavior of External Glazing Systems Under Seismic In-Plane Racking*, Building Research Association of New Zealand (BRANZ), Study Report No. 39.

Memari, A. M., Behr, R. A. and Kremer, P. A., 2003. "Seismic Behavior of Curtain Walls Containing Insulating Glass Units," *Journal of Architectural Engineering*, ASCE, Vol. 9, No. 2, pp. 70-85.

Memari, A. M., Kremer, P. A. and Behr, R. A., 2004. "Dynamic Racking Crescendo Tests on Architectural Glass Fitted with Anchored "PET" Film," *Journal of Architectural Engineering*, ASCE, Vol. 10. No. 1, pp. 5-14.

Memari, A. M., Kremer, P. A., and Behr, R. A., 2006a. "Architectural Glass Panels with Rounded Corners to Mitigate Earthquake Damage," *Earthquake Spectra Journal*, Volume 22, No. 1, pp. 129-150.

Memari, A. M., Chen, X., Kremer, P. A., and Behr, R. A., 2006b. "Seismic Performance of Two-Side Structural Silicone Glazing Systems," *Journal of ASTM International (JIA)*, Vol. 3 No. 10, pp. 1-10.

Memari, A. M., Shirazi, A. and Kremer, P. A., (2007). "Static Finite Element Analysis of Architectural Glass Curtain Walls Under In-Plane Loads and Corresponding Full-Scale Test," *Structural Engineering and Mechanics Journal*, Vol. 25, No. 4, pp. 365-382.

Nakata, S., H. Itoh, A. Baba, and S. Okamoto, 1984. "US-Japan Cooperative Research on R/C Full-Scale Building Test," *Proceedings of the Eighth World Conference on Earthquake Engineering*, July 21-28, 1984, San Francisco CA, Englewood Cliffs NJ: Prentice-Hall, Inc., vol. VI, pp. 611-618.

National Institute of Building Sciences (NIBS), 2008. *Whole Building Design Guide.* www.wbdg.org, prepared by the National Institute of Building Sciences, July 15, 2008.

Porter, K. A. and Kiremidjian, A. S., 2001. *Assembly-Based Vulnerability of Buildings and its Uses in Seismic Performance Evaluation and Risk-Management Decision-Making, Report 139,* John A. Blume Earthquake Engineering Research Center, Stanford, CA.

Porter, K. A., 2006. *ATC-58 Fragility Functions: Curtain Wall, Version 1.0*, www.atcouncil.org, 2007.

Porter, K.A., 2007. *ATC-58 Fragility Function Calculator Mini-Manual Version 1.01*, www.atcouncil.org, 2007.

Schwartz, T., 1984. "How to Avoid Glass Fractures," *Glass Digest*, March 15, 1984, pp. 58-61.

Schwartz, T., 2001. "Glass and Metal Curtain-Wall Fundamentals," *Association for Preservation Technology Bulletin*, Vol. 32, No. 1, pp. 37-45.

Sucuoglu, H. and Vallabhan, C. V. G., 1997. "Behavior of Window Glass Panels During Earthquakes," *Engineering Structures*, Vol. 19**,** No. 8, pp. 685-694.

Appendix A

Fragility Function Data

In this appendix, Section A.1 presents the experimental data converted from drifts into drift ratio values. Section A.2 presents the detailed information about glass configurations according to limit states that were input into the *Fragility Function Calculator version 1.02* software. Section A.3 contains the results as produced from the software. Section A.4 shows the fragility function plots for all glass configurations and limit states.

A.1 Failure Data

The following tables **A.1** through **A.18** present the experimental data in terms of failure drifts (inches and millimeters) and determined drift ratios. Preceding the data values are information regarding the specimen tested, which includes "Original Specimen Numbering," "Glass Type," "Corner Shape," "Edge Condition," "Corner Condition," "Nominal Glass Thickness," "Average Clearance," and "Glass Manufacturer." Then, experimental data for each specimen is presented (if available) for glass-to-frame contact, gasket failure limit state, cracking failure limit state, and the fallout limit state.

For the cracking limit state, only one set of failure data is given for monolithic, laminated, or symmetric IGU configurations. These values represent the accepted failure values for those panes or units. For asymmetric IGU's, cracking failure data is given for both the inner and outer panes. This is because sometimes the inner pane of an asymmetric IGU experienced the failure earlier than the outer pane, and vice versa. A column then denotes the lowest cracking failure drift ratio considering both panels, where this column specifically applies to glass configurations (3-5, 19, and 20).

For the fallout limit state, only one set of failure data is presented for all glass configurations. This is because for the asymmetric IGU's fallout was experienced in the inner panel first for every specimen.

Table A.1: Specimen information for glass configurations (1-3)

ID	Original Specimen Numbering	Glass Type	Corner Shape	Edge Condition	Corner Condition	Glass Nominal Thickness (in.)	Average Clearance (in.)	Glass Manufacturer
Annealed Monolithic								
1	1-1	AN Mono	rectangular	cut	cut	0.25	0.43	Centre Glass
1	1-2	AN Mono	rectangular	cut	cut	0.25	0.43	Centre Glass
1	1-3	AN Mono	rectangular	cut	cut	0.25	0.43	Centre Glass
1	1-4	AN Mono	rectangular	cut	cut	0.25	0.43	Centre Glass
1	1-5	AN Mono	rectangular	cut	cut	0.25	0.43	Oldcastle
1	1-6	AN Mono	rectangular	cut	cut	0.25	0.43	Oldcastle
1	added 4/17/08	AN Mono	rectangular	cut	cut	0.25	0.43	
Annealed Insulating Glass Units								
2		AN IGU	rectangular	cut	cut	1.00	0.43	
2		AN IGU	rectangular	cut	cut	1.00	0.43	
2		AN IGU	rectangular	cut	cut	1.00	0.43	
2		AN IGU	rectangular	cut	cut	1.00	0.43	
2		AN IGU	rectangular	cut	cut	1.00	0.43	
2		AN IGU	rectangular	cut	cut	1.00	0.43	
2	added 4/17/08	AN IGU	rectangular	cut	cut	1.00	0.43	
Asymmetric Insulating Glass Units								
3	A-1	Asymmetric IGU	rectangular	cut	cut	1.013	0.43	
3	A-2	Asymmetric IGU	rectangular	cut	cut	1.013	0.43	
3	A-3	Asymmetric IGU	rectangular	cut	cut	1.013	0.43	
3	A-4	Asymmetric IGU	rectangular	cut	cut	1.013	0.43	
3	A-5	Asymmetric IGU	rectangular	cut	cut	1.013	0.43	
3	A-6	Asymmetric IGU	rectangular	cut	cut	1.013	0.43	

Table A.2: Experimental failure data for glass configurations (1-3)

ID	Glass-to-Frame Contact			Gasket Failure			Cracking							Fallout		
							Single or Inner Pane-IGU			Outer Pane-IGU			Lowest	Single or Inner Pane-IGU		
	in.	mm	D.R.	in.	mm	D.R.	in.	mm	D.R.	in.	mm	D.R.	D.R.	in.	mm	D.R.
Asymmetric Insulating Glass Units																
1							1.15	29.2	0.0142					1.88	47.7	0.0232
1							0.93	23.7	0.0115					2.01	51.0	0.0248
1							1.15	29.2	0.0142					2.21	56.0	0.0272
1	0.073	1.9	0.0009				1.15	29.2	0.0142					2.01	51.0	0.0248
1							1.15	29.2	0.0142					1.36	34.6	0.0168
1							1.15	29.2	0.0142					1.36	34.6	0.0168
1							1.15	29.2	0.0142					1.79	45.6	0.0221
Annealed Insulating Glass Units																
2	0.72	18.2	0.0089				1.79	45.6	0.0221					3.08	78.3	0.0381
2	0.72	18.2	0.0089				2.44	61.9	0.0301					2.65	67.4	0.0328
2	0.50	12.8	0.0062				1.58	40.1	0.0195					2.22	56.5	0.0275
2	0.72	18.2	0.0089				1.58	40.1	0.0195					2.22	56.5	0.0275
2	0.50	12.8	0.0062				2.22	56.5	0.0275					3.08	78.3	0.0381
2	0.72	18.2	0.0089				2.01	51.0	0.0248					2.22	56.5	0.0275
2							1.79	45.6	0.0221					2.22	56.5	0.0275
Asymmetric Insulating Glass Units																
3	0.93	23.7	0.0115	2.22	56.48	0.0275	2.22	56.5	0.0275	2.65	67.4	0.0328	0.0275	2.44	61.9	0.0301
3	0.72	18.2	0.0089	2.01	51.02	0.0248	2.22	56.5	0.0275	2.65	67.4	0.0328	0.0275	2.44	61.9	0.0301
3	0.72	18.2	0.0089	2.65	67.40	0.0328	2.44	61.9	0.0301	2.65	67.4	0.0328	0.0301	2.65	67.4	0.0328
3	0.72	18.2	0.0089	1.79	45.56	0.0221	2.01	51.0	0.0248	2.44	61.9	0.0301	0.0248	2.22	56.5	0.0275
3	0.29	7.3	0.0036	1.79	45.56	0.0221	1.79	45.6	0.0221	2.01	51.0	0.0248	0.0221	2.01	51.0	0.0248
3	0.72	18.2	0.0089	2.87	72.87	0.0354	2.87	72.9	0.0354	3.08	78.3	0.0381	0.0354	3.08	78.3	0.0381

Table A.3: Specimen information for glass configurations (4 and 5)

ID	Original Specimen Numbering	Glass Type	Corner Shape	Edge Condition	Corner Condition	Glass Nominal Thickness (in.)	Average Clearance (in.)	Glass Manufacturer
	Asymmetric Insulating Glass Units							
4	B-1	Asymmetric IGU	rectangular	cut	cut	1.043	0.43	
4	B-2	Asymmetric IGU	rectangular	cut	cut	1.043	0.43	
4	B-3	Asymmetric IGU	rectangular	cut	cut	1.043	0.43	
4	B-4	Asymmetric IGU	rectangular	cut	cut	1.043	0.43	
4	B-5	Asymmetric IGU	rectangular	cut	cut	1.043	0.43	
4	B-6	Asymmetric IGU	rectangular	cut	cut	1.043	0.43	
5	C-1	Asymmetric IGU	rectangular	cut	cut	1.038	0.43	
5	C-2	Asymmetric IGU	rectangular	cut	cut	1.038	0.43	
5	C-3	Asymmetric IGU	rectangular	cut	cut	1.038	0.43	
5	C-4	Asymmetric IGU	rectangular	cut	cut	1.038	0.43	
5	C-5	Asymmetric IGU	rectangular	cut	cut	1.038	0.43	
5	C-6	Asymmetric IGU	rectangular	cut	cut	1.038	0.43	

Table A.4: Experimental failure data for glass configurations (4 and 5)

ID	Glass-to-Frame Contact			Gasket Failure			Cracking							Fallout		
							Single or Inner Pane-IGU			Outer Pane-IGU			Lowest	Single or Inner Pane-IGU		
	in.	mm	D.R.	in.	mm	D.R.	in.	mm	D.R.	in.	mm	D.R.	D.R.	in.	mm	D.R.
Asymmetric Insulating Glass Units																
4	1.79	45.6	0.0221	2.65	67.40	0.0328	2.94	74.6	0.0363	2.65	67.4	0.0328	0.0328	3.08	78.3	0.0381
4	Unknown	Unknown	Unknown	2.22	56.48	0.0275	2.87	72.9	0.0354	2.44	61.9	0.0301	0.0301	2.87	72.9	0.0354
4	1.15	29.2	0.0142	2.22	56.48	0.0275	2.57	65.2	0.0317	2.22	56.5	0.0275	0.0275	2.65	67.4	0.0328
4	0.93	23.7	0.0115	1.79	45.56	0.0221	1.79	45.6	0.0221	2.29	58.2	0.0283	0.0221	1.79	45.6	0.0221
4	0.72	18.2	0.0089	1.58	40.10	0.0195	1.58	40.1	0.0195	n/a	n/a	n/a	0.0195	1.79	45.6	0.0221
4	1.15	29.2	0.0142	2.44	61.94	0.0301	2.65	67.4	0.0328	2.44	61.9	0.0301	0.0301	2.65	67.4	0.0328
5	0.72	18.2	0.0089	1.79	45.56	0.0221	1.79	45.6	0.0221	3.64	92.5	0.0450	0.0221	3.11	79.0	0.0384
5	0.50	12.8	0.0062	2.22	56.48	0.0275	2.65	67.4	0.0328	2.87	72.9	0.0354	0.0328	2.65	67.4	0.0328
5	0.50	12.8	0.0062	2.22	56.48	0.0275	2.22	56.5	0.0275	3.41	86.6	0.0421	0.0275	2.87	72.9	0.0354
5	0.29	7.3	0.0036	2.01	51.02	0.0248	2.44	61.9	0.0301	2.01	51.0	0.0248	0.0248	2.44	61.9	0.0301
5	0.72	18.2	0.0089	2.01	51.02	0.0248	2.01	51.0	0.0248	3.00	76.1	0.0370	0.0248	2.51	63.7	0.0310
5	0.50	12.8	0.0062	2.44	61.94	0.0301	2.44	61.9	0.0301	2.94	74.6	0.0363	0.0301	2.98	75.7	0.0368

Table A.5: Specimen information for glass configuration (6)

ID	Original Specimen Numbering	Glass Type	Corner Shape	Edge Condition	Corner Condition	Glass Nominal Thickness (in.)	Average Clearance (in.)	Glass Manufacturer
	Annealed Laminated							
6	III G	AN Lam	rectangular	cut	cut	0.25	0.43	
6	III G	AN Lam	rectangular	cut	cut	0.25	0.43	
6	III G	AN Lam	rectangular	cut	cut	0.25	0.43	
6	III G	AN Lam	rectangular	cut	cut	0.25	0.43	
6	III G	AN Lam	rectangular	cut	cut	0.25	0.43	
6	III G	AN Lam	rectangular	cut	cut	0.25	0.43	
6	SR 41	AN Lam	rectangular	cut	cut	0.25	0.43	
6	SR 41	AN Lam	rectangular	cut	cut	0.25	0.43	
6	SR 41	AN Lam	rectangular	cut	cut	0.25	0.43	
6	SR 41	AN Lam	rectangular	cut	cut	0.25	0.43	
6	SR 41	AN Lam	rectangular	cut	cut	0.25	0.43	
6	SR 41	AN Lam	rectangular	cut	cut	0.25	0.43	
6	Config G and UMR	AN Lam	rectangular	cut	cut	0.25	0.43	
6	Config G and UMR	AN Lam	rectangular	cut	cut	0.25	0.43	
6	Config G and UMR	AN Lam	rectangular	cut	cut	0.25	0.43	
6	Config G and UMR	AN Lam	rectangular	cut	cut	0.25	0.43	
6	Config G and UMR	AN Lam	rectangular	cut	cut	0.25	0.43	
6	Config G and UMR	AN Lam	rectangular	cut	cut	0.25	0.43	
6	Config G and UMR	AN Lam	rectangular	cut	cut	0.25	0.43	
6	Config G and UMR	AN Lam	rectangular	cut	cut	0.25	0.43	
6	Config G and UMR	AN Lam	rectangular	cut	cut	0.25	0.43	
6	Config G and UMR	AN Lam	rectangular	cut	cut	0.25	0.43	
6	Config G and UMR	AN Lam	rectangular	cut	cut	0.25	0.43	
6	Config G and UMR	AN Lam	rectangular	cut	cut	0.25	0.43	

Table A.6: Experimental failure data for glass configuration (6)

ID	Glass-to-Frame Contact			Gasket Failure			Cracking							Fallout		
							Single or Inner Pane-IGU			Outer Pane-IGU			Lowest	Single or Inner Pane-IGU		
	in.	mm	D.R.	in.	mm	D.R.	in.	mm	D.R.	in.	mm	D.R.	D.R.	in.	mm	D.R.
	Annealed Laminated															
6							1.15	29.2	0.0142					5.19	131.9	0.0641
6							1.15	29.2	0.0142					4.44	112.8	0.0548
6							1.36	34.6	0.0168					4.41	112.0	0.0544
6							0.93	23.7	0.0115					3.49	88.6	0.0431
6							0.93	23.7	0.0115					5.18	131.6	0.0640
6							1.36	34.6	0.0168					4.94	125.5	0.0610
6							0.93	23.7	0.0115					5.21	132.3	0.0643
6							0.93	23.7	0.0115					2.78	70.7	0.0344
6							1.15	29.2	0.0142					3.54	89.9	0.0437
6							0.93	23.7	0.0115					3.39	86.2	0.0419
6							1.15	29.2	0.0142					4.80	121.8	0.0592
6							0.93	23.7	0.0115					4.98	126.4	0.0614
6							1.79	45.6	0.0221					5.02	127.5	0.0620
6							1.15	29.2	0.0142					3.08	78.3	0.0381
6							1.36	34.6	0.0168					5.02	127.5	0.0620
6							1.36	34.6	0.0168					5.02	127.5	0.0620
6							1.15	29.2	0.0142					5.02	127.5	0.0620
6							1.36	34.6	0.0168					5.02	127.5	0.0620
6							1.79	45.6	0.0221					5.02	127.5	0.0620
6							1.79	45.6	0.0221					5.02	127.5	0.0620
6							1.58	40.1	0.0195					5.02	127.5	0.0620
6							1.79	45.6	0.0221					5.02	127.5	0.0620
6							1.58	40.1	0.0195					5.02	127.5	0.0620
6							1.58	40.1	0.0195					5.02	127.5	0.0620

Table A.7: Specimen information for glass configurations (7 and 8)

ID	Original Specimen Numbering	Glass Type	Corner Shape	Edge Condition	Corner Condition	Glass Nominal Thickness (in.)	Average Clearance (in.)	Glass Manufacturer
	Annealed Monolithic - Storefront							
7	1-1	AN Mono	rectangular	cut	cut	0.25	0.41	
7	1-2	AN Mono	rectangular	cut	cut	0.25	0.41	
7	1-3	AN Mono	rectangular	cut	cut	0.25	0.41	
7	2-1	AN Mono	rectangular	cut	cut	0.25	0.41	
7	2-2	AN Mono	rectangular	cut	cut	0.25	0.41	
7	2-3	AN Mono	rectangular	cut	cut	0.25	0.41	
7	3-1	AN Mono	rectangular	cut	cut	0.25	0.41	
7	3-2	AN Mono	rectangular	cut	cut	0.25	0.41	
7	3-3	AN Mono	rectangular	cut	cut	0.25	0.41	
7	4-1	AN Mono	rectangular	cut	cut	0.25	0.41	
7	4-2	AN Mono	rectangular	cut	cut	0.25	0.41	
7	4-3	AN Mono	rectangular	cut	cut	0.25	0.41	
	Annealed Insulating Glass Units - Storefront							
8	1-1	AN IGU	rectangular	cut	cut	1.00	0.59	
8	1-2	AN IGU	rectangular	cut	cut	1.00	0.59	
8	1-3	AN IGU	rectangular	cut	cut	1.00	0.59	
8	2-1	AN IGU	rectangular	cut	cut	1.00	0.59	
8	2-2	AN IGU	rectangular	cut	cut	1.00	0.59	
8	2-3	AN IGU	rectangular	cut	cut	1.00	0.59	
8	3-1	AN IGU	rectangular	cut	cut	1.00	0.59	
8	3-2	AN IGU	rectangular	cut	cut	1.00	0.59	
8	3-3	AN IGU	rectangular	cut	cut	1.00	0.59	
8	4-1	AN IGU	rectangular	cut	cut	1.00	0.59	
8	4-2	AN IGU	rectangular	cut	cut	1.00	0.59	
8	4-3	AN IGU	rectangular	cut	cut	1.00	0.59	

Table A.8: Experimental failure data for glass configurations (7 and 8)

ID	Glass-to-Frame Contact			Gasket Failure			Cracking							Fallout		
							Single or Inner Pane-IGU			Outer Pane-IGU			Lowest	Single or Inner Pane-IGU		
	in.	mm	D.R.	in.	mm	D.R.	in.	mm	D.R.	in.	mm	D.R.	D.R.	in.	mm	D.R.
Annealed Monolithic - Storefront																
7				2.00	50.80	0.0247	2.75	69.9	0.0340					4.20	106.7	0.0519
7				3.38	85.85	0.0417	3.25	82.6	0.0401					3.40	86.4	0.0420
7				3.63	92.20	0.0448	4.25	108.0	0.0525					5.30	134.6	0.0654
7				3.13	79.50	0.0386	3.25	82.6	0.0401					3.30	83.8	0.0407
7				2.25	57.15	0.0278	3.50	88.9	0.0432					4.50	114.3	0.0556
7				2.50	63.50	0.0309	4.25	108.0	0.0525					5.00	127.0	0.0617
7				2.50	63.50	0.0309	3.00	76.2	0.0370					4.35	110.5	0.0537
7				0.75	19.05	0.0093	3.25	82.6	0.0401					4.25	108.0	0.0525
7				3.25	82.55	0.0401	3.50	88.9	0.0432					4.15	105.4	0.0512
7				2.25	57.15	0.0278	3.00	76.2	0.0370					3.50	88.9	0.0432
7				3.50	88.90	0.0432	3.50	88.9	0.0432					4.35	110.5	0.0537
7				2.25	57.15	0.0278	3.00	76.2	0.0370					3.75	95.3	0.0463
7				2.00	50.80	0.0247	2.75	69.9	0.0340					4.20	106.7	0.0519
7				3.38	85.85	0.0417	3.25	82.6	0.0401					3.40	86.4	0.0420
Annealed Insulating Glass Units - Storefront																
8				2.50	63.50	0.0309	4.75	120.7	0.0586					5.55	141.0	0.0685
8				2.88	73.15	0.0356	4.75	120.7	0.0586					5.25	133.4	0.0648
8				3.63	92.20	0.0448	4.75	120.7	0.0586					4.95	125.7	0.0611
8				3.75	95.25	0.0463	4.50	114.3	0.0556					5.75	146.1	0.0710
8				3.50	88.90	0.0432	4.50	114.3	0.0556					5.50	139.7	0.0679
8				3.50	88.90	0.0432	4.50	114.3	0.0556					5.40	137.2	0.0667
8				3.75	95.25	0.0463	5.00	127.0	0.0617					5.25	133.4	0.0648
8				4.00	101.60	0.0494	4.50	114.3	0.0556					5.25	133.4	0.0648
8				2.75	69.85	0.0340	4.75	120.7	0.0586					5.25	133.4	0.0648
8				4.13	104.90	0.0510	5.50	139.7	0.0679					5.50	139.7	0.0679
8				4.25	107.95	0.0525	5.25	133.4	0.0648					5.50	139.7	0.0679
8				3.00	76.20	0.0370	4.75	120.7	0.0586					5.50	139.7	0.0679

Table A.9: Specimen information for glass configurations (9-13)

ID	Original Specimen Numbering	Glass Type	Corner Shape	Edge Condition	Corner Condition	Glass Nominal Thickness (in.)	Average Clearance (in.)	Glass Manufacturer
	Annealed Laminated - Storefront							
9	1-1	AN Lam	rectangular	cut	cut	0.25	0.41	
9	1-2	AN Lam	rectangular	cut	cut	0.25	0.41	
9	1-3	AN Lam	rectangular	cut	cut	0.25	0.41	
9	2-1	AN Lam	rectangular	cut	cut	0.25	0.41	
9	2-2	AN Lam	rectangular	cut	cut	0.25	0.41	
9	2-3	AN Lam	rectangular	cut	cut	0.25	0.41	
9	3-1	AN Lam	rectangular	cut	cut	0.25	0.41	
9	3-2	AN Lam	rectangular	cut	cut	0.25	0.41	
9	3-3	AN Lam	rectangular	cut	cut	0.25	0.41	
9	4-1	AN Lam	rectangular	cut	cut	0.25	0.41	
9	4-2	AN Lam	rectangular	cut	cut	0.25	0.41	
9	4-3	AN Lam	rectangular	cut	cut	0.25	0.41	
	Annealed Monolithic - 0" Clearance							
10	added 11/27/2007	AN Mono	rectangular	cut	cut	0.25	0	
10	added 3/14/2008	AN Mono	rectangular	cut	cut	0.25	0	
	Annealed Monolithic - 1/8" Clearance							
11	added 2007	AN Mono	rectangular	cut	cut	0.25	0.125	
11	added 2/18/2008	AN Mono	rectangular	cut	cut	0.25	0.125	
	Annealed Monolithic - 1/4" Clearance							
12	added 10/30/2007	AN Mono	rectangular	cut	cut	0.25	0.25	
12	added 3/28/2008	AN Mono	rectangular	cut	cut	0.25	0.25	
12	added 2007	AN Mono	rectangular	cut	cut	0.25	0.25	
	Annealed Insulating Glass Unit - 1/4" Clearance							
13	added 4/9/2008	AN IGU	rectangular	cut	cut	1.00	0.25	

Table A.10: Experimental failure data for glass configurations (9-13)

ID	Glass-to-Frame Contact			Gasket Failure			Cracking							Fallout		
							Single or Inner Pane-IGU			Outer Pane-IGU			Lowest	Single or Inner Pane-IGU		
	in.	mm	D.R.	in.	mm	D.R.	in.	mm	D.R.	in.	mm	D.R.	D.R.	in.	mm	D.R.
Annealed Laminated - Storefront																
9				2.63	66.80	0.0325	5.25	133.4	0.0648					6.00[1]	152.4	0.0741
9				2.75	69.85	0.0340	5.00	127.0	0.0617					6.00	152.4	0.0741
9				3.13	79.50	0.0386	3.75	95.3	0.0463					5.50	139.7	0.0679
9				0.75	19.05	0.0093	4.00	101.6	0.0494					6.00[1]	152.4	0.0741
9				3.00	76.20	0.0370	4.25	108.0	0.0525					6.00[1]	152.4	0.0741
9				2.75	69.85	0.0340	4.25	108.0	0.0525					6.00[1]	152.4	0.0741
9				3.25	82.55	0.0401	5.50	139.7	0.0679					5.50	139.7	0.0679
9				2.25	57.15	0.0278	4.25	108.0	0.0525					6.00[1]	152.4	0.0741
9				2.13	54.10	0.0263	5.50	139.7	0.0679					5.75	146.1	0.0710
9				n/a	n/a	n/a	n/a	n/a	n/a					n/a	n/a	n/a
9				n/a	n/a	n/a	n/a	n/a	n/a					n/a	n/a	n/a
9				n/a	n/a	n/a	n/a	n/a	n/a					n/a	n/a	n/a
9				2.63	66.80	0.0325	5.25	133.4	0.0648					6.00[1]	152.4	0.0741
9				2.75	69.85	0.0340	5.00	127.0	0.0617					6.00	152.4	0.0741
Annealed Monolithic - 0" Clearance																
10							0.70	17.7	0.0086					0.86	21.9	0.0106
10							0.73	18.5	0.0090					0.89	22.5	0.0110
Annealed Monolithic - 1/8" Clearance																
11							0.72	18.2	0.0089					0.72	18.2	0.0089
11							0.65	16.6	0.0080					1.04	26.4	0.0128
Annealed Monolithic - 1/4" Clearance																
12							1.22	30.9	0.0150					1.22	30.9	0.0150
12							1.15	29.2	0.0142					1.36	34.6	0.0168
12							1.21	30.7	0.0149					1.42	35.9	0.0175
Annealed Insulating Glass Unit - 1/4" Clearance																
13							1.15	29.2	0.0142					1.79	45.6	0.0221

Table A.11: Specimen information for glass configurations (14-17)

ID	Original Specimen Numbering	Glass Type	Corner Shape	Edge Condition	Corner Condition	Glass Nominal Thickness (in.)	Average Clearance (in.)	Glass Manufacturer
Annealed Monolithic – 2:1 Aspect Ratio								
14	Dec 2006	AN Mono	rectangular	cut	cut	0.25	0.43	Oldcastle
14	Dec 2006	AN Mono	rectangular	cut	cut	0.25	0.43	Oldcastle
Annealed Monolithic - 1:2 Aspect Ratio								
15	Dec 2006	AN Mono	rectangular	cut	cut	0.25	0.43	Oldcastle
15	Dec 2006	AN Mono	rectangular	cut	cut	0.25	0.43	Oldcastle
Heat-Strengthened Monolithic								
16	UMR -1	HS Mono	rectangular	cut	cut	0.25	0.43	
16	UMR -2	HS Mono	rectangular	cut	cut	0.25	0.43	
16	UMR -3	HS Mono	rectangular	cut	cut	0.25	0.43	
16	UMR -4	HS Mono	rectangular	cut	cut	0.25	0.43	
16	UMR -5	HS Mono	rectangular	cut	cut	0.25	0.43	
16	UMR -6	HS Mono	rectangular	cut	cut	0.25	0.43	
16	UMR -7	HS Mono	rectangular	cut	cut	0.25	0.43	
16	UMR -8	HS Mono	rectangular	cut	cut	0.25	0.43	
Heat-Strengthened IGU								
17	UMR -1	HS IGU	rectangular	cut	cut	1.00	0.43	
17	UMR -2	HS IGU	rectangular	cut	cut	1.00	0.43	
17	UMR -3	HS IGU	rectangular	cut	cut	1.00	0.43	
17	UMR -4	HS IGU	rectangular	cut	cut	1.00	0.43	
17	UMR -5	HS IGU	rectangular	cut	cut	1.00	0.43	
17	UMR -6	HS IGU	rectangular	cut	cut	1.00	0.43	

Table A.12: Experimental failure data for glass configurations (14-17)

ID	Glass-to-Frame Contact			Gasket Failure			Cracking							Fallout		
							Single or Inner Pane-IGU			Outer Pane-IGU			Lowest	Single or Inner Pane-IGU		
	in.	mm	D.R.	in.	mm	D.R.	in.	mm	D.R.	in.	mm	D.R.	D.R.	in.	mm	D.R.
Annealed Monolithic - 2:1 Aspect Ratio																
14							1.79	45.6	0.0171					2.22	56.5	0.0212
14							2.01	51.0	0.0191					2.22	56.5	0.0212
Annealed Monolithic - 1:2 Aspect Ratio																
15							1.15	29.2	0.0202					1.36	34.6	0.0239
15							1.36	34.6	0.0239					1.58	40.1	0.0277
Heat-Strengthened Monolithic																
16	1.15	29.2	0.0142				2.44	61.9	0.0301					2.55	64.7	0.0314
16	1.15	29.2	0.0142				1.79	45.6	0.0221					1.79	45.6	0.0221
16	0.72	18.2	0.0089				1.79	45.6	0.0221					1.79	45.6	0.0221
16	0.72	18.2	0.0089				1.58	40.1	0.0195					2.01	51.0	0.0248
16	0.72	18.2	0.0089				2.01	51.0	0.0248					2.01	51.0	0.0248
16	1.15	29.2	0.0142				1.79	45.6	0.0221					1.79	45.6	0.0221
16	0.29	7.3	0.0036				2.22	56.5	0.0275					2.22	56.5	0.0275
16	0.72	18.2	0.0089				2.01	51.0	0.0248					2.01	51.0	0.0248
Heat-Strengthened IGU																
17	0.72	18.2	0.0089				1.79	45.6	0.0221					1.79	45.6	0.0221
17	0.72	18.2	0.0089				2.87	72.9	0.0354					2.87	72.9	0.0354
17	0.50	12.8	0.0062				2.01	51.0	0.0248					2.22	56.5	0.0275
17	0.72	18.2	0.0089				2.01	51.0	0.0248					2.01	51.0	0.0248
17	0.72	18.2	0.0089				2.22	56.5	0.0275					2.22	56.5	0.0275
17	0.72	18.2	0.0089				2.01	51.0	0.0248					2.01	51.0	0.0248

Table A.13: Specimen information for glass configurations (18-20)

ID	Original Specimen Numbering	Glass Type	Corner Shape	Edge Condition	Corner Condition	Glass Nominal Thickness (in.)	Average Clearance (in.)	Glass Manufacturer
	Heat-Strengthened Laminated							
18	UMR -1	HS LAM	rectangular	cut	cut	0.38	0.43	
18	UMR -2	HS LAM	rectangular	cut	cut	0.38	0.43	
18	UMR -3	HS LAM	rectangular	cut	cut	0.38	0.43	
18	UMR -4	HS LAM	rectangular	cut	cut	0.38	0.43	
18	UMR -5	HS LAM	rectangular	cut	cut	0.38	0.43	
18	UMR -6	HS LAM	rectangular	cut	cut	0.38	0.43	
	Asymmetric (HS) Insulating Glass Unit							
19	D-1	Asymmetric IGU (HS)	rectangular	cut	cut	1.038	0.43	
19	D-2	Asymmetric IGU (HS)	rectangular	cut	cut	1.038	0.43	
19	D-3	Asymmetric IGU (HS)	rectangular	cut	cut	1.038	0.43	
19	D-4	Asymmetric IGU (HS)	rectangular	cut	cut	1.038	0.43	
19	D-5	Asymmetric IGU (HS)	rectangular	cut	cut	1.038	0.43	
19	D-6	Asymmetric IGU (HS)	rectangular	cut	cut	1.038	0.43	
20	E-1	Asymmetric IGU (HS)	rectangular	cut	cut	1.253	0.43	
20	E-2	Asymmetric IGU (HS)	rectangular	cut	cut	1.253	0.43	
20	E-3	Asymmetric IGU (HS)	rectangular	cut	cut	1.253	0.43	
20	E-4	Asymmetric IGU (HS)	rectangular	cut	cut	1.253	0.43	
20	E-5	Asymmetric IGU (HS)	rectangular	cut	cut	1.253	0.43	

Table A.14: Experimental failure data for glass configurations (18-20)

ID	Glass-to-Frame Contact			Gasket Failure			Cracking							Fallout		
							Single or Inner Pane-IGU			Outer Pane-IGU			Lowest	Single or Inner Pane-IGU		
	in.	mm	D.R.	in.	mm	D.R.	in.	mm	D.R.	in.	mm	D.R.	D.R.	in.	mm	D.R.
Heat-Strengthened Laminated																
18	0.72	18.2	0.0089				1.36	34.6	0.0168					5.02[1]	127.5	0.0620
18	1.15	29.2	0.0142				1.79	45.6	0.0221					4.16	105.6	0.0513
18	0.72	18.2	0.0089				2.01	51.0	0.0248					4.37	111.1	0.0540
18	0.72	18.2	0.0089				1.79	45.6	0.0221					3.94	100.2	0.0487
18	0.72	18.2	0.0089				1.79	45.6	0.0221					3.73	94.7	0.0460
18	0.72	18.2	0.0089				2.01	51.0	0.0248					5.02[1]	127.5	0.0620
Asymmetric (HS) Insulating Glass Unit																
19	0.72	18.2	0.0089				2.01	51.0	0.0248	2.81	71.3	0.0347	0.0248	2.38	60.4	0.0294
19	1.36	34.6	0.0168				3.00	76.1	0.0370	2.44	61.9	0.0301	0.0301	3.04	77.2	0.0375
19	0.72	18.2	0.0089				3.02	76.8	0.0373	2.22	56.5	0.0275	0.0275	3.02	76.8	0.0373
19	0.93	23.7	0.0115				2.87	72.9	0.0354	2.22	56.5	0.0275	0.0275	3.00	76.1	0.0370
19	0.29	7.3	0.0036				1.79	45.6	0.0221	2.44	61.9	0.0301	0.0221	2.44	61.9	0.0301
19	0.50	12.8	0.0062				2.46	62.6	0.0304	2.01	51.0	0.0248	0.0248	2.61	66.3	0.0322
20	0.72	18.2	0.0089				2.44	61.9	0.0301	3.86	98.0	0.0476	0.0301	2.65	67.4	0.0328
20	0.50	12.8	0.0062				2.44	61.9	0.0301	2.87	72.9	0.0354	0.0301	2.87	72.9	0.0354
20	0.50	12.8	0.0062				2.65	67.4	0.0328	4.80	122.0	0.0593	0.0328	2.77	70.2	0.0341
20	0.07	1.9	0.0009				1.58	40.1	0.0195	3.73	94.7	0.0460	0.0195	2.22	56.5	0.0275
20	0.50	12.8	0.0062				2.44	61.9	0.0301	4.33	110.0	0.0535	0.0301	2.65	67.4	0.0328

Table A.15: Specimen information for glass configurations (21 and 22)

ID	Original Specimen Numbering	Glass Type	Corner Shape	Edge Condition	Corner Condition	Glass Nominal Thickness (in.)	Average Clearance (in.)	Glass Manufacturer
	Fully-Tempered Monolithic							
21	UMR -1	FT mono	rectangular	cut	cut	0.25	0.43	
21	UMR -2	FT mono	rectangular	cut	cut	0.25	0.43	
21	UMR -3	FT mono	rectangular	cut	cut	0.25	0.43	
21	UMR -4	FT mono	rectangular	cut	cut	0.25	0.43	
21	UMR -5	FT mono	rectangular	cut	cut	0.25	0.43	
21	UMR -6	FT mono	rectangular	cut	cut	0.25	0.43	
	Fully-Tempered Monolithic - Storefront							
22	1-1	Storefront - FT mono	rectangular	cut	cut	0.25	0.41	
22	1-2	Storefront - FT mono	rectangular	cut	cut	0.25	0.41	
22	1-3	Storefront - FT mono	rectangular	cut	cut	0.25	0.41	
22	2-1	Storefront - FT mono	rectangular	cut	cut	0.25	0.41	
22	2-2	Storefront - FT mono	rectangular	cut	cut	0.25	0.41	
22	2-3	Storefront - FT mono	rectangular	cut	cut	0.25	0.41	
22	3-1	Storefront - FT mono	rectangular	cut	cut	0.25	0.41	
22	3-2	Storefront - FT mono	rectangular	cut	cut	0.25	0.41	
22	3-3	Storefront - FT mono	rectangular	cut	cut	0.25	0.41	
22	4-1	Storefront - FT mono	rectangular	cut	cut	0.25	0.41	
22	4-2	Storefront - FT mono	rectangular	cut	cut	0.25	0.41	

Table A.16: Experimental failure data for glass configurations (21 and 22)

ID	Glass-to-Frame Contact			Gasket Failure			Cracking							Fallout		
							Single or Inner Pane-IGU			Outer Pane-IGU			Lowest	Single or Inner Pane-IGU		
	in.	mm	D.R.	in.	mm	D.R.	in.	mm	D.R.	in.	mm	D.R.	D.R.	in.	mm	D.R.
Fully-Tempered Monolithic																
21	0.93	23.7	0.0115				2.22	56.5	0.0275					2.22	56.5	0.0275
21	0.93	23.7	0.0115				1.79	45.6	0.0221					1.79	45.6	0.0221
21	0.72	18.2	0.0089				2.01	51.0	0.0248					2.01	51.0	0.0248
21	0.93	23.7	0.0115				2.65	67.4	0.0328					2.65	67.4	0.0328
21	0.72	18.2	0.0089				1.15	29.2	0.0142					1.15	29.2	0.0142
21	1.15	29.2	0.0142				2.01	51.0	0.0248					2.01	51.0	0.0248
Fully-Tempered Monolithic - Storefront																
22														3.85	97.8	0.0475
22														3.75	95.3	0.0463
22														4.00	101.6	0.0494
22														3.25	82.6	0.0401
22														3.25	82.6	0.0401
22														3.90	99.1	0.0481
22														3.50	88.9	0.0432
22														3.55	90.2	0.0438
22														4.00	101.6	0.0494
22														4.00	101.6	0.0494
22														4.25	108.0	0.0525

Table A.17: Specimen information for glass configurations (23 and 24)

ID	Original Specimen Numbering	Glass Type	Corner Shape	Edge Condition	Corner Condition	Glass Nominal Thickness (in.)	Average Clearance (in.)	Glass Manufacturer
Fully-Tempered Insulating Glass Unit- Storefront								
23	1-1	Storefront - FT IGU	rectangular	cut	cut	1.00	0.59	
23	1-2	Storefront - FT IGU	rectangular	cut	cut	1.00	0.59	
23	1-3	Storefront - FT IGU	rectangular	cut	cut	1.00	0.59	
23	2-1	Storefront - FT IGU	rectangular	cut	cut	1.00	0.59	
23	2-2	Storefront - FT IGU	rectangular	cut	cut	1.00	0.59	
23	2-3	Storefront - FT IGU	rectangular	cut	cut	1.00	0.59	
23	3-1	Storefront - FT IGU	rectangular	cut	cut	1.00	0.59	
23	3-2	Storefront - FT IGU	rectangular	cut	cut	1.00	0.59	
23	3-3	Storefront - FT IGU	rectangular	cut	cut	1.00	0.59	
23	4-1	Storefront - FT IGU	rectangular	cut	cut	1.00	0.59	
23	4-2	Storefront - FT IGU	rectangular	cut	cut	1.00	0.59	
23	4-3	Storefront - FT IGU	rectangular	cut	cut	1.00	0.59	
Asymmetric (FT) Insulating Glass Unit								
24	F-1	Assymetric IGU (FT)	rectangular	cut	cut	1.238	0.43	
24	F-2	Assymetric IGU (FT)	rectangular	cut	cut	1.238	0.43	
24	F-3	Assymetric IGU (FT)	rectangular	cut	cut	1.238	0.43	
24	F-4	Assymetric IGU (FT)	rectangular	cut	cut	1.238	0.43	
24	F-5	Assymetric IGU (FT)	rectangular	cut	cut	1.238	0.43	
24	F-6	Assymetric IGU (FT)	rectangular	cut	cut	1.238	0.43	

Table A.18: Experimental failure data for glass configurations (23 and 24)

ID	Glass-to-Frame Contact			Gasket Failure			Cracking							Fallout		
							Single or Inner Pane-IGU			Outer Pane-IGU			Lowest	Single or Inner Pane-IGU		
	in.	mm	D.R.	in.	mm	D.R.	in.	mm	D.R.	in.	mm	D.R.	D.R.	in.	mm	D.R.
Fully-Tempered Insulating Glass Unit- Storefront																
23														5.75	146.1	0.0710
23														5.75	146.1	0.0710
23														5.50	139.7	0.0679
23														5.50	139.7	0.0679
23														5.25	133.4	0.0648
23														4.75	120.7	0.0586
23														6.00	152.4	0.0741
23														5.50	139.7	0.0679
23														5.00	127.0	0.0617
23														4.55	115.6	0.0562
23														3.40	86.4	0.0420
23														5.00	127.0	0.0617
Asymmetric (FT) Insulating Glass Unit																
22	0.29	7.3	0.0036				2.65	67.4	0.0328	2.65	67.4	0.0328	0.0328	2.78	70.7	0.0344
22	0.72	18.2	0.0089				3.08	78.3	0.0381	3.73	94.7	0.0460	0.0381	3.30	83.8	0.0407
22	0.51	12.9	0.0063				2.87	72.9	0.0354	3.30	83.8	0.0407	0.0354	3.08	78.3	0.0381
22	0.72	18.2	0.0089				2.65	67.4	0.0328	3.02	76.8	0.0373	0.0328	2.87	72.9	0.0354
22	0.50	12.8	0.0062				2.22	56.5	0.0275	3.07	77.9	0.0379	0.0275	2.22	56.5	0.0275
22	0.72	18.2	0.0089				2.65	67.4	0.0328	2.87	72.9	0.0354	0.0328	2.65	67.4	0.0328

A.2 Software Information Input

In this section, information that was input into the *Fragility Function Calculator version 1.02* software for each glass configuration and failure limit state was compiled, of which the subjects included: Component ID, Component Description, Describe Specimen, Describe Excitation, Demand Parameter, Damage Evidence, and Damage Measure. Tables **A.19** through **A.22** provide input information for the serviceability limit states of cracking and gasket degradation for glass configurations, while tables **A.23** through **A.26** provide input information for the ultimate limit state of glass fallout.

Table A.19: Input information for glass configurations (1-6) for serviceability limit states

Glass ID	PACT ID	Component Description:	Describe Specimens:	Describe Excitation:	Demand Parameter:	Damage Evidence:	Damage Measure:
1	B2022.001	Curtain wall, monolithic, annealed glass, aluminum framing, square corners, cut corner finish, cut edge finish	5 ft W x 6 ft H (1.5 m x 1.8 m) size, 6:5 aspect ratio, 1/4 in. (6 mm) thick glass, 0.43 in. (11 mm) glass-to-frame clearance, Kawneer 1600 curtain wall framing	Displacement controlled cyclic racking loading	Cracking Transient Interstory Drift Ratio	glass-to-frame contact, corner crushing, fallout, gasket/sealant damage, cracking	Serviceability type failure
2	B2022.002	Curtain wall, IGU, annealed glass, aluminum framing, square corners, cut corner finish, cut edge finish	5 ft W x 6 ft H (1.5 m x 1.8 m) size, 6:5 aspect ratio, inner/outer AN 1/4 in. (6 mm) thick glass, 0.43 in. (11 mm) glass-to-frame clearance, Kawneer 1600 curtain wall framing	Displacement controlled cyclic racking loading	Cracking Transient Interstory Drift Ratio	glass-to-frame contact, corner crushing, fallout, gasket/sealant damage, cracking	Serviceability type failure
3	B2022.003	Curtain wall, IGU, asymmetric glass, aluminum framing, square corners, cut corner finish, cut edge finish	5 ft W x 6 ft H (1.5 m x 1.8 m) size, 6:5 aspect ratio, 1/4 in. (6 mm) inner AN mono glass, 1/4 in. (6 mm) outer AN lam. (0.030 PVB) outer glass, 0.43 in. (11 mm) average glass-to-frame clearance, Kawneer 1600 curtain wall framing	Displacement controlled cyclic racking loading	First Cracking Overall Transient Interstory Drift Ratio observed in glass unit or Gasket Transient Interstory Drift Ratio	glass-to-frame contact, corner crushing, fallout, gasket/sealant damage, cracking	Serviceability type failure
4	B2022.004	Curtain wall, IGU, asymmetric glass, aluminum framing, square corners, cut corner finish, cut edge finish	5 ft W x 6 ft H (1.5 m x 1.8 m) size, 6:5 aspect ratio, 1/4 in. (6 mm) inner AN mono glass, 1/4 in. (6 mm) outer AN lam. (0.060 PVB) outer glass, 0.43 in. (11 mm) average glass-to-frame clearance, Kawneer 1600 curtain wall framing	Displacement controlled cyclic racking loading	First Cracking Overall Transient Interstory Drift Ratio observed in glass unit or Gasket Transient Interstory Drift Ratio	glass-to-frame contact, corner crushing, fallout, gasket/sealant damage, cracking	Serviceability type failure
5	B2022.005	Curtain wall, IGU, asymmetric glass, aluminum framing, square corners, cut corner finish, cut edge finish	5 ft W x 6 ft H (1.5 m x 1.8 m) size, 6:5 aspect ratio, 1/4 in. (6 mm) inner AN mono glass, 1/2 in. (13 mm) outer AN lam. (0.030 PVB) outer glass, 0.43 in. (11 mm) average glass-to-frame clearance, Kawneer 1600 curtain wall framing	Displacement controlled cyclic racking loading	First Cracking Overall Transient Interstory Drift Ratio observed in glass unit or Gasket Transient Interstory Drift Ratio	glass-to-frame contact, corner crushing, fallout, gasket/sealant damage, cracking	Serviceability type failure
6	B2022.006	Curtain wall, laminated, annealed glass, aluminum framing, square corners, cut corner finish, cut edge finish	5 ft W x 6 ft H (1.5 m x 1.8 m) size, 6:5 aspect ratio, 1/4 in. (6 mm) thick glass (0.030 PVB), 0.43 in. (11 mm) glass-to-frame clearance, Kawneer 1600 curtain wall framing	Displacement controlled cyclic racking loading	Cracking Transient Interstory Drift Ratio	glass-to-frame contact, corner crushing, fallout, gasket/sealant damage, cracking	Serviceability type failure

Table A.20: Input information for glass configurations (7-12) for serviceability limit states

Glass ID	PACT ID	Component Description:	Describe Specimens:	Describe Excitation:	Demand Parameter:	Damage Evidence:	Damage Measure:
7	B2022.007	Storefront, monolithic, annealed glass, aluminum framing, square corners, cut corner finish, cut edge finish	5 ft W x 6 ft H (1.5 m x 1.8 m) size, 6:5 aspect ratio, 1/4 in. (6 mm) thick glass, 0.41 in. (10 mm) average glass-to-frame clearance, Kawneer TriFab II 451 Storefront curtain wall framing	Displacement controlled cyclic racking loading	Cracking Transient Interstory Drift Ratio or Gasket Transient Interstory Drift Ratio	glass-to-frame contact, corner crushing, fallout, gasket/sealant damage, cracking	Serviceability type failure
8	B2022.008	Storefront, IGU, annealed glass, aluminum framing, square corners, cut corner finish, cut edge finish	5 ft W x 6 ft H (1.5 m x 1.8 m) size, 6:5 aspect ratio, inner/outer AN 1/4 in. (6 mm) thick glass, 0.59 in. (15 mm) average glass-to-frame clearance, Kawneer TriFab II 451 Storefront curtain wall framing	Displacement controlled cyclic racking loading	First Cracking Overall Transient Interstory Drift Ratio observed in glass unit or Gasket Transient Interstory Drift Ratio	glass-to-frame contact, corner crushing, fallout, gasket/sealant damage, cracking	Serviceability type failure
9	B2022.009	Storefront, laminated, annealed glass, aluminum framing, square corners, cut corner finish, cut edge finish	5 ft W x 6 ft H (1.5 m x 1.8 m) size, 6:5 aspect ratio, 1/4 in. (6 mm) thick glass (0.030 PVB), 0.41 in. (10 mm) average glass-to-frame clearance, Kawneer TriFab II 451 Storefront curtain wall framing	Displacement controlled cyclic racking loading	Cracking Transient Interstory Drift Ratio or Gasket Transient Interstory Drift Ratio	glass-to-frame contact, corner crushing, fallout, gasket/sealant damage, cracking	Serviceability type failure
10	B2022.010	Curtain wall, monolithic, annealed glass, aluminum framing, square corners, cut corner finish, cut edge finish	5 ft W x 6 ft H (1.5 m x 1.8 m) size, 6:5 aspect ratio, 1/4 in. (6 mm) thick glass, 0 in. (0 mm) glass-to-frame clearance, Kawneer 1600 curtain wall framing	Displacement controlled cyclic racking loading	Cracking Transient Interstory Drift Ratio	glass-to-frame contact, corner crushing, fallout, gasket/sealant damage, cracking	Serviceability type failure
11	B2022.011	Curtain wall, monolithic, annealed glass, aluminum framing, square corners, cut corner finish, cut edge finish	5 ft W x 6 ft H (1.5 m x 1.8 m) size, 6:5 aspect ratio, 1/4 in. (6 mm) thick glass, 1/8 in. (3 mm) glass-to-frame clearance, Kawneer 1600 curtain wall framing	Displacement controlled cyclic racking loading	Cracking Transient Interstory Drift Ratio	glass-to-frame contact, corner crushing, fallout, gasket/sealant damage, cracking	Serviceability type failure
12	B2022.012	Curtain wall, monolithic, annealed glass, aluminum framing, square corners, cut corner finish, cut edge finish	5 ft W x 6 ft H (1.5 m x 1.8 m) size, 6:5 aspect ratio, 1/4 in. (6 mm) thick glass, 1/4 in. (6 mm) glass-to-frame clearance, Kawneer 1600 curtain wall framing	Displacement controlled cyclic racking loading	Cracking Transient Interstory Drift Ratio	glass-to-frame contact, corner crushing, fallout, gasket/sealant damage, cracking	Serviceability type failure

Table A.21: Input information for glass configurations (13-18) for serviceability limit states

Glass ID	PACT ID	Component Description:	Describe Specimens:	Describe Excitation:	Demand Parameter:	Damage Evidence:	Damage Measure:
13	B2022.013	Curtain wall, IGU, annealed glass, aluminum framing, square corners, cut corner finish, cut edge finish	5 ft W x 6 ft H (1.5 m x 1.8 m) size, 6:5 aspect ratio, inner/outer AN 1/4 in. (6 mm) thick glass, 1/2 in. (13 mm) glass-to-frame clearance, Kawneer 1600 curtain wall framing	Displacement controlled cyclic racking loading	Cracking Transient Interstory Drift Ratio	glass-to-frame contact, corner crushing, fallout, gasket/sealant damage, cracking	Serviceability type failure
14	B2022.014	Curtain wall, monolithic, annealed glass, aluminum framing, square corners, cut corner finish, cut edge finish	4 ft W x 8 ft H (1.2 m x 2.4 m) size, 2:1 aspect ratio, 1/4 in. (6 mm) thick glass, 0.43 in. (11 mm) glass-to-frame clearance, Kawneer 1600 curtain wall framing	Displacement controlled cyclic racking loading	Cracking Transient Interstory Drift Ratio	glass-to-frame contact, corner crushing, fallout, gasket/sealant damage, cracking	Serviceability type failure
15	B2022.015	Curtain wall, monolithic, annealed glass, aluminum framing, square corners, cut corner finish, cut edge finish	8 ft W x 4 ft H (2.4 m x 1.2 m) size, 1:2 aspect ratio, 1/4 in. (6 mm) thick glass, 0.43 in. (11 mm) glass-to-frame clearance, Kawneer 1600 curtain wall framing	Displacement controlled cyclic racking loading	Cracking Transient Interstory Drift Ratio	glass-to-frame contact, corner crushing, fallout, gasket/sealant damage, cracking	Serviceability type failure
16	not available	Curtain wall, monolithic, heat-strengthened glass, aluminum framing, square corners, cut corner finish, cut edge finish	5 ft W x 6 ft H (1.5 m x 1.8 m) size, 6:5 aspect ratio, 1/4 in. (6 mm) thick glass, 0.43 in. (11 mm) glass-to-frame clearance, Kawneer 1600 curtain wall framing	Displacement controlled cyclic racking loading	Cracking Transient Interstory Drift Ratio	glass-to-frame contact, corner crushing, fallout, gasket/sealant damage, cracking	Serviceability type failure
17	not available	Curtain wall, IGU, heat-strengthened glass, aluminum framing, square corners, cut corner finish, cut edge finish	5 ft W x 6 ft H (1.5 m x 1.8 m) size, 6:5 aspect ratio, inner/outer HS 1/4 in. (6 mm) thick glass, 0.43 in. (11 mm) glass-to-frame clearance, Kawneer 1600 curtain wall framing	Displacement controlled cyclic racking loading	Cracking Transient Interstory Drift Ratio	glass-to-frame contact, corner crushing, fallout, gasket/sealant damage, cracking	Serviceability type failure
18	not available	Curtain wall, laminated, heat-strengthened glass, aluminum framing, square corners, cut corner finish, cut edge finish	5 ft W x 6 ft H (1.5 m x 1.8 m) size, 6:5 aspect ratio, 3/8 in. (10 mm) thick glass (0.030 PVB), 0.43 in. (11 mm) glass-to-frame clearance, Kawneer 1600 curtain wall framing	Displacement controlled cyclic racking loading	Cracking Transient Interstory Drift Ratio	glass-to-frame contact, corner crushing, fallout, gasket/sealant damage, cracking	Serviceability type failure

Table A.22: Input information for glass configurations (19-24) for serviceability limit states

Glass ID	PACT ID	Component Description:	Describe Specimens:	Describe Excitation:	Demand Parameter:	Damage Evidence:	Damage Measure:
19	not available	Curtain wall, IGU, asymmetric glass, aluminum framing, square corners, cut corner finish, cut edge finish	5 ft W x 6 ft H (1.5 m x 1.8 m) size, 6:5 aspect ratio, 1/4 in. (6 mm) inner AN mono glass, 1/4 in. (6 mm) outer HS lam. (0.060 PVB) outer glass, 0.43 in. (11 mm) average glass-to-frame clearance, Kawneer 1600 curtain wall framing	Displacement controlled cyclic racking loading	First Cracking Overall Transient Interstory Drift Ratio observed in glass unit or Gasket Transient Interstory Drift Ratio	glass-to-frame contact, corner crushing, fallout, gasket/sealant damage, cracking	Serviceability type failure
20	not available	Curtain wall, IGU, asymmetric glass, aluminum framing, square corners, cut corner finish, cut edge finish	5 ft W x 6 ft H (1.5 m x 1.8 m) size, 6:5 aspect ratio, 1/4 in. (6 mm) inner AN mono glass, 1/2 in. (13 mm) outer HS lam. (0.060 PVB) outer glass, 0.43 in. (11 mm) average glass-to-frame clearance, Kawneer 1600 curtain wall framing	Displacement controlled cyclic racking loading	First Cracking Overall Transient Interstory Drift Ratio observed in glass unit or Gasket Transient Interstory Drift Ratio	glass-to-frame contact, corner crushing, fallout, gasket/sealant damage, cracking	Serviceability type failure
21	not available	Curtain wall, monolithic, fully-tempered glass, aluminum framing, square corners, cut corner finish, cut edge finish	5 ft W x 6 ft H (1.5 m x 1.8 m) size, 6:5 aspect ratio, 1/4 in. (6 mm) thick glass, 0.43 in. (11 mm) glass-to-frame clearance, Kawneer 1600 curtain wall framing	Displacement controlled cyclic racking loading	Cracking Transient Interstory Drift Ratio	glass-to-frame contact, corner crushing, fallout, gasket/sealant damage, cracking	Serviceability type failure
22	not available	Storefront, monolithic, fully-tempered glass, aluminum framing, square corners, cut corner finish, cut edge finish	5 ft W x 6 ft H (1.5 m x 1.8 m) size, 6:5 aspect ratio, 1/4 in. (6 mm) thick glass, 0.41 in. (10 mm) average glass-to-frame clearance, Kawneer TriFab II 451 Storefront curtain wall framing	Displacement controlled cyclic racking loading	No Cracking Data Available	glass-to-frame contact, corner crushing, fallout, gasket/sealant damage, cracking	Serviceability type failure
23	not available	Storefront, IGU, fully-tempered glass, aluminum framing, square corners, cut corner finish, cut edge finish	5 ft W x 6 ft H (1.5 m x 1.8 m) size, 6:5 aspect ratio, inner/outer FT 1/4 in. (6 mm) thick glass, 0.59 in. (15 mm) average glass-to-frame clearance, Kawneer TriFab II 451 Storefront curtain wall framing	Displacement controlled cyclic racking loading	No Cracking Data Available	glass-to-frame contact, corner crushing, fallout, gasket/sealant damage, cracking	Serviceability type failure
24	not available	Curtain wall, IGU, asymmetric glass, aluminum framing, square corners, cut corner finish, cut edge finish	5 ft W x 6 ft H (1.5 m x 1.8 m) size, 6:5 aspect ratio, 1/4 in. (6 mm) inner AN mono glass, 1/2 in. (13 mm) outer FT lam. (0.060 PVB) outer glass, 0.43 in. (11 mm) average glass-to-frame clearance, Kawneer 1600 curtain wall framing	Displacement controlled cyclic racking loading	First Cracking Overall Transient Interstory Drift Ratio observed in glass unit or Gasket Transient Interstory Drift Ratio	glass-to-frame contact, corner crushing, fallout, gasket/sealant damage, cracking	Serviceability type failure

Table A.23: Input information for glass configurations (1-6) for ultimate limit state

Glass ID	PACT ID	Component Description:	Describe Specimens:	Describe Excitation:	Demand Parameter:	Damage Evidence:	Damage Measure:
1	B2022.001	Curtain wall, monolithic, annealed glass, aluminum framing, square corners, cut corner finish, cut edge finish	5 ft W x 6 ft H (1.5 m x 1.8 m) size, 6:5 aspect ratio, 1/4 in. (6 mm) thick glass, 0.43 in. (11 mm) glass-to-frame clearance, Kawneer 1600 curtain wall framing	Displacement controlled cyclic racking loading	Fallout Transient Interstory Drift Ratio	glass-to-frame contact, corner crushing, fallout, gasket/sealant damage, cracking	Ultimate type failure
2	B2022.002	Curtain wall, IGU, annealed glass, aluminum framing, square corners, cut corner finish, cut edge finish	5 ft W x 6 ft H (1.5 m x 1.8 m) size, 6:5 aspect ratio, inner/outer AN 1/4 in. (6 mm) thick glass, 0.43 in. (11 mm) glass-to-frame clearance, Kawneer 1600 curtain wall framing	Displacement controlled cyclic racking loading	Fallout Transient Interstory Drift Ratio	glass-to-frame contact, corner crushing, fallout, gasket/sealant damage, cracking	Ultimate type failure
3	B2022.003	Curtain wall, IGU, assymetric glass, aluminum framing, square corners, cut corner finish, cut edge finish	5 ft W x 6 ft H (1.5 m x 1.8 m) size, 6:5 aspect ratio, 1/4 in. (6 mm) inner AN mono glass, 1/4 in. (6 mm) outer AN lam. (0.030 PVB) outer glass, 0.43 in. (11 mm) average glass-to-frame clearance, Kawneer 1600 curtain wall framing	Displacement controlled cyclic racking loading	First Overall Fallout Transient Interstory Drift Ratio observed in glass unit	glass-to-frame contact, corner crushing, fallout, gasket/sealant damage, cracking	Ultimate type failure
4	B2022.004	Curtain wall, IGU, assymetric glass, aluminum framing, square corners, cut corner finish, cut edge finish	5 ft W x 6 ft H (1.5 m x 1.8 m) size, 6:5 aspect ratio, 1/4 in. (6 mm) inner AN mono glass, 1/4 in. (6 mm) outer AN lam. (0.060 PVB) outer glass, 0.43 in. (11 mm) average glass-to-frame clearance, Kawneer 1600 curtain wall framing	Displacement controlled cyclic racking loading	First Overall Fallout Transient Interstory Drift Ratio observed in glass unit	glass-to-frame contact, corner crushing, fallout, gasket/sealant damage, cracking	Ultimate type failure
5	B2022.005	Curtain wall, IGU, assymetric glass, aluminum framing, square corners, cut corner finish, cut edge finish	5 ft W x 6 ft H (1.5 m x 1.8 m) size, 6:5 aspect ratio, 1/4 in. (6 mm) inner AN mono glass, 1/2 in. (13 mm) outer AN lam. (0.030 PVB) outer glass, 0.43 in. (11 mm) average glass-to-frame clearance, Kawneer 1600 curtain wall framing	Displacement controlled cyclic racking loading	First Overall Fallout Transient Interstory Drift Ratio observed in glass unit	glass-to-frame contact, corner crushing, fallout, gasket/sealant damage, cracking	Ultimate type failure
6	B2022.006	Curtain wall, laminated, annealed glass, aluminum framing, square corners, cut corner finish, cut edge finish	5 ft W x 6 ft H (1.5 m x 1.8 m) size, 6:5 aspect ratio, 1/4 in. (6 mm) thick glass (0.030 PVB), 0.43 in. (11 mm) glass-to-frame clearance, Kawneer 1600 curtain wall framing	Displacement controlled cyclic racking loading	Fallout Transient Interstory Drift Ratio	glass-to-frame contact, corner crushing, fallout, gasket/sealant damage, cracking	Ultimate type failure

Table A.24: Input information for glass configurations (7-12) for ultimate limit state

Glass ID	PACT ID	Component Description:	Describe Specimens:	Describe Excitation:	Demand Parameter:	Damage Evidence:	Damage Measure:
7	B2022.007	Storefront, monolithic, annealed glass, aluminum framing, square corners, cut corner finish, cut edge finish	5 ft W x 6 ft H (1.5 m x 1.8 m) size, 6:5 aspect ratio, 1/4 in. (6 mm) thick glass, 0.41 in. (10 mm) average glass-to-frame clearance, Kawneer TriFab II 451 Storefront curtain wall framing	Displacement controlled cyclic racking loading	Fallout Transient Interstory Drift Ratio	glass-to-frame contact, corner crushing, fallout, gasket/sealant damage, cracking	Ultimate type failure
8	B2022.008	Storefront, IGU, annealed glass, aluminum framing, square corners, cut corner finish, cut edge finish	5 ft W x 6 ft H (1.5 m x 1.8 m) size, 6:5 aspect ratio, inner/outer AN 1/4 in. (6 mm) thick glass, 0.59 in. (15 mm) average glass-to-frame clearance, Kawneer TriFab II 451 Storefront curtain wall framing	Displacement controlled cyclic racking loading	First Overall Fallout Transient Interstory Drift Ratio observed in glass unit	glass-to-frame contact, corner crushing, fallout, gasket/sealant damage, cracking	Ultimate type failure
9	B2022.009	Storefront, laminated, annealed glass, aluminum framing, square corners, cut corner finish, cut edge finish	5 ft W x 6 ft H (1.5 m x 1.8 m) size, 6:5 aspect ratio, 1/4 in. (6 mm) thick glass (0.030 PVB), 0.41 in. (10 mm) average glass-to-frame clearance, Kawneer TriFab II 451 Storefront curtain wall framing	Displacement controlled cyclic racking loading	Fallout Transient Interstory Drift Ratio	glass-to-frame contact, corner crushing, fallout, gasket/sealant damage, cracking	Ultimate type failure
10	B2022.010	Curtain wall, monolithic, annealed glass, aluminum framing, square corners, cut corner finish, cut edge finish	5 ft W x 6 ft H (1.5 m x 1.8 m) size, 6:5 aspect ratio, 1/4 in. (6 mm) thick glass, 0 in. (0 mm) glass-to-frame clearance, Kawneer 1600 curtain wall framing	Displacement controlled cyclic racking loading	Fallout Transient Interstory Drift Ratio	glass-to-frame contact, corner crushing, fallout, gasket/sealant damage, cracking	Ultimate type failure
11	B2022.011	Curtain wall, monolithic, annealed glass, aluminum framing, square corners, cut corner finish, cut edge finish	5 ft W x 6 ft H (1.5 m x 1.8 m) size, 6:5 aspect ratio, 1/4 in. (6 mm) thick glass, 1/8 in. (3 mm) glass-to-frame clearance, Kawneer 1600 curtain wall framing	Displacement controlled cyclic racking loading	Fallout Transient Interstory Drift Ratio	glass-to-frame contact, corner crushing, fallout, gasket/sealant damage, cracking	Ultimate type failure
12	B2022.012	Curtain wall, monolithic, annealed glass, aluminum framing, square corners, cut corner finish, cut edge finish	5 ft W x 6 ft H (1.5 m x 1.8 m) size, 6:5 aspect ratio, 1/4 in. (6 mm) thick glass, 1/4 in. (6 mm) glass-to-frame clearance, Kawneer 1600 curtain wall framing	Displacement controlled cyclic racking loading	Fallout Transient Interstory Drift Ratio	glass-to-frame contact, corner crushing, fallout, gasket/sealant damage, cracking	Ultimate type failure

Table A.25: Input information for glass configurations (13-18) for ultimate limit state

Glass ID	PACT ID	Component Description:	Describe Specimens:	Describe Excitation:	Demand Parameter:	Damage Evidence:	Damage Measure:
13	B2022.013	Curtain wall, IGU, annealed glass, aluminum framing, square corners, cut corner finish, cut edge finish	5 ft W x 6 ft H (1.5 m x 1.8 m) size, 6:5 aspect ratio, inner/outer AN 1/4 in. (6 mm) thick glass, 1/2 in. (13 mm) glass-to-frame clearance, Kawneer 1600 curtain wall framing	Displacement controlled cyclic racking loading	Fallout Transient Interstory Drift Ratio	glass-to-frame contact, corner crushing, fallout, gasket/sealant damage, cracking	Ultimate type failure
14	B2022.014	Curtain wall, monolithic, annealed glass, aluminum framing, square corners, cut corner finish, cut edge finish	4 ft W x 8 ft H (1.2 m x 2.4 m) size, 2:1 aspect ratio, 1/4 in. (6 mm) thick glass, 0.43 in. (11 mm) glass-to-frame clearance, Kawneer 1600 curtain wall framing	Displacement controlled cyclic racking loading	Fallout Transient Interstory Drift Ratio	glass-to-frame contact, corner crushing, fallout, gasket/sealant damage, cracking	Ultimate type failure
15	B2022.015	Curtain wall, monolithic, annealed glass, aluminum framing, square corners, cut corner finish, cut edge finish	8 ft W x 4 ft H (2.4 m x 1.2 m) size, 1:2 aspect ratio, 1/4 in. (6 mm) thick glass, 0.43 in. (11 mm) glass-to-frame clearance, Kawneer 1600 curtain wall framing	Displacement controlled cyclic racking loading	Fallout Transient Interstory Drift Ratio	glass-to-frame contact, corner crushing, fallout, gasket/sealant damage, cracking	Ultimate type failure
16	not available	Curtain wall, monolithic, heat-strengthened glass, aluminum framing, square corners, cut corner finish, cut edge finish	5 ft W x 6 ft H (1.5 m x 1.8 m) size, 6:5 aspect ratio, 1/4 in. (6 mm) thick glass, 0.43 in. (11 mm) glass-to-frame clearance, Kawneer 1600 curtain wall framing	Displacement controlled cyclic racking loading	Fallout Transient Interstory Drift Ratio	glass-to-frame contact, corner crushing, fallout, gasket/sealant damage, cracking	Ultimate type failure
17	not available	Curtain wall, IGU, heat-strengthened glass, aluminum framing, square corners, cut corner finish, cut edge finish	5 ft W x 6 ft H (1.5 m x 1.8 m) size, 6:5 aspect ratio, inner/outer HS 1/4 in. (6 mm) thick glass, 0.43 in. (11 mm) glass-to-frame clearance, Kawneer 1600 curtain wall framing	Displacement controlled cyclic racking loading	Fallout Transient Interstory Drift Ratio	glass-to-frame contact, corner crushing, fallout, gasket/sealant damage, cracking	Ultimate type failure
18	not available	Curtain wall, laminated, heat-strengthened glass, aluminum framing, square corners, cut corner finish, cut edge finish	5 ft W x 6 ft H (1.5 m x 1.8 m) size, 6:5 aspect ratio, 3/8 in. (10 mm) thick glass (0.030 PVB), 0.43 in. (11 mm) glass-to-frame clearance, Kawneer 1600 curtain wall framing	Displacement controlled cyclic racking loading	Fallout Transient Interstory Drift Ratio	glass-to-frame contact, corner crushing, fallout, gasket/sealant damage, cracking	Ultimate type failure

Table A.26: Input information for glass configurations (19-24) for ultimate limit state

Glass ID	PACT ID	Component Description:	Describe Specimens:	Describe Excitation:	Demand Parameter:	Damage Evidence:	Damage Measure:
19	not available	Curtain wall, IGU, asymmetric glass, aluminum framing, square corners, cut corner finish, cut edge finish	5 ft W x 6 ft H (1.5 m x 1.8 m) size, 6:5 aspect ratio, 1/4 in. (6 mm) inner AN mono glass, 1/4 in. (6 mm) outer HS lam. (0.060 PVB) outer glass, 0.43 in. (11 mm) average glass-to-frame clearance, Kawneer 1600 curtain wall framing	Displacement controlled cyclic racking loading	First Overall Fallout Transient Interstory Drift Ratio observed in glass unit	glass-to-frame contact, corner crushing, fallout, gasket/sealant damage, cracking	Ultimate type failure
20	not available	Curtain wall, IGU, asymmetric glass, aluminum framing, square corners, cut corner finish, cut edge finish	5 ft W x 6 ft H (1.5 m x 1.8 m) size, 6:5 aspect ratio, 1/4 in. (6 mm) inner AN mono glass, 1/2 in. (13 mm) outer HS lam. (0.060 PVB) outer glass, 0.43 in. (11 mm) average glass-to-frame clearance, Kawneer 1600 curtain wall framing	Displacement controlled cyclic racking loading	First Overall Fallout Transient Interstory Drift Ratio observed in glass unit	glass-to-frame contact, corner crushing, fallout, gasket/sealant damage, cracking	Ultimate type failure
21	not available	Curtain wall, monolithic, fully-tempered glass, aluminum framing, square corners, cut corner finish, cut edge finish	5 ft W x 6 ft H (1.5 m x 1.8 m) size, 6:5 aspect ratio, 1/4 in. (6 mm) thick glass, 0.43 in. (11 mm) glass-to-frame clearance, Kawneer 1600 curtain wall framing	Displacement controlled cyclic racking loading	Fallout Transient Interstory Drift Ratio	glass-to-frame contact, corner crushing, fallout, gasket/sealant damage, cracking	Ultimate type failure
22	not available	Storefront, monolithic, fully-tempered glass, aluminum framing, square corners, cut corner finish, cut edge finish	5 ft W x 6 ft H (1.5 m x 1.8 m) size, 6:5 aspect ratio, 1/4 in. (6 mm) thick glass, 0.41 in. (10 mm) average glass-to-frame clearance, Kawneer TriFab II 451 Storefront curtain wall framing	Displacement controlled cyclic racking loading	Fallout Transient Interstory Drift Ratio	glass-to-frame contact, corner crushing, fallout, gasket/sealant damage, cracking	Ultimate type failure
23	not available	Storefront, IGU, fully-tempered glass, aluminum framing, square corners, cut corner finish, cut edge finish	5 ft W x 6 ft H (1.5 m x 1.8 m) size, 6:5 aspect ratio, inner/outer FT 1/4 in. (6 mm) thick glass, 0.59 in. (15 mm) average glass-to-frame clearance, Kawneer TriFab II 451 Storefront curtain wall framing	Displacement controlled cyclic racking loading	Fallout Transient Interstory Drift Ratio	glass-to-frame contact, corner crushing, fallout, gasket/sealant damage, cracking	Ultimate type failure
24	not available	Curtain wall, IGU, asymmetric glass, aluminum framing, square corners, cut corner finish, cut edge finish	5 ft W x 6 ft H (1.5 m x 1.8 m) size, 6:5 aspect ratio, 1/4 in. (6 mm) inner AN mono glass, 1/2 in. (13 mm) outer FT lam. (0.060 PVB) outer glass, 0.43 in. (11 mm) average glass-to-frame clearance, Kawneer 1600 curtain wall framing	Displacement controlled cyclic racking loading	First Overall Fallout Transient Interstory Drift Ratio observed in glass unit	glass-to-frame contact, corner crushing, fallout, gasket/sealant damage, cracking	Ultimate type failure

A.3 Software Output

The following figures **Figure A.1** through **A.29** contain the outputs from the *Fragility Function Calculator version 1.02* software for all glass configurations listed in Table 3.1, and for applicable cracking, fallout, and gasket limit states. The output provides the median interstory drift ratio value (θ), the random dispersion value (β_r), and whether the data passes the Lilliefors Goodness of Fit test.

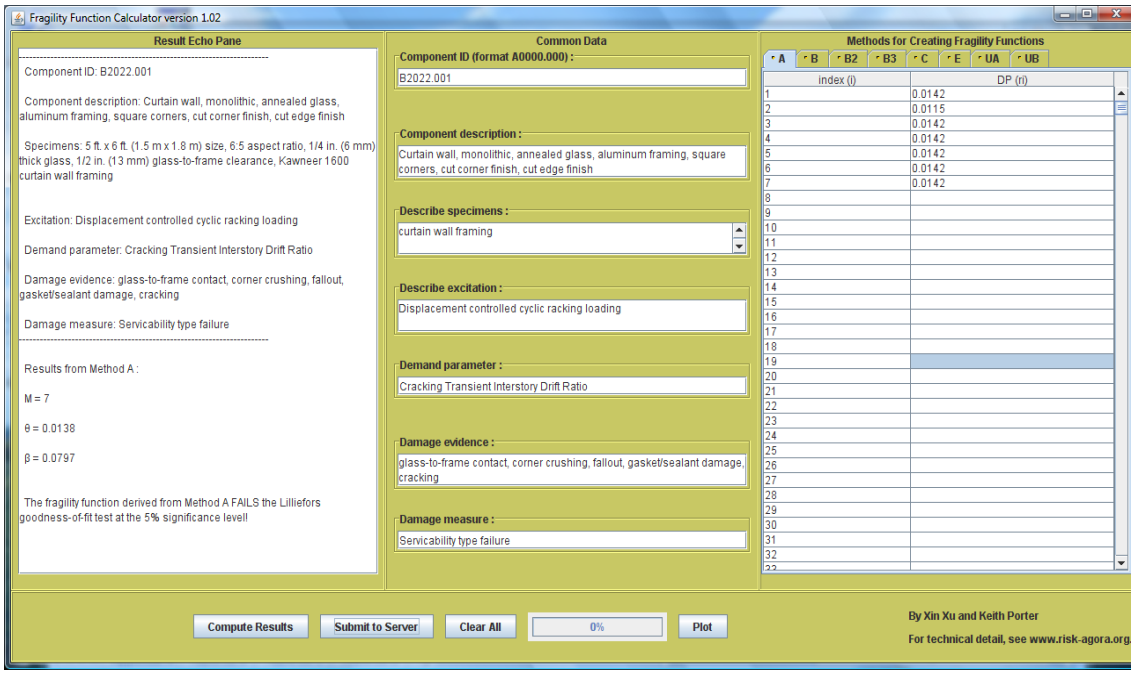

(a)

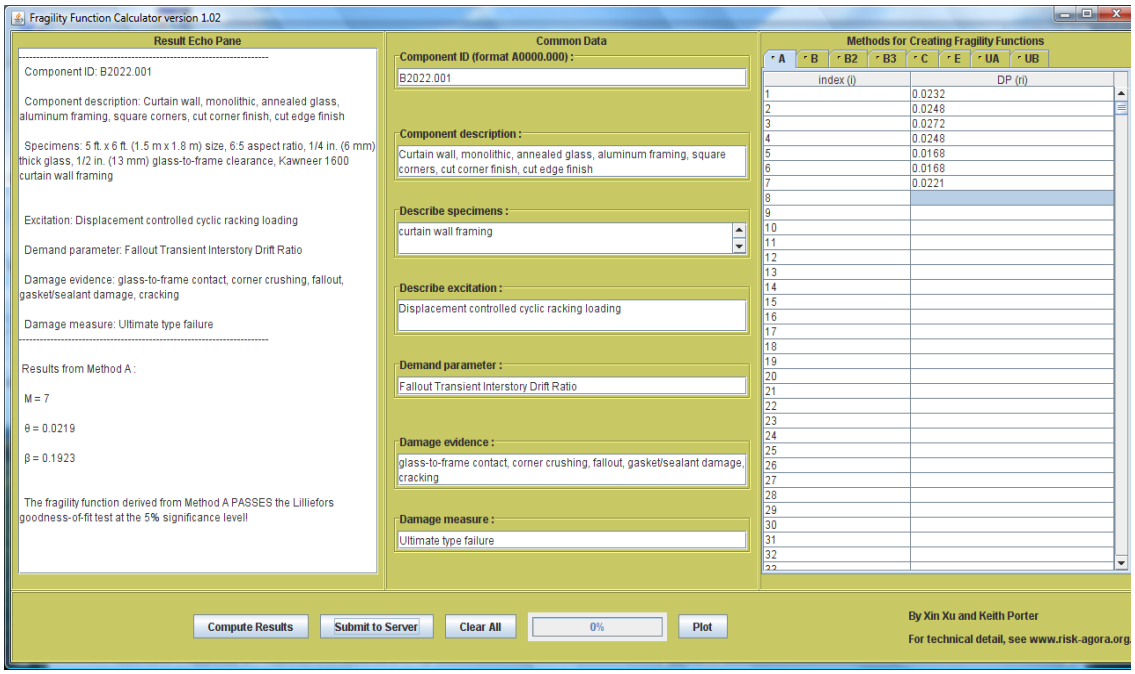

(b)

Figure A.1: Output of glass configuration (1) for (a) cracking and (b) fallout limit states

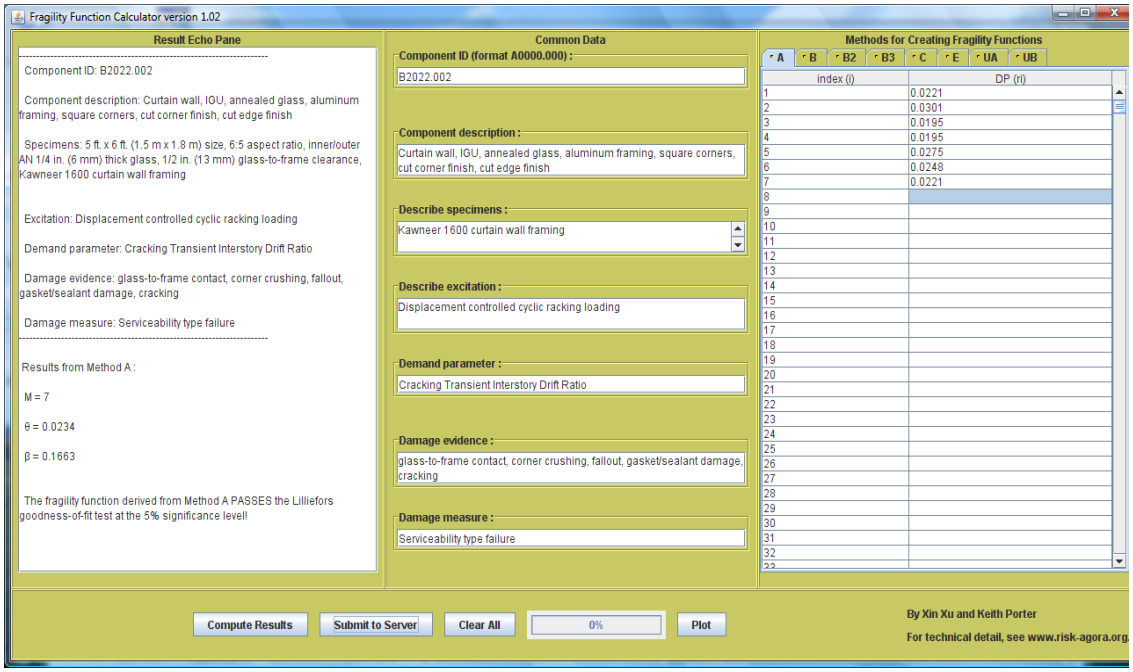

(a)

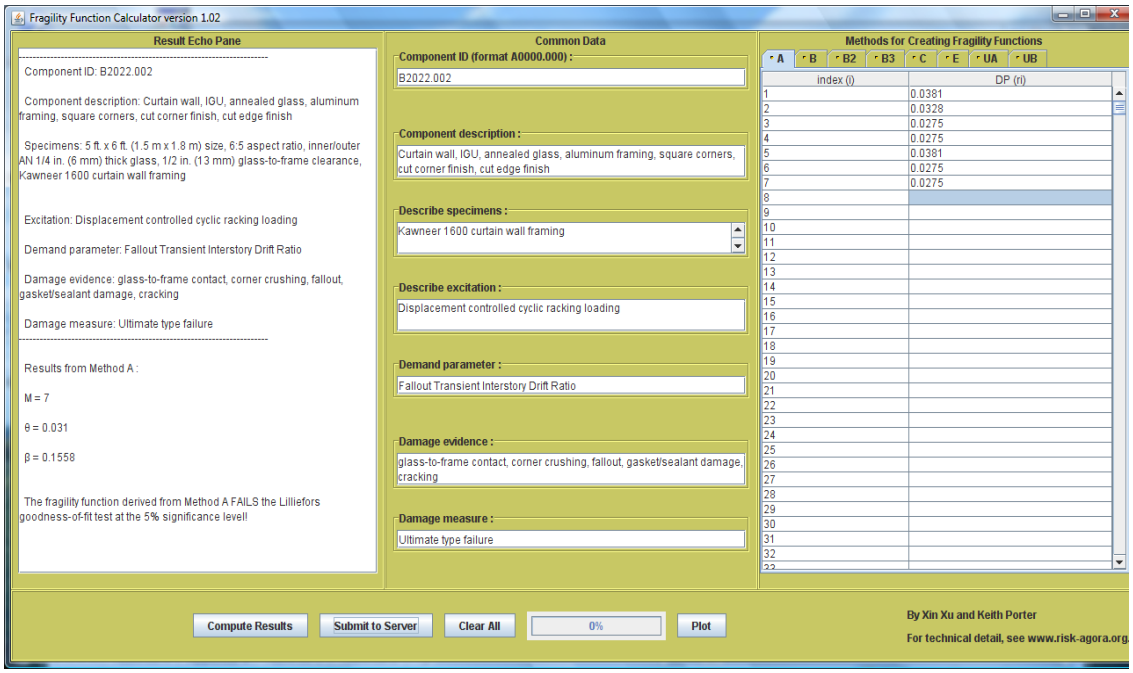

(b)

Figure A.2: Output of glass configuration (2) for (a) cracking and (b) fallout limit states

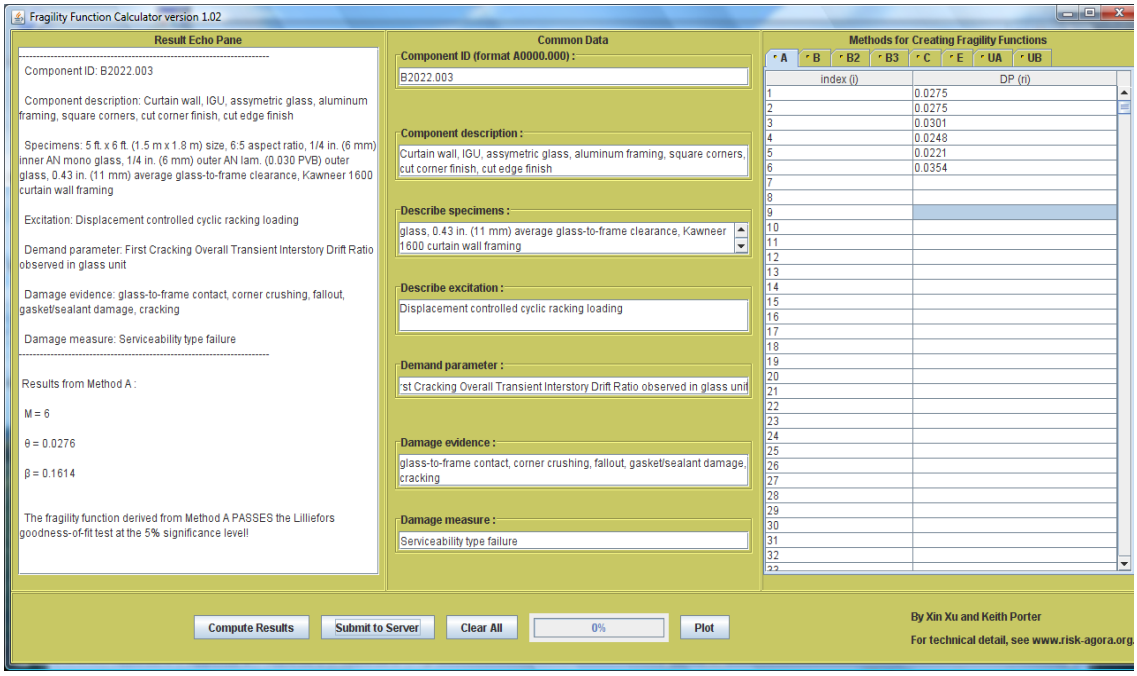

(a)

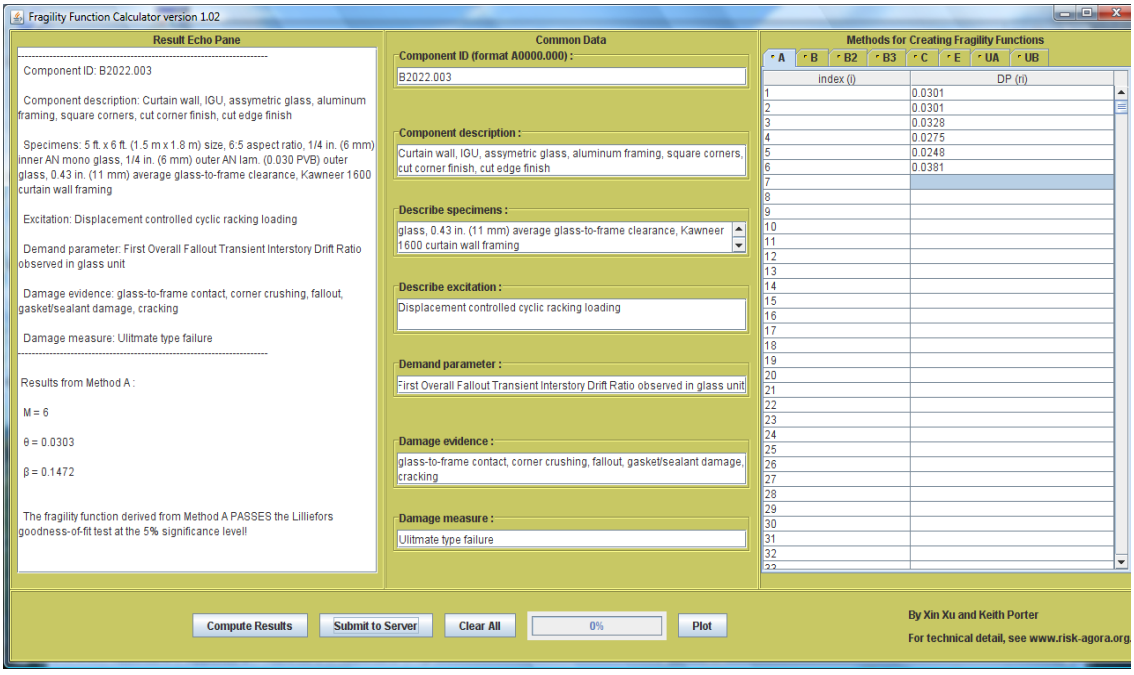

(b)

Figure A.3: Output of glass configuration (3) for (a) cracking and (b) fallout limit states

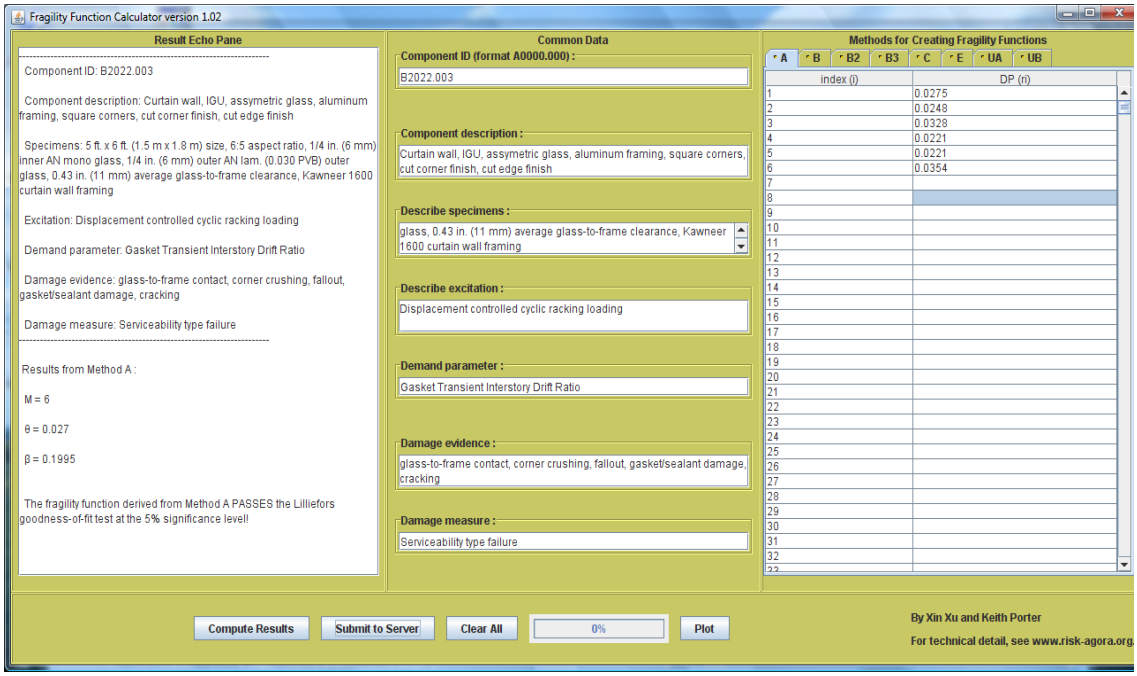

Figure A.4: Output of glass configuration (3) for gasket degradation limit state

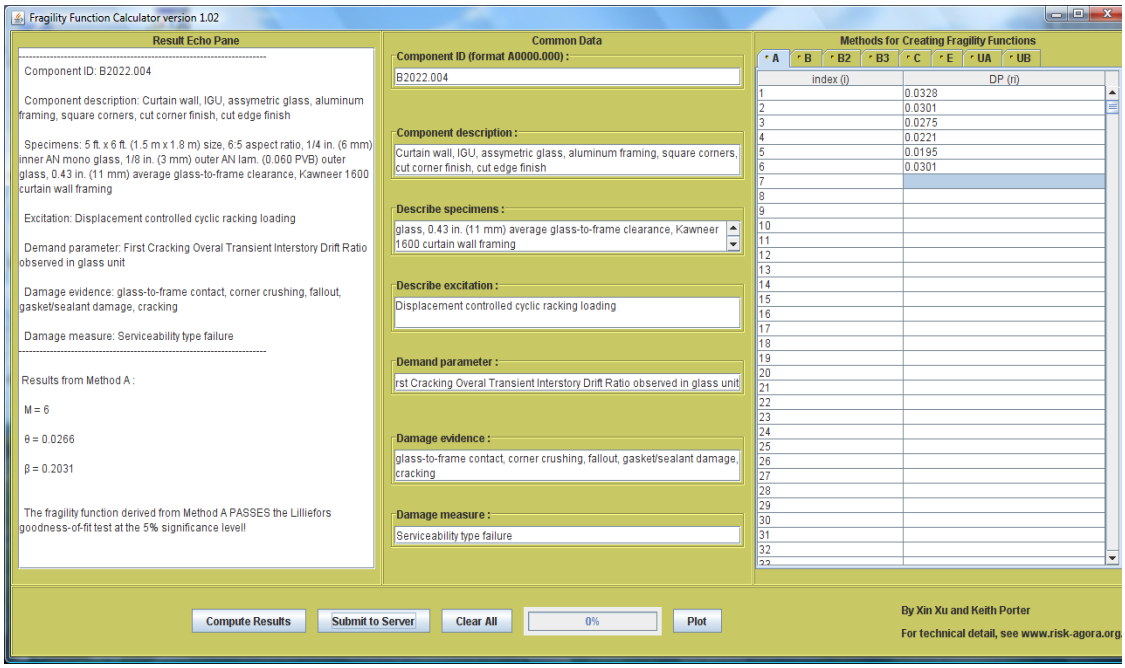

(a)

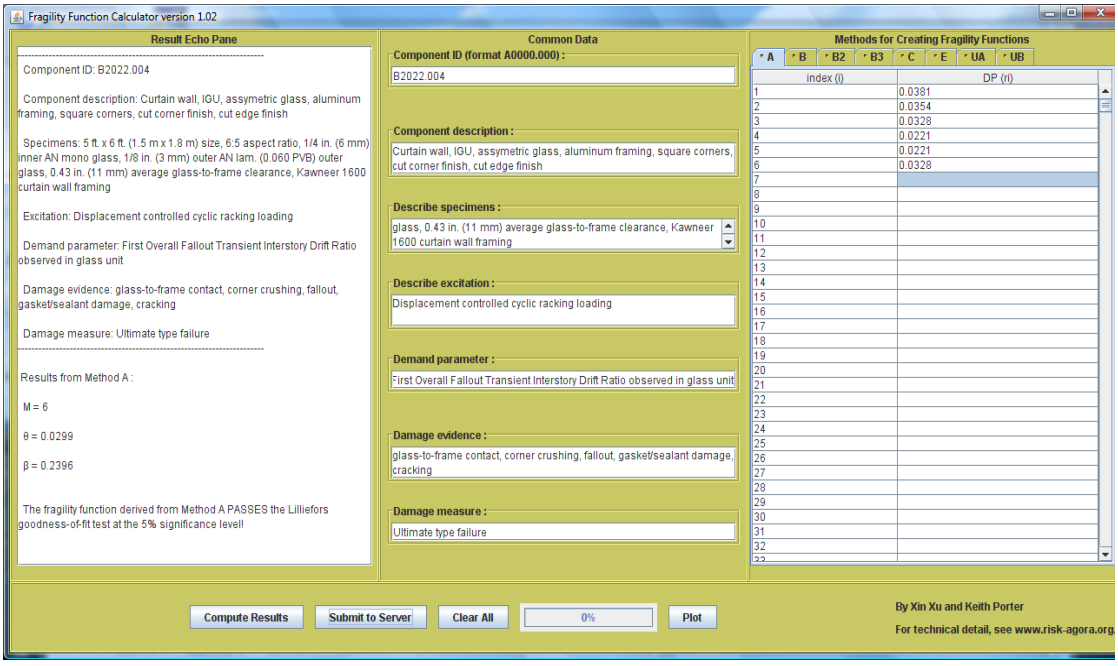

(b)

Figure A.5: Output of glass configuration (4) for (a) cracking and (b) fallout limit states

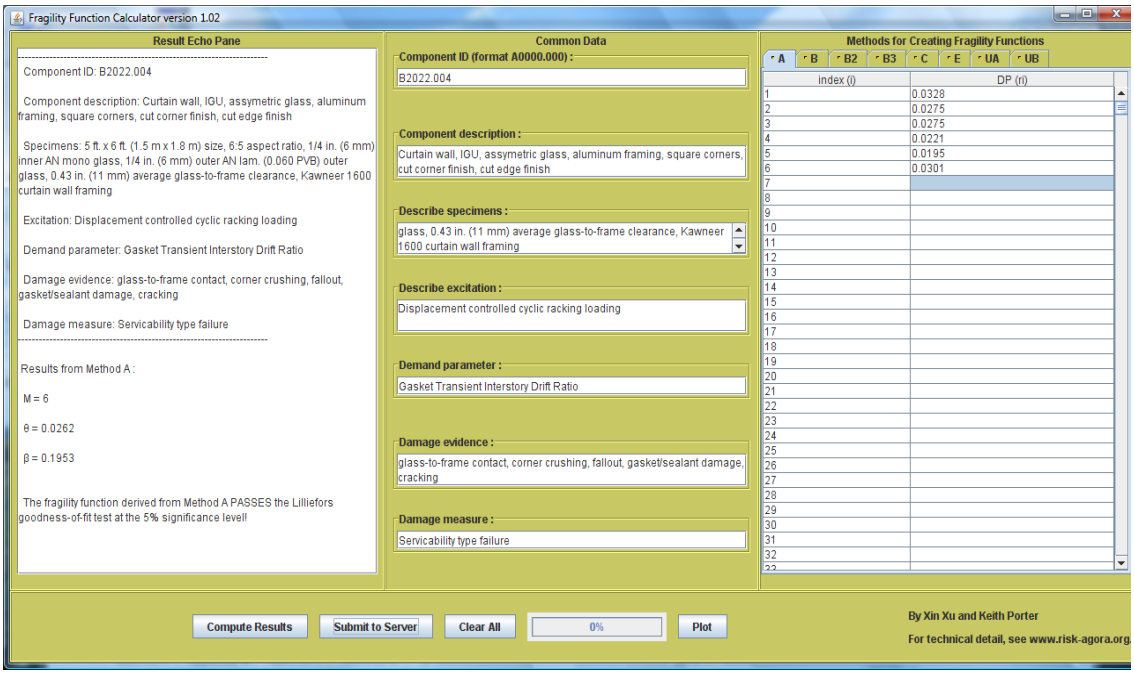

Figure A.6: Output of glass configuration (4) for gasket degradation limit state

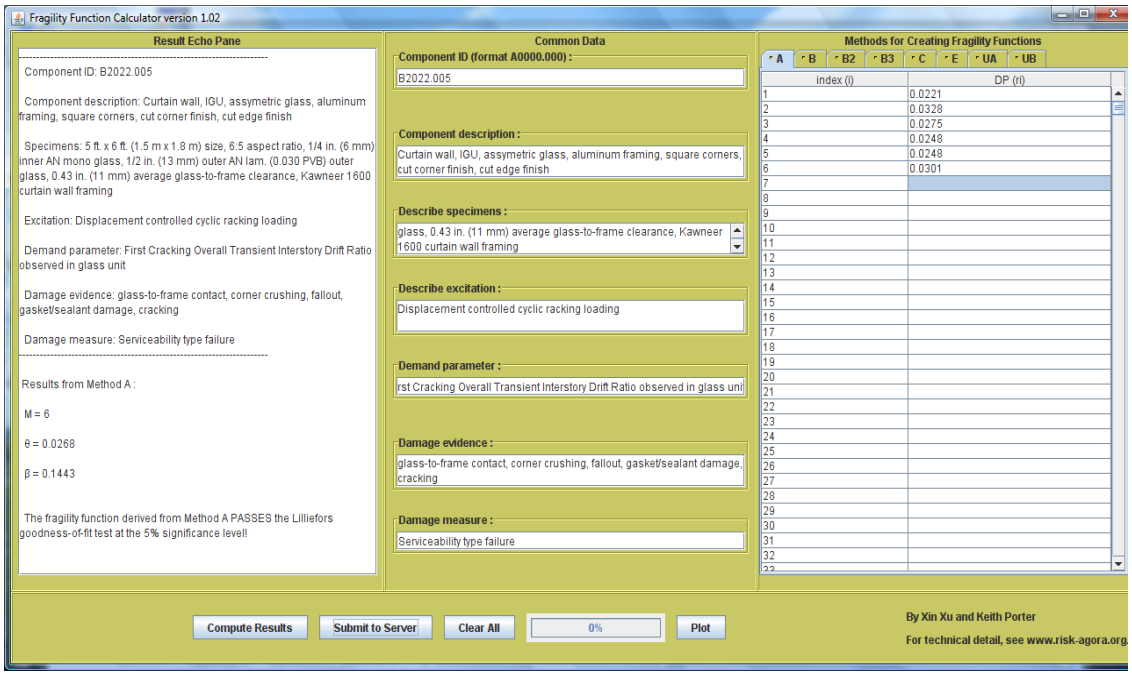

(a)

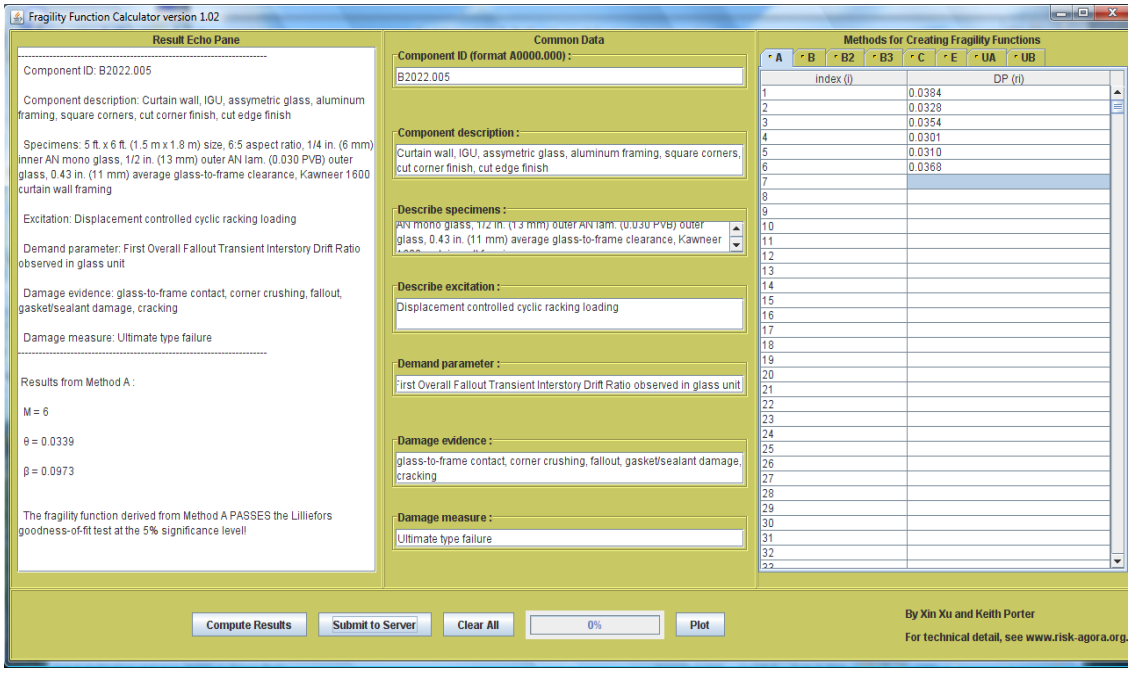

(b)

Figure A.7: Output of glass configuration (5) for (a) cracking and (b) fallout limit states

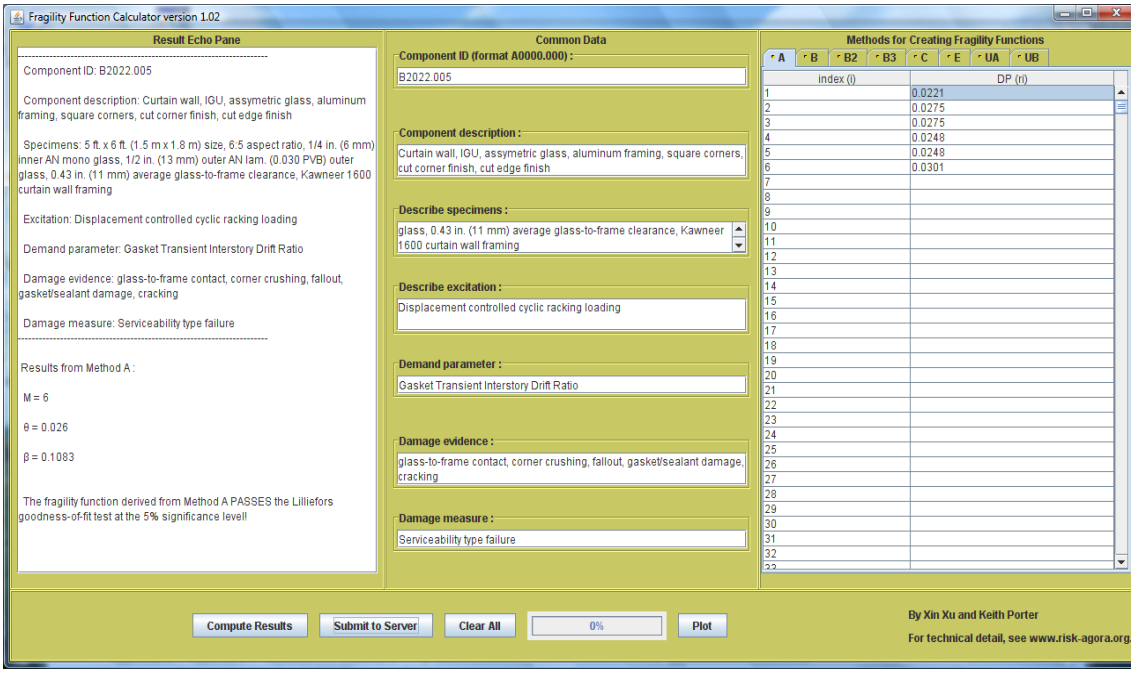

Figure A.8: Output of glass configuration (5) for gasket degradation limit state

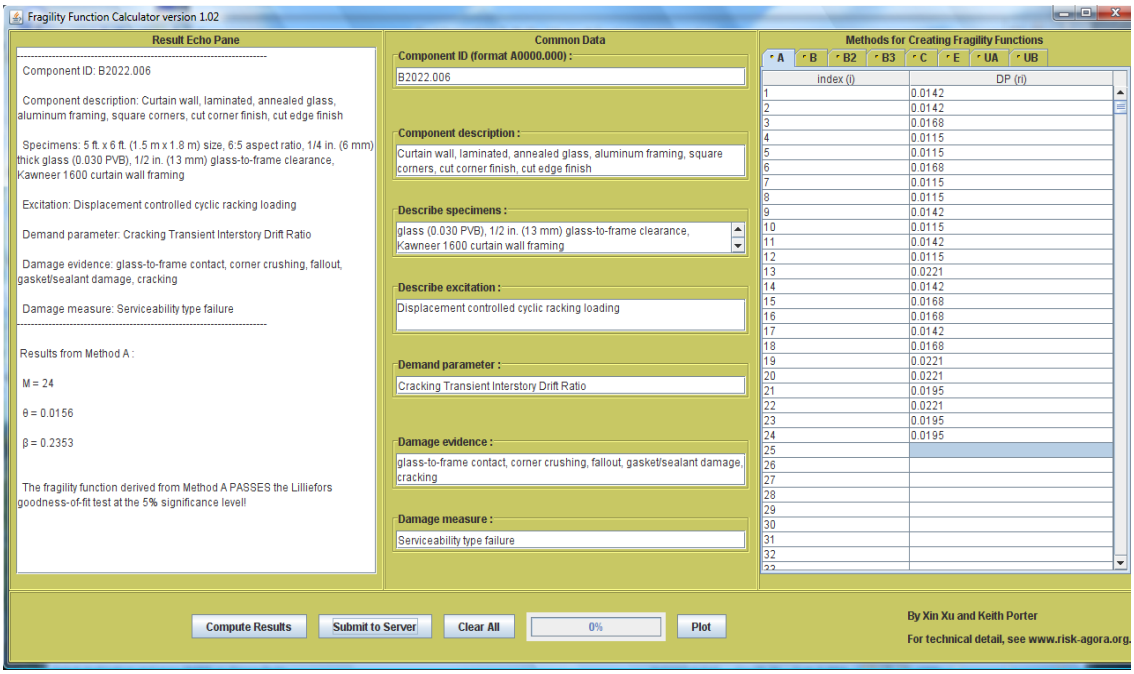

(a)

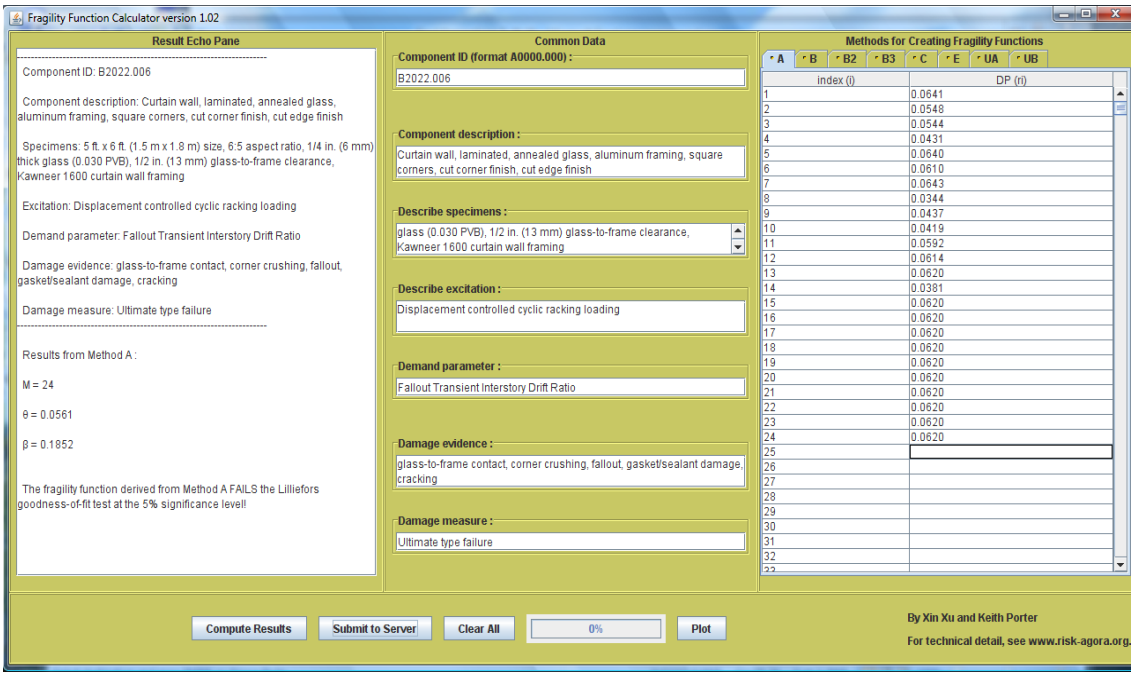

(b)

Figure A.9: Output of glass configuration (6) for (a) cracking and (b) fallout limit states

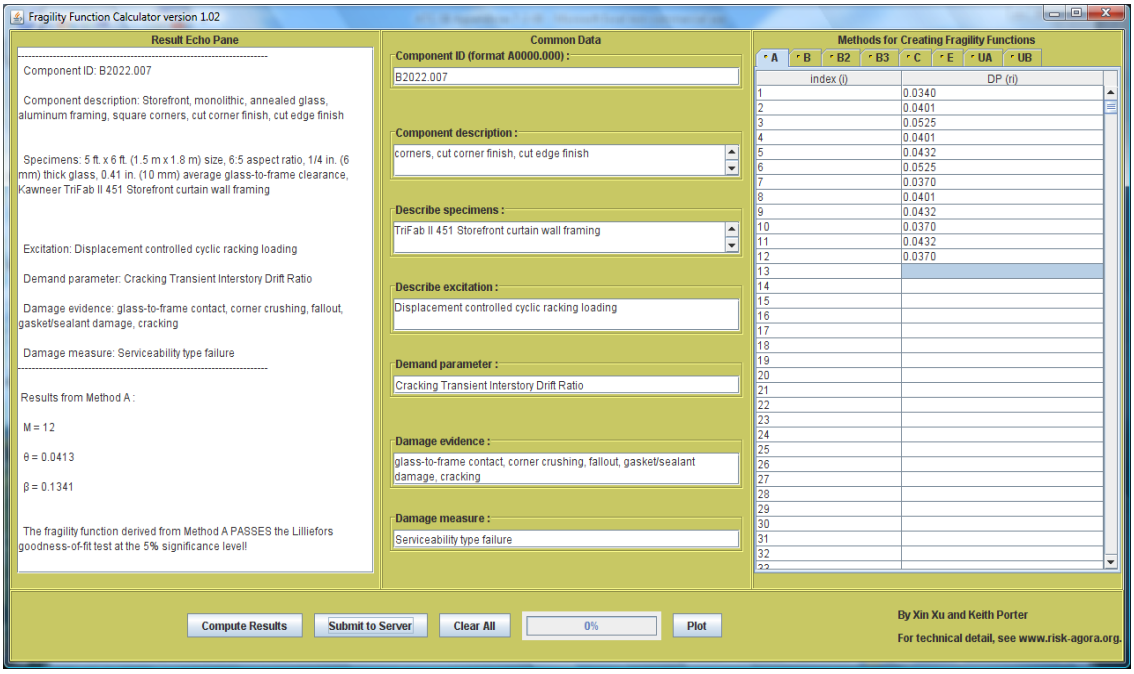

(a)

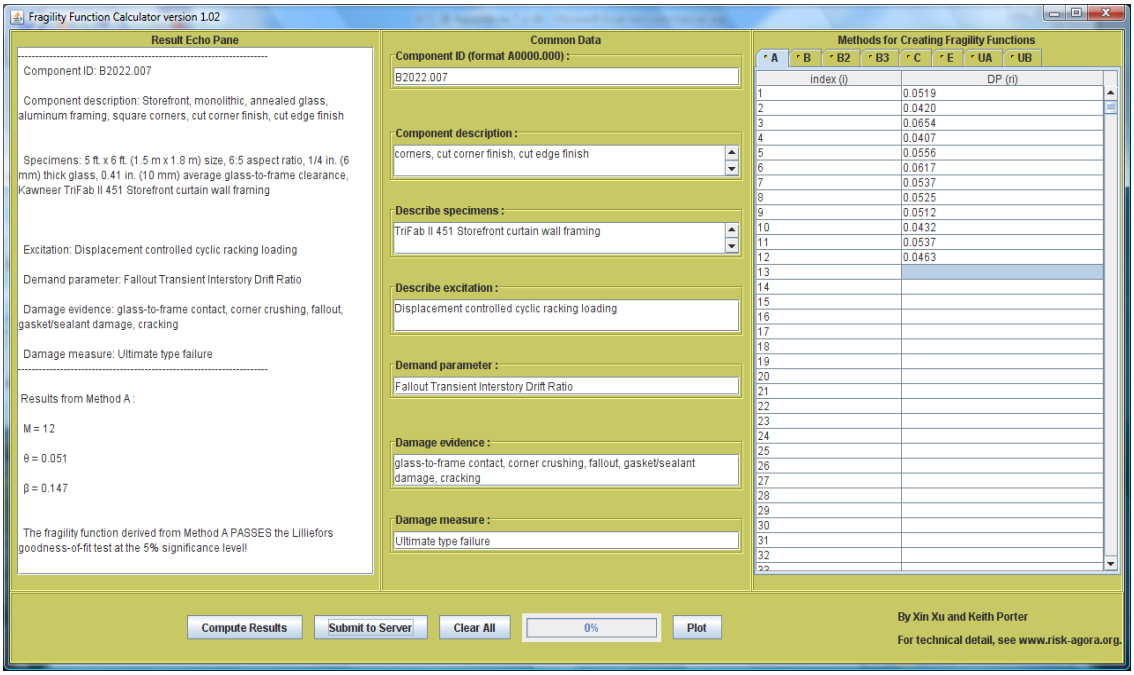

(b)

Figure A.10: Output of glass configuration (7) for (a) cracking and (b) fallout limit states

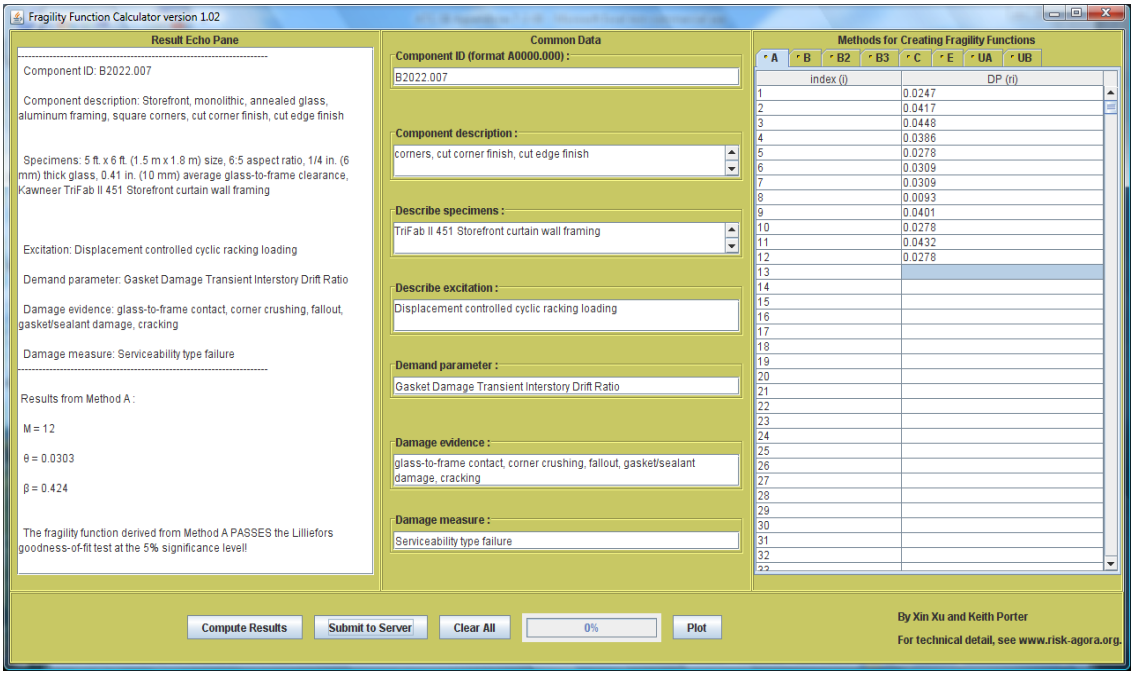

Figure A.11: Output of glass configuration (7) for gasket degradation limit state

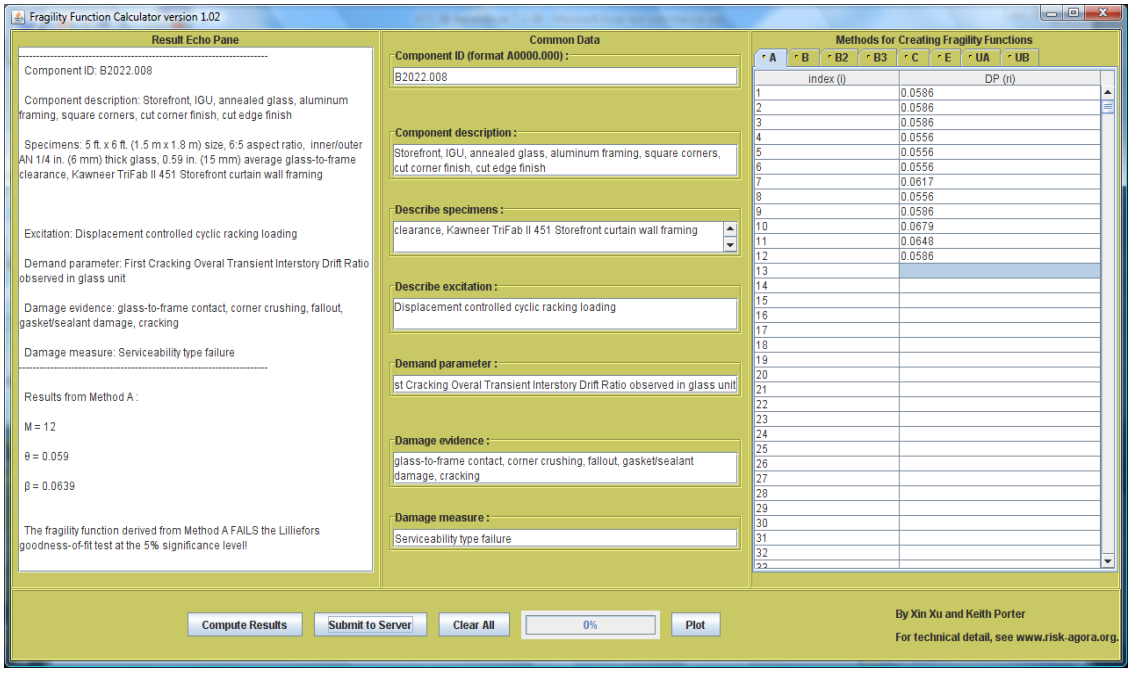

(a)

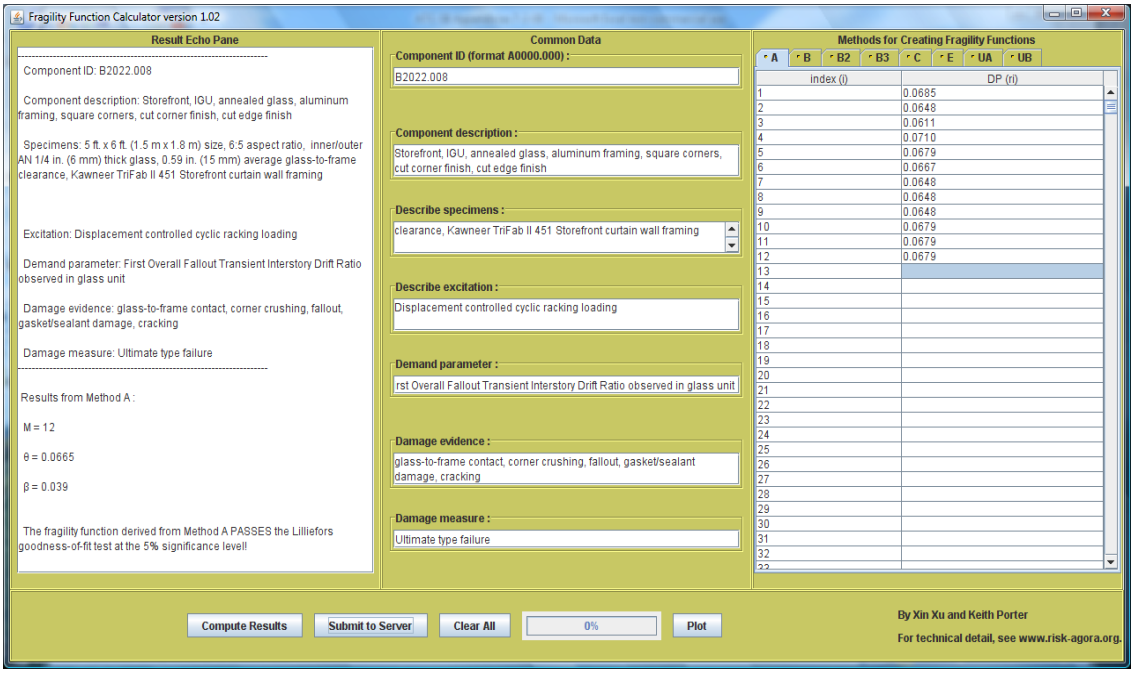

(b)

Figure A.12: Output of glass configuration (8) for (a) cracking and (b) fallout limit states

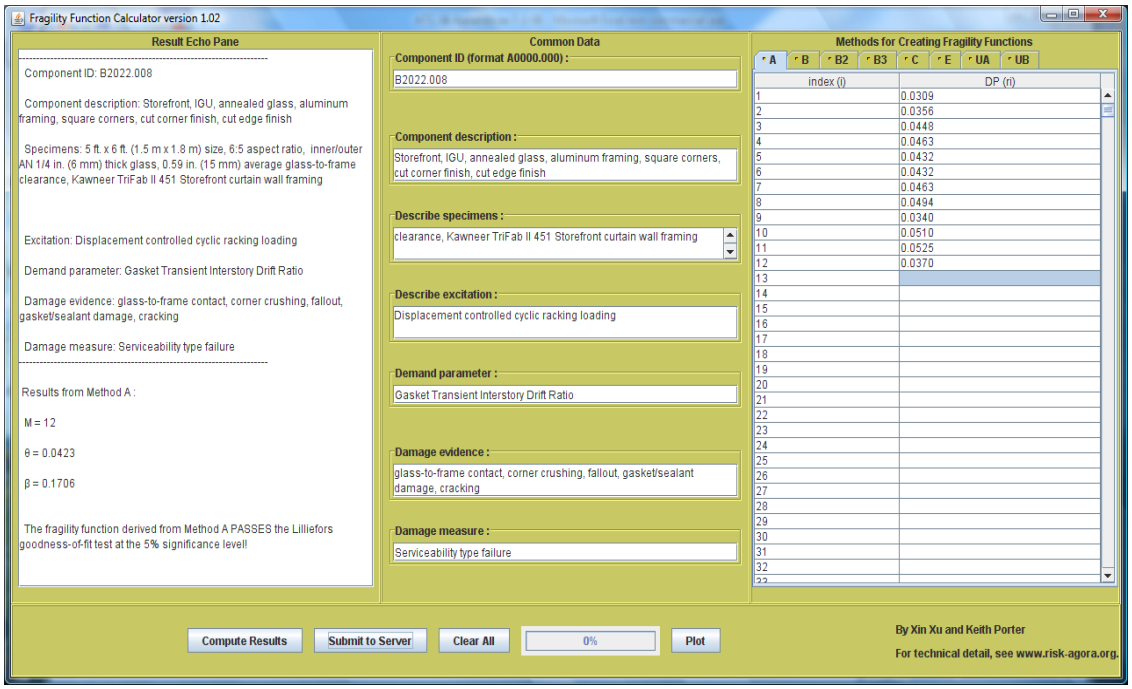

Figure A.13: Output of glass configuration (8) for gasket degradation limit state

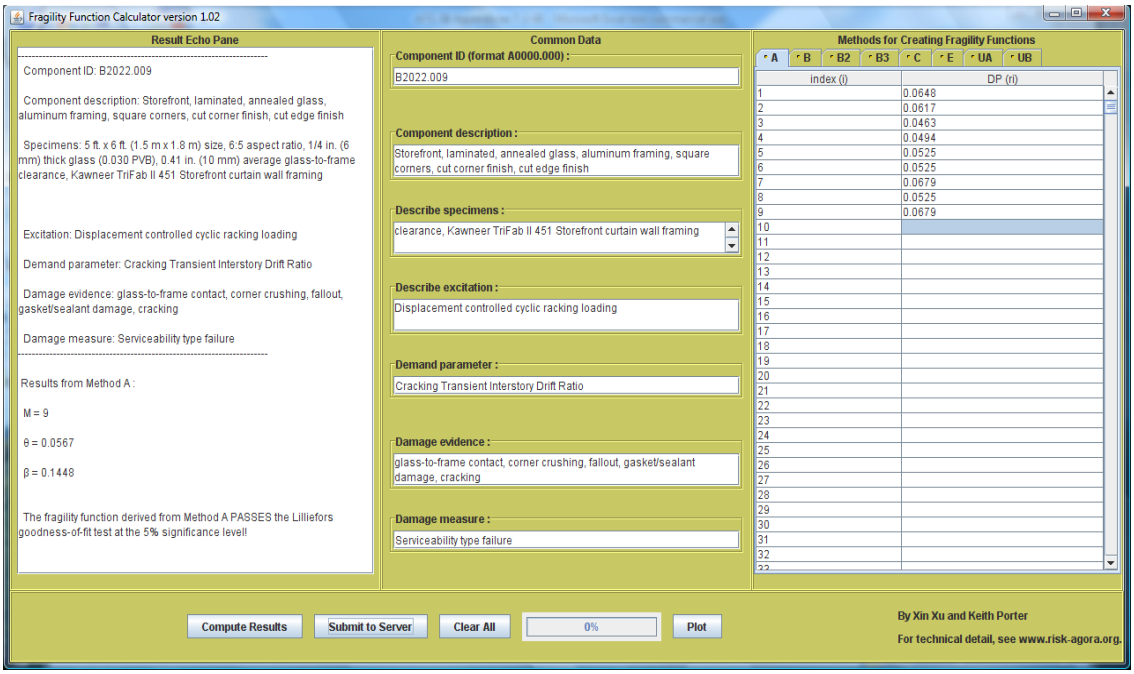

(a)

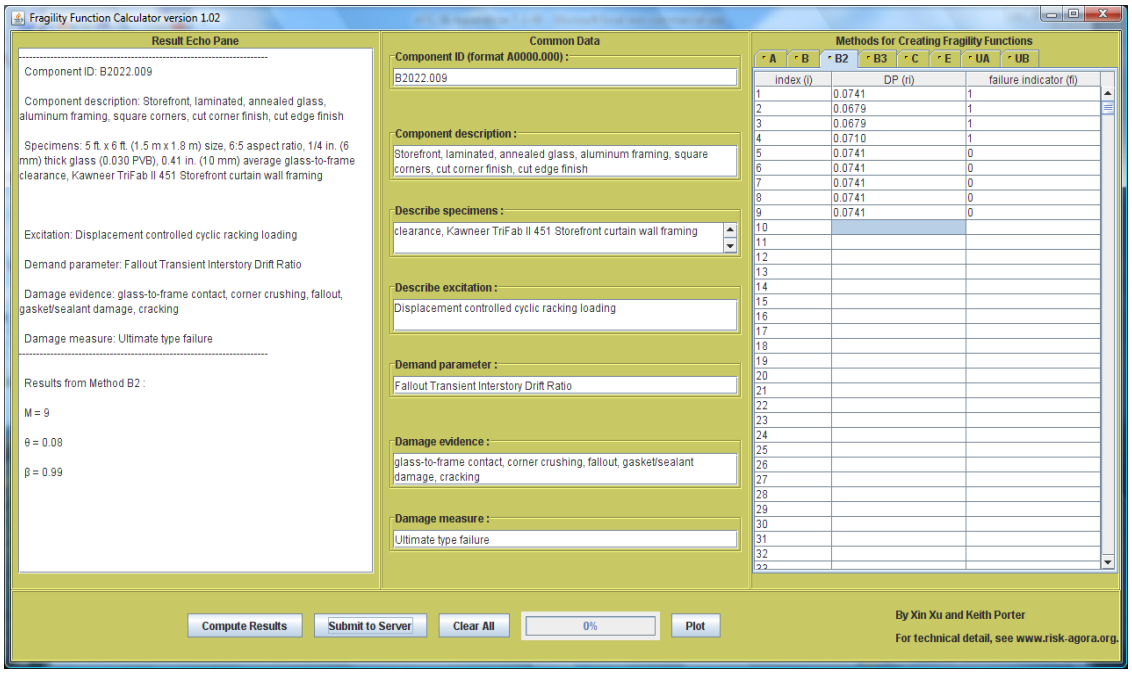

(b)

Figure A.14: Output of glass configuration (9) for (a) cracking and (b) fallout limit states

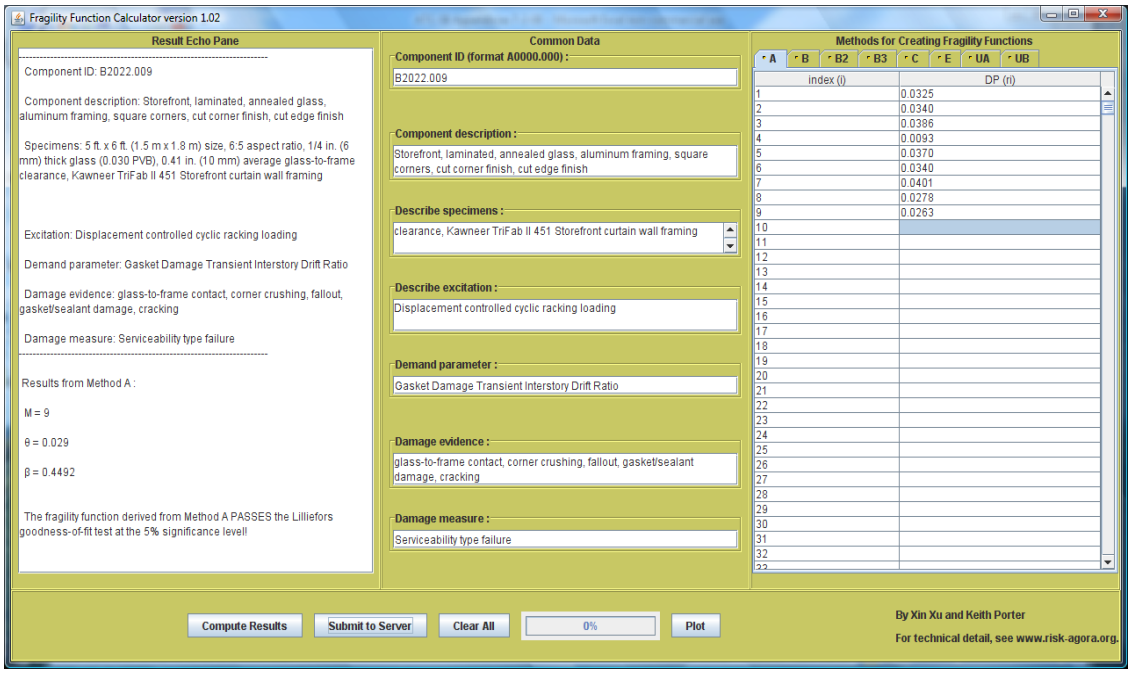

Figure A.15: Output of glass configuration (9) for gasket degradation limit state

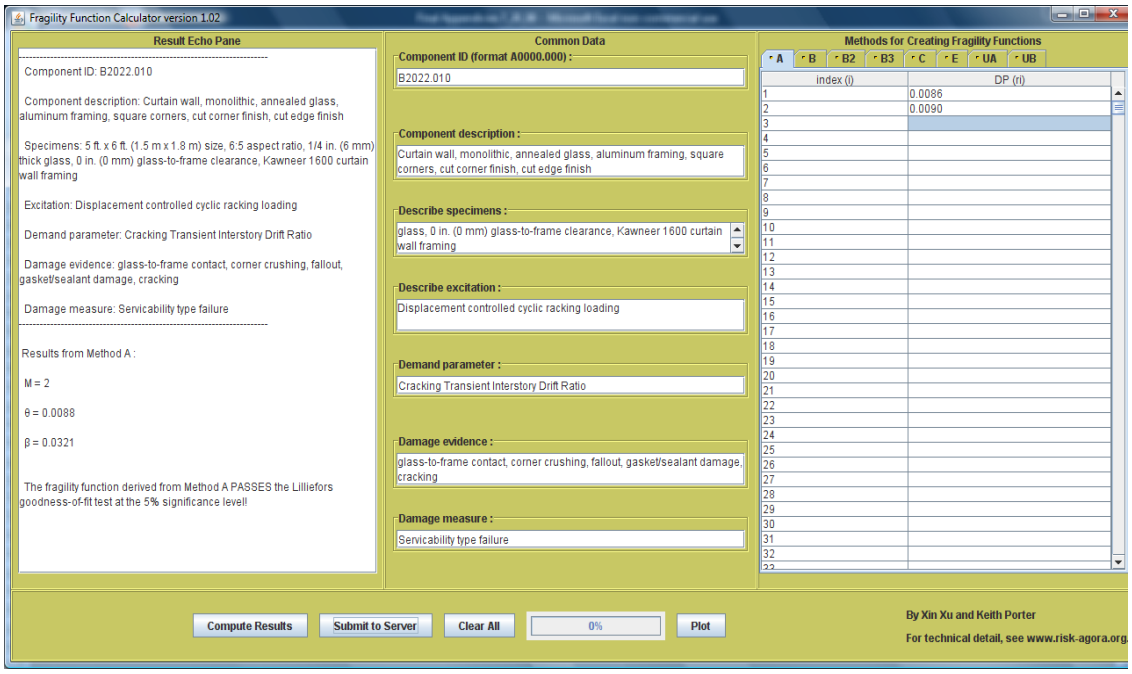

(a)

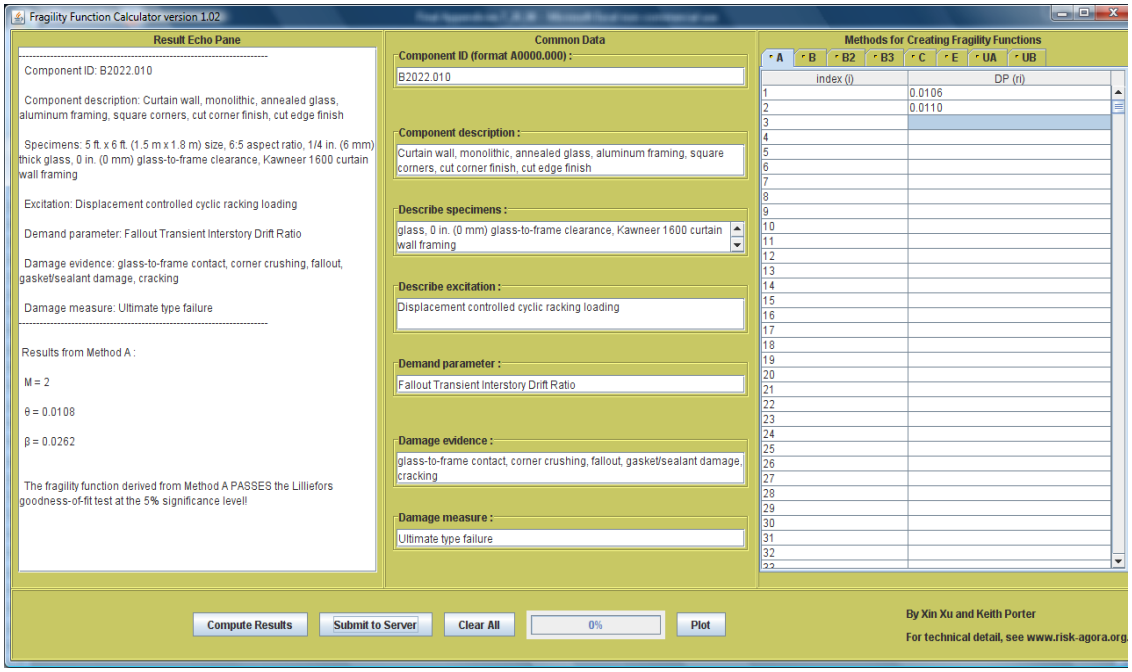

(b)

Figure A.16: Output of glass configuration (10) for (a) cracking and (b) fallout

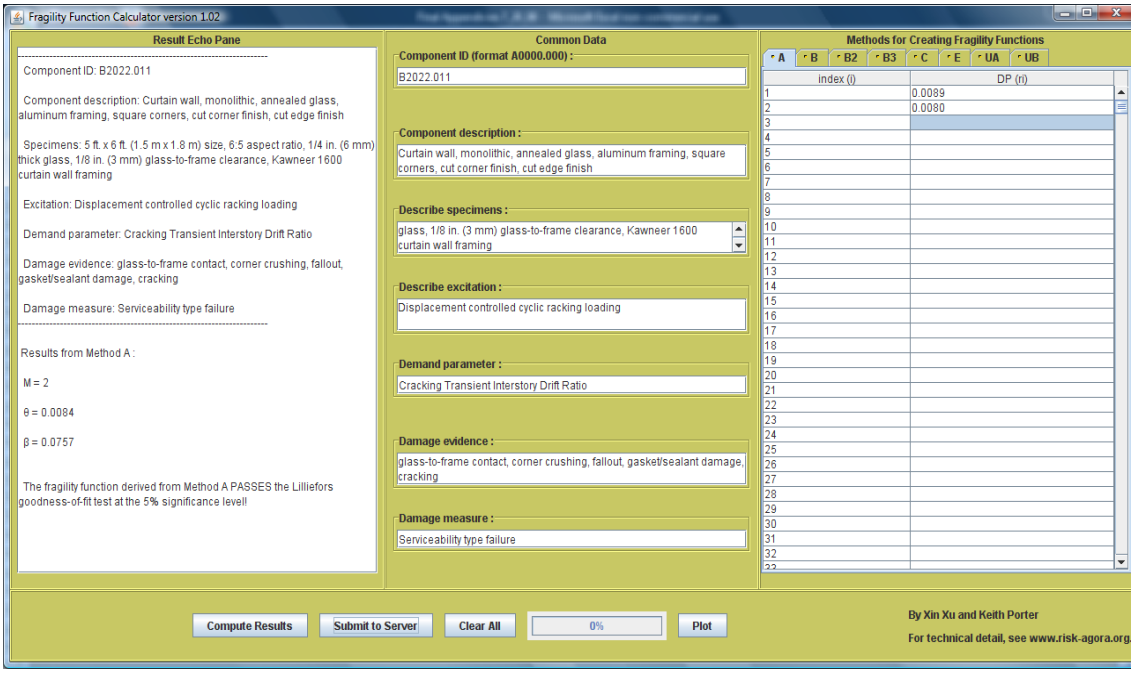

(a)

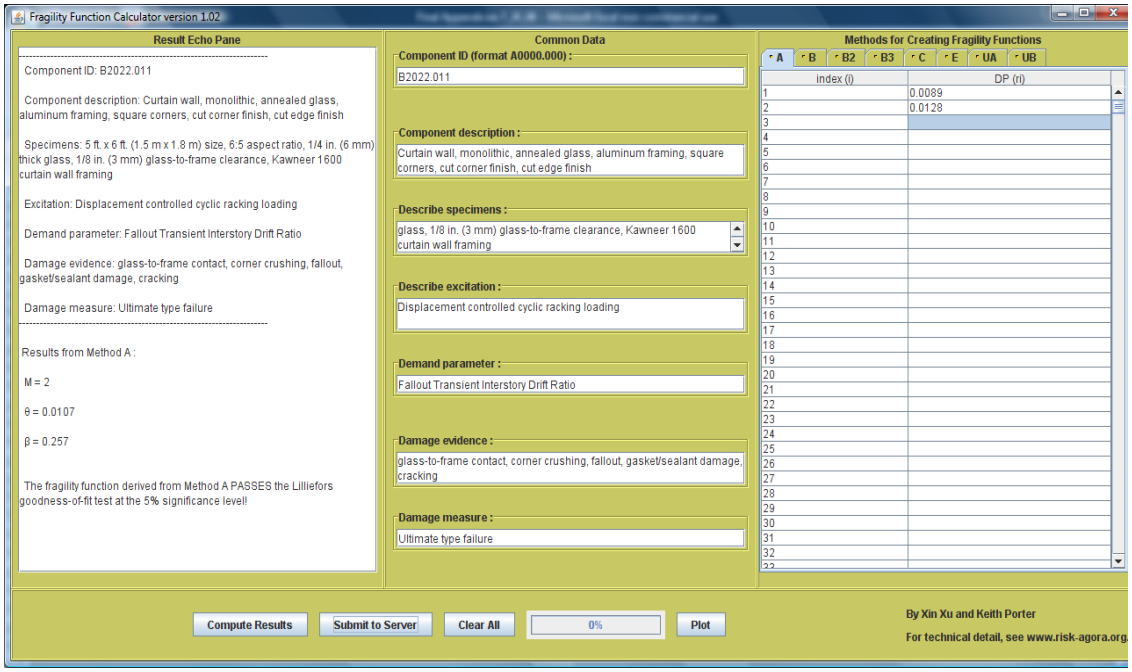

(b)

Figure A.17: Output of glass configuration (11) for (a) cracking and (b) fallout

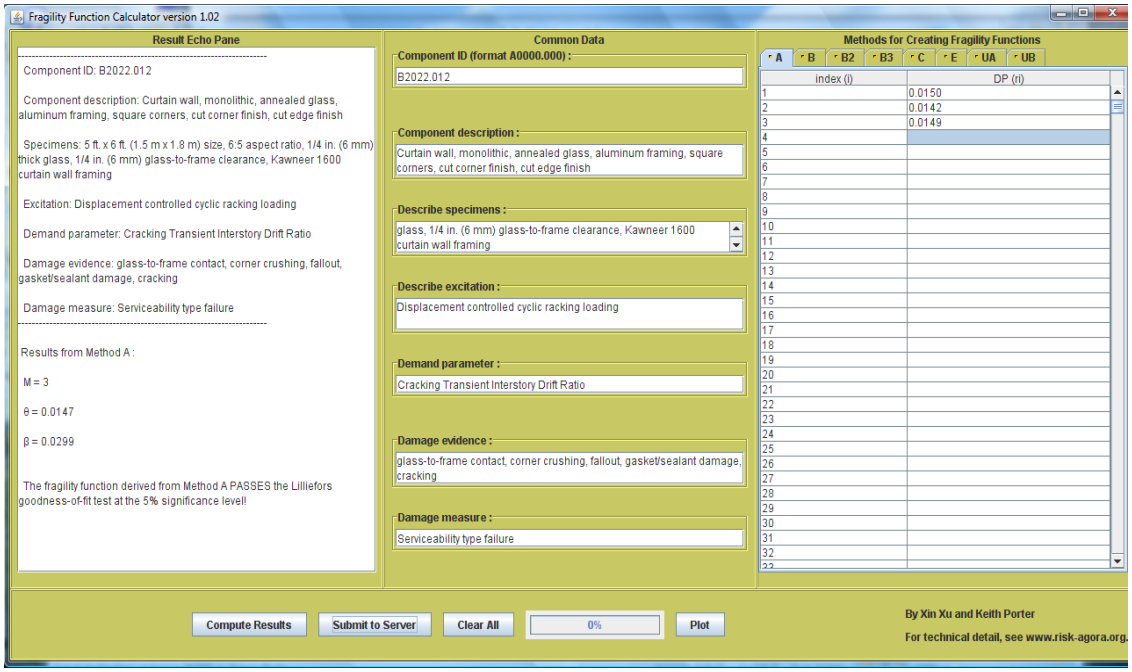

(a)

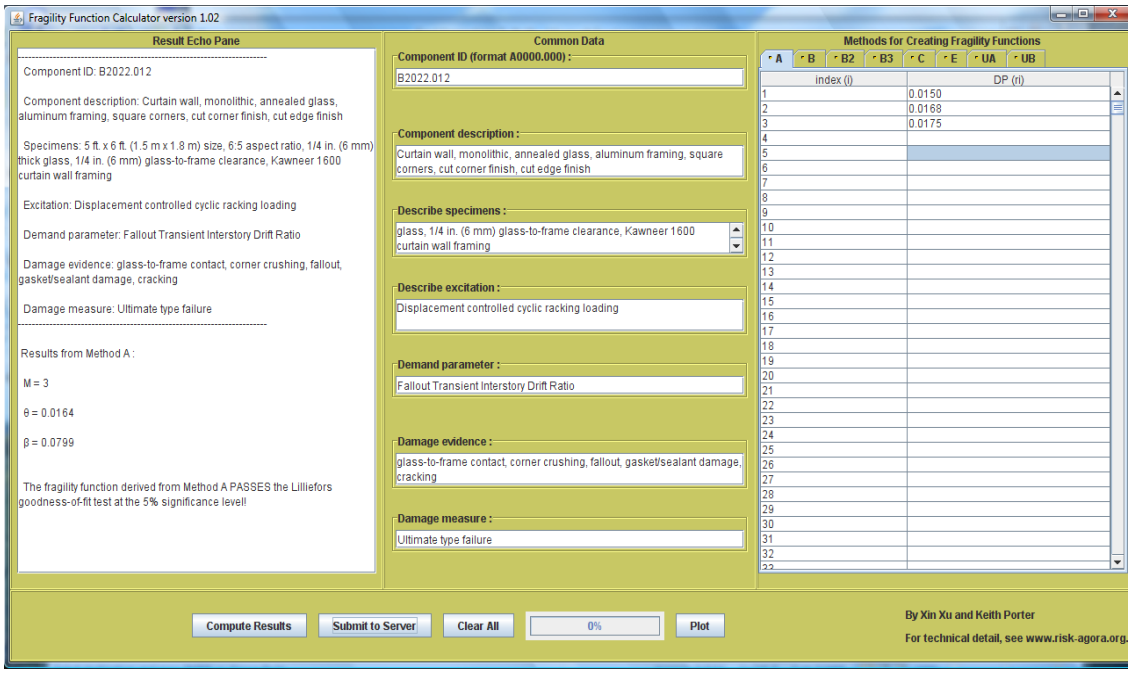

(b)

Figure A.18: Output of glass configuration (12) for (a) cracking and (b) fallout

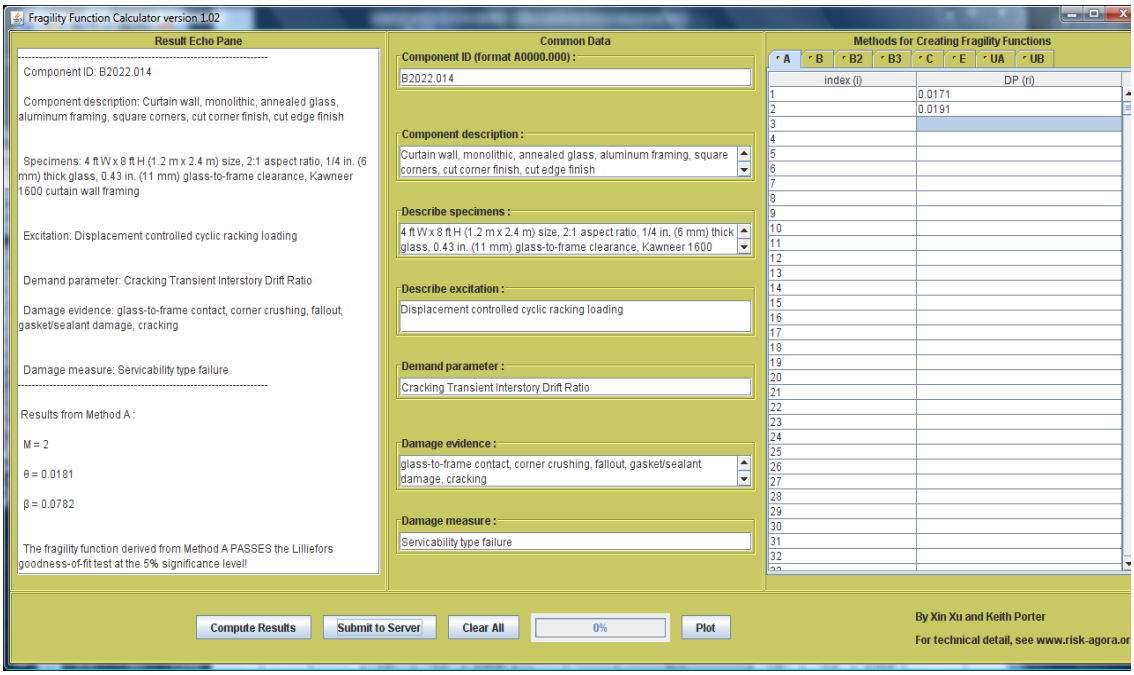

(a)

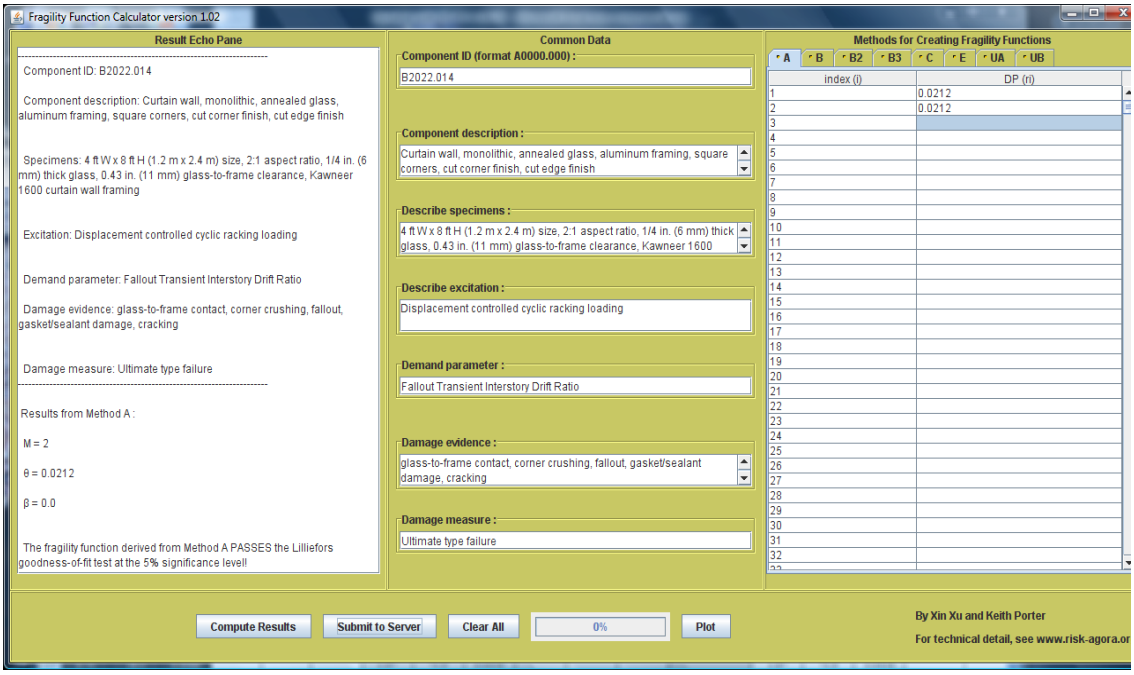

Figure A.19: Output of glass configuration (14) for (a) cracking and (b) fallout

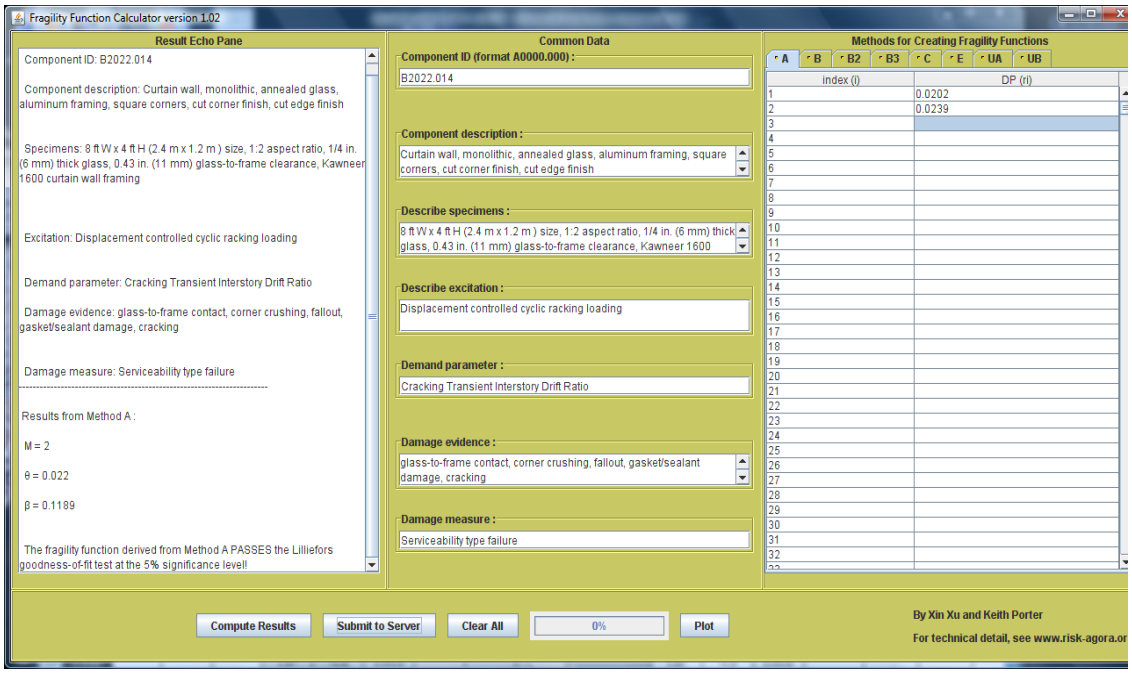

(a)

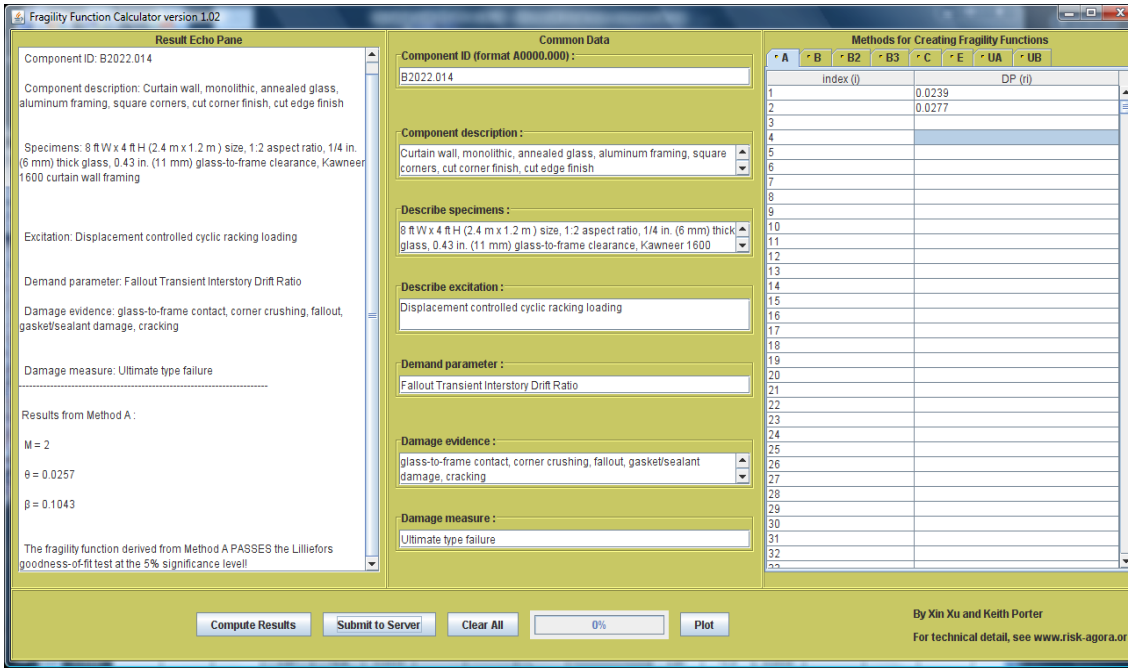

Figure A.20: Output of glass configuration (15) for (a) cracking and (b) fallout

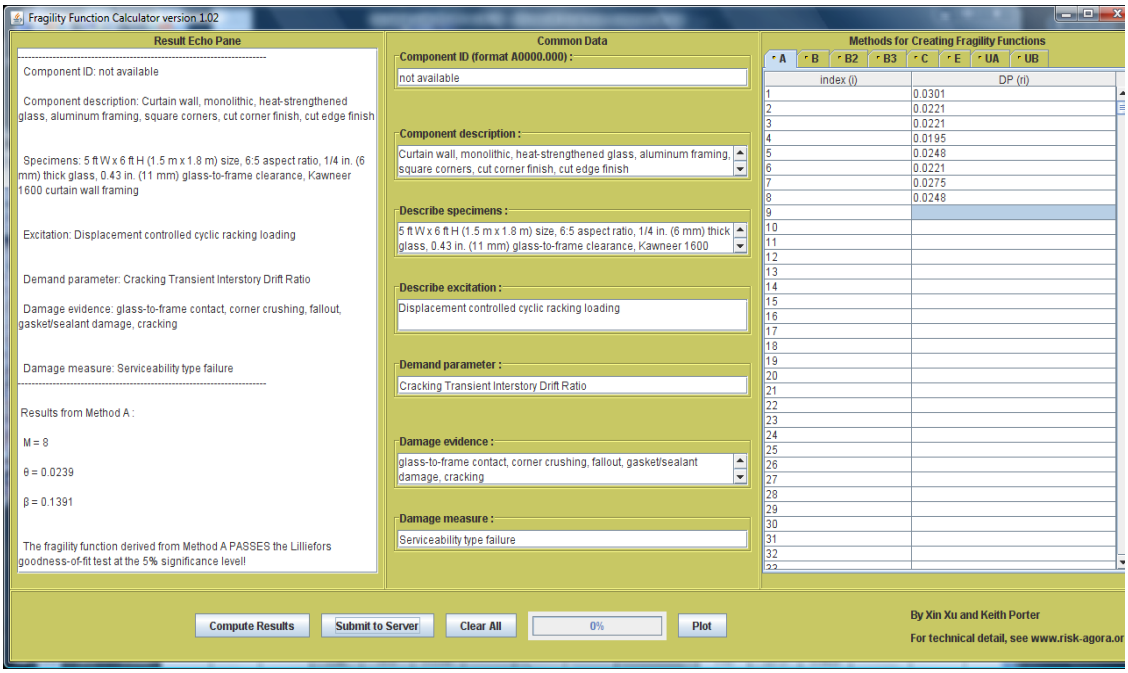

(a)

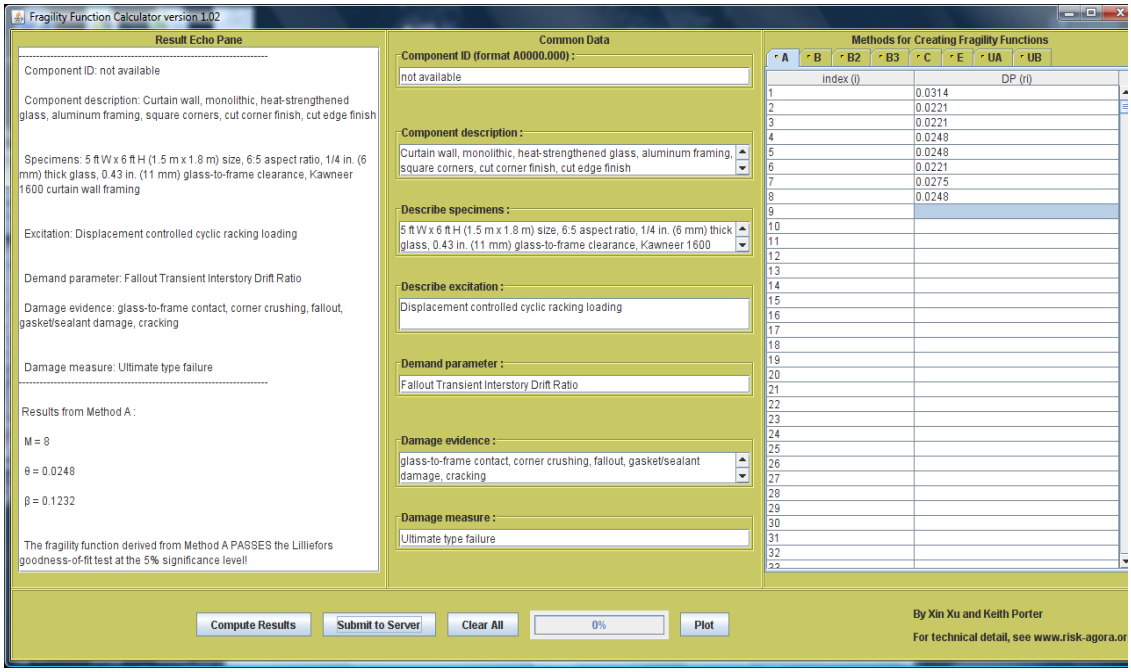

(b)

Figure A.21: Output of glass configuration (16) for (a) cracking and (b) fallout

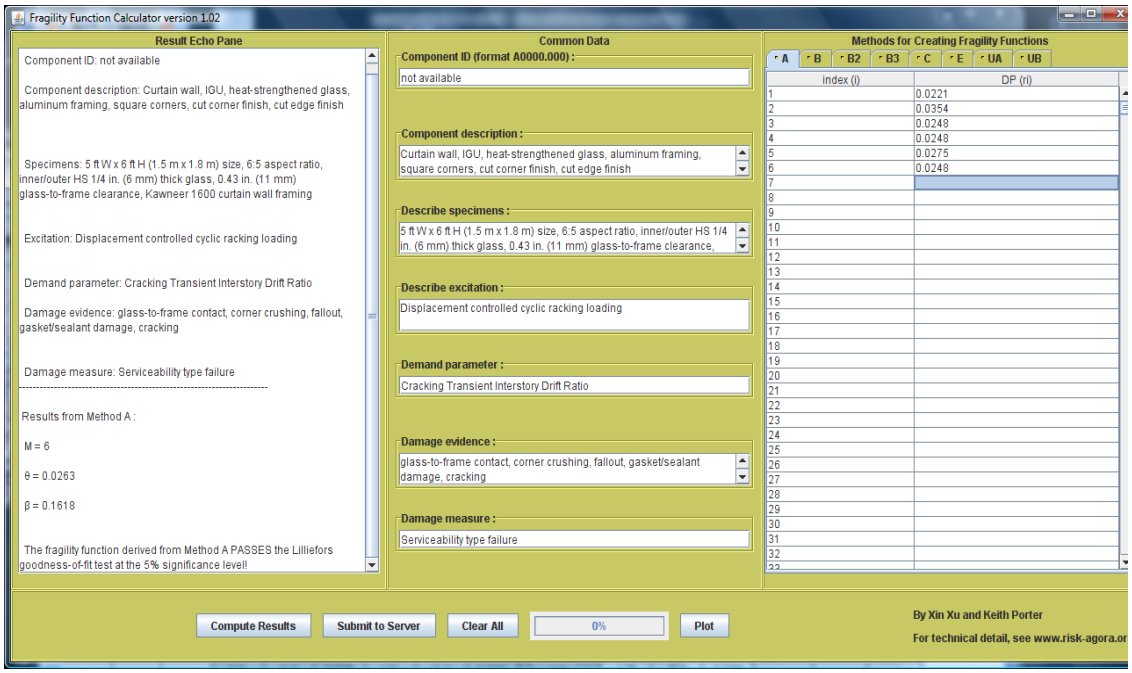

(a)

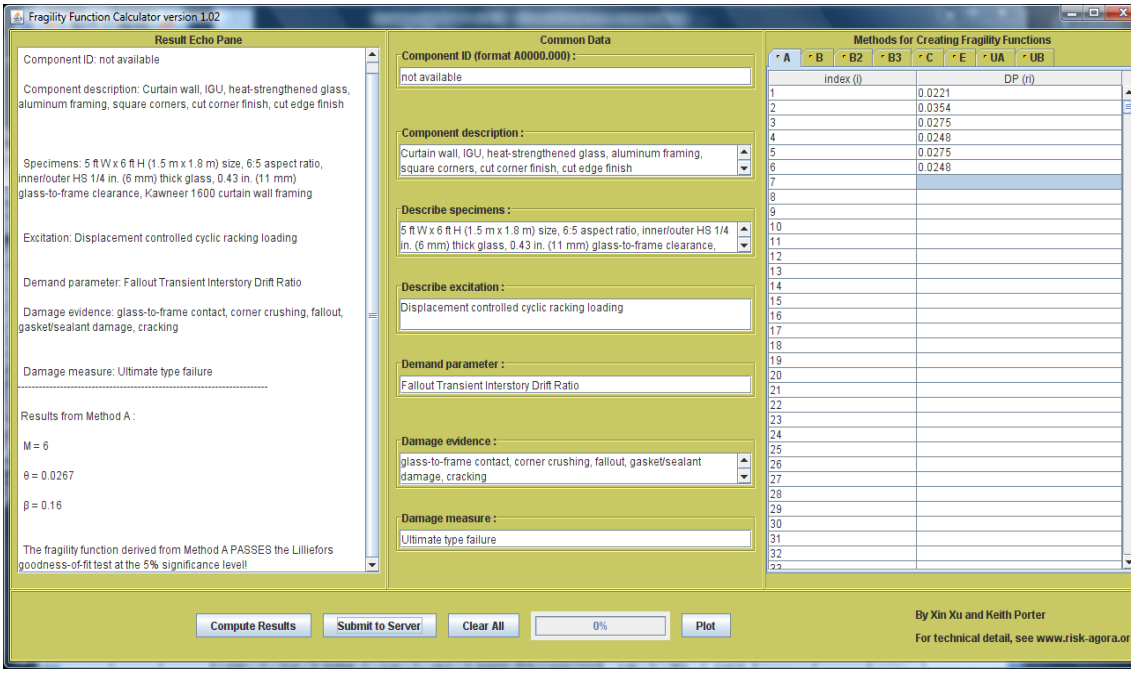

(b)

Figure A.22: Output of glass configuration (17) for (a) cracking and (b) fallout

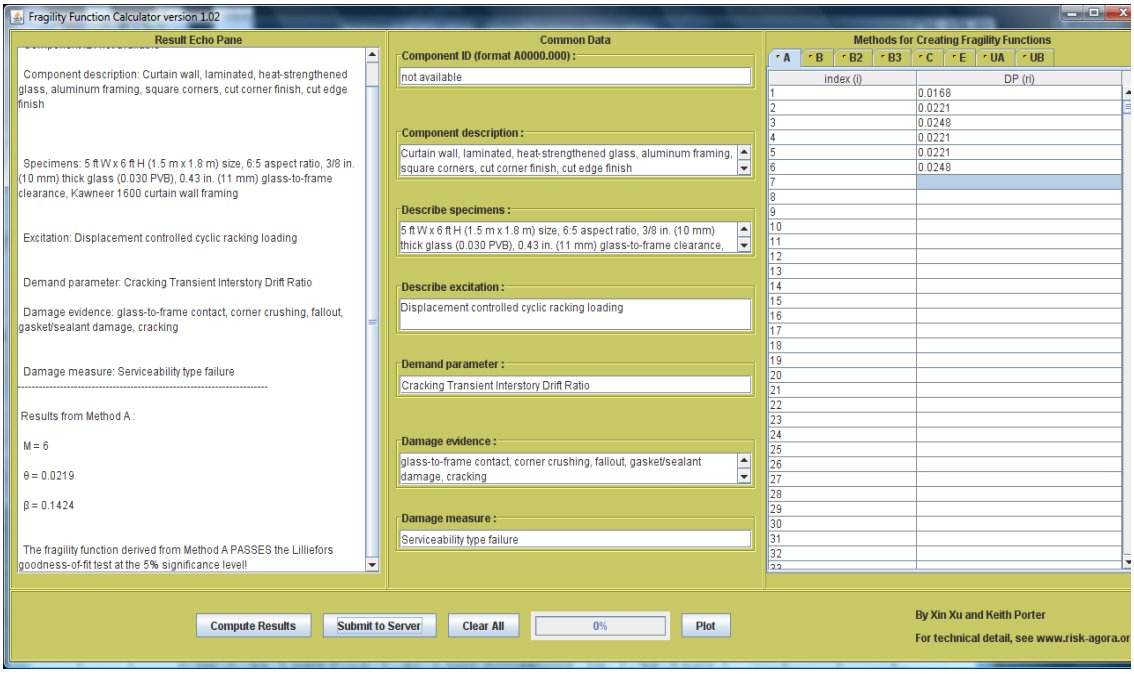

(a)

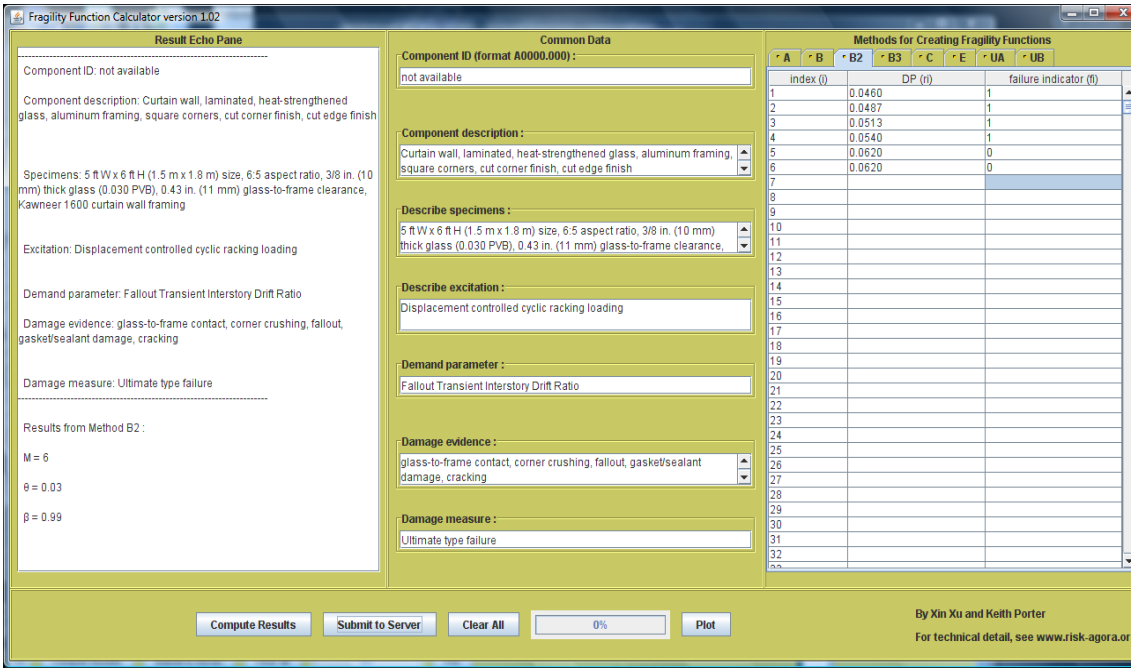

(b)

Figure A.23: Output of glass configuration (18) for (a) cracking and (b) fallout

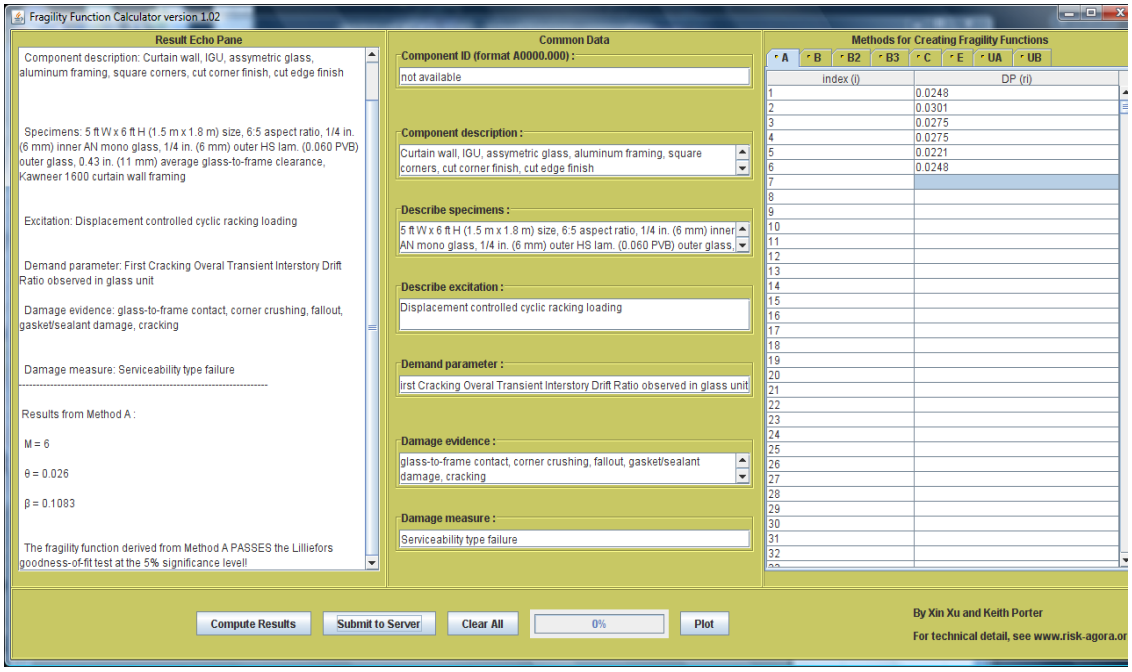

(a)

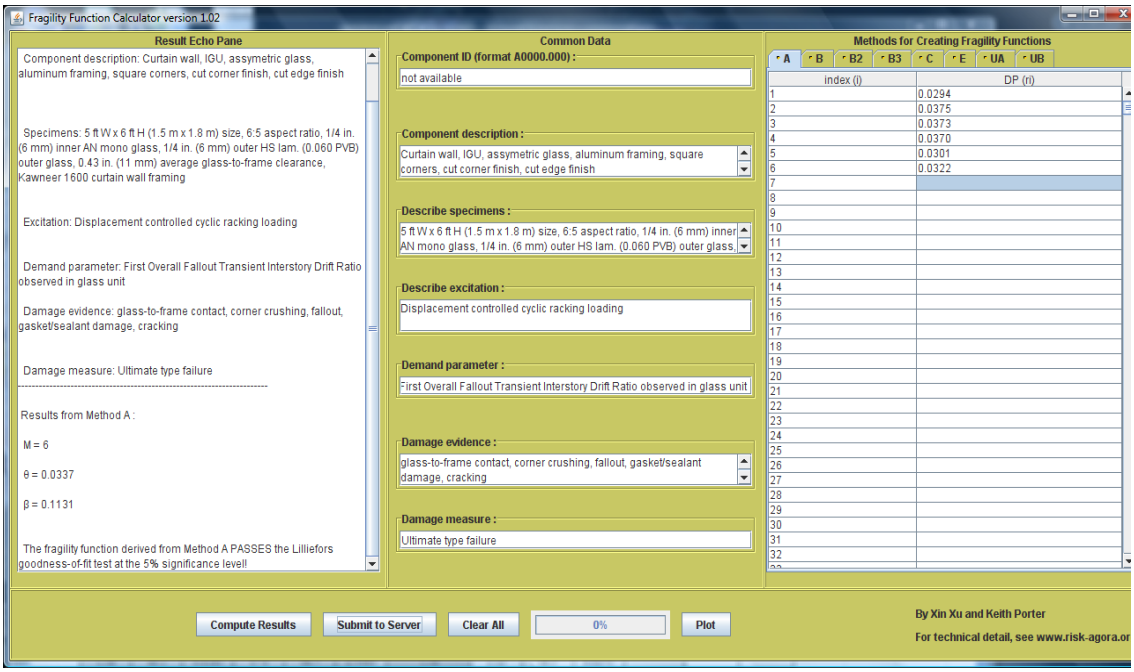

(b)

Figure A.24: Output of glass configuration (19) for (a) cracking and (b) fallout

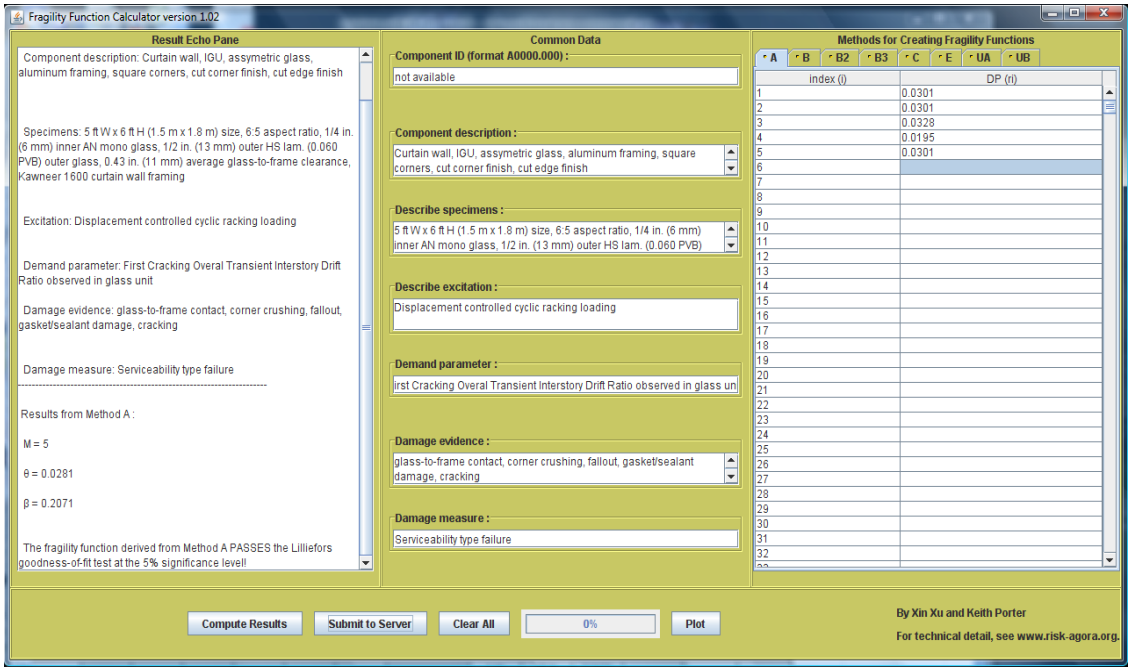

(a)

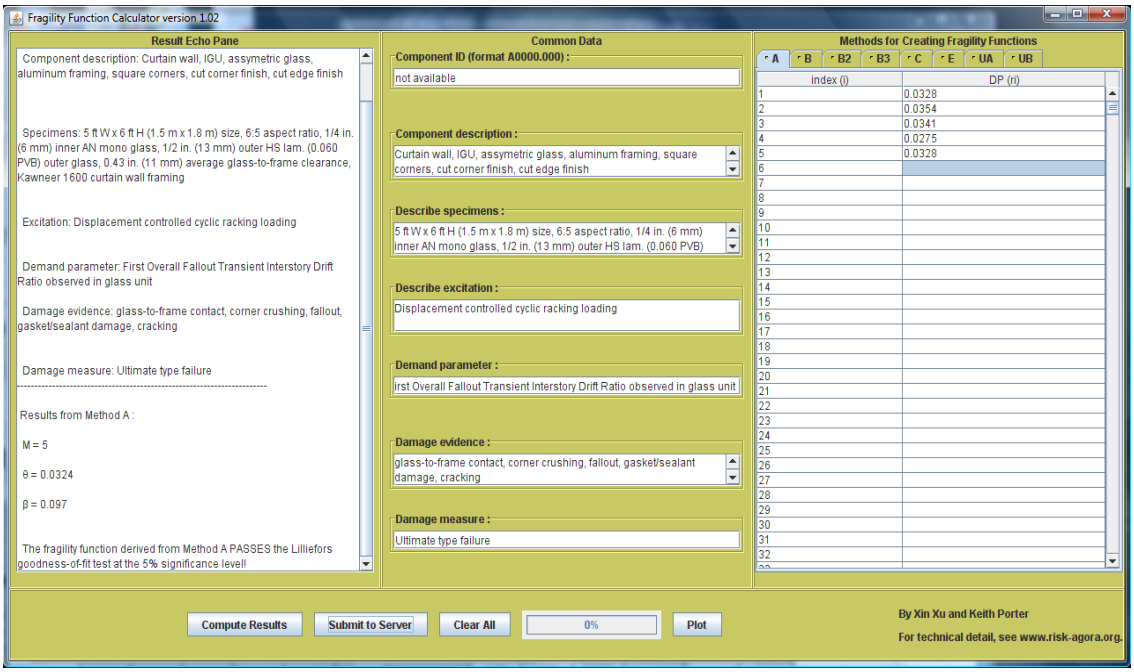

(b)

Figure A.25: Output of glass configuration (20) for (a) cracking and (b) fallout

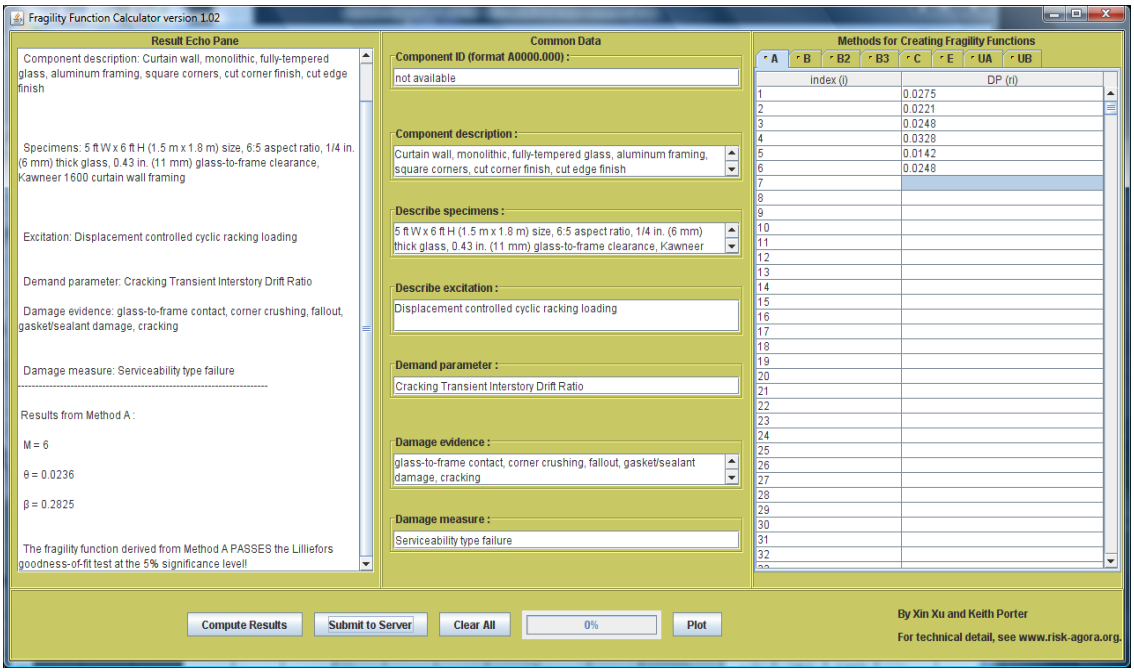

(a)

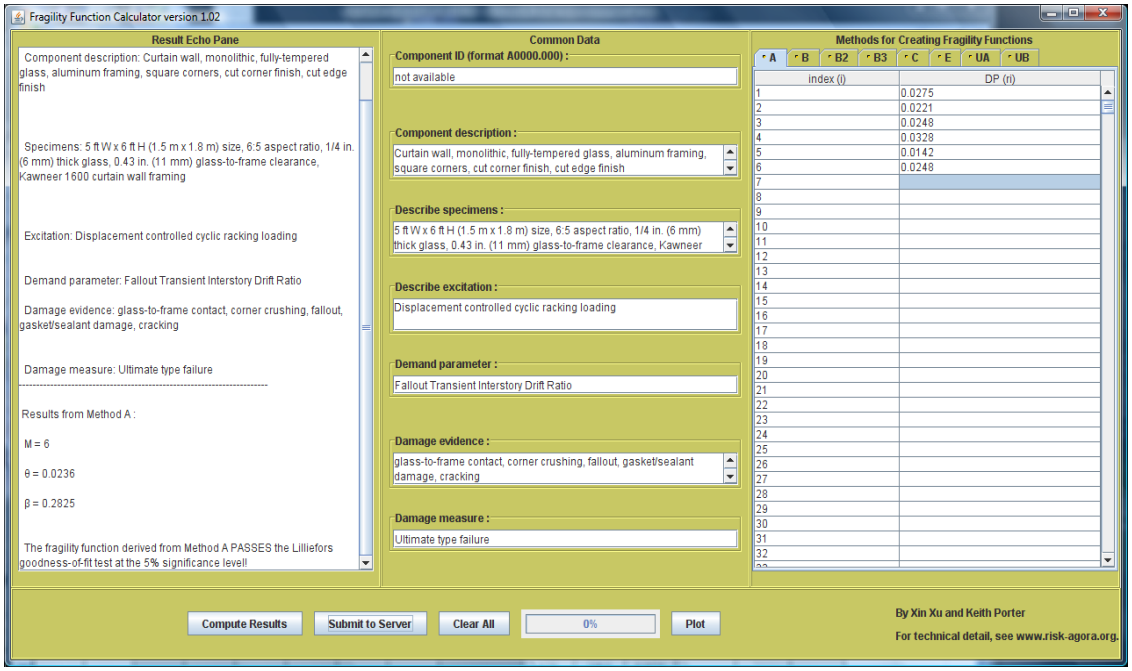

(b)

Figure A.26: Output of glass configuration (21) for (a) cracking and (b) fallout

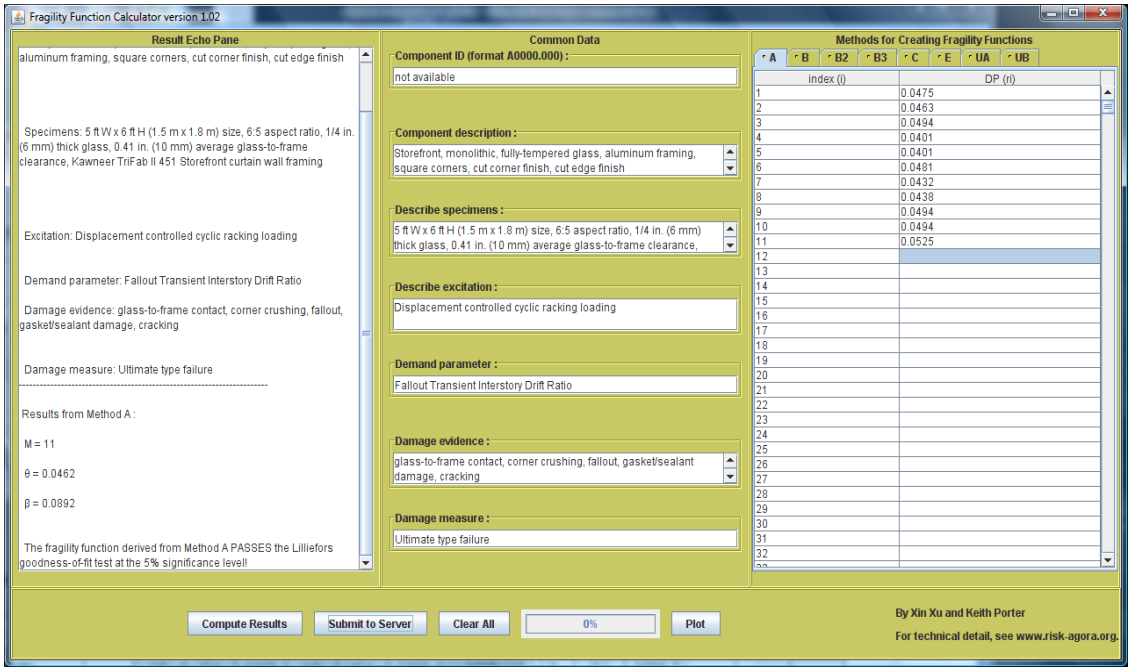

Figure **A.27**: Output of glass configuration (22) for fallout limit state

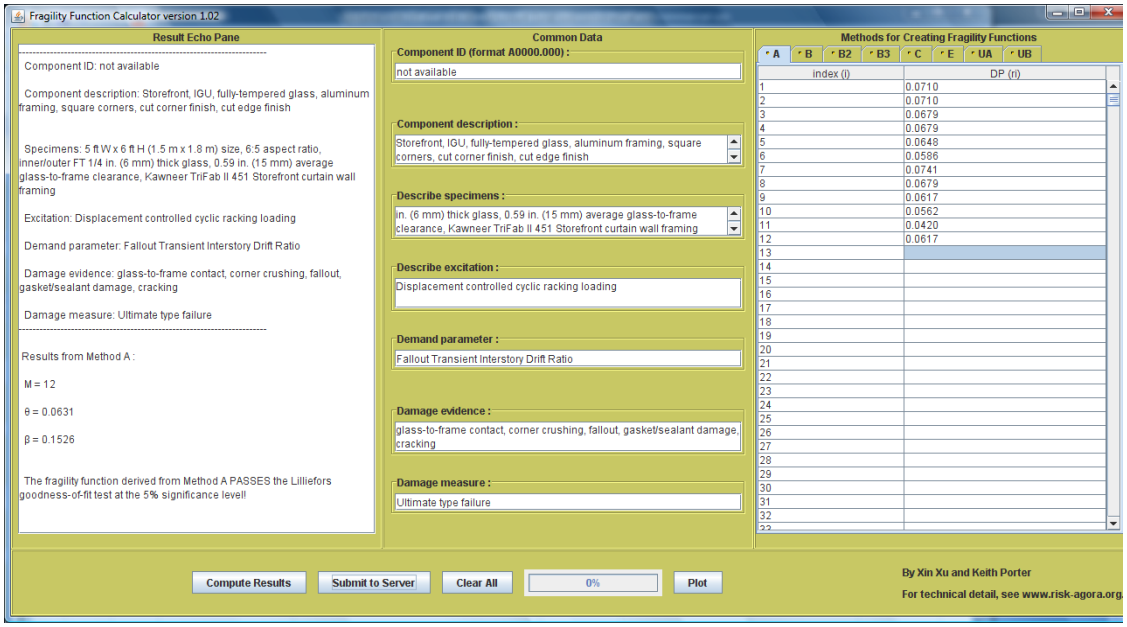

Figure A.28: Output of glass configuration (23) for fallout limit state

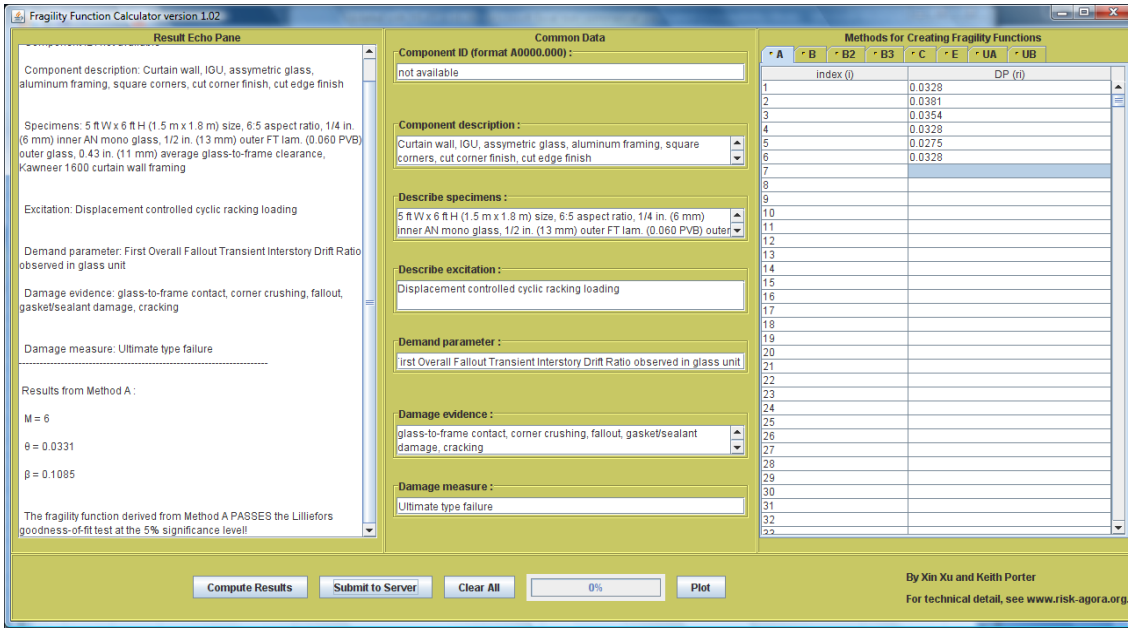

(a)

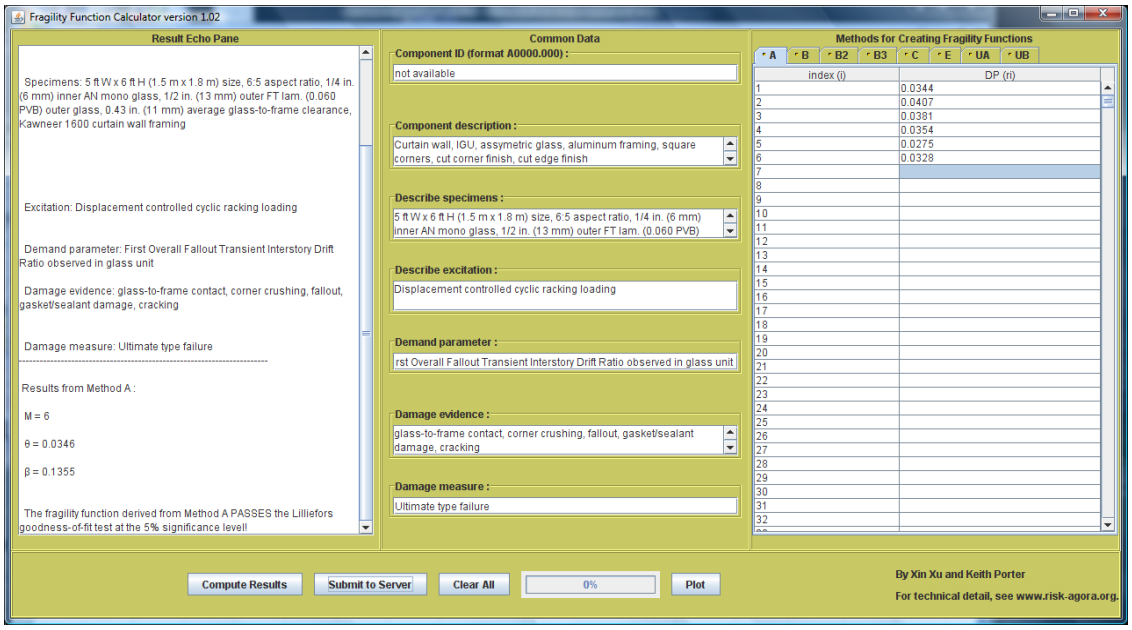

(b)

Figure A.29: Output of glass configuration (24) for (a) cracking and (b) fallout

A.4 Plotted Fragility Curves

The plots of the developed fragility functions are presented here. Figures **Figure A.30** through **A.58** give fragility plots for each of the available limit states (cracking, fallout, and gasket) of the glass configurations listed in Table 3.1. Along with each of the plotted fragilities, a table is provided in the figure which lists the values of the data points along the curves. Each table lists probability values in increments of one percent and then the corresponding drift ratios as a function of the fragility curve. These tables were provided for reference purposes, so that values can be looked up on the tables as opposed to having to manually calculate needed values on the curve.

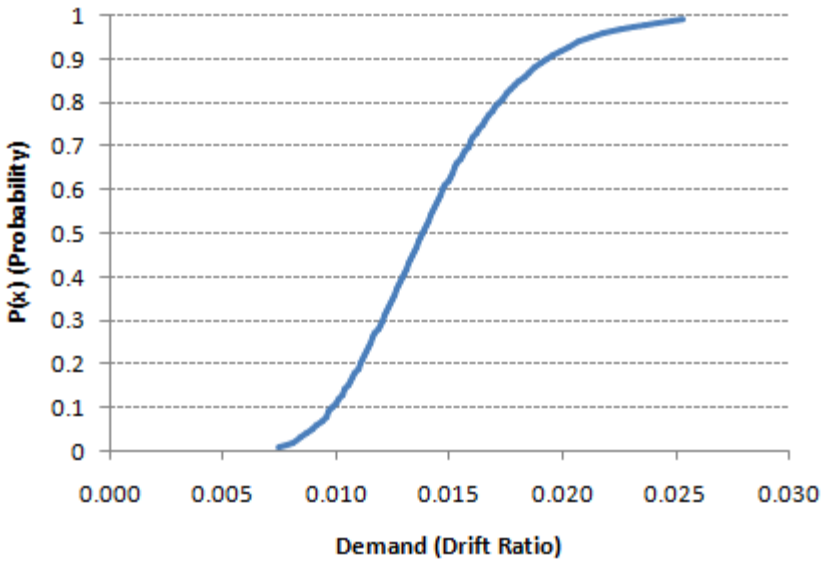

(a)

P(x)	θ	P(x)	θ	P(x)	θ	P(x)	θ	P(x)	θ
0.01	0.0075	0.21	0.0112	0.41	0.0130	0.61	0.0148	0.81	0.0174
0.02	0.0081	0.22	0.0113	0.42	0.0131	0.62	0.0149	0.82	0.0175
0.03	0.0084	0.23	0.0114	0.43	0.0132	0.63	0.0151	0.83	0.0177
0.04	0.0087	0.24	0.0115	0.44	0.0133	0.64	0.0152	0.84	0.0179
0.05	**0.0090**	**0.25**	**0.0116**	**0.45**	**0.0134**	**0.65**	**0.0153**	**0.85**	**0.0181**
0.06	0.0092	0.26	0.0117	0.46	0.0134	0.66	0.0154	0.86	0.0183
0.07	0.0094	0.27	0.0118	0.47	0.0135	0.67	0.0155	0.87	0.0185
0.08	0.0095	0.28	0.0118	0.48	0.0136	0.68	0.0156	0.88	0.0188
0.09	0.0097	0.29	0.0119	0.49	0.0137	0.69	0.0157	0.89	0.0190
0.10	**0.0099**	**0.30**	**0.0120**	**0.50**	**0.0138**	**0.70**	**0.0158**	**0.90**	**0.0193**
0.11	0.0100	0.31	0.0121	0.51	0.0139	0.71	0.0160	0.91	0.0196
0.12	0.0101	0.32	0.0122	0.52	0.0140	0.72	0.0161	0.92	0.0199
0.13	0.0103	0.33	0.0123	0.53	0.0141	0.73	0.0162	0.93	0.0203
0.14	0.0104	0.34	0.0124	0.54	0.0142	0.74	0.0163	0.94	0.0207
0.15	**0.0105**	**0.35**	**0.0125**	**0.55**	**0.0143**	**0.75**	**0.0165**	**0.95**	**0.0212**
0.16	0.0106	0.36	0.0126	0.56	0.0144	0.76	0.0166	0.96	0.0218
0.17	0.0107	0.37	0.0127	0.57	0.0145	0.77	0.0167	0.97	0.0226
0.18	0.0109	0.38	0.0127	0.58	0.0145	0.78	0.0169	0.98	0.0236
0.19	0.0110	0.39	0.0128	0.59	0.0146	0.79	0.0170	0.99	0.0254
0.20	**0.0111**	**0.40**	**0.0129**	**0.60**	**0.0147**	**0.80**	**0.0172**		

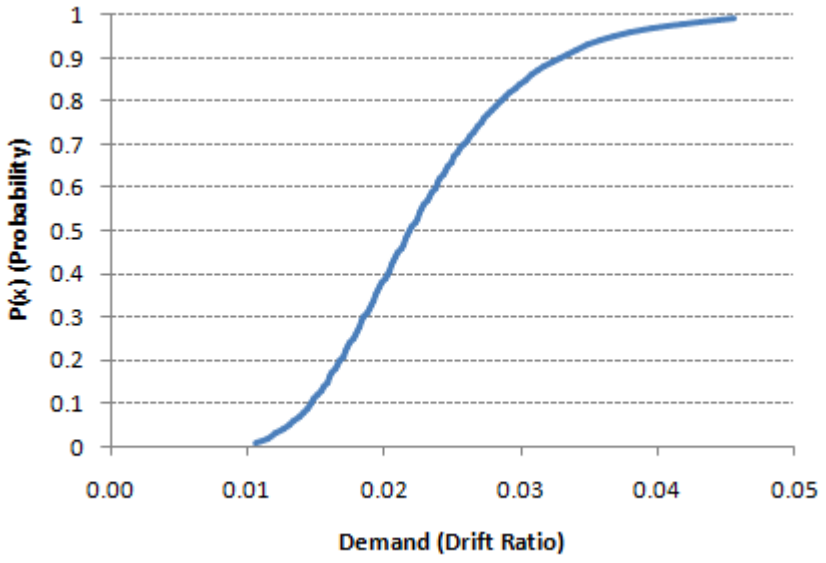

(b)

P(x)	θ	P(x)	θ	P(x)	θ	P(x)	θ	P(x)	θ
0.01	0.0105	0.21	0.0170	0.41	0.0204	0.61	0.0239	0.81	0.0289
0.02	0.0115	0.22	0.0172	0.42	0.0206	0.62	0.0241	0.82	0.0292
0.03	0.0121	0.23	0.0174	0.43	0.0207	0.63	0.0243	0.83	0.0296
0.04	0.0126	0.24	0.0175	0.44	0.0209	0.64	0.0245	0.84	0.0300
0.05	**0.0130**	**0.25**	**0.0177**	**0.45**	**0.0211**	**0.65**	**0.0247**	**0.85**	**0.0304**
0.06	0.0134	0.26	0.0179	0.46	0.0212	0.66	0.0249	0.86	0.0308
0.07	0.0138	0.27	0.0181	0.47	0.0214	0.67	0.0252	0.87	0.0312
0.08	0.0141	0.28	0.0182	0.48	0.0216	0.68	0.0254	0.88	0.0317
0.09	0.0144	0.29	0.0184	0.49	0.0217	0.69	0.0256	0.89	0.0322
0.10	**0.0146**	**0.30**	**0.0186**	**0.50**	**0.0219**	**0.70**	**0.0258**	**0.90**	**0.0328**
0.11	0.0149	0.31	0.0187	0.51	0.0221	0.71	0.0261	0.91	0.0334
0.12	0.0151	0.32	0.0189	0.52	0.0222	0.72	0.0263	0.92	0.0341
0.13	0.0154	0.33	0.0191	0.53	0.0224	0.73	0.0266	0.93	0.0349
0.14	0.0156	0.34	0.0192	0.54	0.0226	0.74	0.0268	0.94	0.0357
0.15	**0.0158**	**0.35**	**0.0194**	**0.55**	**0.0228**	**0.75**	**0.0271**	**0.95**	**0.0368**
0.16	0.0160	0.36	0.0196	0.56	0.0230	0.76	0.0274	0.96	0.0380
0.17	0.0162	0.37	0.0197	0.57	0.0232	0.77	0.0276	0.97	0.0396
0.18	0.0164	0.38	0.0199	0.58	0.0233	0.78	0.0279	0.98	0.0418
0.19	0.0166	0.39	0.0201	0.59	0.0235	0.79	0.0282	0.99	0.0456
0.20	**0.0168**	**0.40**	**0.0202**	**0.60**	**0.0237**	**0.80**	**0.0285**		

Figure A.30: Plotted fragility curve and information for glass configuration (1) for the (a) cracking and (b) fallout limit state

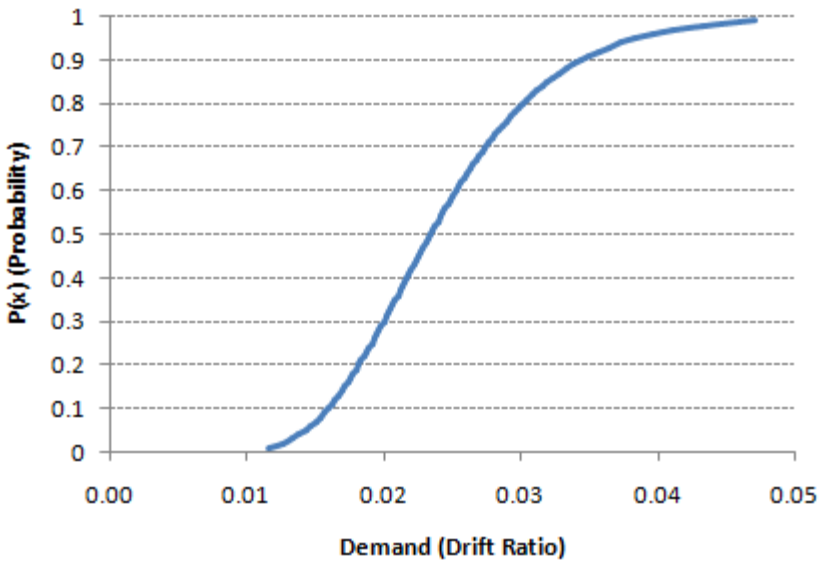

(a)

P(x)	θ	P(x)	θ	P(x)	θ	P(x)	θ	P(x)	θ
0.01	0.0116	0.21	0.0184	0.41	0.0219	0.61	0.0254	0.81	0.0305
0.02	0.0126	0.22	0.0186	0.42	0.0220	0.62	0.0256	0.82	0.0308
0.03	0.0133	0.23	0.0187	0.43	0.0222	0.63	0.0258	0.83	0.0312
0.04	0.0138	0.24	0.0189	0.44	0.0224	0.64	0.0261	0.84	0.0315
0.05	**0.0143**	**0.25**	**0.0191**	**0.45**	**0.0225**	**0.65**	**0.0263**	**0.85**	**0.0319**
0.06	0.0147	0.26	0.0193	0.46	0.0227	0.66	0.0265	0.86	0.0324
0.07	0.0150	0.27	0.0195	0.47	0.0229	0.67	0.0267	0.87	0.0328
0.08	0.0154	0.28	0.0196	0.48	0.0231	0.68	0.0269	0.88	0.0333
0.09	0.0157	0.29	0.0198	0.49	0.0232	0.69	0.0272	0.89	0.0338
0.10	**0.0159**	**0.30**	**0.0200**	**0.50**	**0.0234**	**0.70**	**0.0274**	**0.90**	**0.0344**
0.11	0.0162	0.31	0.0202	0.51	0.0236	0.71	0.0276	0.91	0.0350
0.12	0.0164	0.32	0.0203	0.52	0.0238	0.72	0.0279	0.92	0.0357
0.13	0.0167	0.33	0.0205	0.53	0.0239	0.73	0.0281	0.93	0.0364
0.14	0.0169	0.34	0.0207	0.54	0.0241	0.74	0.0284	0.94	0.0373
0.15	**0.0171**	**0.35**	**0.0208**	**0.55**	**0.0243**	**0.75**	**0.0286**	**0.95**	**0.0383**
0.16	0.0174	0.36	0.0210	0.56	0.0245	0.76	0.0289	0.96	0.0396
0.17	0.0176	0.37	0.0212	0.57	0.0247	0.77	0.0292	0.97	0.0411
0.18	0.0178	0.38	0.0214	0.58	0.0249	0.78	0.0295	0.98	0.0433
0.19	0.0180	0.39	0.0215	0.59	0.0251	0.79	0.0298	0.99	0.0470
0.20	**0.0182**	**0.40**	**0.0217**	**0.60**	**0.0252**	**0.80**	**0.0301**		

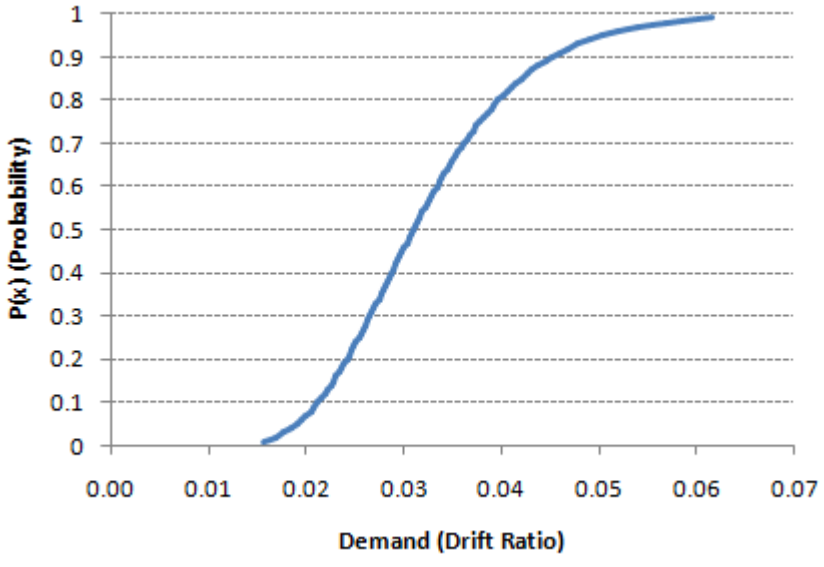

(b)

P(x)	θ	P(x)	θ	P(x)	θ	P(x)	θ	P(x)	θ
0.01	0.0156	0.21	0.0244	0.41	0.0290	0.61	0.0337	0.81	0.0402
0.02	0.0169	0.22	0.0247	0.42	0.0292	0.62	0.0339	0.82	0.0406
0.03	0.0178	0.23	0.0249	0.43	0.0294	0.63	0.0342	0.83	0.0411
0.04	0.0185	0.24	0.0252	0.44	0.0296	0.64	0.0345	0.84	0.0416
0.05	**0.0191**	**0.25**	**0.0254**	**0.45**	**0.0299**	**0.65**	**0.0347**	**0.85**	**0.0421**
0.06	0.0196	0.26	0.0256	0.46	0.0301	0.66	0.0350	0.86	0.0426
0.07	0.0201	0.27	0.0259	0.47	0.0303	0.67	0.0353	0.87	0.0432
0.08	0.0205	0.28	0.0261	0.48	0.0305	0.68	0.0356	0.88	0.0438
0.09	0.0209	0.29	0.0263	0.49	0.0308	0.69	0.0359	0.89	0.0445
0.10	**0.0212**	**0.30**	**0.0266**	**0.50**	**0.0310**	**0.70**	**0.0362**	**0.90**	**0.0452**
0.11	0.0216	0.31	0.0268	0.51	0.0312	0.71	0.0365	0.91	0.0460
0.12	0.0219	0.32	0.0270	0.52	0.0315	0.72	0.0368	0.92	0.0469
0.13	0.0222	0.33	0.0272	0.53	0.0317	0.73	0.0371	0.93	0.0479
0.14	0.0225	0.34	0.0274	0.54	0.0319	0.74	0.0375	0.94	0.0490
0.15	**0.0228**	**0.35**	**0.0277**	**0.55**	**0.0322**	**0.75**	**0.0378**	**0.95**	**0.0504**
0.16	0.0231	0.36	0.0279	0.56	0.0324	0.76	0.0382	0.96	0.0520
0.17	0.0234	0.37	0.0281	0.57	0.0327	0.77	0.0385	0.97	0.0540
0.18	0.0237	0.38	0.0283	0.58	0.0329	0.78	0.0389	0.98	0.0568
0.19	0.0239	0.39	0.0285	0.59	0.0332	0.79	0.0393	0.99	0.0616
0.20	**0.0242**	**0.40**	**0.0288**	**0.60**	**0.0334**	**0.80**	**0.0397**		

Figure A.31: Plotted fragility curve and information for glass configuration (2) for the (a) cracking and (b) fallout limit state

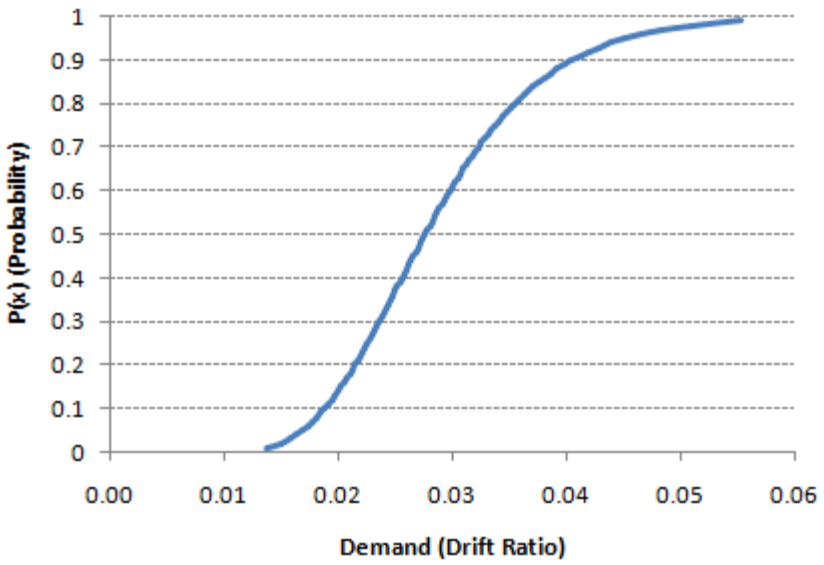

(a)

P(x)	θ	P(x)	θ	P(x)	θ	P(x)	θ	P(x)	θ
0.01	0.0138	0.21	0.0217	0.41	0.0258	0.61	0.0300	0.81	0.0359
0.02	0.0150	0.22	0.0219	0.42	0.0260	0.62	0.0302	0.82	0.0363
0.03	0.0158	0.23	0.0221	0.43	0.0262	0.63	0.0305	0.83	0.0367
0.04	0.0164	0.24	0.0224	0.44	0.0264	0.64	0.0307	0.84	0.0371
0.05	**0.0169**	**0.25**	**0.0226**	**0.45**	**0.0266**	**0.65**	**0.0310**	**0.85**	**0.0376**
0.06	0.0174	0.26	0.0228	0.46	0.0268	0.66	0.0312	0.86	0.0381
0.07	0.0178	0.27	0.0230	0.47	0.0270	0.67	0.0315	0.87	0.0386
0.08	0.0182	0.28	0.0232	0.48	0.0272	0.68	0.0317	0.88	0.0392
0.09	0.0185	0.29	0.0234	0.49	0.0274	0.69	0.0320	0.89	0.0398
0.10	**0.0188**	**0.30**	**0.0236**	**0.50**	**0.0276**	**0.70**	**0.0323**	**0.90**	**0.0404**
0.11	0.0192	0.31	0.0238	0.51	0.0278	0.71	0.0325	0.91	0.0412
0.12	0.0194	0.32	0.0240	0.52	0.0280	0.72	0.0328	0.92	0.0420
0.13	0.0197	0.33	0.0242	0.53	0.0282	0.73	0.0331	0.93	0.0428
0.14	0.0200	0.34	0.0244	0.54	0.0284	0.74	0.0334	0.94	0.0439
0.15	**0.0203**	**0.35**	**0.0246**	**0.55**	**0.0287**	**0.75**	**0.0337**	**0.95**	**0.0451**
0.16	0.0205	0.36	0.0248	0.56	0.0289	0.76	0.0341	0.96	0.0465
0.17	0.0208	0.37	0.0250	0.57	0.0291	0.77	0.0344	0.97	0.0483
0.18	0.0210	0.38	0.0252	0.58	0.0293	0.78	0.0347	0.98	0.0509
0.19	0.0212	0.39	0.0254	0.59	0.0295	0.79	0.0351	0.99	0.0552
0.20	**0.0215**	**0.40**	**0.0256**	**0.60**	**0.0298**	**0.80**	**0.0355**		

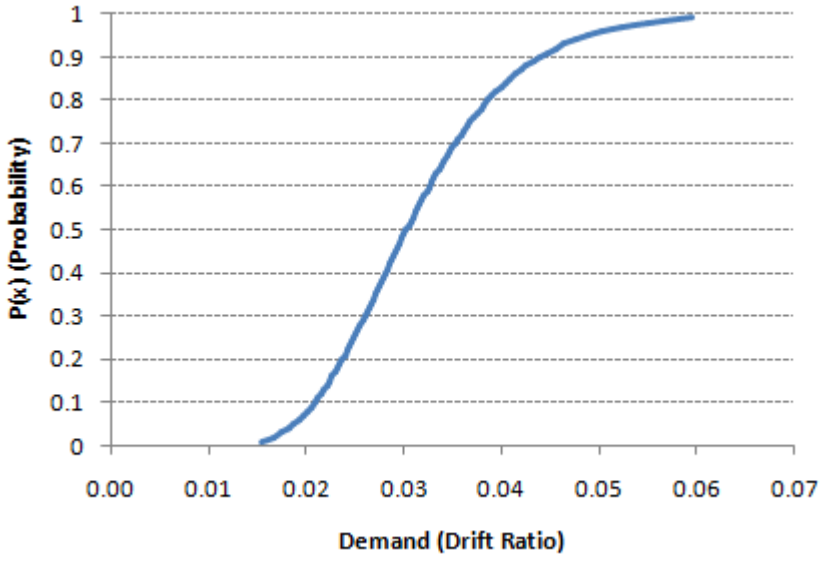

(b)

P(x)	θ	P(x)	θ	P(x)	θ	P(x)	θ	P(x)	θ
0.01	0.0154	0.21	0.0240	0.41	0.0284	0.61	0.0329	0.81	0.0391
0.02	0.0167	0.22	0.0242	0.42	0.0286	0.62	0.0331	0.82	0.0395
0.03	0.0176	0.23	0.0245	0.43	0.0288	0.63	0.0334	0.83	0.0400
0.04	0.0182	0.24	0.0247	0.44	0.0290	0.64	0.0336	0.84	0.0404
0.05	**0.0188**	**0.25**	**0.0249**	**0.45**	**0.0292**	**0.65**	**0.0339**	**0.85**	**0.0409**
0.06	0.0193	0.26	0.0251	0.46	0.0294	0.66	0.0341	0.86	0.0414
0.07	0.0198	0.27	0.0254	0.47	0.0296	0.67	0.0344	0.87	0.0420
0.08	0.0202	0.28	0.0256	0.48	0.0299	0.68	0.0347	0.88	0.0426
0.09	0.0205	0.29	0.0258	0.49	0.0301	0.69	0.0350	0.89	0.0432
0.10	**0.0209**	**0.30**	**0.0260**	**0.50**	**0.0303**	**0.70**	**0.0353**	**0.90**	**0.0439**
0.11	0.0212	0.31	0.0262	0.51	0.0305	0.71	0.0356	0.91	0.0447
0.12	0.0216	0.32	0.0265	0.52	0.0307	0.72	0.0359	0.92	0.0455
0.13	0.0219	0.33	0.0267	0.53	0.0310	0.73	0.0362	0.93	0.0465
0.14	0.0222	0.34	0.0269	0.54	0.0312	0.74	0.0365	0.94	0.0476
0.15	**0.0224**	**0.35**	**0.0271**	**0.55**	**0.0314**	**0.75**	**0.0368**	**0.95**	**0.0488**
0.16	0.0227	0.36	0.0273	0.56	0.0317	0.76	0.0372	0.96	0.0503
0.17	0.0230	0.37	0.0275	0.57	0.0319	0.77	0.0375	0.97	0.0523
0.18	0.0232	0.38	0.0277	0.58	0.0321	0.78	0.0379	0.98	0.0550
0.19	0.0235	0.39	0.0279	0.59	0.0324	0.79	0.0383	0.99	0.0595
0.20	**0.0237**	**0.40**	**0.0282**	**0.60**	**0.0326**	**0.80**	**0.0387**		

Figure A.32: Plotted fragility curve and information for glass configuration (3) for the (a) cracking and (b) fallout limit state

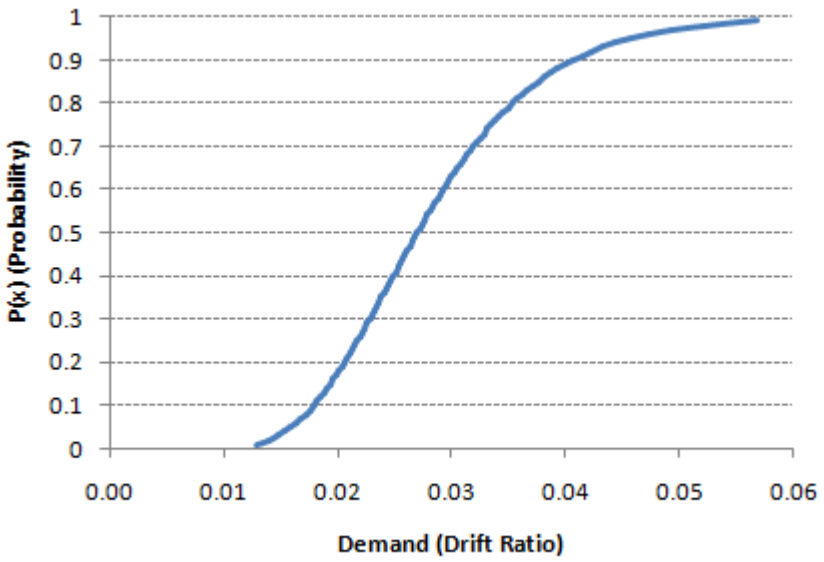

P(x)	θ	P(x)	θ	P(x)	θ	P(x)	θ	P(x)	θ
0.01	0.0128	0.21	0.0209	0.41	0.0251	0.61	0.0295	0.81	0.0358
0.02	0.0140	0.22	0.0211	0.42	0.0253	0.62	0.0298	0.82	0.0362
0.03	0.0148	0.23	0.0213	0.43	0.0255	0.63	0.0300	0.83	0.0366
0.04	0.0154	0.24	0.0215	0.44	0.0257	0.64	0.0303	0.84	0.0371
0.05	**0.0160**	**0.25**	**0.0218**	**0.45**	**0.0259**	**0.65**	**0.0305**	**0.85**	**0.0376**
0.06	0.0164	0.26	0.0220	0.46	0.0261	0.66	0.0308	0.86	0.0382
0.07	0.0168	0.27	0.0222	0.47	0.0264	0.67	0.0311	0.87	0.0387
0.08	0.0172	0.28	0.0224	0.48	0.0266	0.68	0.0314	0.88	0.0393
0.09	0.0176	0.29	0.0226	0.49	0.0268	0.69	0.0316	0.89	0.0400
0.10	**0.0179**	**0.30**	**0.0228**	**0.50**	**0.0270**	**0.70**	**0.0319**	**0.90**	**0.0407**
0.11	0.0182	0.31	0.0230	0.51	0.0272	0.71	0.0322	0.91	0.0415
0.12	0.0185	0.32	0.0232	0.52	0.0274	0.72	0.0325	0.92	0.0423
0.13	0.0188	0.33	0.0235	0.53	0.0277	0.73	0.0328	0.93	0.0433
0.14	0.0191	0.34	0.0237	0.54	0.0279	0.74	0.0332	0.94	0.0444
0.15	**0.0194**	**0.35**	**0.0239**	**0.55**	**0.0281**	**0.75**	**0.0335**	**0.95**	**0.0457**
0.16	0.0196	0.36	0.0241	0.56	0.0283	0.76	0.0338	0.96	0.0473
0.17	0.0199	0.37	0.0243	0.57	0.0286	0.77	0.0342	0.97	0.0493
0.18	0.0201	0.38	0.0245	0.58	0.0288	0.78	0.0346	0.98	0.0521
0.19	0.0204	0.39	0.0247	0.59	0.0290	0.79	0.0349	0.99	0.0568
0.20	**0.0206**	**0.40**	**0.0249**	**0.60**	**0.0293**	**0.80**	**0.0353**		

Figure A.33: Plotted fragility curve and information of glass configuration (3) for the gasket degradation limit state

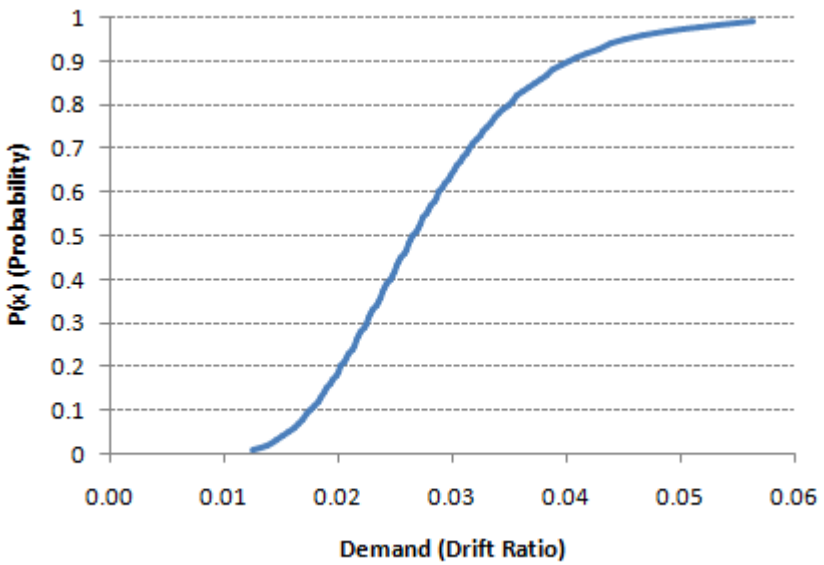

(a)

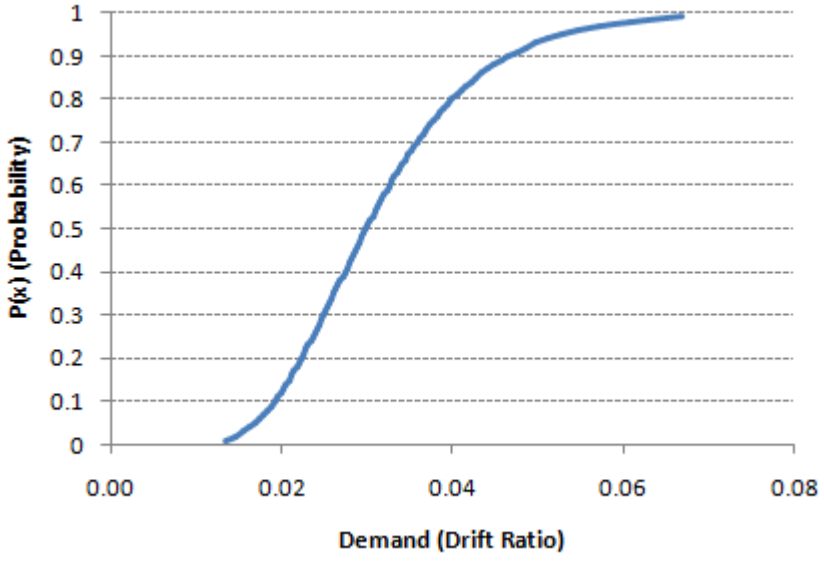

(b)

P(x)	θ	P(x)	θ	P(x)	θ	P(x)	θ	P(x)	θ
0.01	0.0126	0.21	0.0205	0.41	0.0247	0.61	0.0291	0.81	0.0353
0.02	0.0137	0.22	0.0207	0.42	0.0249	0.62	0.0293	0.82	0.0357
0.03	0.0145	0.23	0.0210	0.43	0.0251	0.63	0.0296	0.83	0.0362
0.04	0.0151	0.24	0.0212	0.44	0.0253	0.64	0.0299	0.84	0.0366
0.05	**0.0157**	**0.25**	**0.0214**	**0.45**	**0.0255**	**0.65**	**0.0301**	**0.85**	**0.0371**
0.06	0.0161	0.26	0.0216	0.46	0.0258	0.66	0.0304	0.86	0.0377
0.07	0.0165	0.27	0.0218	0.47	0.0260	0.67	0.0306	0.87	0.0382
0.08	0.0169	0.28	0.0220	0.48	0.0262	0.68	0.0309	0.88	0.0388
0.09	0.0173	0.29	0.0223	0.49	0.0264	0.69	0.0312	0.89	0.0395
0.10	**0.0176**	**0.30**	**0.0225**	**0.50**	**0.0266**	**0.70**	**0.0315**	**0.90**	**0.0402**
0.11	0.0179	0.31	0.0227	0.51	0.0268	0.71	0.0318	0.91	0.0410
0.12	0.0182	0.32	0.0229	0.52	0.0270	0.72	0.0321	0.92	0.0418
0.13	0.0185	0.33	0.0231	0.53	0.0273	0.73	0.0324	0.93	0.0428
0.14	0.0188	0.34	0.0233	0.54	0.0275	0.74	0.0327	0.94	0.0439
0.15	**0.0191**	**0.35**	**0.0235**	**0.55**	**0.0277**	**0.75**	**0.0331**	**0.95**	**0.0452**
0.16	0.0193	0.36	0.0237	0.56	0.0279	0.76	0.0334	0.96	0.0467
0.17	0.0196	0.37	0.0239	0.57	0.0282	0.77	0.0337	0.97	0.0487
0.18	0.0198	0.38	0.0241	0.58	0.0284	0.78	0.0341	0.98	0.0515
0.19	0.0200	0.39	0.0243	0.59	0.0286	0.79	0.0345	0.99	0.0563
0.20	**0.0203**	**0.40**	**0.0245**	**0.60**	**0.0289**	**0.80**	**0.0349**		

P(x)	θ	P(x)	θ	P(x)	θ	P(x)	θ	P(x)	θ
0.01	0.0134	0.21	0.0226	0.41	0.0276	0.61	0.0329	0.81	0.0405
0.02	0.0147	0.22	0.0229	0.42	0.0279	0.62	0.0332	0.82	0.0410
0.03	0.0156	0.23	0.0232	0.43	0.0281	0.63	0.0335	0.83	0.0416
0.04	0.0163	0.24	0.0234	0.44	0.0284	0.64	0.0338	0.84	0.0422
0.05	**0.0169**	**0.25**	**0.0237**	**0.45**	**0.0286**	**0.65**	**0.0342**	**0.85**	**0.0428**
0.06	0.0175	0.26	0.0239	0.46	0.0289	0.66	0.0345	0.86	0.0435
0.07	0.0179	0.27	0.0242	0.47	0.0291	0.67	0.0348	0.87	0.0441
0.08	0.0184	0.28	0.0244	0.48	0.0294	0.68	0.0352	0.88	0.0449
0.09	0.0188	0.29	0.0247	0.49	0.0296	0.69	0.0355	0.89	0.0457
0.10	**0.0192**	**0.30**	**0.0249**	**0.50**	**0.0299**	**0.70**	**0.0358**	**0.90**	**0.0466**
0.11	0.0196	0.31	0.0252	0.51	0.0302	0.71	0.0362	0.91	0.0475
0.12	0.0199	0.32	0.0254	0.52	0.0304	0.72	0.0366	0.92	0.0486
0.13	0.0202	0.33	0.0257	0.53	0.0307	0.73	0.0370	0.93	0.0498
0.14	0.0206	0.34	0.0259	0.54	0.0310	0.74	0.0374	0.94	0.0512
0.15	**0.0209**	**0.35**	**0.0262**	**0.55**	**0.0312**	**0.75**	**0.0378**	**0.95**	**0.0528**
0.16	0.0212	0.36	0.0264	0.56	0.0315	0.76	0.0382	0.96	0.0548
0.17	0.0215	0.37	0.0267	0.57	0.0318	0.77	0.0386	0.97	0.0573
0.18	0.0218	0.38	0.0269	0.58	0.0321	0.78	0.0391	0.98	0.0609
0.19	0.0221	0.39	0.0271	0.59	0.0323	0.79	0.0395	0.99	0.0669
0.20	**0.0223**	**0.40**	**0.0274**	**0.60**	**0.0326**	**0.80**	**0.0400**		

Figure A.34: Plotted fragility curve and information for glass configuration (4) for the (a) cracking and (b) fallout limit state

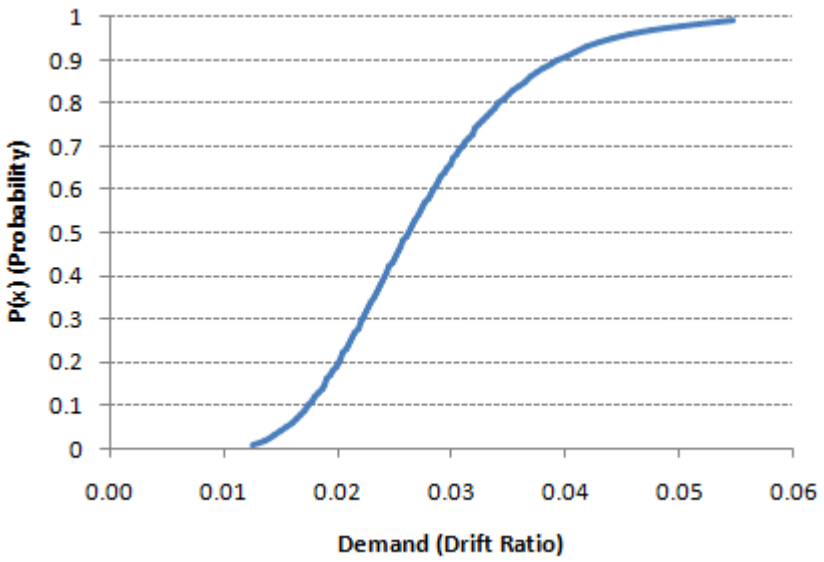

P(x)	θ	P(x)	θ	P(x)	θ	P(x)	θ	P(x)	θ
0.01	0.0125	0.21	0.0203	0.41	0.0244	0.61	0.0286	0.81	0.0346
0.02	0.0137	0.22	0.0205	0.42	0.0246	0.62	0.0289	0.82	0.0350
0.03	0.0144	0.23	0.0207	0.43	0.0248	0.63	0.0291	0.83	0.0355
0.04	0.0150	0.24	0.0209	0.44	0.0250	0.64	0.0294	0.84	0.0359
0.05	**0.0156**	**0.25**	**0.0212**	**0.45**	**0.0252**	**0.65**	**0.0296**	**0.85**	**0.0364**
0.06	0.0160	0.26	0.0214	0.46	0.0254	0.66	0.0299	0.86	0.0369
0.07	0.0164	0.27	0.0216	0.47	0.0256	0.67	0.0301	0.87	0.0374
0.08	0.0168	0.28	0.0218	0.48	0.0258	0.68	0.0304	0.88	0.0380
0.09	0.0171	0.29	0.0220	0.49	0.0260	0.69	0.0307	0.89	0.0387
0.10	**0.0175**	**0.30**	**0.0222**	**0.50**	**0.0262**	**0.70**	**0.0309**	**0.90**	**0.0393**
0.11	0.0178	0.31	0.0224	0.51	0.0264	0.71	0.0312	0.91	0.0401
0.12	0.0181	0.32	0.0226	0.52	0.0266	0.72	0.0315	0.92	0.0409
0.13	0.0183	0.33	0.0228	0.53	0.0268	0.73	0.0318	0.93	0.0418
0.14	0.0186	0.34	0.0230	0.54	0.0270	0.74	0.0321	0.94	0.0429
0.15	**0.0189**	**0.35**	**0.0232**	**0.55**	**0.0273**	**0.75**	**0.0324**	**0.95**	**0.0441**
0.16	0.0191	0.36	0.0234	0.56	0.0275	0.76	0.0328	0.96	0.0456
0.17	0.0194	0.37	0.0236	0.57	0.0277	0.77	0.0331	0.97	0.0476
0.18	0.0196	0.38	0.0238	0.58	0.0279	0.78	0.0335	0.98	0.0502
0.19	0.0198	0.39	0.0240	0.59	0.0282	0.79	0.0338	0.99	0.0548
0.20	**0.0201**	**0.40**	**0.0242**	**0.60**	**0.0284**	**0.80**	**0.0342**		

Figure A.35: Plotted fragility curve and information of glass configuration (4) for the gasket degradation limit state

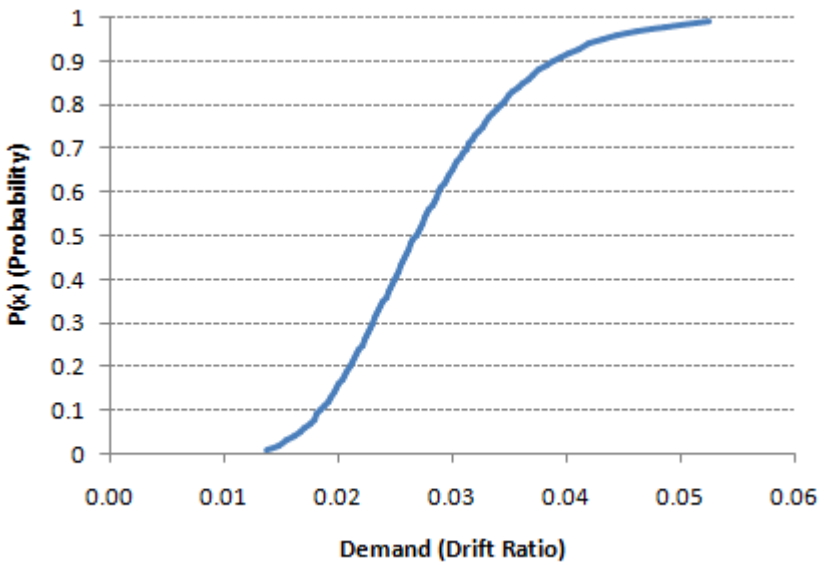

(a)

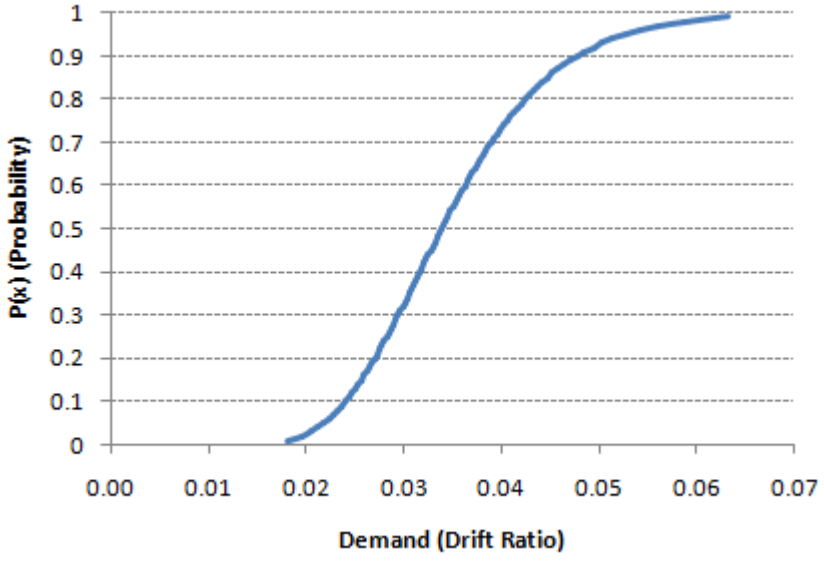

(b)

P(x)	θ	P(x)	θ	P(x)	θ	P(x)	θ	P(x)	θ
0.01	0.0137	0.21	0.0212	0.41	0.0251	0.61	0.0291	0.81	0.0345
0.02	0.0148	0.22	0.0214	0.42	0.0253	0.62	0.0293	0.82	0.0349
0.03	0.0156	0.23	0.0216	0.43	0.0255	0.63	0.0295	0.83	0.0353
0.04	0.0162	0.24	0.0219	0.44	0.0257	0.64	0.0297	0.84	0.0357
0.05	**0.0167**	**0.25**	**0.0221**	**0.45**	**0.0258**	**0.65**	**0.0300**	**0.85**	**0.0362**
0.06	0.0171	0.26	0.0223	0.46	0.0260	0.66	0.0302	0.86	0.0366
0.07	0.0175	0.27	0.0225	0.47	0.0262	0.67	0.0304	0.87	0.0371
0.08	0.0179	0.28	0.0226	0.48	0.0264	0.68	0.0307	0.88	0.0376
0.09	0.0182	0.29	0.0228	0.49	0.0266	0.69	0.0309	0.89	0.0382
0.10	**0.0185**	**0.30**	**0.0230**	**0.50**	**0.0268**	**0.70**	**0.0312**	**0.90**	**0.0388**
0.11	0.0188	0.31	0.0232	0.51	0.0270	0.71	0.0314	0.91	0.0395
0.12	0.0191	0.32	0.0234	0.52	0.0272	0.72	0.0317	0.92	0.0402
0.13	0.0194	0.33	0.0236	0.53	0.0274	0.73	0.0320	0.93	0.0411
0.14	0.0196	0.34	0.0238	0.54	0.0276	0.74	0.0323	0.94	0.0420
0.15	**0.0199**	**0.35**	**0.0240**	**0.55**	**0.0278**	**0.75**	**0.0326**	**0.95**	**0.0431**
0.16	0.0201	0.36	0.0242	0.56	0.0280	0.76	0.0329	0.96	0.0444
0.17	0.0203	0.37	0.0243	0.57	0.0282	0.77	0.0332	0.97	0.0462
0.18	0.0206	0.38	0.0245	0.58	0.0284	0.78	0.0335	0.98	0.0485
0.19	0.0208	0.39	0.0247	0.59	0.0286	0.79	0.0338	0.99	0.0525
0.20	**0.0210**	**0.40**	**0.0249**	**0.60**	**0.0288**	**0.80**	**0.0342**		

P(x)	θ	P(x)	θ	P(x)	θ	P(x)	θ	P(x)	θ
0.01	0.0182	0.21	0.0273	0.41	0.0319	0.61	0.0365	0.81	0.0429
0.02	0.0196	0.22	0.0276	0.42	0.0321	0.62	0.0368	0.82	0.0433
0.03	0.0205	0.23	0.0278	0.43	0.0323	0.63	0.0371	0.83	0.0438
0.04	0.0212	0.24	0.0281	0.44	0.0326	0.64	0.0373	0.84	0.0443
0.05	**0.0218**	**0.25**	**0.0283**	**0.45**	**0.0328**	**0.65**	**0.0376**	**0.85**	**0.0448**
0.06	0.0223	0.26	0.0285	0.46	0.0330	0.66	0.0379	0.86	0.0453
0.07	0.0228	0.27	0.0288	0.47	0.0332	0.67	0.0381	0.87	0.0458
0.08	0.0233	0.28	0.0290	0.48	0.0334	0.68	0.0384	0.88	0.0464
0.09	0.0237	0.29	0.0292	0.49	0.0337	0.69	0.0387	0.89	0.0471
0.10	**0.0240**	**0.30**	**0.0295**	**0.50**	**0.0339**	**0.70**	**0.0390**	**0.90**	**0.0478**
0.11	0.0244	0.31	0.0297	0.51	0.0341	0.71	0.0393	0.91	0.0486
0.12	0.0247	0.32	0.0299	0.52	0.0344	0.72	0.0396	0.92	0.0494
0.13	0.0251	0.33	0.0301	0.53	0.0346	0.73	0.0400	0.93	0.0503
0.14	0.0254	0.34	0.0304	0.54	0.0348	0.74	0.0403	0.94	0.0514
0.15	**0.0257**	**0.35**	**0.0306**	**0.55**	**0.0351**	**0.75**	**0.0406**	**0.95**	**0.0527**
0.16	0.0260	0.36	0.0308	0.56	0.0353	0.76	0.0410	0.96	0.0542
0.17	0.0263	0.37	0.0310	0.57	0.0355	0.77	0.0413	0.97	0.0561
0.18	0.0265	0.38	0.0312	0.58	0.0358	0.78	0.0417	0.98	0.0588
0.19	0.0268	0.39	0.0315	0.59	0.0360	0.79	0.0421	0.99	0.0632
0.20	**0.0271**	**0.40**	**0.0317**	**0.60**	**0.0363**	**0.80**	**0.0425**		

Figure A.36: Plotted fragility curve and information for glass configuration (5) for the (a) cracking and (b) fallout limit state

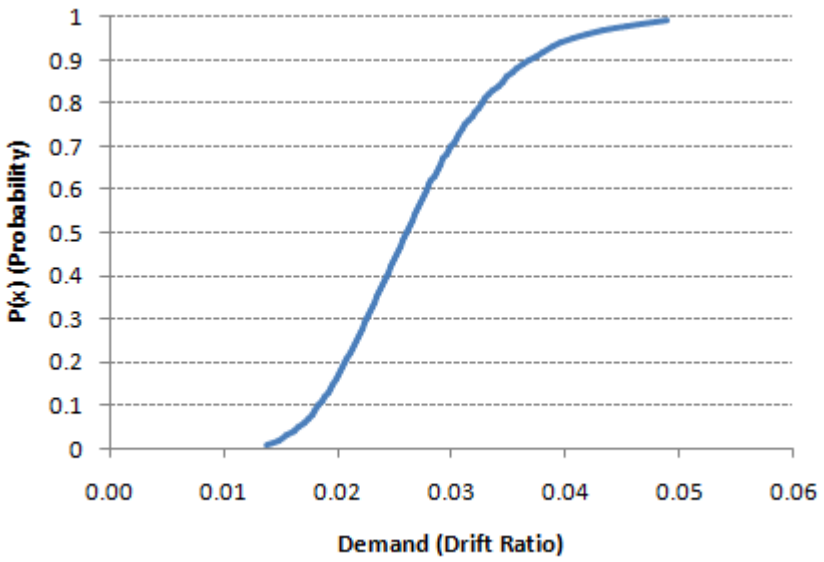

P(x)	θ	P(x)	θ	P(x)	θ	P(x)	θ	P(x)	θ
0.01	0.0138	0.21	0.0209	0.41	0.0244	0.61	0.0281	0.81	0.0330
0.02	0.0149	0.22	0.0211	0.42	0.0246	0.62	0.0283	0.82	0.0334
0.03	0.0156	0.23	0.0213	0.43	0.0248	0.63	0.0285	0.83	0.0337
0.04	0.0161	0.24	0.0215	0.44	0.0250	0.64	0.0287	0.84	0.0341
0.05	**0.0166**	**0.25**	**0.0216**	**0.45**	**0.0251**	**0.65**	**0.0289**	**0.85**	**0.0345**
0.06	0.0170	0.26	0.0218	0.46	0.0253	0.66	0.0291	0.86	0.0349
0.07	0.0174	0.27	0.0220	0.47	0.0255	0.67	0.0293	0.87	0.0353
0.08	0.0177	0.28	0.0222	0.48	0.0256	0.68	0.0295	0.88	0.0358
0.09	0.0181	0.29	0.0224	0.49	0.0258	0.69	0.0298	0.89	0.0363
0.10	**0.0183**	**0.30**	**0.0225**	**0.50**	**0.0260**	**0.70**	**0.0300**	**0.90**	**0.0368**
0.11	0.0186	0.31	0.0227	0.51	0.0262	0.71	0.0302	0.91	0.0374
0.12	0.0189	0.32	0.0229	0.52	0.0264	0.72	0.0305	0.92	0.0381
0.13	0.0191	0.33	0.0231	0.53	0.0265	0.73	0.0307	0.93	0.0388
0.14	0.0194	0.34	0.0232	0.54	0.0267	0.74	0.0310	0.94	0.0397
0.15	**0.0196**	**0.35**	**0.0234**	**0.55**	**0.0269**	**0.75**	**0.0312**	**0.95**	**0.0407**
0.16	0.0198	0.36	0.0236	0.56	0.0271	0.76	0.0315	0.96	0.0419
0.17	0.0201	0.37	0.0238	0.57	0.0273	0.77	0.0318	0.97	0.0434
0.18	0.0203	0.38	0.0239	0.58	0.0275	0.78	0.0321	0.98	0.0455
0.19	0.0205	0.39	0.0241	0.59	0.0277	0.79	0.0324	0.99	0.0490
0.20	**0.0207**	**0.40**	**0.0243**	**0.60**	**0.0279**	**0.80**	**0.0327**		

Figure A.37: Plotted fragility curve and information of glass configuration (5) for the gasket degradation limit state

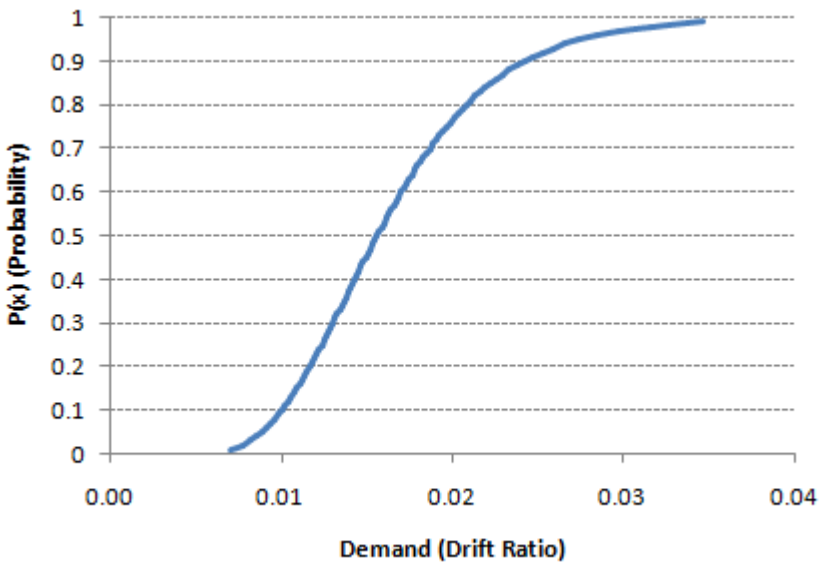

(a)

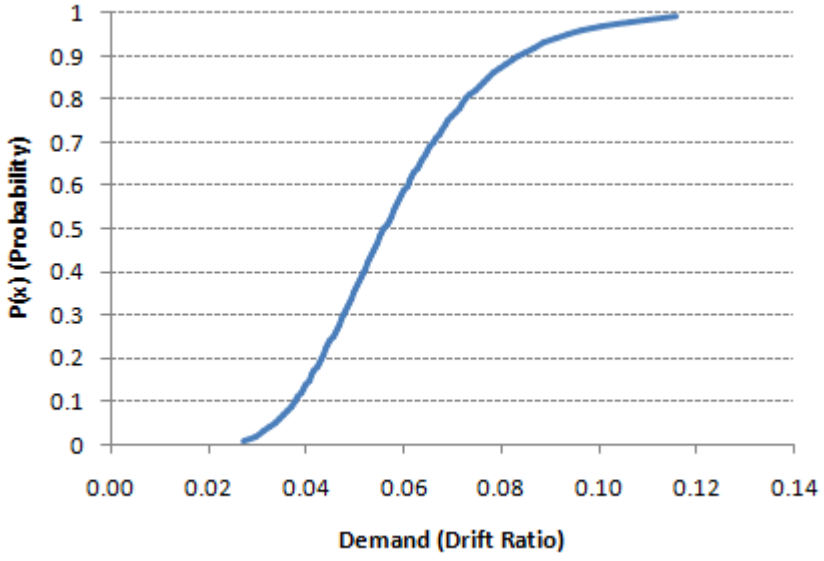

(b)

P(x)	θ	P(x)	θ	P(x)	θ	P(x)	θ	P(x)	θ
0.01	0.0070	0.21	0.0118	0.41	0.0144	0.61	0.0172	0.81	0.0211
0.02	0.0077	0.22	0.0120	0.42	0.0146	0.62	0.0173	0.82	0.0214
0.03	0.0082	0.23	0.0121	0.43	0.0147	0.63	0.0175	0.83	0.0216
0.04	0.0086	0.24	0.0122	0.44	0.0148	0.64	0.0176	0.84	0.0219
0.05	**0.0089**	**0.25**	**0.0124**	**0.45**	**0.0149**	**0.65**	**0.0178**	**0.85**	**0.0223**
0.06	0.0092	0.26	0.0125	0.46	0.0151	0.66	0.0180	0.86	0.0226
0.07	0.0094	0.27	0.0126	0.47	0.0152	0.67	0.0181	0.87	0.0230
0.08	0.0096	0.28	0.0128	0.48	0.0153	0.68	0.0183	0.88	0.0233
0.09	0.0098	0.29	0.0129	0.49	0.0155	0.69	0.0185	0.89	0.0238
0.10	**0.0101**	**0.30**	**0.0130**	**0.50**	**0.0156**	**0.70**	**0.0187**	**0.90**	**0.0242**
0.11	0.0102	0.31	0.0132	0.51	0.0157	0.71	0.0189	0.91	0.0247
0.12	0.0104	0.32	0.0133	0.52	0.0159	0.72	0.0191	0.92	0.0253
0.13	0.0106	0.33	0.0134	0.53	0.0160	0.73	0.0192	0.93	0.0259
0.14	0.0108	0.34	0.0135	0.54	0.0161	0.74	0.0195	0.94	0.0266
0.15	**0.0109**	**0.35**	**0.0137**	**0.55**	**0.0163**	**0.75**	**0.0197**	**0.95**	**0.0274**
0.16	0.0111	0.36	0.0138	0.56	0.0164	0.76	0.0199	0.96	0.0284
0.17	0.0112	0.37	0.0139	0.57	0.0166	0.77	0.0201	0.97	0.0297
0.18	0.0114	0.38	0.0140	0.58	0.0167	0.78	0.0203	0.98	0.0316
0.19	0.0115	0.39	0.0142	0.59	0.0169	0.79	0.0206	0.99	0.0346
0.20	**0.0117**	**0.40**	**0.0143**	**0.60**	**0.0170**	**0.80**	**0.0208**		

P(x)	θ	P(x)	θ	P(x)	θ	P(x)	θ	P(x)	θ
0.01	0.0272	0.21	0.0437	0.41	0.0523	0.61	0.0612	0.81	0.0737
0.02	0.0296	0.22	0.0441	0.42	0.0527	0.62	0.0617	0.82	0.0746
0.03	0.0313	0.23	0.0446	0.43	0.0531	0.63	0.0622	0.83	0.0755
0.04	0.0325	0.24	0.0450	0.44	0.0535	0.64	0.0627	0.84	0.0764
0.05	**0.0336**	**0.25**	**0.0455**	**0.45**	**0.0539**	**0.65**	**0.0632**	**0.85**	**0.0774**
0.06	0.0346	0.26	0.0459	0.46	0.0544	0.66	0.0638	0.86	0.0785
0.07	0.0355	0.27	0.0464	0.47	0.0548	0.67	0.0643	0.87	0.0796
0.08	0.0362	0.28	0.0468	0.48	0.0552	0.68	0.0649	0.88	0.0808
0.09	0.0370	0.29	0.0472	0.49	0.0557	0.69	0.0655	0.89	0.0822
0.10	**0.0377**	**0.30**	**0.0477**	**0.50**	**0.0561**	**0.70**	**0.0660**	**0.90**	**0.0836**
0.11	0.0383	0.31	0.0481	0.51	0.0565	0.71	0.0666	0.91	0.0851
0.12	0.0389	0.32	0.0485	0.52	0.0570	0.72	0.0672	0.92	0.0868
0.13	0.0395	0.33	0.0489	0.53	0.0574	0.73	0.0679	0.93	0.0888
0.14	0.0401	0.34	0.0493	0.54	0.0579	0.74	0.0685	0.94	0.0910
0.15	**0.0406**	**0.35**	**0.0498**	**0.55**	**0.0583**	**0.75**	**0.0692**	**0.95**	**0.0936**
0.16	0.0412	0.36	0.0502	0.56	0.0588	0.76	0.0699	0.96	0.0967
0.17	0.0417	0.37	0.0506	0.57	0.0593	0.77	0.0706	0.97	0.1007
0.18	0.0422	0.38	0.0510	0.58	0.0597	0.78	0.0713	0.98	0.1063
0.19	0.0427	0.39	0.0514	0.59	0.0602	0.79	0.0721	0.99	0.1157
0.20	**0.0432**	**0.40**	**0.0518**	**0.60**	**0.0607**	**0.80**	**0.0729**		

Figure A.38: Plotted fragility curve and information for glass configuration (6) for the (a) cracking and (b) fallout limit state

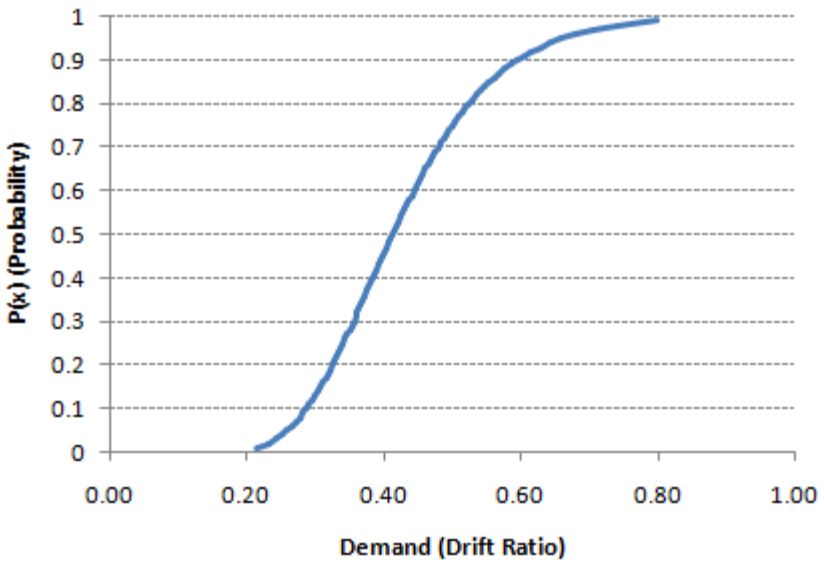

(a)

P(x)	θ	P(x)	θ	P(x)	θ	P(x)	θ	P(x)	θ
0.01	0.2133	0.21	0.3285	0.41	0.3872	0.61	0.4471	0.81	0.5299
0.02	0.2305	0.22	0.3317	0.42	0.3900	0.62	0.4504	0.82	0.5356
0.03	0.2421	0.23	0.3348	0.43	0.3928	0.63	0.4538	0.83	0.5415
0.04	0.2512	0.24	0.3379	0.44	0.3957	0.64	0.4573	0.84	0.5478
0.05	**0.2589**	**0.25**	**0.3410**	**0.45**	**0.3985**	**0.65**	**0.4608**	**0.85**	**0.5543**
0.06	0.2656	0.26	0.3440	0.46	0.4014	0.66	0.4643	0.86	0.5613
0.07	0.2716	0.27	0.3470	0.47	0.4043	0.67	0.4680	0.87	0.5687
0.08	0.2771	0.28	0.3500	0.48	0.4072	0.68	0.4717	0.88	0.5766
0.09	0.2822	0.29	0.3529	0.49	0.4101	0.69	0.4755	0.89	0.5851
0.10	**0.2870**	**0.30**	**0.3559**	**0.50**	**0.4130**	**0.70**	**0.4793**	**0.90**	**0.5943**
0.11	0.2915	0.31	0.3588	0.51	0.4160	0.71	0.4833	0.91	0.6044
0.12	0.2958	0.32	0.3616	0.52	0.4189	0.72	0.4873	0.92	0.6155
0.13	0.2999	0.33	0.3645	0.53	0.4219	0.73	0.4915	0.93	0.6280
0.14	0.3039	0.34	0.3673	0.54	0.4249	0.74	0.4958	0.94	0.6423
0.15	**0.3077**	**0.35**	**0.3702**	**0.55**	**0.4280**	**0.75**	**0.5002**	**0.95**	**0.6589**
0.16	0.3114	0.36	0.3730	0.56	0.4311	0.76	0.5047	0.96	0.6790
0.17	0.3150	0.37	0.3759	0.57	0.4342	0.77	0.5094	0.97	0.7046
0.18	0.3185	0.38	0.3787	0.58	0.4374	0.78	0.5143	0.98	0.7400
0.19	0.3219	0.39	0.3815	0.59	0.4406	0.79	0.5193	0.99	0.7996
0.20	**0.3252**	**0.40**	**0.3843**	**0.60**	**0.4438**	**0.80**	**0.5245**		

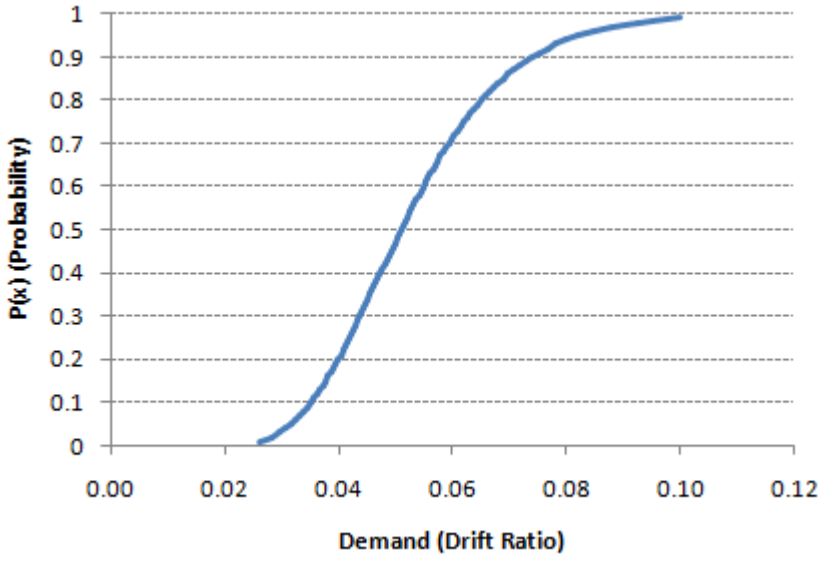

(b)

P(x)	θ	P(x)	θ	P(x)	θ	P(x)	θ	P(x)	θ
0.01	0.0260	0.21	0.0404	0.41	0.0477	0.61	0.0553	0.81	0.0658
0.02	0.0281	0.22	0.0408	0.42	0.0481	0.62	0.0557	0.82	0.0665
0.03	0.0296	0.23	0.0412	0.43	0.0485	0.63	0.0562	0.83	0.0673
0.04	0.0307	0.24	0.0416	0.44	0.0488	0.64	0.0566	0.84	0.0680
0.05	**0.0317**	**0.25**	**0.0419**	**0.45**	**0.0492**	**0.65**	**0.0570**	**0.85**	**0.0689**
0.06	0.0325	0.26	0.0423	0.46	0.0495	0.66	0.0575	0.86	0.0698
0.07	0.0332	0.27	0.0427	0.47	0.0499	0.67	0.0579	0.87	0.0707
0.08	0.0339	0.28	0.0431	0.48	0.0503	0.68	0.0584	0.88	0.0717
0.09	0.0346	0.29	0.0434	0.49	0.0506	0.69	0.0589	0.89	0.0728
0.10	**0.0352**	**0.30**	**0.0438**	**0.50**	**0.0510**	**0.70**	**0.0594**	**0.90**	**0.0740**
0.11	0.0357	0.31	0.0442	0.51	0.0514	0.71	0.0599	0.91	0.0752
0.12	0.0363	0.32	0.0445	0.52	0.0517	0.72	0.0604	0.92	0.0767
0.13	0.0368	0.33	0.0449	0.53	0.0521	0.73	0.0609	0.93	0.0782
0.14	0.0373	0.34	0.0453	0.54	0.0525	0.74	0.0615	0.94	0.0801
0.15	**0.0378**	**0.35**	**0.0456**	**0.55**	**0.0529**	**0.75**	**0.0620**	**0.95**	**0.0822**
0.16	0.0382	0.36	0.0460	0.56	0.0533	0.76	0.0626	0.96	0.0847
0.17	0.0387	0.37	0.0463	0.57	0.0537	0.77	0.0632	0.97	0.0880
0.18	0.0391	0.38	0.0467	0.58	0.0541	0.78	0.0638	0.98	0.0925
0.19	0.0395	0.39	0.0470	0.59	0.0545	0.79	0.0644	0.99	0.1001
0.20	**0.0400**	**0.40**	**0.0474**	**0.60**	**0.0549**	**0.80**	**0.0651**		

Figure A.39: Plotted fragility curve and information for glass configuration (7) for the (a) cracking and (b) fallout limit state

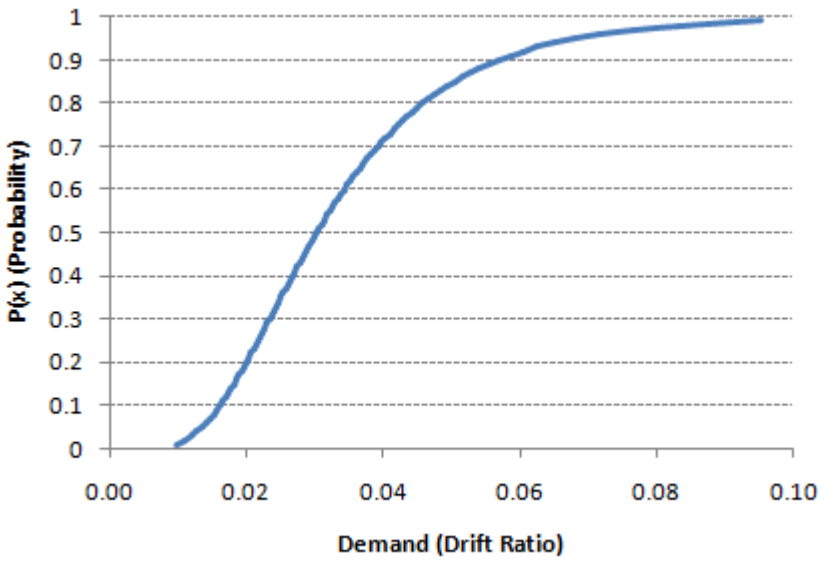

P(x)	θ	P(x)	θ	P(x)	θ	P(x)	θ	P(x)	θ
0.01	0.0096	0.21	0.0204	0.41	0.0271	0.61	0.0348	0.81	0.0467
0.02	0.0110	0.22	0.0207	0.42	0.0274	0.62	0.0352	0.82	0.0475
0.03	0.0120	0.23	0.0211	0.43	0.0278	0.63	0.0357	0.83	0.0485
0.04	0.0128	0.24	0.0214	0.44	0.0281	0.64	0.0361	0.84	0.0494
0.05	**0.0135**	**0.25**	**0.0217**	**0.45**	**0.0285**	**0.65**	**0.0366**	**0.85**	**0.0505**
0.06	0.0141	0.26	0.0221	0.46	0.0288	0.66	0.0371	0.86	0.0516
0.07	0.0147	0.27	0.0224	0.47	0.0292	0.67	0.0376	0.87	0.0527
0.08	0.0152	0.28	0.0227	0.48	0.0296	0.68	0.0381	0.88	0.0540
0.09	0.0157	0.29	0.0231	0.49	0.0299	0.69	0.0387	0.89	0.0554
0.10	**0.0161**	**0.30**	**0.0234**	**0.50**	**0.0303**	**0.70**	**0.0392**	**0.90**	**0.0569**
0.11	0.0166	0.31	0.0237	0.51	0.0307	0.71	0.0398	0.91	0.0586
0.12	0.0170	0.32	0.0241	0.52	0.0311	0.72	0.0404	0.92	0.0605
0.13	0.0174	0.33	0.0244	0.53	0.0314	0.73	0.0410	0.93	0.0626
0.14	0.0178	0.34	0.0247	0.54	0.0318	0.74	0.0416	0.94	0.0651
0.15	**0.0182**	**0.35**	**0.0251**	**0.55**	**0.0322**	**0.75**	**0.0422**	**0.95**	**0.0681**
0.16	0.0186	0.36	0.0254	0.56	0.0326	0.76	0.0429	0.96	0.0717
0.17	0.0189	0.37	0.0257	0.57	0.0330	0.77	0.0436	0.97	0.0764
0.18	0.0193	0.38	0.0261	0.58	0.0335	0.78	0.0443	0.98	0.0832
0.19	0.0197	0.39	0.0264	0.59	0.0339	0.79	0.0451	0.99	0.0952
0.20	**0.0200**	**0.40**	**0.0267**	**0.60**	**0.0343**	**0.80**	**0.0458**		

Figure A.40: Plotted fragility curve and information of glass configuration (7) for the gasket degradation limit state

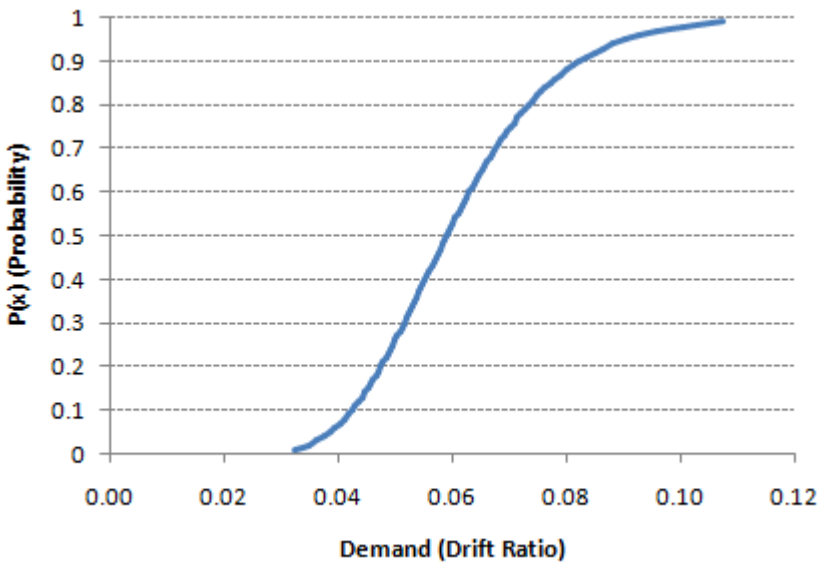

(a)

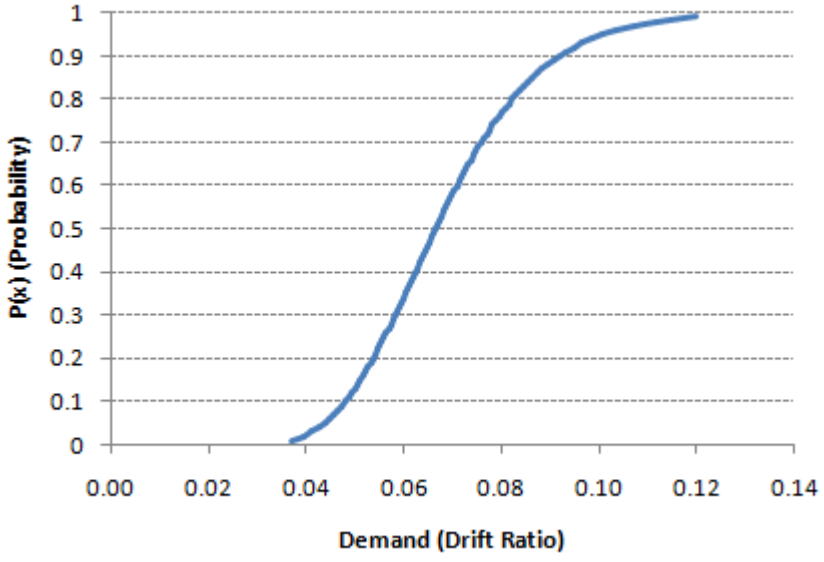

(b)

P(x)	θ	P(x)	θ	P(x)	θ	P(x)	θ	P(x)	θ
0.01	0.0324	0.21	0.0479	0.41	0.0556	0.61	0.0634	0.81	0.0740
0.02	0.0347	0.22	0.0483	0.42	0.0560	0.62	0.0638	0.82	0.0747
0.03	0.0363	0.23	0.0488	0.43	0.0564	0.63	0.0643	0.83	0.0755
0.04	0.0376	0.24	0.0492	0.44	0.0567	0.64	0.0647	0.84	0.0763
0.05	**0.0386**	**0.25**	**0.0496**	**0.45**	**0.0571**	**0.65**	**0.0652**	**0.85**	**0.0771**
0.06	0.0395	0.26	0.0500	0.46	0.0575	0.66	0.0656	0.86	0.0780
0.07	0.0403	0.27	0.0504	0.47	0.0579	0.67	0.0661	0.87	0.0789
0.08	0.0411	0.28	0.0508	0.48	0.0582	0.68	0.0666	0.88	0.0799
0.09	0.0417	0.29	0.0512	0.49	0.0586	0.69	0.0671	0.89	0.0810
0.10	**0.0424**	**0.30**	**0.0515**	**0.50**	**0.0590**	**0.70**	**0.0675**	**0.90**	**0.0821**
0.11	0.0430	0.31	0.0519	0.51	0.0594	0.71	0.0681	0.91	0.0834
0.12	0.0436	0.32	0.0523	0.52	0.0598	0.72	0.0686	0.92	0.0848
0.13	0.0441	0.33	0.0527	0.53	0.0602	0.73	0.0691	0.93	0.0863
0.14	0.0446	0.34	0.0530	0.54	0.0605	0.74	0.0697	0.94	0.0881
0.15	**0.0452**	**0.35**	**0.0534**	**0.55**	**0.0609**	**0.75**	**0.0702**	**0.95**	**0.0902**
0.16	0.0456	0.36	0.0538	0.56	0.0613	0.76	0.0708	0.96	0.0927
0.17	0.0461	0.37	0.0542	0.57	0.0617	0.77	0.0714	0.97	0.0958
0.18	0.0466	0.38	0.0545	0.58	0.0622	0.78	0.0720	0.98	0.1002
0.19	0.0470	0.39	0.0549	0.59	0.0626	0.79	0.0726	0.99	0.1075
0.20	**0.0475**	**0.40**	**0.0553**	**0.60**	**0.0630**	**0.80**	**0.0733**		

P(x)	θ	P(x)	θ	P(x)	θ	P(x)	θ	P(x)	θ
0.01	0.0369	0.21	0.0542	0.41	0.0628	0.61	0.0714	0.81	0.0830
0.02	0.0396	0.22	0.0547	0.42	0.0632	0.62	0.0718	0.82	0.0838
0.03	0.0413	0.23	0.0552	0.43	0.0636	0.63	0.0723	0.83	0.0847
0.04	0.0427	0.24	0.0556	0.44	0.0640	0.64	0.0728	0.84	0.0855
0.05	**0.0439**	**0.25**	**0.0561**	**0.45**	**0.0644**	**0.65**	**0.0733**	**0.85**	**0.0864**
0.06	0.0449	0.26	0.0565	0.46	0.0648	0.66	0.0738	0.86	0.0874
0.07	0.0458	0.27	0.0569	0.47	0.0652	0.67	0.0743	0.87	0.0884
0.08	0.0466	0.28	0.0574	0.48	0.0657	0.68	0.0749	0.88	0.0895
0.09	0.0474	0.29	0.0578	0.49	0.0661	0.69	0.0754	0.89	0.0907
0.10	**0.0481**	**0.30**	**0.0582**	**0.50**	**0.0665**	**0.70**	**0.0759**	**0.90**	**0.0920**
0.11	0.0488	0.31	0.0587	0.51	0.0669	0.71	0.0765	0.91	0.0934
0.12	0.0494	0.32	0.0591	0.52	0.0673	0.72	0.0771	0.92	0.0949
0.13	0.0500	0.33	0.0595	0.53	0.0678	0.73	0.0777	0.93	0.0966
0.14	0.0506	0.34	0.0599	0.54	0.0682	0.74	0.0783	0.94	0.0985
0.15	**0.0512**	**0.35**	**0.0603**	**0.55**	**0.0686**	**0.75**	**0.0789**	**0.95**	**0.1008**
0.16	0.0517	0.36	0.0607	0.56	0.0691	0.76	0.0795	0.96	0.1036
0.17	0.0522	0.37	0.0611	0.57	0.0695	0.77	0.0802	0.97	0.1070
0.18	0.0528	0.38	0.0616	0.58	0.0700	0.78	0.0808	0.98	0.1118
0.19	0.0533	0.39	0.0620	0.59	0.0704	0.79	0.0816	0.99	0.1198
0.20	**0.0537**	**0.40**	**0.0624**	**0.60**	**0.0709**	**0.80**	**0.0823**		

Figure A.41: Plotted fragility curve and information for glass configuration (8) for the (a) cracking and (b) fallout limit state

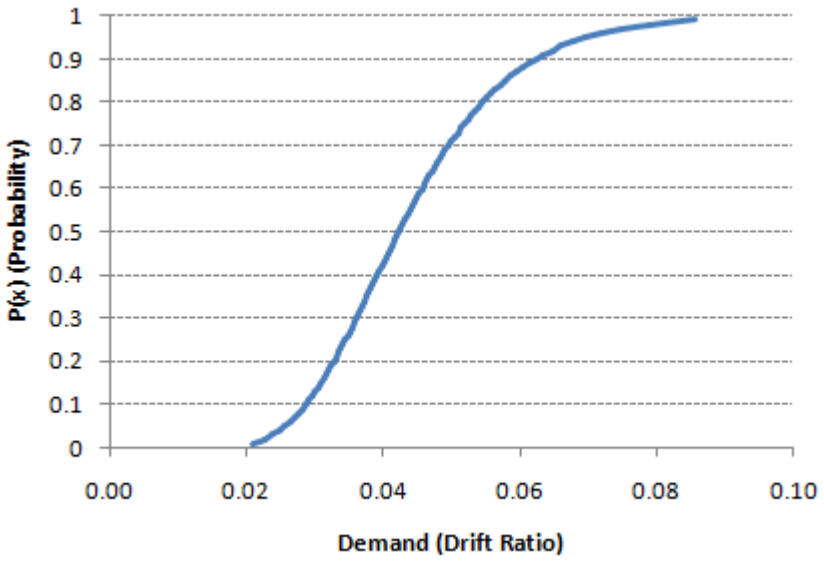

P(x)	θ	P(x)	θ	P(x)	θ	P(x)	θ	P(x)	θ
0.01	0.0209	0.21	0.0331	0.41	0.0395	0.61	0.0460	0.81	0.0552
0.02	0.0227	0.22	0.0335	0.42	0.0398	0.62	0.0464	0.82	0.0558
0.03	0.0239	0.23	0.0338	0.43	0.0401	0.63	0.0468	0.83	0.0565
0.04	0.0249	0.24	0.0342	0.44	0.0404	0.64	0.0472	0.84	0.0572
0.05	**0.0257**	**0.25**	**0.0345**	**0.45**	**0.0407**	**0.65**	**0.0475**	**0.85**	**0.0579**
0.06	0.0264	0.26	0.0348	0.46	0.0410	0.66	0.0479	0.86	0.0587
0.07	0.0270	0.27	0.0351	0.47	0.0413	0.67	0.0483	0.87	0.0595
0.08	0.0276	0.28	0.0355	0.48	0.0417	0.68	0.0487	0.88	0.0604
0.09	0.0282	0.29	0.0358	0.49	0.0420	0.69	0.0492	0.89	0.0613
0.10	**0.0287**	**0.30**	**0.0361**	**0.50**	**0.0423**	**0.70**	**0.0496**	**0.90**	**0.0624**
0.11	0.0292	0.31	0.0364	0.51	0.0426	0.71	0.0500	0.91	0.0635
0.12	0.0296	0.32	0.0367	0.52	0.0429	0.72	0.0505	0.92	0.0647
0.13	0.0301	0.33	0.0370	0.53	0.0433	0.73	0.0509	0.93	0.0662
0.14	0.0305	0.34	0.0373	0.54	0.0436	0.74	0.0514	0.94	0.0678
0.15	**0.0309**	**0.35**	**0.0376**	**0.55**	**0.0439**	**0.75**	**0.0519**	**0.95**	**0.0696**
0.16	0.0313	0.36	0.0379	0.56	0.0443	0.76	0.0524	0.96	0.0719
0.17	0.0317	0.37	0.0383	0.57	0.0446	0.77	0.0529	0.97	0.0748
0.18	0.0321	0.38	0.0386	0.58	0.0450	0.78	0.0535	0.98	0.0788
0.19	0.0324	0.39	0.0389	0.59	0.0453	0.79	0.0540	0.99	0.0856
0.20	**0.0328**	**0.40**	**0.0392**	**0.60**	**0.0457**	**0.80**	**0.0546**		

Figure A.42: Plotted fragility curve and information of glass configuration (8) for the gasket degradation limit state

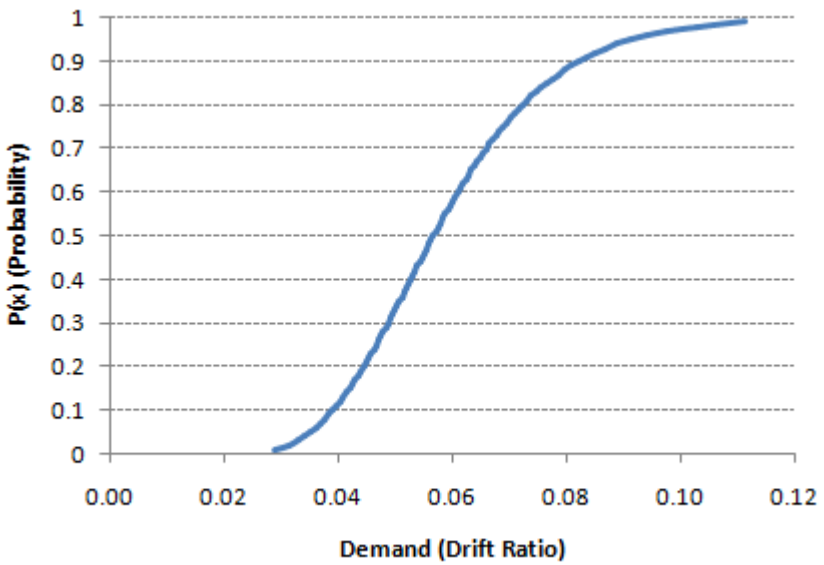

(a)

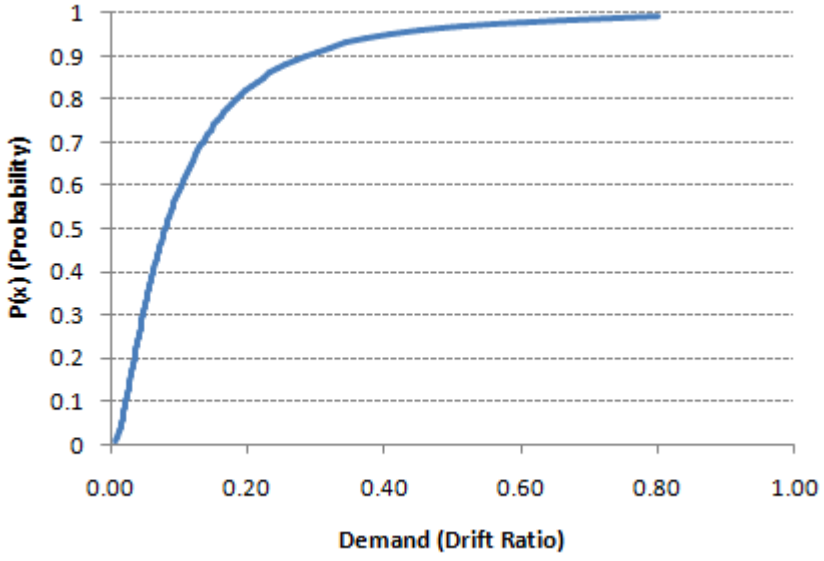

(b)

P(x)	θ	P(x)	θ	P(x)	θ	P(x)	θ	P(x)	θ
0.01	0.0289	0.21	0.0449	0.41	0.0531	0.61	0.0615	0.81	0.0731
0.02	0.0313	0.22	0.0454	0.42	0.0535	0.62	0.0619	0.82	0.0739
0.03	0.0329	0.23	0.0458	0.43	0.0539	0.63	0.0624	0.83	0.0747
0.04	0.0342	0.24	0.0462	0.44	0.0543	0.64	0.0629	0.84	0.0756
0.05	**0.0352**	**0.25**	**0.0467**	**0.45**	**0.0547**	**0.65**	**0.0634**	**0.85**	**0.0765**
0.06	0.0362	0.26	0.0471	0.46	0.0551	0.66	0.0639	0.86	0.0775
0.07	0.0370	0.27	0.0475	0.47	0.0555	0.67	0.0644	0.87	0.0785
0.08	0.0378	0.28	0.0479	0.48	0.0559	0.68	0.0649	0.88	0.0796
0.09	0.0385	0.29	0.0483	0.49	0.0563	0.69	0.0654	0.89	0.0808
0.10	**0.0392**	**0.30**	**0.0487**	**0.50**	**0.0567**	**0.70**	**0.0660**	**0.90**	**0.0821**
0.11	0.0398	0.31	0.0491	0.51	0.0571	0.71	0.0665	0.91	0.0835
0.12	0.0404	0.32	0.0495	0.52	0.0575	0.72	0.0671	0.92	0.0851
0.13	0.0409	0.33	0.0499	0.53	0.0579	0.73	0.0677	0.93	0.0869
0.14	0.0415	0.34	0.0503	0.54	0.0584	0.74	0.0683	0.94	0.0889
0.15	**0.0420**	**0.35**	**0.0507**	**0.55**	**0.0588**	**0.75**	**0.0689**	**0.95**	**0.0912**
0.16	0.0425	0.36	0.0511	0.56	0.0592	0.76	0.0695	0.96	0.0940
0.17	0.0430	0.37	0.0515	0.57	0.0597	0.77	0.0702	0.97	0.0976
0.18	0.0435	0.38	0.0519	0.58	0.0601	0.78	0.0709	0.98	0.1026
0.19	0.0440	0.39	0.0523	0.59	0.0606	0.79	0.0716	0.99	0.1111
0.20	**0.0445**	**0.40**	**0.0527**	**0.60**	**0.0610**	**0.80**	**0.0723**		

P(x)	θ	P(x)	θ	P(x)	θ	P(x)	θ	P(x)	θ
0.01	0.0080	0.21	0.0360	0.41	0.0639	0.61	0.1055	0.81	0.1908
0.02	0.0105	0.22	0.0372	0.42	0.0655	0.62	0.1083	0.82	0.1980
0.03	0.0124	0.23	0.0385	0.43	0.0672	0.63	0.1111	0.83	0.2057
0.04	0.0141	0.24	0.0398	0.44	0.0689	0.64	0.1141	0.84	0.2141
0.05	**0.0157**	**0.25**	**0.0410**	**0.45**	**0.0706**	**0.65**	**0.1172**	**0.85**	**0.2232**
0.06	0.0172	0.26	0.0423	0.46	0.0724	0.66	0.1203	0.86	0.2331
0.07	0.0186	0.27	0.0436	0.47	0.0743	0.67	0.1237	0.87	0.2440
0.08	0.0199	0.28	0.0449	0.48	0.0761	0.68	0.1271	0.88	0.2560
0.09	0.0212	0.29	0.0463	0.49	0.0780	0.69	0.1307	0.89	0.2694
0.10	**0.0225**	**0.30**	**0.0476**	**0.50**	**0.0800**	**0.70**	**0.1344**	**0.90**	**0.2845**
0.11	0.0238	0.31	0.0490	0.51	0.0820	0.71	0.1384	0.91	0.3017
0.12	0.0250	0.32	0.0504	0.52	0.0841	0.72	0.1425	0.92	0.3215
0.13	0.0262	0.33	0.0518	0.53	0.0862	0.73	0.1467	0.93	0.3448
0.14	0.0275	0.34	0.0532	0.54	0.0884	0.74	0.1513	0.94	0.3729
0.15	**0.0287**	**0.35**	**0.0546**	**0.55**	**0.0906**	**0.75**	**0.1560**	**0.95**	**0.4077**
0.16	0.0299	0.36	0.0561	0.56	0.0929	0.76	0.1610	0.96	0.4527
0.17	0.0311	0.37	0.0576	0.57	0.0953	0.77	0.1662	0.97	0.5149
0.18	0.0323	0.38	0.0591	0.58	0.0977	0.78	0.1718	0.98	0.6111
0.19	0.0335	0.39	0.0607	0.59	0.1002	0.79	0.1778	0.99	0.8004
0.20	**0.0348**	**0.40**	**0.0623**	**0.60**	**0.1028**	**0.80**	**0.1841**		

Figure A.43: Plotted fragility curve and information for glass configuration (9) for the (a) cracking and (b) fallout limit state

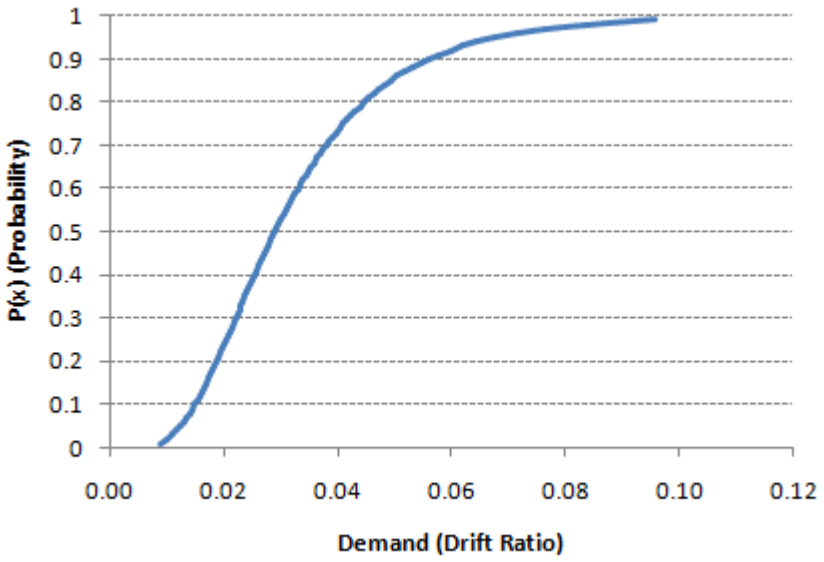

P(x)	θ	P(x)	θ	P(x)	θ	P(x)	θ	P(x)	θ
0.01	0.0088	0.21	0.0192	0.41	0.0258	0.61	0.0335	0.81	0.0455
0.02	0.0101	0.22	0.0195	0.42	0.0261	0.62	0.0339	0.82	0.0464
0.03	0.0110	0.23	0.0198	0.43	0.0265	0.63	0.0344	0.83	0.0474
0.04	0.0118	0.24	0.0202	0.44	0.0268	0.64	0.0349	0.84	0.0483
0.05	0.0125	**0.25**	0.0205	**0.45**	0.0272	**0.65**	0.0354	**0.85**	0.0494
0.06	0.0130	0.26	0.0208	0.46	0.0275	0.66	0.0358	0.86	0.0505
0.07	0.0136	0.27	0.0212	0.47	0.0279	0.67	0.0364	0.87	0.0517
0.08	0.0141	0.28	0.0215	0.48	0.0283	0.68	0.0369	0.88	0.0531
0.09	0.0146	0.29	0.0218	0.49	0.0286	0.69	0.0374	0.89	0.0545
0.10	0.0150	**0.30**	0.0221	**0.50**	0.0290	**0.70**	0.0380	**0.90**	0.0560
0.11	0.0154	0.31	0.0225	0.51	0.0294	0.71	0.0385	0.91	0.0578
0.12	0.0159	0.32	0.0228	0.52	0.0298	0.72	0.0391	0.92	0.0597
0.13	0.0163	0.33	0.0231	0.53	0.0301	0.73	0.0397	0.93	0.0619
0.14	0.0166	0.34	0.0235	0.54	0.0305	0.74	0.0404	0.94	0.0645
0.15	0.0170	**0.35**	0.0238	**0.55**	0.0309	**0.75**	0.0410	**0.95**	0.0675
0.16	0.0174	0.36	0.0241	0.56	0.0313	0.76	0.0417	0.96	0.0713
0.17	0.0178	0.37	0.0245	0.57	0.0318	0.77	0.0424	0.97	0.0763
0.18	0.0181	0.38	0.0248	0.58	0.0322	0.78	0.0431	0.98	0.0833
0.19	0.0185	0.39	0.0251	0.59	0.0326	0.79	0.0439	0.99	0.0959
0.20	0.0188	**0.40**	0.0255	**0.60**	0.0330	**0.80**	0.0447		

Figure A.44: Plotted fragility curve and information of glass configuration (9) for the gasket degradation limit state

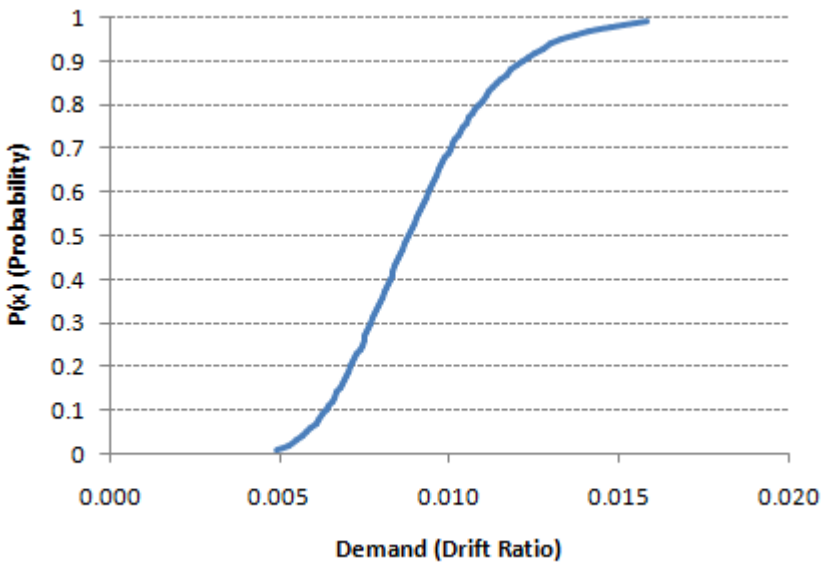

(a)

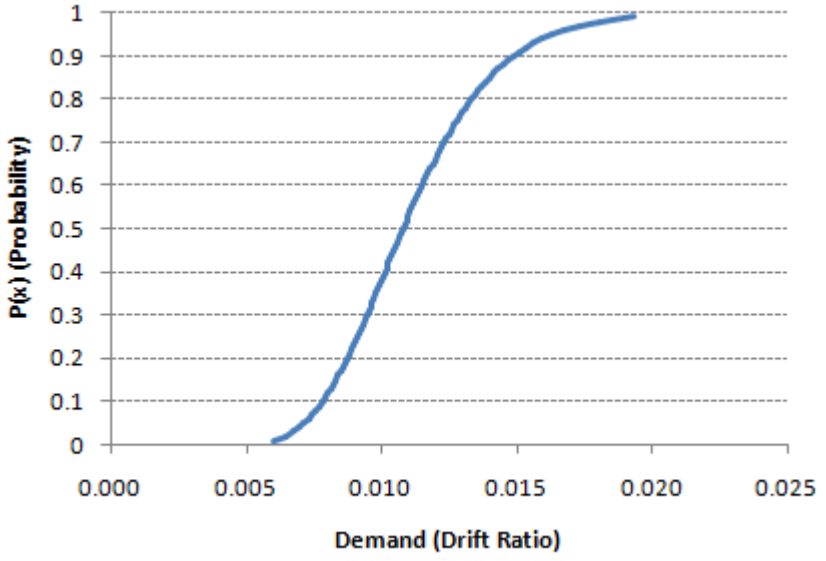

(b)

P(x)	θ	P(x)	θ	P(x)	θ	P(x)	θ	P(x)	θ
0.01	0.0049	0.21	0.0072	0.41	0.0083	0.61	0.0094	0.81	0.0110
0.02	0.0052	0.22	0.0072	0.42	0.0084	0.62	0.0095	0.82	0.0111
0.03	0.0055	0.23	0.0073	0.43	0.0084	0.63	0.0096	0.83	0.0112
0.04	0.0057	0.24	0.0074	0.44	0.0085	0.64	0.0096	0.84	0.0113
0.05	**0.0058**	**0.25**	**0.0074**	**0.45**	**0.0085**	**0.65**	**0.0097**	**0.85**	**0.0114**
0.06	0.0059	0.26	0.0075	0.46	0.0086	0.66	0.0098	0.86	0.0116
0.07	0.0061	0.27	0.0075	0.47	0.0086	0.67	0.0098	0.87	0.0117
0.08	0.0062	0.28	0.0076	0.48	0.0087	0.68	0.0099	0.88	0.0118
0.09	0.0063	0.29	0.0077	0.49	0.0087	0.69	0.0100	0.89	0.0120
0.10	**0.0064**	**0.30**	**0.0077**	**0.50**	**0.0088**	**0.70**	**0.0100**	**0.90**	**0.0122**
0.11	0.0065	0.31	0.0078	0.51	0.0089	0.71	0.0101	0.91	0.0123
0.12	0.0065	0.32	0.0078	0.52	0.0089	0.72	0.0102	0.92	0.0125
0.13	0.0066	0.33	0.0079	0.53	0.0090	0.73	0.0103	0.93	0.0128
0.14	0.0067	0.34	0.0079	0.54	0.0090	0.74	0.0103	0.94	0.0130
0.15	**0.0068**	**0.35**	**0.0080**	**0.55**	**0.0091**	**0.75**	**0.0104**	**0.95**	**0.0133**
0.16	0.0068	0.36	0.0080	0.56	0.0091	0.76	0.0105	0.96	0.0137
0.17	0.0069	0.37	0.0081	0.57	0.0092	0.77	0.0106	0.97	0.0141
0.18	0.0070	0.38	0.0081	0.58	0.0093	0.78	0.0107	0.98	0.0148
0.19	0.0071	0.39	0.0082	0.59	0.0093	0.79	0.0108	0.99	0.0158
0.20	**0.0071**	**0.40**	**0.0083**	**0.60**	**0.0094**	**0.80**	**0.0109**		

P(x)	θ	P(x)	θ	P(x)	θ	P(x)	θ	P(x)	θ
0.01	0.0060	0.21	0.0088	0.41	0.0102	0.61	0.0116	0.81	0.0135
0.02	0.0064	0.22	0.0089	0.42	0.0103	0.62	0.0117	0.82	0.0136
0.03	0.0067	0.23	0.0090	0.43	0.0103	0.63	0.0117	0.83	0.0137
0.04	0.0070	0.24	0.0090	0.44	0.0104	0.64	0.0118	0.84	0.0139
0.05	**0.0071**	**0.25**	**0.0091**	**0.45**	**0.0105**	**0.65**	**0.0119**	**0.85**	**0.0140**
0.06	0.0073	0.26	0.0092	0.46	0.0105	0.66	0.0120	0.86	0.0142
0.07	0.0075	0.27	0.0093	0.47	0.0106	0.67	0.0121	0.87	0.0143
0.08	0.0076	0.28	0.0093	0.48	0.0107	0.68	0.0121	0.88	0.0145
0.09	0.0077	0.29	0.0094	0.49	0.0107	0.69	0.0122	0.89	0.0147
0.10	**0.0078**	**0.30**	**0.0095**	**0.50**	**0.0108**	**0.70**	**0.0123**	**0.90**	**0.0149**
0.11	0.0079	0.31	0.0095	0.51	0.0109	0.71	0.0124	0.91	0.0151
0.12	0.0080	0.32	0.0096	0.52	0.0109	0.72	0.0125	0.92	0.0154
0.13	0.0081	0.33	0.0097	0.53	0.0110	0.73	0.0126	0.93	0.0156
0.14	0.0082	0.34	0.0097	0.54	0.0111	0.74	0.0127	0.94	0.0160
0.15	**0.0083**	**0.35**	**0.0098**	**0.55**	**0.0111**	**0.75**	**0.0128**	**0.95**	**0.0163**
0.16	0.0084	0.36	0.0099	0.56	0.0112	0.76	0.0129	0.96	0.0168
0.17	0.0085	0.37	0.0099	0.57	0.0113	0.77	0.0130	0.97	0.0173
0.18	0.0086	0.38	0.0100	0.58	0.0114	0.78	0.0131	0.98	0.0181
0.19	0.0087	0.39	0.0101	0.59	0.0114	0.79	0.0132	0.99	0.0194
0.20	**0.0087**	**0.40**	**0.0101**	**0.60**	**0.0115**	**0.80**	**0.0133**		

Figure A.45: Plotted fragility curve and information for glass configuration (10) for the (a) cracking and (b) fallout limit state

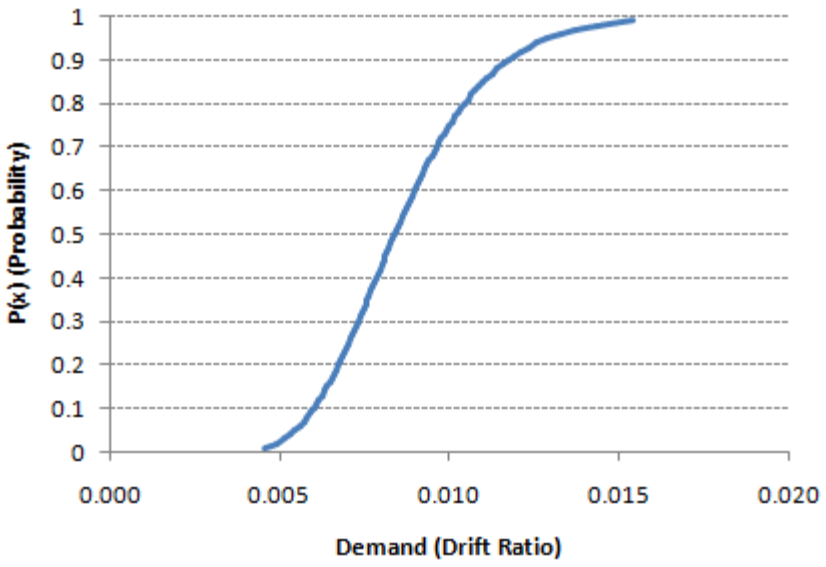

(a)

P(x)	θ	P(x)	θ	P(x)	θ	P(x)	θ	P(x)	θ
0.01	0.0046	0.21	0.0068	0.41	0.0079	0.61	0.0090	0.81	0.0106
0.02	0.0049	0.22	0.0069	0.42	0.0080	0.62	0.0091	0.82	0.0107
0.03	0.0051	0.23	0.0069	0.43	0.0080	0.63	0.0092	0.83	0.0108
0.04	0.0053	0.24	0.0070	0.44	0.0081	0.64	0.0092	0.84	0.0109
0.05	**0.0055**	**0.25**	**0.0070**	**0.45**	**0.0081**	**0.65**	**0.0093**	**0.85**	**0.0110**
0.06	0.0056	0.26	0.0071	0.46	0.0082	0.66	0.0094	0.86	0.0111
0.07	0.0057	0.27	0.0072	0.47	0.0082	0.67	0.0094	0.87	0.0113
0.08	0.0058	0.28	0.0072	0.48	0.0083	0.68	0.0095	0.88	0.0114
0.09	0.0059	0.29	0.0073	0.49	0.0083	0.69	0.0096	0.89	0.0116
0.10	**0.0060**	**0.30**	**0.0073**	**0.50**	**0.0084**	**0.70**	**0.0096**	**0.90**	**0.0117**
0.11	0.0061	0.31	0.0074	0.51	0.0085	0.71	0.0097	0.91	0.0119
0.12	0.0062	0.32	0.0074	0.52	0.0085	0.72	0.0098	0.92	0.0121
0.13	0.0063	0.33	0.0075	0.53	0.0086	0.73	0.0099	0.93	0.0123
0.14	0.0063	0.34	0.0075	0.54	0.0086	0.74	0.0099	0.94	0.0126
0.15	**0.0064**	**0.35**	**0.0076**	**0.55**	**0.0087**	**0.75**	**0.0100**	**0.95**	**0.0129**
0.16	0.0065	0.36	0.0076	0.56	0.0087	0.76	0.0101	0.96	0.0133
0.17	0.0065	0.37	0.0077	0.57	0.0088	0.77	0.0102	0.97	0.0137
0.18	0.0066	0.38	0.0078	0.58	0.0089	0.78	0.0103	0.98	0.0144
0.19	0.0067	0.39	0.0078	0.59	0.0089	0.79	0.0104	0.99	0.0154
0.20	**0.0067**	**0.40**	**0.0079**	**0.60**	**0.0090**	**0.80**	**0.0105**		

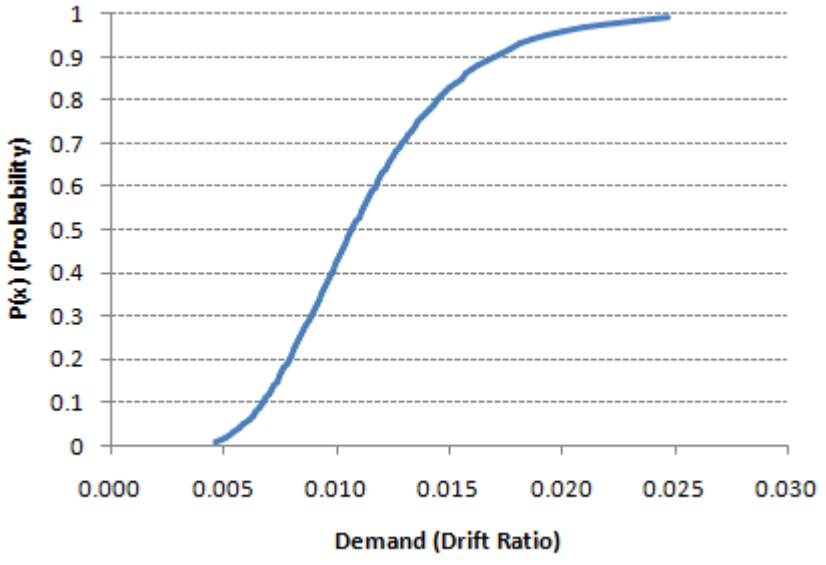

(b)

P(x)	θ	P(x)	θ	P(x)	θ	P(x)	θ	P(x)	θ
0.01	0.0046	0.21	0.0080	0.41	0.0099	0.61	0.0118	0.81	0.0147
0.02	0.0051	0.22	0.0081	0.42	0.0100	0.62	0.0119	0.82	0.0149
0.03	0.0054	0.23	0.0082	0.43	0.0100	0.63	0.0121	0.83	0.0151
0.04	0.0057	0.24	0.0083	0.44	0.0101	0.64	0.0122	0.84	0.0153
0.05	**0.0059**	**0.25**	**0.0084**	**0.45**	**0.0102**	**0.65**	**0.0123**	**0.85**	**0.0155**
0.06	0.0061	0.26	0.0085	0.46	0.0103	0.66	0.0124	0.86	0.0158
0.07	0.0063	0.27	0.0086	0.47	0.0104	0.67	0.0125	0.87	0.0160
0.08	0.0065	0.28	0.0087	0.48	0.0105	0.68	0.0127	0.88	0.0163
0.09	0.0066	0.29	0.0088	0.49	0.0106	0.69	0.0128	0.89	0.0166
0.10	**0.0068**	**0.30**	**0.0089**	**0.50**	**0.0107**	**0.70**	**0.0129**	**0.90**	**0.0170**
0.11	0.0069	0.31	0.0090	0.51	0.0108	0.71	0.0131	0.91	0.0173
0.12	0.0070	0.32	0.0090	0.52	0.0109	0.72	0.0132	0.92	0.0177
0.13	0.0071	0.33	0.0091	0.53	0.0110	0.73	0.0133	0.93	0.0182
0.14	0.0073	0.34	0.0092	0.54	0.0111	0.74	0.0135	0.94	0.0187
0.15	**0.0074**	**0.35**	**0.0093**	**0.55**	**0.0112**	**0.75**	**0.0136**	**0.95**	**0.0193**
0.16	0.0075	0.36	0.0094	0.56	0.0113	0.76	0.0138	0.96	0.0201
0.17	0.0076	0.37	0.0095	0.57	0.0114	0.77	0.0140	0.97	0.0210
0.18	0.0077	0.38	0.0096	0.58	0.0115	0.78	0.0141	0.98	0.0224
0.19	0.0078	0.39	0.0097	0.59	0.0116	0.79	0.0143	0.99	0.0247
0.20	**0.0079**	**0.40**	**0.0098**	**0.60**	**0.0117**	**0.80**	**0.0145**		

Figure A.46: Plotted fragility curve and information for glass configuration (11) for the (a) cracking and (b) fallout limit state

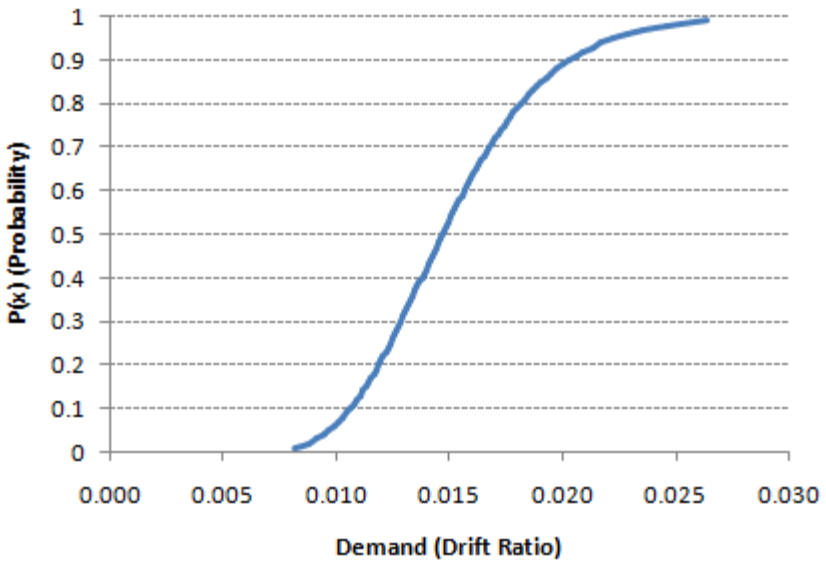

(a)

P(x)	θ	P(x)	θ	P(x)	θ	P(x)	θ	P(x)	θ
0.01	0.0082	0.21	0.0120	0.41	0.0139	0.61	0.0158	0.81	0.0183
0.02	0.0088	0.22	0.0121	0.42	0.0140	0.62	0.0159	0.82	0.0185
0.03	0.0092	0.23	0.0122	0.43	0.0141	0.63	0.0160	0.83	0.0187
0.04	0.0095	0.24	0.0123	0.44	0.0142	0.64	0.0161	0.84	0.0189
0.05	**0.0097**	**0.25**	**0.0124**	**0.45**	**0.0142**	**0.65**	**0.0162**	**0.85**	**0.0191**
0.06	0.0099	0.26	0.0125	0.46	0.0143	0.66	0.0163	0.86	0.0193
0.07	0.0101	0.27	0.0126	0.47	0.0144	0.67	0.0164	0.87	0.0195
0.08	0.0103	0.28	0.0127	0.48	0.0145	0.68	0.0165	0.88	0.0198
0.09	0.0105	0.29	0.0128	0.49	0.0146	0.69	0.0167	0.89	0.0200
0.10	**0.0106**	**0.30**	**0.0129**	**0.50**	**0.0147**	**0.70**	**0.0168**	**0.90**	**0.0203**
0.11	0.0108	0.31	0.0130	0.51	0.0148	0.71	0.0169	0.91	0.0206
0.12	0.0109	0.32	0.0131	0.52	0.0149	0.72	0.0170	0.92	0.0209
0.13	0.0111	0.33	0.0132	0.53	0.0150	0.73	0.0172	0.93	0.0213
0.14	0.0112	0.34	0.0132	0.54	0.0151	0.74	0.0173	0.94	0.0218
0.15	**0.0113**	**0.35**	**0.0133**	**0.55**	**0.0152**	**0.75**	**0.0174**	**0.95**	**0.0223**
0.16	0.0114	0.36	0.0134	0.56	0.0153	0.76	0.0176	0.96	0.0229
0.17	0.0116	0.37	0.0135	0.57	0.0154	0.77	0.0177	0.97	0.0236
0.18	0.0117	0.38	0.0136	0.58	0.0155	0.78	0.0179	0.98	0.0247
0.19	0.0118	0.39	0.0137	0.59	0.0156	0.79	0.0180	0.99	0.0264
0.20	**0.0119**	**0.40**	**0.0138**	**0.60**	**0.0157**	**0.80**	**0.0182**		

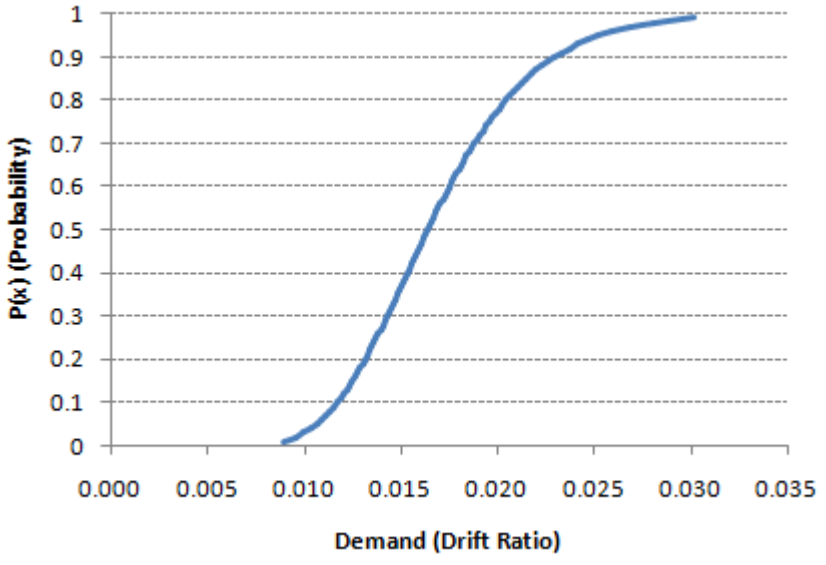

(b)

P(x)	θ	P(x)	θ	P(x)	θ	P(x)	θ	P(x)	θ
0.01	0.0089	0.21	0.0133	0.41	0.0155	0.61	0.0176	0.81	0.0206
0.02	0.0096	0.22	0.0134	0.42	0.0156	0.62	0.0178	0.82	0.0208
0.03	0.0100	0.23	0.0135	0.43	0.0157	0.63	0.0179	0.83	0.0211
0.04	0.0104	0.24	0.0136	0.44	0.0158	0.64	0.0180	0.84	0.0213
0.05	**0.0107**	**0.25**	**0.0137**	**0.45**	**0.0159**	**0.65**	**0.0181**	**0.85**	**0.0215**
0.06	0.0109	0.26	0.0139	0.46	0.0160	0.66	0.0183	0.86	0.0218
0.07	0.0111	0.27	0.0140	0.47	0.0161	0.67	0.0184	0.87	0.0220
0.08	0.0113	0.28	0.0141	0.48	0.0162	0.68	0.0185	0.88	0.0223
0.09	0.0115	0.29	0.0142	0.49	0.0163	0.69	0.0187	0.89	0.0226
0.10	**0.0117**	**0.30**	**0.0143**	**0.50**	**0.0164**	**0.70**	**0.0188**	**0.90**	**0.0229**
0.11	0.0119	0.31	0.0144	0.51	0.0165	0.71	0.0190	0.91	0.0233
0.12	0.0121	0.32	0.0145	0.52	0.0166	0.72	0.0191	0.92	0.0237
0.13	0.0122	0.33	0.0146	0.53	0.0167	0.73	0.0193	0.93	0.0241
0.14	0.0124	0.34	0.0147	0.54	0.0168	0.74	0.0194	0.94	0.0246
0.15	**0.0125**	**0.35**	**0.0148**	**0.55**	**0.0169**	**0.75**	**0.0196**	**0.95**	**0.0252**
0.16	0.0126	0.36	0.0149	0.56	0.0171	0.76	0.0197	0.96	0.0259
0.17	0.0128	0.37	0.0150	0.57	0.0172	0.77	0.0199	0.97	0.0268
0.18	0.0129	0.38	0.0151	0.58	0.0173	0.78	0.0201	0.98	0.0281
0.19	0.0130	0.39	0.0152	0.59	0.0174	0.79	0.0203	0.99	0.0302
0.20	**0.0132**	**0.40**	**0.0153**	**0.60**	**0.0175**	**0.80**	**0.0204**		

Figure A.47: Plotted fragility curve and information for glass configuration (12) for the (a) cracking and (b) fallout limit state

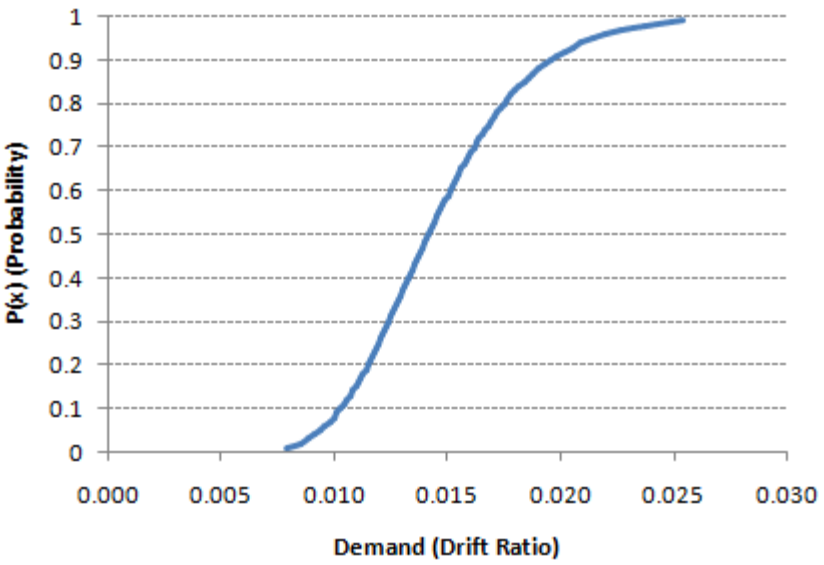

(a)

P(x)	θ	P(x)	θ	P(x)	θ	P(x)	θ	P(x)	θ
0.01	0.0079	0.21	0.0116	0.41	0.0134	0.61	0.0152	0.81	0.0177
0.02	0.0085	0.22	0.0117	0.42	0.0135	0.62	0.0153	0.82	0.0179
0.03	0.0089	0.23	0.0118	0.43	0.0136	0.63	0.0154	0.83	0.0180
0.04	0.0092	0.24	0.0119	0.44	0.0137	0.64	0.0155	0.84	0.0182
0.05	**0.0094**	**0.25**	**0.0120**	**0.45**	**0.0138**	**0.65**	**0.0156**	**0.85**	**0.0184**
0.06	0.0096	0.26	0.0121	0.46	0.0138	0.66	0.0157	0.86	0.0186
0.07	0.0098	0.27	0.0122	0.47	0.0139	0.67	0.0159	0.87	0.0188
0.08	0.0100	0.28	0.0123	0.48	0.0140	0.68	0.0160	0.88	0.0190
0.09	0.0102	0.29	0.0124	0.49	0.0141	0.69	0.0161	0.89	0.0193
0.10	**0.0103**	**0.30**	**0.0125**	**0.50**	**0.0142**	**0.70**	**0.0162**	**0.90**	**0.0196**
0.11	0.0105	0.31	0.0125	0.51	0.0143	0.71	0.0163	0.91	0.0199
0.12	0.0106	0.32	0.0126	0.52	0.0144	0.72	0.0164	0.92	0.0202
0.13	0.0107	0.33	0.0127	0.53	0.0145	0.73	0.0166	0.93	0.0205
0.14	0.0108	0.34	0.0128	0.54	0.0146	0.74	0.0167	0.94	0.0209
0.15	**0.0110**	**0.35**	**0.0129**	**0.55**	**0.0147**	**0.75**	**0.0168**	**0.95**	**0.0214**
0.16	0.0111	0.36	0.0130	0.56	0.0147	0.76	0.0169	0.96	0.0220
0.17	0.0112	0.37	0.0131	0.57	0.0148	0.77	0.0171	0.97	0.0227
0.18	0.0113	0.38	0.0132	0.58	0.0149	0.78	0.0172	0.98	0.0237
0.19	0.0114	0.39	0.0132	0.59	0.0150	0.79	0.0174	0.99	0.0254
0.20	**0.0115**	**0.40**	**0.0133**	**0.60**	**0.0151**	**0.80**	**0.0175**		

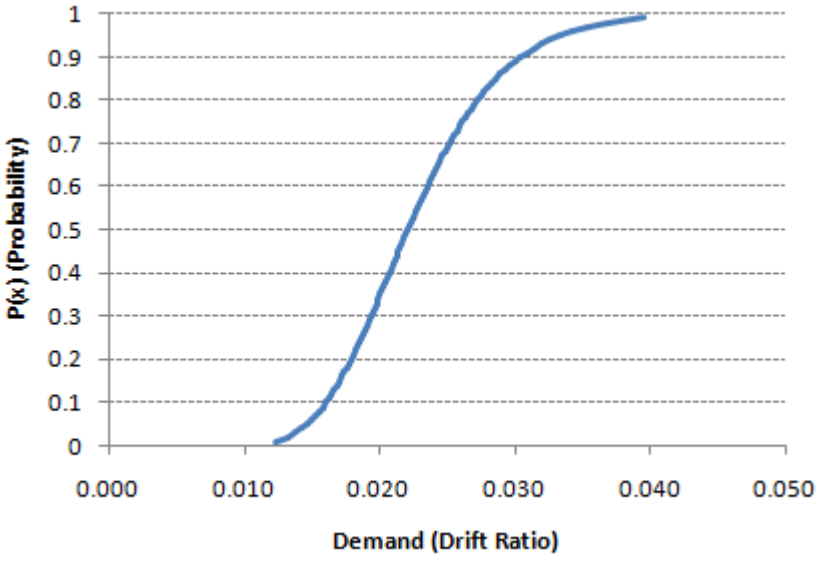

(b)

P(x)	θ	P(x)	θ	P(x)	θ	P(x)	θ	P(x)	θ
0.01	0.0124	0.21	0.0181	0.41	0.0209	0.61	0.0237	0.81	0.0275
0.02	0.0132	0.22	0.0182	0.42	0.0210	0.62	0.0239	0.82	0.0278
0.03	0.0138	0.23	0.0184	0.43	0.0211	0.63	0.0240	0.83	0.0281
0.04	0.0143	0.24	0.0185	0.44	0.0213	0.64	0.0242	0.84	0.0283
0.05	**0.0146**	**0.25**	**0.0187**	**0.45**	**0.0214**	**0.65**	**0.0243**	**0.85**	**0.0286**
0.06	0.0150	0.26	0.0188	0.46	0.0216	0.66	0.0245	0.86	0.0290
0.07	0.0153	0.27	0.0190	0.47	0.0217	0.67	0.0247	0.87	0.0293
0.08	0.0156	0.28	0.0191	0.48	0.0218	0.68	0.0248	0.88	0.0296
0.09	0.0158	0.29	0.0192	0.49	0.0220	0.69	0.0250	0.89	0.0300
0.10	**0.0160**	**0.30**	**0.0194**	**0.50**	**0.0221**	**0.70**	**0.0252**	**0.90**	**0.0304**
0.11	0.0163	0.31	0.0195	0.51	0.0222	0.71	0.0254	0.91	0.0309
0.12	0.0165	0.32	0.0197	0.52	0.0224	0.72	0.0256	0.92	0.0314
0.13	0.0167	0.33	0.0198	0.53	0.0225	0.73	0.0258	0.93	0.0320
0.14	0.0169	0.34	0.0199	0.54	0.0227	0.74	0.0260	0.94	0.0326
0.15	**0.0171**	**0.35**	**0.0201**	**0.55**	**0.0228**	**0.75**	**0.0262**	**0.95**	**0.0333**
0.16	0.0172	0.36	0.0202	0.56	0.0230	0.76	0.0264	0.96	0.0342
0.17	0.0174	0.37	0.0203	0.57	0.0231	0.77	0.0266	0.97	0.0354
0.18	0.0176	0.38	0.0205	0.58	0.0232	0.78	0.0268	0.98	0.0369
0.19	0.0177	0.39	0.0206	0.59	0.0234	0.79	0.0270	0.99	0.0395
0.20	**0.0179**	**0.40**	**0.0207**	**0.60**	**0.0235**	**0.80**	**0.0273**		

Figure A.48: Plotted fragility curve and information for glass configuration (13) for the (a) cracking and (b) fallout limit state

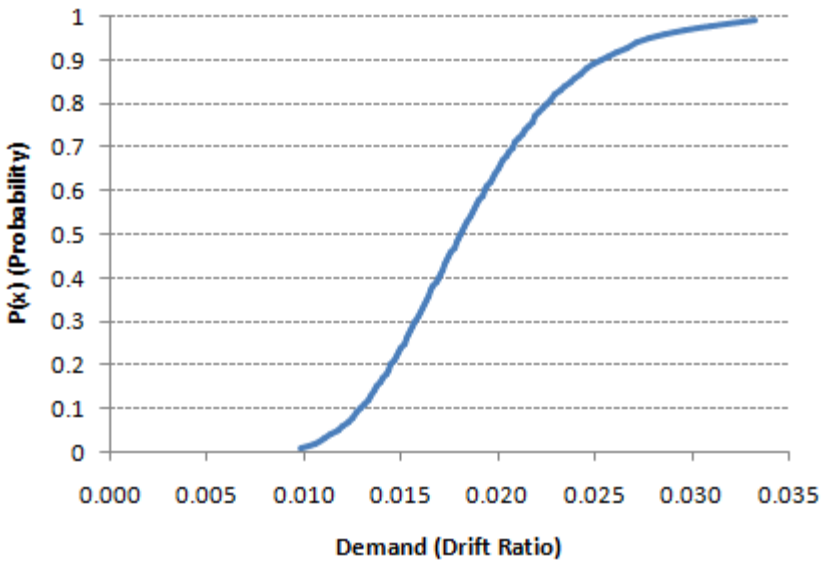

(a)

P(x)	θ	P(x)	θ	P(x)	θ	P(x)	θ	P(x)	θ
0.01	0.0098	0.21	0.0147	0.41	0.0171	0.61	0.0195	0.81	0.0228
0.02	0.0106	0.22	0.0148	0.42	0.0172	0.62	0.0196	0.82	0.0230
0.03	0.0111	0.23	0.0149	0.43	0.0173	0.63	0.0197	0.83	0.0232
0.04	0.0114	0.24	0.0150	0.44	0.0174	0.64	0.0199	0.84	0.0235
0.05	**0.0118**	**0.25**	**0.0152**	**0.45**	**0.0175**	**0.65**	**0.0200**	**0.85**	**0.0237**
0.06	0.0120	0.26	0.0153	0.46	0.0176	0.66	0.0202	0.86	0.0240
0.07	0.0123	0.27	0.0154	0.47	0.0177	0.67	0.0203	0.87	0.0243
0.08	0.0125	0.28	0.0155	0.48	0.0179	0.68	0.0205	0.88	0.0246
0.09	0.0127	0.29	0.0157	0.49	0.0180	0.69	0.0206	0.89	0.0250
0.10	**0.0129**	**0.30**	**0.0158**	**0.50**	**0.0181**	**0.70**	**0.0208**	**0.90**	**0.0253**
0.11	0.0131	0.31	0.0159	0.51	0.0182	0.71	0.0209	0.91	0.0257
0.12	0.0133	0.32	0.0160	0.52	0.0183	0.72	0.0211	0.92	0.0262
0.13	0.0135	0.33	0.0161	0.53	0.0185	0.73	0.0213	0.93	0.0266
0.14	0.0136	0.34	0.0162	0.54	0.0186	0.74	0.0214	0.94	0.0272
0.15	**0.0138**	**0.35**	**0.0164**	**0.55**	**0.0187**	**0.75**	**0.0216**	**0.95**	**0.0279**
0.16	0.0139	0.36	0.0165	0.56	0.0188	0.76	0.0218	0.96	0.0286
0.17	0.0141	0.37	0.0166	0.57	0.0190	0.77	0.0220	0.97	0.0296
0.18	0.0142	0.38	0.0167	0.58	0.0191	0.78	0.0222	0.98	0.0310
0.19	0.0144	0.39	0.0168	0.59	0.0192	0.79	0.0224	0.99	0.0333
0.20	**0.0145**	**0.40**	**0.0169**	**0.60**	**0.0193**	**0.80**	**0.0226**		

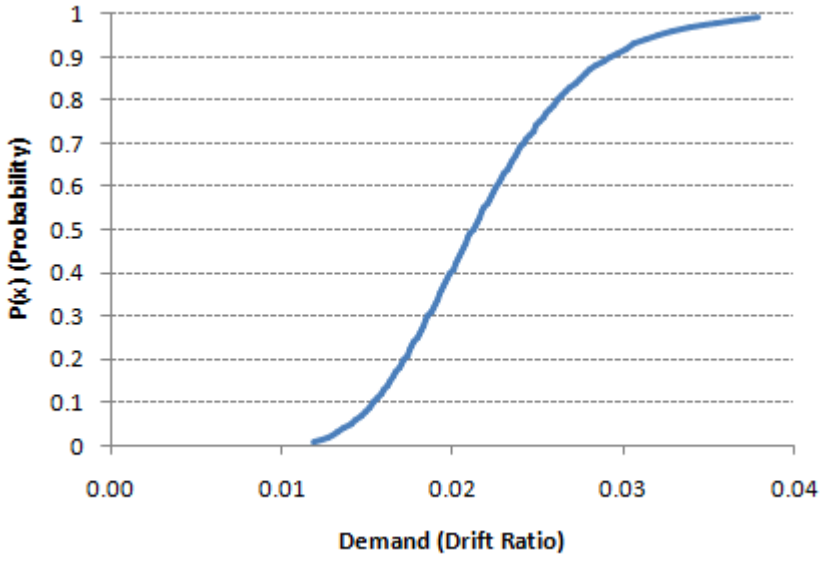

(b)

P(x)	θ	P(x)	θ	P(x)	θ	P(x)	θ	P(x)	θ
0.01	0.0119	0.21	0.0173	0.41	0.0200	0.61	0.0227	0.81	0.0264
0.02	0.0127	0.22	0.0175	0.42	0.0202	0.62	0.0229	0.82	0.0267
0.03	0.0132	0.23	0.0176	0.43	0.0203	0.63	0.0230	0.83	0.0269
0.04	0.0137	0.24	0.0178	0.44	0.0204	0.64	0.0232	0.84	0.0272
0.05	**0.0141**	**0.25**	**0.0179**	**0.45**	**0.0205**	**0.65**	**0.0233**	**0.85**	**0.0275**
0.06	0.0144	0.26	0.0181	0.46	0.0207	0.66	0.0235	0.86	0.0278
0.07	0.0147	0.27	0.0182	0.47	0.0208	0.67	0.0237	0.87	0.0281
0.08	0.0149	0.28	0.0183	0.48	0.0209	0.68	0.0238	0.88	0.0284
0.09	0.0152	0.29	0.0185	0.49	0.0211	0.69	0.0240	0.89	0.0288
0.10	**0.0154**	**0.30**	**0.0186**	**0.50**	**0.0212**	**0.70**	**0.0242**	**0.90**	**0.0292**
0.11	0.0156	0.31	0.0187	0.51	0.0213	0.71	0.0243	0.91	0.0296
0.12	0.0158	0.32	0.0189	0.52	0.0215	0.72	0.0245	0.92	0.0301
0.13	0.0160	0.33	0.0190	0.53	0.0216	0.73	0.0247	0.93	0.0307
0.14	0.0162	0.34	0.0191	0.54	0.0217	0.74	0.0249	0.94	0.0313
0.15	**0.0164**	**0.35**	**0.0193**	**0.55**	**0.0219**	**0.75**	**0.0251**	**0.95**	**0.0320**
0.16	0.0165	0.36	0.0194	0.56	0.0220	0.76	0.0253	0.96	0.0328
0.17	0.0167	0.37	0.0195	0.57	0.0222	0.77	0.0255	0.97	0.0339
0.18	0.0169	0.38	0.0196	0.58	0.0223	0.78	0.0257	0.98	0.0354
0.19	0.0170	0.39	0.0198	0.59	0.0224	0.79	0.0259	0.99	0.0379
0.20	**0.0172**	**0.40**	**0.0199**	**0.60**	**0.0226**	**0.80**	**0.0262**		

Figure A.49: Plotted fragility curve and information for glass configuration (14) for the (a) cracking and (b) fallout limit state

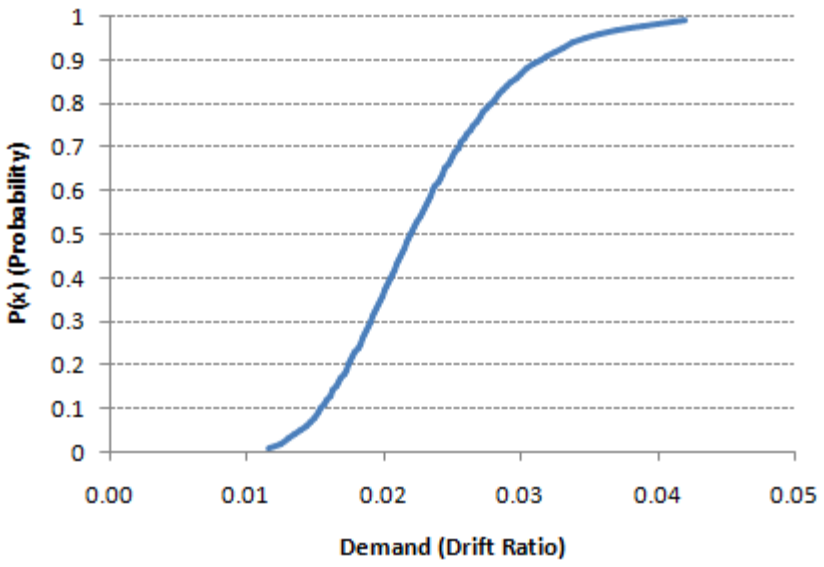

(a)

P(x)	θ	P(x)	θ	P(x)	θ	P(x)	θ	P(x)	θ
0.01	0.0115	0.21	0.0176	0.41	0.0207	0.61	0.0238	0.81	0.0281
0.02	0.0125	0.22	0.0178	0.42	0.0208	0.62	0.0239	0.82	0.0283
0.03	0.0131	0.23	0.0179	0.43	0.0210	0.63	0.0241	0.83	0.0287
0.04	0.0135	0.24	0.0181	0.44	0.0211	0.64	0.0243	0.84	0.0290
0.05	**0.0139**	**0.25**	**0.0183**	**0.45**	**0.0212**	**0.65**	**0.0245**	**0.85**	**0.0293**
0.06	0.0143	0.26	0.0184	0.46	0.0214	0.66	0.0247	0.86	0.0297
0.07	0.0146	0.27	0.0186	0.47	0.0215	0.67	0.0249	0.87	0.0301
0.08	0.0149	0.28	0.0187	0.48	0.0217	0.68	0.0250	0.88	0.0305
0.09	0.0152	0.29	0.0189	0.49	0.0218	0.69	0.0252	0.89	0.0309
0.10	**0.0154**	**0.30**	**0.0190**	**0.50**	**0.0220**	**0.70**	**0.0254**	**0.90**	**0.0314**
0.11	0.0157	0.31	0.0192	0.51	0.0222	0.71	0.0256	0.91	0.0319
0.12	0.0159	0.32	0.0193	0.52	0.0223	0.72	0.0259	0.92	0.0325
0.13	0.0161	0.33	0.0195	0.53	0.0225	0.73	0.0261	0.93	0.0331
0.14	0.0163	0.34	0.0196	0.54	0.0226	0.74	0.0263	0.94	0.0338
0.15	**0.0165**	**0.35**	**0.0198**	**0.55**	**0.0228**	**0.75**	**0.0265**	**0.95**	**0.0347**
0.16	0.0167	0.36	0.0199	0.56	0.0229	0.76	0.0268	0.96	0.0357
0.17	0.0169	0.37	0.0201	0.57	0.0231	0.77	0.0270	0.97	0.0370
0.18	0.0171	0.38	0.0202	0.58	0.0233	0.78	0.0272	0.98	0.0389
0.19	0.0173	0.39	0.0204	0.59	0.0234	0.79	0.0275	0.99	0.0419
0.20	**0.0174**	**0.40**	**0.0205**	**0.60**	**0.0236**	**0.80**	**0.0278**		

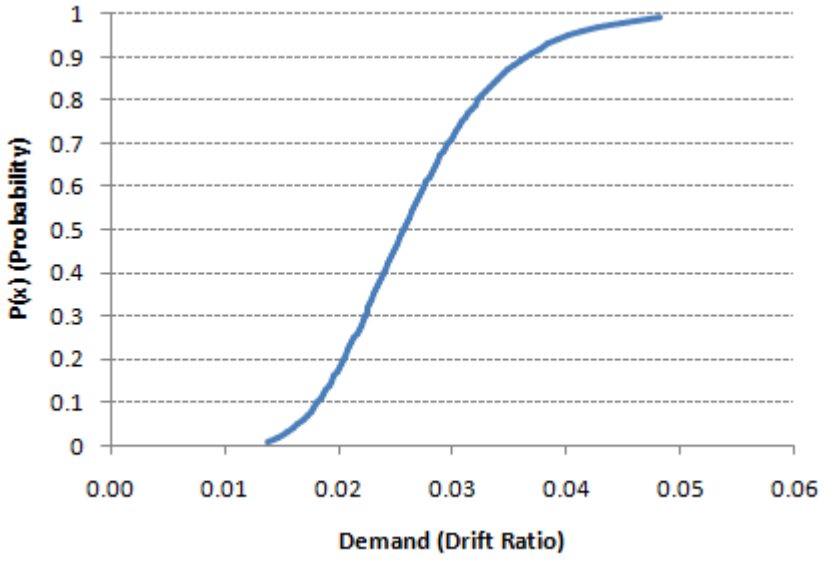

(b)

P(x)	θ	P(x)	θ	P(x)	θ	P(x)	θ	P(x)	θ
0.01	0.0137	0.21	0.0207	0.41	0.0242	0.61	0.0277	0.81	0.0326
0.02	0.0147	0.22	0.0208	0.42	0.0243	0.62	0.0279	0.82	0.0329
0.03	0.0154	0.23	0.0210	0.43	0.0245	0.63	0.0281	0.83	0.0333
0.04	0.0160	0.24	0.0212	0.44	0.0247	0.64	0.0283	0.84	0.0336
0.05	**0.0165**	**0.25**	**0.0214**	**0.45**	**0.0248**	**0.65**	**0.0285**	**0.85**	**0.0340**
0.06	0.0169	0.26	0.0216	0.46	0.0250	0.66	0.0287	0.86	0.0344
0.07	0.0172	0.27	0.0218	0.47	0.0252	0.67	0.0290	0.87	0.0349
0.08	0.0176	0.28	0.0219	0.48	0.0254	0.68	0.0292	0.88	0.0353
0.09	0.0179	0.29	0.0221	0.49	0.0255	0.69	0.0294	0.89	0.0358
0.10	**0.0182**	**0.30**	**0.0223**	**0.50**	**0.0257**	**0.70**	**0.0296**	**0.90**	**0.0364**
0.11	0.0184	0.31	0.0225	0.51	0.0259	0.71	0.0299	0.91	0.0370
0.12	0.0187	0.32	0.0226	0.52	0.0261	0.72	0.0301	0.92	0.0376
0.13	0.0189	0.33	0.0228	0.53	0.0262	0.73	0.0303	0.93	0.0383
0.14	0.0192	0.34	0.0230	0.54	0.0264	0.74	0.0306	0.94	0.0392
0.15	**0.0194**	**0.35**	**0.0232**	**0.55**	**0.0266**	**0.75**	**0.0309**	**0.95**	**0.0401**
0.16	0.0196	0.36	0.0233	0.56	0.0268	0.76	0.0311	0.96	0.0413
0.17	0.0198	0.37	0.0235	0.57	0.0270	0.77	0.0314	0.97	0.0428
0.18	0.0201	0.38	0.0237	0.58	0.0271	0.78	0.0317	0.98	0.0448
0.19	0.0203	0.39	0.0238	0.59	0.0273	0.79	0.0320	0.99	0.0483
0.20	**0.0205**	**0.40**	**0.0240**	**0.60**	**0.0275**	**0.80**	**0.0323**		

Figure A.50: Plotted fragility curve and information for glass configuration (15) for the (a) cracking and (b) fallout limit state

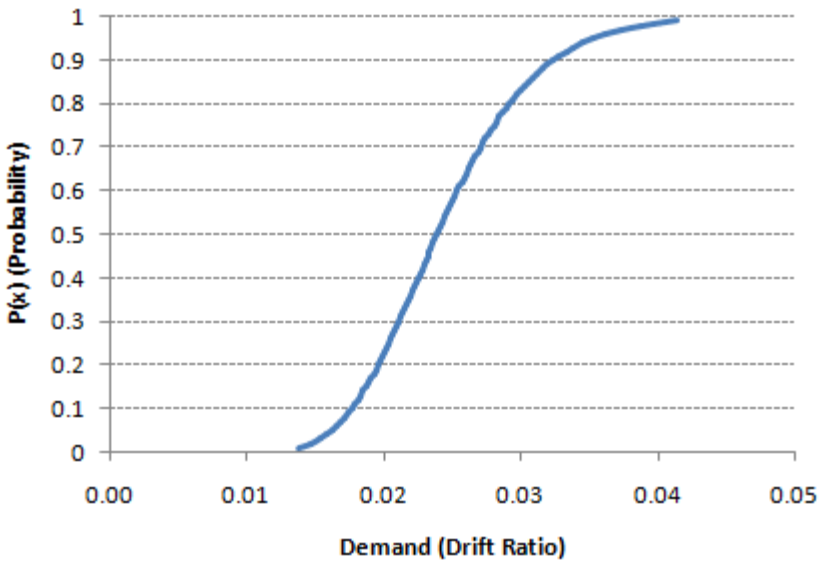

(a)

P(x)	θ	P(x)	θ	P(x)	θ	P(x)	θ	P(x)	θ
0.01	0.0138	0.21	0.0198	0.41	0.0227	0.61	0.0255	0.81	0.0294
0.02	0.0147	0.22	0.0199	0.42	0.0228	0.62	0.0257	0.82	0.0297
0.03	0.0153	0.23	0.0201	0.43	0.0229	0.63	0.0258	0.83	0.0299
0.04	0.0158	0.24	0.0202	0.44	0.0231	0.64	0.0260	0.84	0.0302
0.05	**0.0162**	**0.25**	**0.0204**	**0.45**	**0.0232**	**0.65**	**0.0262**	**0.85**	**0.0305**
0.06	0.0166	0.26	0.0205	0.46	0.0233	0.66	0.0263	0.86	0.0308
0.07	0.0169	0.27	0.0207	0.47	0.0235	0.67	0.0265	0.87	0.0312
0.08	0.0172	0.28	0.0208	0.48	0.0236	0.68	0.0267	0.88	0.0315
0.09	0.0174	0.29	0.0210	0.49	0.0238	0.69	0.0269	0.89	0.0319
0.10	**0.0177**	**0.30**	**0.0211**	**0.50**	**0.0239**	**0.70**	**0.0270**	**0.90**	**0.0323**
0.11	0.0179	0.31	0.0213	0.51	0.0240	0.71	0.0272	0.91	0.0328
0.12	0.0181	0.32	0.0214	0.52	0.0242	0.72	0.0274	0.92	0.0333
0.13	0.0183	0.33	0.0215	0.53	0.0243	0.73	0.0276	0.93	0.0339
0.14	0.0185	0.34	0.0217	0.54	0.0245	0.74	0.0278	0.94	0.0345
0.15	**0.0187**	**0.35**	**0.0218**	**0.55**	**0.0246**	**0.75**	**0.0280**	**0.95**	**0.0352**
0.16	0.0189	0.36	0.0220	0.56	0.0248	0.76	0.0282	0.96	0.0361
0.17	0.0191	0.37	0.0221	0.57	0.0249	0.77	0.0285	0.97	0.0373
0.18	0.0193	0.38	0.0222	0.58	0.0251	0.78	0.0287	0.98	0.0388
0.19	0.0194	0.39	0.0224	0.59	0.0252	0.79	0.0289	0.99	0.0414
0.20	**0.0196**	**0.40**	**0.0225**	**0.60**	**0.0254**	**0.80**	**0.0292**		

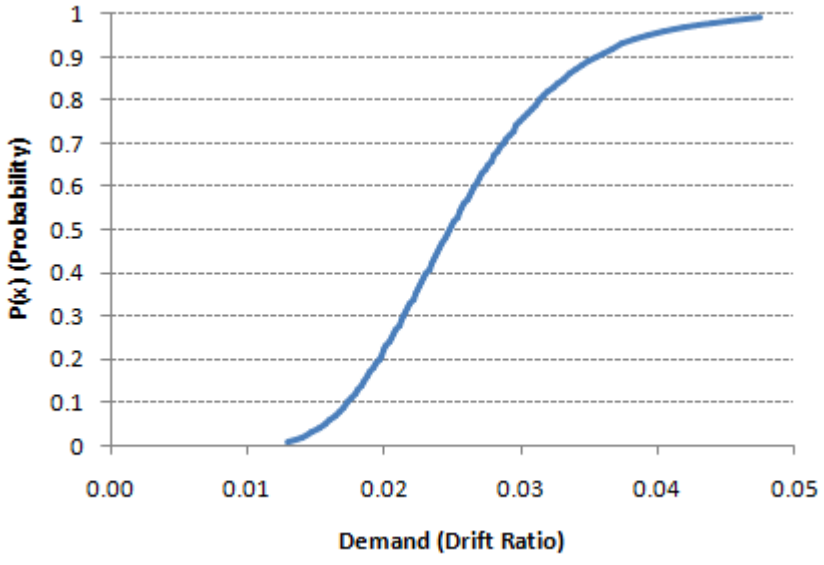

(b)

P(x)	θ	P(x)	θ	P(x)	θ	P(x)	θ	P(x)	θ
0.01	0.0130	0.21	0.0198	0.41	0.0233	0.61	0.0268	0.81	0.0317
0.02	0.0140	0.22	0.0200	0.42	0.0234	0.62	0.0270	0.82	0.0320
0.03	0.0147	0.23	0.0202	0.43	0.0236	0.63	0.0272	0.83	0.0324
0.04	0.0152	0.24	0.0204	0.44	0.0238	0.64	0.0274	0.84	0.0327
0.05	**0.0157**	**0.25**	**0.0205**	**0.45**	**0.0239**	**0.65**	**0.0276**	**0.85**	**0.0331**
0.06	0.0161	0.26	0.0207	0.46	0.0241	0.66	0.0278	0.86	0.0335
0.07	0.0164	0.27	0.0209	0.47	0.0243	0.67	0.0280	0.87	0.0340
0.08	0.0168	0.28	0.0211	0.48	0.0245	0.68	0.0283	0.88	0.0344
0.09	0.0171	0.29	0.0213	0.49	0.0246	0.69	0.0285	0.89	0.0349
0.10	**0.0173**	**0.30**	**0.0214**	**0.50**	**0.0248**	**0.70**	**0.0287**	**0.90**	**0.0355**
0.11	0.0176	0.31	0.0216	0.51	0.0250	0.71	0.0289	0.91	0.0361
0.12	0.0179	0.32	0.0218	0.52	0.0251	0.72	0.0292	0.92	0.0367
0.13	0.0181	0.33	0.0219	0.53	0.0253	0.73	0.0294	0.93	0.0374
0.14	0.0183	0.34	0.0221	0.54	0.0255	0.74	0.0297	0.94	0.0383
0.15	**0.0186**	**0.35**	**0.0223**	**0.55**	**0.0257**	**0.75**	**0.0299**	**0.95**	**0.0392**
0.16	0.0188	0.36	0.0224	0.56	0.0259	0.76	0.0302	0.96	0.0404
0.17	0.0190	0.37	0.0226	0.57	0.0261	0.77	0.0305	0.97	0.0419
0.18	0.0192	0.38	0.0228	0.58	0.0262	0.78	0.0308	0.98	0.0440
0.19	0.0194	0.39	0.0229	0.59	0.0264	0.79	0.0311	0.99	0.0475
0.20	**0.0196**	**0.40**	**0.0231**	**0.60**	**0.0266**	**0.80**	**0.0314**		

Figure A.51: Plotted fragility curve and information for glass configuration (16) for the (a) cracking and (b) fallout limit state

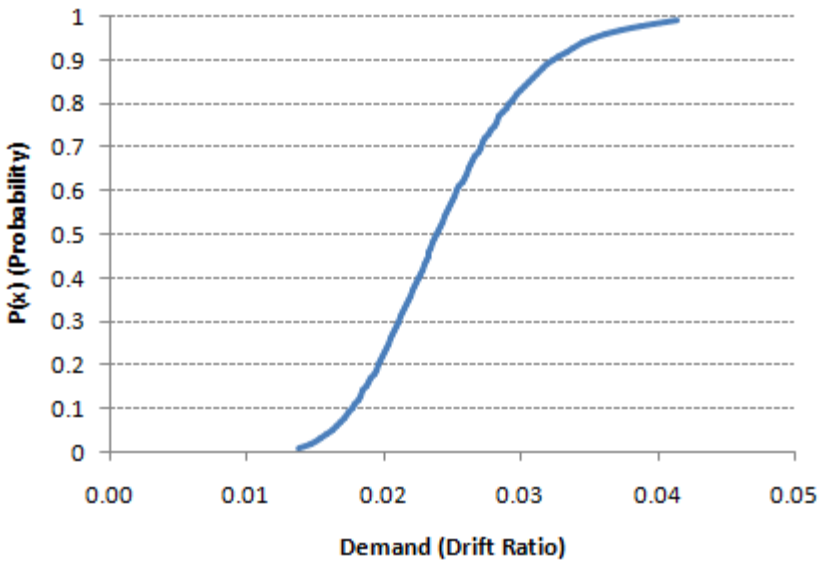

(a)

P(x)	θ	P(x)	θ	P(x)	θ	P(x)	θ	P(x)	θ
0.01	0.0131	0.21	0.0207	0.41	0.0246	0.61	0.0286	0.81	0.0342
0.02	0.0143	0.22	0.0209	0.42	0.0248	0.62	0.0288	0.82	0.0345
0.03	0.0150	0.23	0.0211	0.43	0.0250	0.63	0.0290	0.83	0.0349
0.04	0.0156	0.24	0.0213	0.44	0.0251	0.64	0.0293	0.84	0.0354
0.05	**0.0161**	**0.25**	**0.0215**	**0.45**	**0.0253**	**0.65**	**0.0295**	**0.85**	**0.0358**
0.06	0.0165	0.26	0.0217	0.46	0.0255	0.66	0.0297	0.86	0.0363
0.07	0.0169	0.27	0.0219	0.47	0.0257	0.67	0.0300	0.87	0.0368
0.08	0.0173	0.28	0.0221	0.48	0.0259	0.68	0.0302	0.88	0.0373
0.09	0.0176	0.29	0.0223	0.49	0.0261	0.69	0.0305	0.89	0.0379
0.10	**0.0180**	**0.30**	**0.0225**	**0.50**	**0.0263**	**0.70**	**0.0307**	**0.90**	**0.0385**
0.11	0.0182	0.31	0.0227	0.51	0.0265	0.71	0.0310	0.91	0.0392
0.12	0.0185	0.32	0.0229	0.52	0.0267	0.72	0.0313	0.92	0.0400
0.13	0.0188	0.33	0.0231	0.53	0.0269	0.73	0.0316	0.93	0.0408
0.14	0.0191	0.34	0.0233	0.54	0.0271	0.74	0.0319	0.94	0.0418
0.15	**0.0193**	**0.35**	**0.0234**	**0.55**	**0.0273**	**0.75**	**0.0322**	**0.95**	**0.0429**
0.16	0.0196	0.36	0.0236	0.56	0.0275	0.76	0.0325	0.96	0.0443
0.17	0.0198	0.37	0.0238	0.57	0.0277	0.77	0.0328	0.97	0.0461
0.18	0.0200	0.38	0.0240	0.58	0.0279	0.78	0.0331	0.98	0.0485
0.19	0.0202	0.39	0.0242	0.59	0.0281	0.79	0.0334	0.99	0.0526
0.20	**0.0205**	**0.40**	**0.0244**	**0.60**	**0.0284**	**0.80**	**0.0338**		

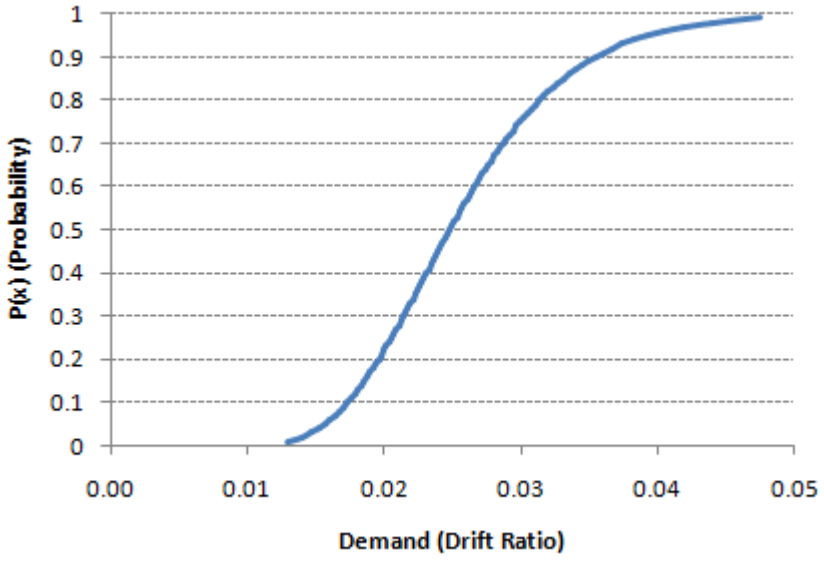

(b)

P(x)	θ	P(x)	θ	P(x)	θ	P(x)	θ	P(x)	θ
0.01	0.0134	0.21	0.0210	0.41	0.0250	0.61	0.0290	0.81	0.0347
0.02	0.0145	0.22	0.0212	0.42	0.0251	0.62	0.0292	0.82	0.0350
0.03	0.0153	0.23	0.0214	0.43	0.0253	0.63	0.0295	0.83	0.0354
0.04	0.0159	0.24	0.0216	0.44	0.0255	0.64	0.0297	0.84	0.0359
0.05	**0.0164**	**0.25**	**0.0219**	**0.45**	**0.0257**	**0.65**	**0.0299**	**0.85**	**0.0363**
0.06	0.0168	0.26	0.0221	0.46	0.0259	0.66	0.0302	0.86	0.0368
0.07	0.0172	0.27	0.0223	0.47	0.0261	0.67	0.0304	0.87	0.0373
0.08	0.0176	0.28	0.0225	0.48	0.0263	0.68	0.0307	0.88	0.0379
0.09	0.0179	0.29	0.0227	0.49	0.0265	0.69	0.0309	0.89	0.0384
0.10	**0.0182**	**0.30**	**0.0228**	**0.50**	**0.0267**	**0.70**	**0.0312**	**0.90**	**0.0391**
0.11	0.0185	0.31	0.0230	0.51	0.0269	0.71	0.0315	0.91	0.0398
0.12	0.0188	0.32	0.0232	0.52	0.0271	0.72	0.0317	0.92	0.0405
0.13	0.0191	0.33	0.0234	0.53	0.0273	0.73	0.0320	0.93	0.0414
0.14	0.0194	0.34	0.0236	0.54	0.0275	0.74	0.0323	0.94	0.0424
0.15	**0.0196**	**0.35**	**0.0238**	**0.55**	**0.0277**	**0.75**	**0.0326**	**0.95**	**0.0435**
0.16	0.0199	0.36	0.0240	0.56	0.0279	0.76	0.0329	0.96	0.0449
0.17	0.0201	0.37	0.0242	0.57	0.0281	0.77	0.0333	0.97	0.0467
0.18	0.0203	0.38	0.0244	0.58	0.0283	0.78	0.0336	0.98	0.0491
0.19	0.0206	0.39	0.0246	0.59	0.0286	0.79	0.0339	0.99	0.0533
0.20	**0.0208**	**0.40**	**0.0248**	**0.60**	**0.0288**	**0.80**	**0.0343**		

Figure A.52: Plotted fragility curve and information for glass configuration (17) for the (a) cracking and (b) fallout limit state

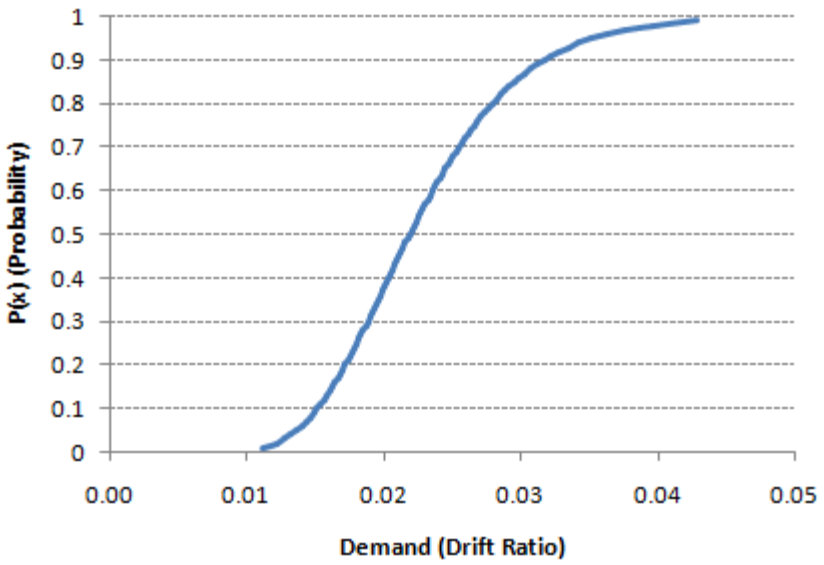

(a)

P(x)	θ	P(x)	θ	P(x)	θ	P(x)	θ	P(x)	θ
0.01	0.0112	0.21	0.0174	0.41	0.0205	0.61	0.0237	0.81	0.0282
0.02	0.0121	0.22	0.0175	0.42	0.0207	0.62	0.0239	0.82	0.0285
0.03	0.0127	0.23	0.0177	0.43	0.0208	0.63	0.0241	0.83	0.0288
0.04	0.0132	0.24	0.0179	0.44	0.0210	0.64	0.0243	0.84	0.0292
0.05	**0.0136**	**0.25**	**0.0180**	**0.45**	**0.0211**	**0.65**	**0.0245**	**0.85**	**0.0295**
0.06	0.0140	0.26	0.0182	0.46	0.0213	0.66	0.0247	0.86	0.0299
0.07	0.0143	0.27	0.0184	0.47	0.0214	0.67	0.0249	0.87	0.0303
0.08	0.0146	0.28	0.0185	0.48	0.0216	0.68	0.0251	0.88	0.0307
0.09	0.0149	0.29	0.0187	0.49	0.0217	0.69	0.0253	0.89	0.0312
0.10	**0.0151**	**0.30**	**0.0188**	**0.50**	**0.0219**	**0.70**	**0.0255**	**0.90**	**0.0317**
0.11	0.0154	0.31	0.0190	0.51	0.0221	0.71	0.0257	0.91	0.0322
0.12	0.0156	0.32	0.0191	0.52	0.0222	0.72	0.0259	0.92	0.0328
0.13	0.0158	0.33	0.0193	0.53	0.0224	0.73	0.0261	0.93	0.0335
0.14	0.0160	0.34	0.0194	0.54	0.0225	0.74	0.0264	0.94	0.0343
0.15	**0.0162**	**0.35**	**0.0196**	**0.55**	**0.0227**	**0.75**	**0.0266**	**0.95**	**0.0352**
0.16	0.0164	0.36	0.0198	0.56	0.0229	0.76	0.0268	0.96	0.0363
0.17	0.0166	0.37	0.0199	0.57	0.0230	0.77	0.0271	0.97	0.0376
0.18	0.0168	0.38	0.0201	0.58	0.0232	0.78	0.0274	0.98	0.0396
0.19	0.0170	0.39	0.0202	0.59	0.0234	0.79	0.0276	0.99	0.0428
0.20	**0.0172**	**0.40**	**0.0204**	**0.60**	**0.0236**	**0.80**	**0.0279**		

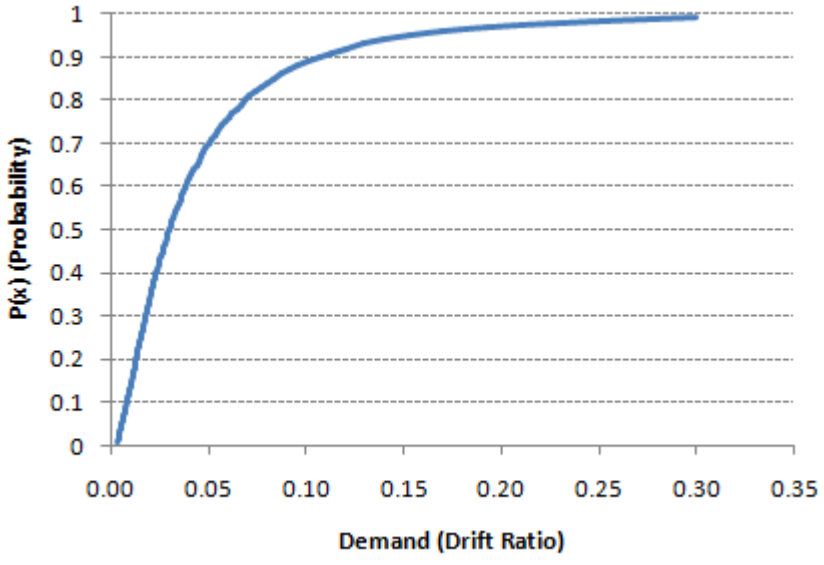

(b)

P(x)	θ	P(x)	θ	P(x)	θ	P(x)	θ	P(x)	θ
0.01	0.0030	0.21	0.0135	0.41	0.0239	0.61	0.0396	0.81	0.0715
0.02	0.0039	0.22	0.0140	0.42	0.0246	0.62	0.0406	0.82	0.0742
0.03	0.0047	0.23	0.0144	0.43	0.0252	0.63	0.0417	0.83	0.0772
0.04	0.0053	0.24	0.0149	0.44	0.0258	0.64	0.0428	0.84	0.0803
0.05	0.0059	**0.25**	0.0154	**0.45**	0.0265	**0.65**	0.0439	**0.85**	0.0837
0.06	0.0064	0.26	0.0159	0.46	0.0272	0.66	0.0451	0.86	0.0874
0.07	0.0070	0.27	0.0164	0.47	0.0278	0.67	0.0464	0.87	0.0915
0.08	0.0075	0.28	0.0168	0.48	0.0285	0.68	0.0477	0.88	0.0960
0.09	0.0080	0.29	0.0173	0.49	0.0293	0.69	0.0490	0.89	0.1010
0.10	0.0084	**0.30**	0.0179	**0.50**	0.0300	**0.70**	0.0504	**0.90**	0.1067
0.11	0.0089	0.31	0.0184	0.51	0.0308	0.71	0.0519	0.91	0.1131
0.12	0.0094	0.32	0.0189	0.52	0.0315	0.72	0.0534	0.92	0.1206
0.13	0.0098	0.33	0.0194	0.53	0.0323	0.73	0.0550	0.93	0.1293
0.14	0.0103	0.34	0.0199	0.54	0.0331	0.74	0.0567	0.94	0.1398
0.15	0.0108	**0.35**	0.0205	**0.55**	0.0340	**0.75**	0.0585	**0.95**	0.1529
0.16	0.0112	0.36	0.0210	0.56	0.0348	0.76	0.0604	0.96	0.1698
0.17	0.0117	0.37	0.0216	0.57	0.0357	0.77	0.0623	0.97	0.1931
0.18	0.0121	0.38	0.0222	0.58	0.0366	0.78	0.0644	0.98	0.2292
0.19	0.0126	0.39	0.0228	0.59	0.0376	0.79	0.0667	0.99	0.3001
0.20	0.0130	**0.40**	0.0233	**0.60**	0.0386	**0.80**	0.0690		

Figure A.53: Plotted fragility curve and information for glass configuration (18) for the (a) cracking and (b) fallout limit state

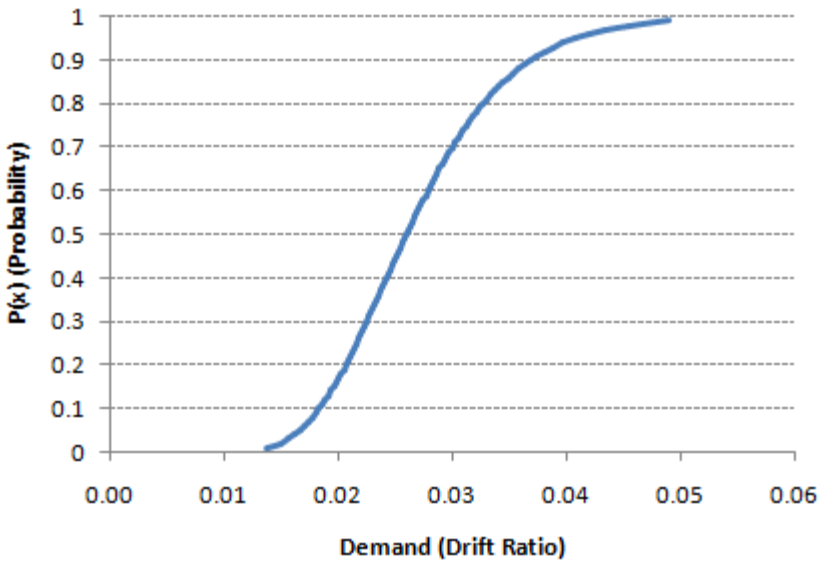

(a)

P(x)	θ	P(x)	θ	P(x)	θ	P(x)	θ	P(x)	θ
0.01	0.0138	0.21	0.0209	0.41	0.0244	0.61	0.0281	0.81	0.0330
0.02	0.0149	0.22	0.0211	0.42	0.0246	0.62	0.0283	0.82	0.0334
0.03	0.0156	0.23	0.0213	0.43	0.0248	0.63	0.0285	0.83	0.0337
0.04	0.0161	0.24	0.0215	0.44	0.0250	0.64	0.0287	0.84	0.0341
0.05	**0.0166**	**0.25**	**0.0216**	**0.45**	**0.0251**	**0.65**	**0.0289**	**0.85**	**0.0345**
0.06	0.0170	0.26	0.0218	0.46	0.0253	0.66	0.0291	0.86	0.0349
0.07	0.0174	0.27	0.0220	0.47	0.0255	0.67	0.0293	0.87	0.0353
0.08	0.0177	0.28	0.0222	0.48	0.0256	0.68	0.0295	0.88	0.0358
0.09	0.0181	0.29	0.0224	0.49	0.0258	0.69	0.0298	0.89	0.0363
0.10	**0.0183**	**0.30**	**0.0225**	**0.50**	**0.0260**	**0.70**	**0.0300**	**0.90**	**0.0368**
0.11	0.0186	0.31	0.0227	0.51	0.0262	0.71	0.0302	0.91	0.0374
0.12	0.0189	0.32	0.0229	0.52	0.0264	0.72	0.0305	0.92	0.0381
0.13	0.0191	0.33	0.0231	0.53	0.0265	0.73	0.0307	0.93	0.0388
0.14	0.0194	0.34	0.0232	0.54	0.0267	0.74	0.0310	0.94	0.0397
0.15	**0.0196**	**0.35**	**0.0234**	**0.55**	**0.0269**	**0.75**	**0.0312**	**0.95**	**0.0407**
0.16	0.0198	0.36	0.0236	0.56	0.0271	0.76	0.0315	0.96	0.0419
0.17	0.0201	0.37	0.0238	0.57	0.0273	0.77	0.0318	0.97	0.0434
0.18	0.0203	0.38	0.0239	0.58	0.0275	0.78	0.0321	0.98	0.0455
0.19	0.0205	0.39	0.0241	0.59	0.0277	0.79	0.0324	0.99	0.0490
0.20	**0.0207**	**0.40**	**0.0243**	**0.60**	**0.0279**	**0.80**	**0.0327**		

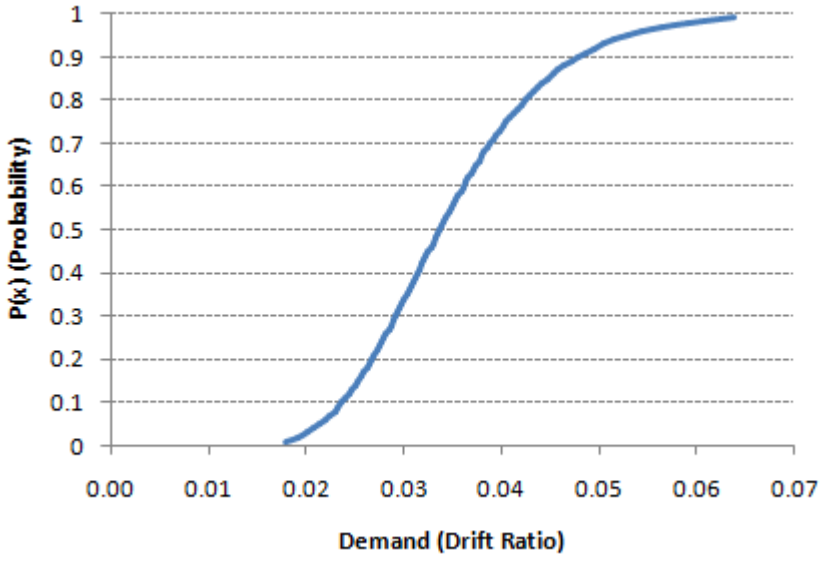

(b)

P(x)	θ	P(x)	θ	P(x)	θ	P(x)	θ	P(x)	θ
0.01	0.0178	0.21	0.0270	0.41	0.0317	0.61	0.0364	0.81	0.0429
0.02	0.0192	0.22	0.0273	0.42	0.0319	0.62	0.0366	0.82	0.0433
0.03	0.0201	0.23	0.0275	0.43	0.0321	0.63	0.0369	0.83	0.0438
0.04	0.0209	0.24	0.0278	0.44	0.0323	0.64	0.0372	0.84	0.0443
0.05	**0.0215**	**0.25**	**0.0280**	**0.45**	**0.0326**	**0.65**	**0.0375**	**0.85**	**0.0448**
0.06	0.0220	0.26	0.0283	0.46	0.0328	0.66	0.0377	0.86	0.0453
0.07	0.0225	0.27	0.0285	0.47	0.0330	0.67	0.0380	0.87	0.0459
0.08	0.0229	0.28	0.0287	0.48	0.0332	0.68	0.0383	0.88	0.0465
0.09	0.0233	0.29	0.0290	0.49	0.0335	0.69	0.0386	0.89	0.0472
0.10	**0.0237**	**0.30**	**0.0292**	**0.50**	**0.0337**	**0.70**	**0.0389**	**0.90**	**0.0479**
0.11	0.0241	0.31	0.0294	0.51	0.0339	0.71	0.0392	0.91	0.0487
0.12	0.0244	0.32	0.0296	0.52	0.0342	0.72	0.0395	0.92	0.0495
0.13	0.0248	0.33	0.0299	0.53	0.0344	0.73	0.0399	0.93	0.0505
0.14	0.0251	0.34	0.0301	0.54	0.0346	0.74	0.0402	0.94	0.0516
0.15	**0.0254**	**0.35**	**0.0303**	**0.55**	**0.0349**	**0.75**	**0.0405**	**0.95**	**0.0529**
0.16	0.0257	0.36	0.0305	0.56	0.0351	0.76	0.0409	0.96	0.0544
0.17	0.0259	0.37	0.0308	0.57	0.0354	0.77	0.0413	0.97	0.0564
0.18	0.0262	0.38	0.0310	0.58	0.0356	0.78	0.0416	0.98	0.0592
0.19	0.0265	0.39	0.0312	0.59	0.0359	0.79	0.0420	0.99	0.0637
0.20	**0.0268**	**0.40**	**0.0314**	**0.60**	**0.0361**	**0.80**	**0.0424**		

Figure A.54: Plotted fragility curve and information for glass configuration (19) for the (a) cracking and (b) fallout limit state

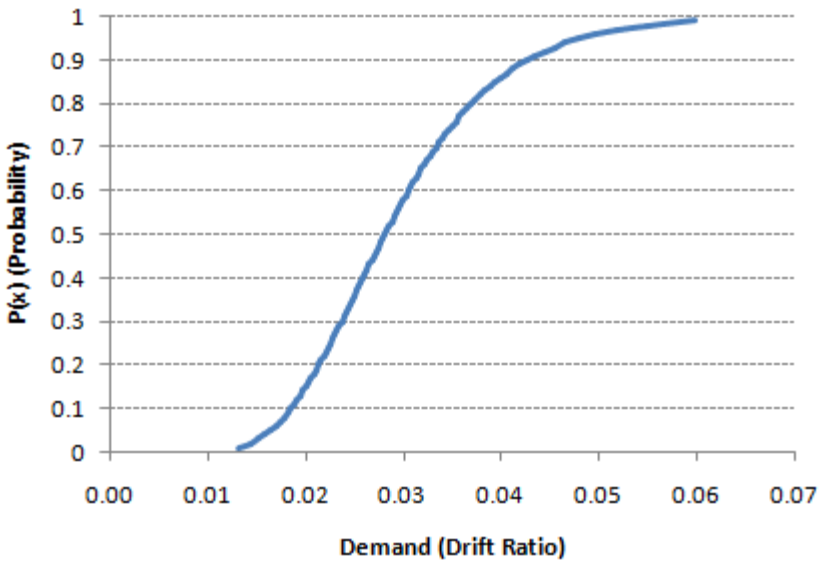

(a)

P(x)	θ	P(x)	θ	P(x)	θ	P(x)	θ	P(x)	θ
0.01	0.0132	0.21	0.0216	0.41	0.0261	0.61	0.0308	0.81	0.0374
0.02	0.0144	0.22	0.0219	0.42	0.0263	0.62	0.0310	0.82	0.0378
0.03	0.0152	0.23	0.0221	0.43	0.0265	0.63	0.0313	0.83	0.0383
0.04	0.0159	0.24	0.0223	0.44	0.0268	0.64	0.0316	0.84	0.0388
0.05	**0.0165**	**0.25**	**0.0226**	**0.45**	**0.0270**	**0.65**	**0.0318**	**0.85**	**0.0394**
0.06	0.0170	0.26	0.0228	0.46	0.0272	0.66	0.0321	0.86	0.0399
0.07	0.0174	0.27	0.0230	0.47	0.0274	0.67	0.0324	0.87	0.0405
0.08	0.0178	0.28	0.0233	0.48	0.0276	0.68	0.0327	0.88	0.0412
0.09	0.0182	0.29	0.0235	0.49	0.0279	0.69	0.0330	0.89	0.0419
0.10	**0.0185**	**0.30**	**0.0237**	**0.50**	**0.0281**	**0.70**	**0.0333**	**0.90**	**0.0426**
0.11	0.0189	0.31	0.0239	0.51	0.0283	0.71	0.0336	0.91	0.0434
0.12	0.0192	0.32	0.0241	0.52	0.0286	0.72	0.0340	0.92	0.0444
0.13	0.0195	0.33	0.0244	0.53	0.0288	0.73	0.0343	0.93	0.0454
0.14	0.0198	0.34	0.0246	0.54	0.0290	0.74	0.0346	0.94	0.0466
0.15	**0.0201**	**0.35**	**0.0248**	**0.55**	**0.0293**	**0.75**	**0.0350**	**0.95**	**0.0480**
0.16	0.0203	0.36	0.0250	0.56	0.0295	0.76	0.0354	0.96	0.0496
0.17	0.0206	0.37	0.0252	0.57	0.0298	0.77	0.0357	0.97	0.0518
0.18	0.0209	0.38	0.0254	0.58	0.0300	0.78	0.0361	0.98	0.0548
0.19	0.0211	0.39	0.0257	0.59	0.0303	0.79	0.0365	0.99	0.0598
0.20	**0.0214**	**0.40**	**0.0259**	**0.60**	**0.0305**	**0.80**	**0.0369**		

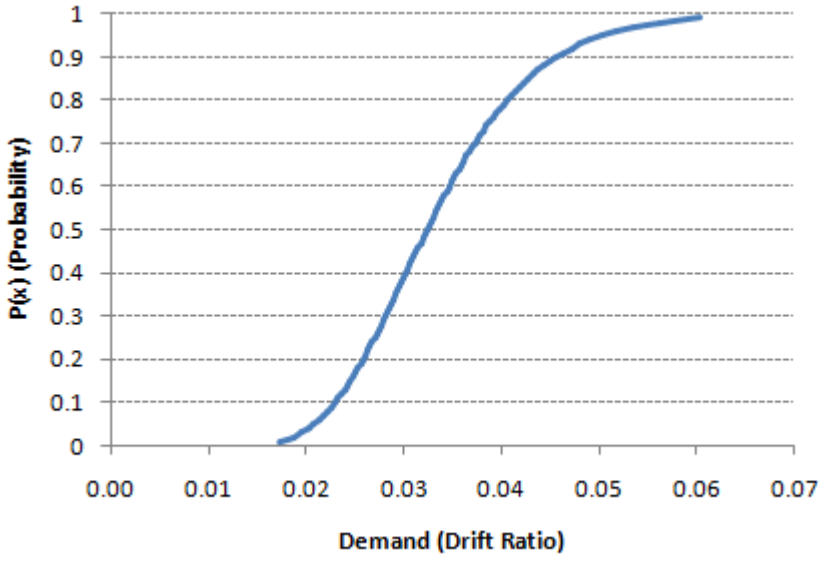

(b)

P(x)	θ	P(x)	θ	P(x)	θ	P(x)	θ	P(x)	θ
0.01	0.0174	0.21	0.0261	0.41	0.0305	0.61	0.0349	0.81	0.0410
0.02	0.0187	0.22	0.0263	0.42	0.0307	0.62	0.0352	0.82	0.0414
0.03	0.0196	0.23	0.0266	0.43	0.0309	0.63	0.0354	0.83	0.0418
0.04	0.0203	0.24	0.0268	0.44	0.0311	0.64	0.0357	0.84	0.0423
0.05	**0.0208**	**0.25**	**0.0270**	**0.45**	**0.0313**	**0.65**	**0.0359**	**0.85**	**0.0428**
0.06	0.0214	0.26	0.0273	0.46	0.0315	0.66	0.0362	0.86	0.0433
0.07	0.0218	0.27	0.0275	0.47	0.0318	0.67	0.0365	0.87	0.0438
0.08	0.0222	0.28	0.0277	0.48	0.0320	0.68	0.0367	0.88	0.0444
0.09	0.0226	0.29	0.0279	0.49	0.0322	0.69	0.0370	0.89	0.0450
0.10	**0.0230**	**0.30**	**0.0282**	**0.50**	**0.0324**	**0.70**	**0.0373**	**0.90**	**0.0457**
0.11	0.0233	0.31	0.0284	0.51	0.0326	0.71	0.0376	0.91	0.0464
0.12	0.0236	0.32	0.0286	0.52	0.0328	0.72	0.0379	0.92	0.0472
0.13	0.0240	0.33	0.0288	0.53	0.0331	0.73	0.0382	0.93	0.0481
0.14	0.0243	0.34	0.0290	0.54	0.0333	0.74	0.0385	0.94	0.0491
0.15	**0.0245**	**0.35**	**0.0292**	**0.55**	**0.0335**	**0.75**	**0.0388**	**0.95**	**0.0503**
0.16	0.0248	0.36	0.0294	0.56	0.0337	0.76	0.0392	0.96	0.0518
0.17	0.0251	0.37	0.0296	0.57	0.0340	0.77	0.0395	0.97	0.0536
0.18	0.0254	0.38	0.0299	0.58	0.0342	0.78	0.0398	0.98	0.0562
0.19	0.0256	0.39	0.0301	0.59	0.0344	0.79	0.0402	0.99	0.0604
0.20	**0.0259**	**0.40**	**0.0303**	**0.60**	**0.0347**	**0.80**	**0.0406**		

Figure A.55: Plotted fragility curve and information for glass configuration (20) for the (a) cracking and (b) fallout limit state

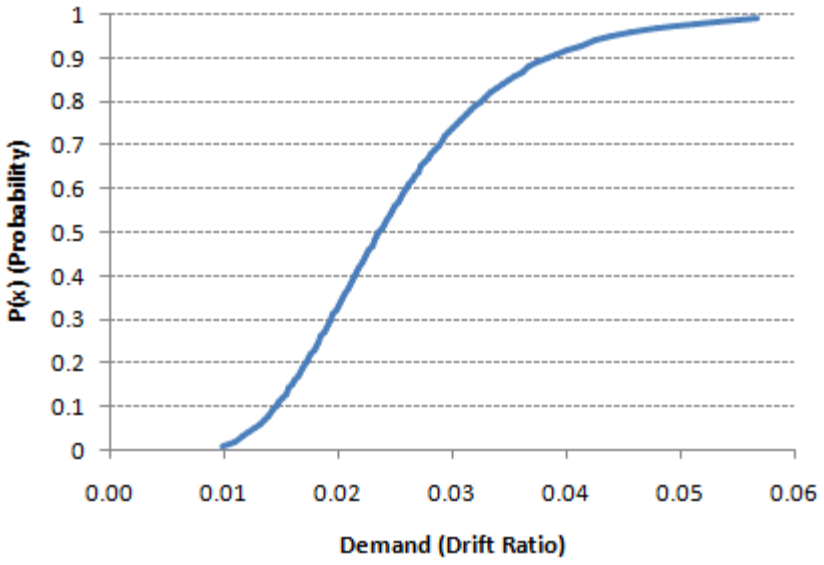

(a)

P(x)	θ	P(x)	θ	P(x)	θ	P(x)	θ	P(x)	θ
0.01	0.0098	0.21	0.0174	0.41	0.0217	0.61	0.0262	0.81	0.0329
0.02	0.0109	0.22	0.0176	0.42	0.0219	0.62	0.0265	0.82	0.0333
0.03	0.0116	0.23	0.0179	0.43	0.0221	0.63	0.0267	0.83	0.0338
0.04	0.0122	0.24	0.0181	0.44	0.0223	0.64	0.0270	0.84	0.0343
0.05	**0.0127**	**0.25**	**0.0183**	**0.45**	**0.0225**	**0.65**	**0.0273**	**0.85**	**0.0349**
0.06	0.0131	0.26	0.0185	0.46	0.0227	0.66	0.0276	0.86	0.0355
0.07	0.0135	0.27	0.0187	0.47	0.0229	0.67	0.0279	0.87	0.0361
0.08	0.0139	0.28	0.0189	0.48	0.0232	0.68	0.0282	0.88	0.0368
0.09	0.0142	0.29	0.0192	0.49	0.0234	0.69	0.0285	0.89	0.0375
0.10	**0.0146**	**0.30**	**0.0194**	**0.50**	**0.0236**	**0.70**	**0.0288**	**0.90**	**0.0383**
0.11	0.0149	0.31	0.0196	0.51	0.0238	0.71	0.0291	0.91	0.0391
0.12	0.0152	0.32	0.0198	0.52	0.0241	0.72	0.0294	0.92	0.0401
0.13	0.0154	0.33	0.0200	0.53	0.0243	0.73	0.0297	0.93	0.0412
0.14	0.0157	0.34	0.0202	0.54	0.0245	0.74	0.0301	0.94	0.0424
0.15	**0.0160**	**0.35**	**0.0204**	**0.55**	**0.0247**	**0.75**	**0.0304**	**0.95**	**0.0439**
0.16	0.0162	0.36	0.0206	0.56	0.0250	0.76	0.0308	0.96	0.0457
0.17	0.0165	0.37	0.0208	0.57	0.0252	0.77	0.0312	0.97	0.0480
0.18	0.0167	0.38	0.0210	0.58	0.0255	0.78	0.0316	0.98	0.0512
0.19	0.0170	0.39	0.0212	0.59	0.0257	0.79	0.0320	0.99	0.0567
0.20	**0.0172**	**0.40**	**0.0215**	**0.60**	**0.0260**	**0.80**	**0.0324**		

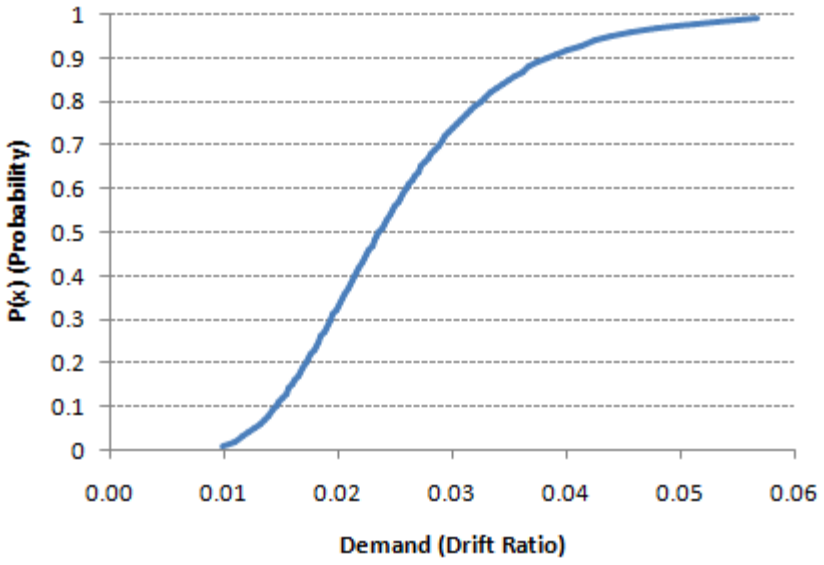

(b)

P(x)	θ	P(x)	θ	P(x)	θ	P(x)	θ	P(x)	θ
0.01	0.0098	0.21	0.0174	0.41	0.0217	0.61	0.0262	0.81	0.0329
0.02	0.0109	0.22	0.0176	0.42	0.0219	0.62	0.0265	0.82	0.0333
0.03	0.0116	0.23	0.0179	0.43	0.0221	0.63	0.0267	0.83	0.0338
0.04	0.0122	0.24	0.0181	0.44	0.0223	0.64	0.0270	0.84	0.0343
0.05	**0.0127**	**0.25**	**0.0183**	**0.45**	**0.0225**	**0.65**	**0.0273**	**0.85**	**0.0349**
0.06	0.0131	0.26	0.0185	0.46	0.0227	0.66	0.0276	0.86	0.0355
0.07	0.0135	0.27	0.0187	0.47	0.0229	0.67	0.0279	0.87	0.0361
0.08	0.0139	0.28	0.0189	0.48	0.0232	0.68	0.0282	0.88	0.0368
0.09	0.0142	0.29	0.0192	0.49	0.0234	0.69	0.0285	0.89	0.0375
0.10	**0.0146**	**0.30**	**0.0194**	**0.50**	**0.0236**	**0.70**	**0.0288**	**0.90**	**0.0383**
0.11	0.0149	0.31	0.0196	0.51	0.0238	0.71	0.0291	0.91	0.0391
0.12	0.0152	0.32	0.0198	0.52	0.0241	0.72	0.0294	0.92	0.0401
0.13	0.0154	0.33	0.0200	0.53	0.0243	0.73	0.0297	0.93	0.0412
0.14	0.0157	0.34	0.0202	0.54	0.0245	0.74	0.0301	0.94	0.0424
0.15	**0.0160**	**0.35**	**0.0204**	**0.55**	**0.0247**	**0.75**	**0.0304**	**0.95**	**0.0439**
0.16	0.0162	0.36	0.0206	0.56	0.0250	0.76	0.0308	0.96	0.0457
0.17	0.0165	0.37	0.0208	0.57	0.0252	0.77	0.0312	0.97	0.0480
0.18	0.0167	0.38	0.0210	0.58	0.0255	0.78	0.0316	0.98	0.0512
0.19	0.0170	0.39	0.0212	0.59	0.0257	0.79	0.0320	0.99	0.0567
0.20	**0.0172**	**0.40**	**0.0215**	**0.60**	**0.0260**	**0.80**	**0.0324**		

Figure A.56: Plotted fragility curve and information for glass configuration (21) for the (a) cracking and (b) fallout limit state

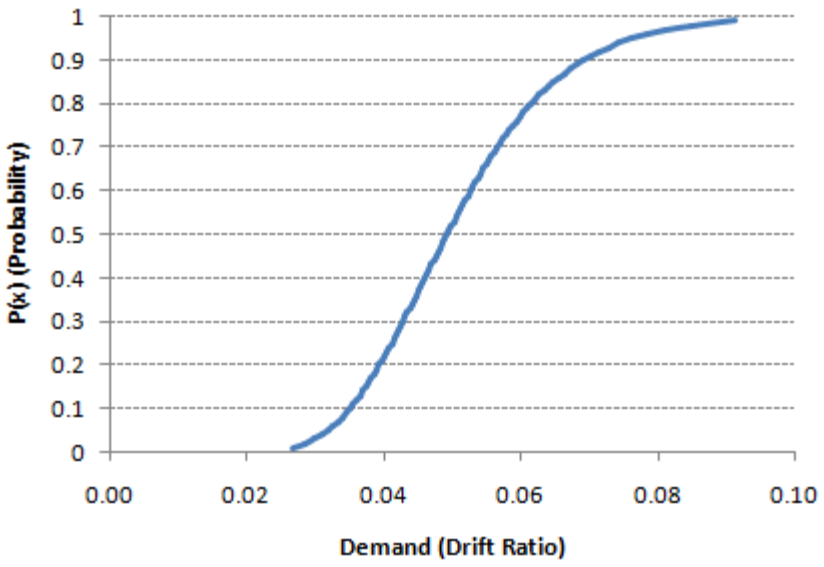

(a)

P(x)	θ	P(x)	θ	P(x)	θ	P(x)	θ	P(x)	θ
0.01	0.0266	0.21	0.0397	0.41	0.0463	0.61	0.0530	0.81	0.0621
0.02	0.0285	0.22	0.0401	0.42	0.0466	0.62	0.0533	0.82	0.0627
0.03	0.0299	0.23	0.0405	0.43	0.0470	0.63	0.0537	0.83	0.0634
0.04	0.0309	0.24	0.0408	0.44	0.0473	0.64	0.0541	0.84	0.0640
0.05	**0.0318**	**0.25**	**0.0411**	**0.45**	**0.0476**	**0.65**	**0.0545**	**0.85**	**0.0648**
0.06	0.0326	0.26	0.0415	0.46	0.0479	0.66	0.0549	0.86	0.0655
0.07	0.0333	0.27	0.0418	0.47	0.0482	0.67	0.0553	0.87	0.0663
0.08	0.0339	0.28	0.0422	0.48	0.0486	0.68	0.0557	0.88	0.0672
0.09	0.0345	0.29	0.0425	0.49	0.0489	0.69	0.0561	0.89	0.0681
0.10	**0.0350**	**0.30**	**0.0428**	**0.50**	**0.0492**	**0.70**	**0.0565**	**0.90**	**0.0691**
0.11	0.0355	0.31	0.0431	0.51	0.0495	0.71	0.0570	0.91	0.0702
0.12	0.0360	0.32	0.0435	0.52	0.0499	0.72	0.0574	0.92	0.0714
0.13	0.0365	0.33	0.0438	0.53	0.0502	0.73	0.0579	0.93	0.0727
0.14	0.0370	0.34	0.0441	0.54	0.0505	0.74	0.0583	0.94	0.0743
0.15	**0.0374**	**0.35**	**0.0444**	**0.55**	**0.0509**	**0.75**	**0.0588**	**0.95**	**0.0761**
0.16	0.0378	0.36	0.0447	0.56	0.0512	0.76	0.0593	0.96	0.0782
0.17	0.0382	0.37	0.0451	0.57	0.0516	0.77	0.0598	0.97	0.0810
0.18	0.0386	0.38	0.0454	0.58	0.0519	0.78	0.0604	0.98	0.0848
0.19	0.0390	0.39	0.0457	0.59	0.0523	0.79	0.0609	0.99	0.0911
0.20	**0.0394**	**0.40**	**0.0460**	**0.60**	**0.0526**	**0.80**	**0.0615**		

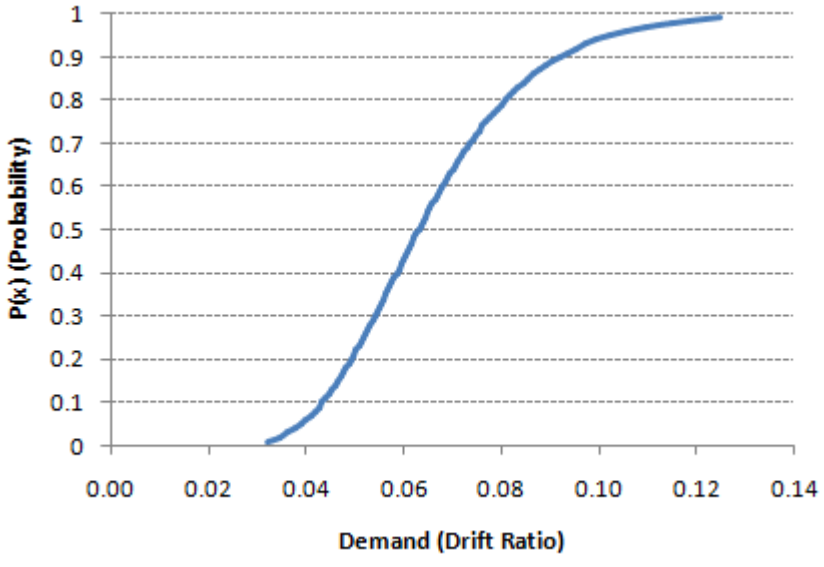

(b)

P(x)	θ	P(x)	θ	P(x)	θ	P(x)	θ	P(x)	θ
0.01	0.0319	0.21	0.0498	0.41	0.0590	0.61	0.0685	0.81	0.0816
0.02	0.0346	0.22	0.0503	0.42	0.0595	0.62	0.0690	0.82	0.0825
0.03	0.0364	0.23	0.0508	0.43	0.0599	0.63	0.0695	0.83	0.0835
0.04	0.0378	0.24	0.0513	0.44	0.0604	0.64	0.0701	0.84	0.0844
0.05	**0.0390**	**0.25**	**0.0518**	**0.45**	**0.0608**	**0.65**	**0.0706**	**0.85**	**0.0855**
0.06	0.0400	0.26	0.0523	0.46	0.0613	0.66	0.0712	0.86	0.0866
0.07	0.0409	0.27	0.0527	0.47	0.0617	0.67	0.0718	0.87	0.0878
0.08	0.0418	0.28	0.0532	0.48	0.0622	0.68	0.0724	0.88	0.0890
0.09	0.0426	0.29	0.0537	0.49	0.0626	0.69	0.0730	0.89	0.0904
0.10	**0.0433**	**0.30**	**0.0541**	**0.50**	**0.0631**	**0.70**	**0.0736**	**0.90**	**0.0919**
0.11	0.0441	0.31	0.0546	0.51	0.0636	0.71	0.0742	0.91	0.0935
0.12	0.0447	0.32	0.0550	0.52	0.0640	0.72	0.0749	0.92	0.0952
0.13	0.0454	0.33	0.0555	0.53	0.0645	0.73	0.0755	0.93	0.0972
0.14	0.0460	0.34	0.0559	0.54	0.0650	0.74	0.0762	0.94	0.0995
0.15	**0.0466**	**0.35**	**0.0564**	**0.55**	**0.0655**	**0.75**	**0.0769**	**0.95**	**0.1022**
0.16	0.0472	0.36	0.0568	0.56	0.0660	0.76	0.0776	0.96	0.1054
0.17	0.0477	0.37	0.0573	0.57	0.0664	0.77	0.0784	0.97	0.1095
0.18	0.0483	0.38	0.0577	0.58	0.0669	0.78	0.0791	0.98	0.1152
0.19	0.0488	0.39	0.0581	0.59	0.0675	0.79	0.0799	0.99	0.1248
0.20	**0.0493**	**0.40**	**0.0586**	**0.60**	**0.0680**	**0.80**	**0.0807**		

Figure A.57: Plotted fragility curve and information for the fallout limit state of (a) configuration (22) and (b) configuration (23)

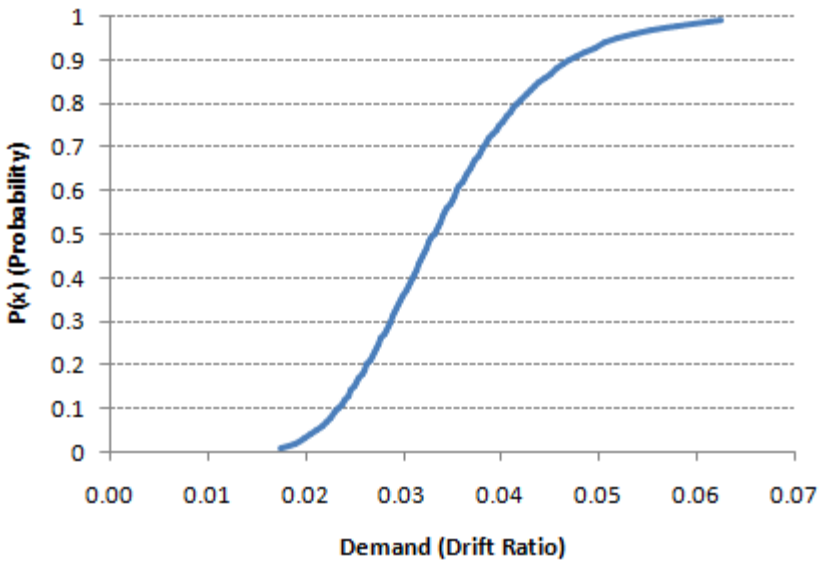

(a)

P(x)	θ	P(x)	θ	P(x)	θ	P(x)	θ	P(x)	θ
0.01	0.0175	0.21	0.0266	0.41	0.0311	0.61	0.0357	0.81	0.0421
0.02	0.0189	0.22	0.0268	0.42	0.0313	0.62	0.0360	0.82	0.0425
0.03	0.0198	0.23	0.0271	0.43	0.0315	0.63	0.0362	0.83	0.0429
0.04	0.0205	0.24	0.0273	0.44	0.0318	0.64	0.0365	0.84	0.0434
0.05	**0.0211**	**0.25**	**0.0275**	**0.45**	**0.0320**	**0.65**	**0.0368**	**0.85**	**0.0439**
0.06	0.0217	0.26	0.0278	0.46	0.0322	0.66	0.0370	0.86	0.0445
0.07	0.0221	0.27	0.0280	0.47	0.0324	0.67	0.0373	0.87	0.0450
0.08	0.0226	0.28	0.0282	0.48	0.0326	0.68	0.0376	0.88	0.0456
0.09	0.0230	0.29	0.0285	0.49	0.0329	0.69	0.0379	0.89	0.0463
0.10	**0.0233**	**0.30**	**0.0287**	**0.50**	**0.0331**	**0.70**	**0.0382**	**0.90**	**0.0470**
0.11	0.0237	0.31	0.0289	0.51	0.0333	0.71	0.0385	0.91	0.0477
0.12	0.0240	0.32	0.0291	0.52	0.0336	0.72	0.0388	0.92	0.0486
0.13	0.0243	0.33	0.0294	0.53	0.0338	0.73	0.0391	0.93	0.0495
0.14	0.0246	0.34	0.0296	0.54	0.0340	0.74	0.0395	0.94	0.0506
0.15	**0.0249**	**0.35**	**0.0298**	**0.55**	**0.0343**	**0.75**	**0.0398**	**0.95**	**0.0519**
0.16	0.0252	0.36	0.0300	0.56	0.0345	0.76	0.0401	0.96	0.0534
0.17	0.0255	0.37	0.0302	0.57	0.0347	0.77	0.0405	0.97	0.0553
0.18	0.0258	0.38	0.0305	0.58	0.0350	0.78	0.0409	0.98	0.0580
0.19	0.0260	0.39	0.0307	0.59	0.0352	0.79	0.0413	0.99	0.0625
0.20	**0.0263**	**0.40**	**0.0309**	**0.60**	**0.0355**	**0.80**	**0.0416**		

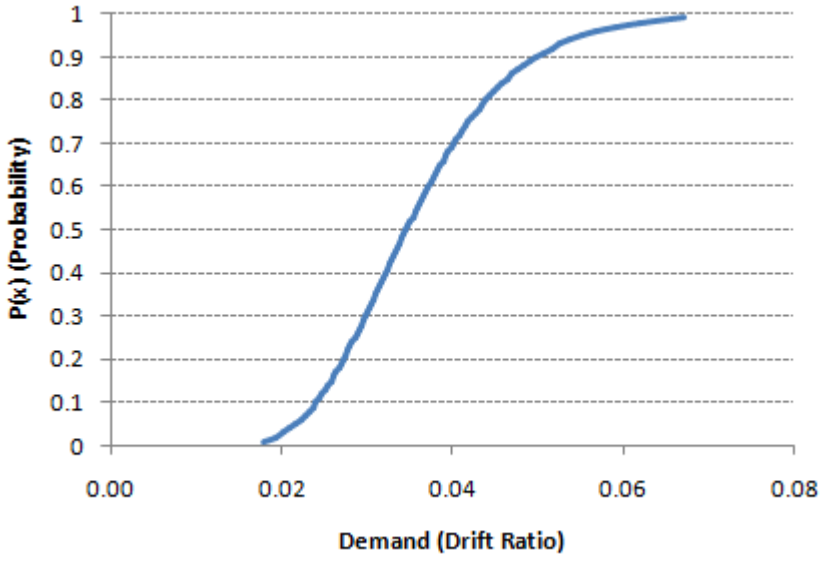

(b)

P(x)	θ	P(x)	θ	P(x)	θ	P(x)	θ	P(x)	θ
0.01	0.0179	0.21	0.0275	0.41	0.0324	0.61	0.0375	0.81	0.0444
0.02	0.0193	0.22	0.0278	0.42	0.0327	0.62	0.0377	0.82	0.0449
0.03	0.0203	0.23	0.0281	0.43	0.0329	0.63	0.0380	0.83	0.0454
0.04	0.0210	0.24	0.0283	0.44	0.0331	0.64	0.0383	0.84	0.0459
0.05	**0.0217**	**0.25**	**0.0286**	**0.45**	**0.0334**	**0.65**	**0.0386**	**0.85**	**0.0464**
0.06	0.0222	0.26	0.0288	0.46	0.0336	0.66	0.0389	0.86	0.0470
0.07	0.0228	0.27	0.0291	0.47	0.0339	0.67	0.0392	0.87	0.0476
0.08	0.0232	0.28	0.0293	0.48	0.0341	0.68	0.0395	0.88	0.0483
0.09	0.0236	0.29	0.0296	0.49	0.0344	0.69	0.0398	0.89	0.0490
0.10	**0.0240**	**0.30**	**0.0298**	**0.50**	**0.0346**	**0.70**	**0.0402**	**0.90**	**0.0498**
0.11	0.0244	0.31	0.0301	0.51	0.0348	0.71	0.0405	0.91	0.0506
0.12	0.0248	0.32	0.0303	0.52	0.0351	0.72	0.0408	0.92	0.0516
0.13	0.0251	0.33	0.0305	0.53	0.0353	0.73	0.0412	0.93	0.0526
0.14	0.0255	0.34	0.0308	0.54	0.0356	0.74	0.0415	0.94	0.0538
0.15	**0.0258**	**0.35**	**0.0310**	**0.55**	**0.0359**	**0.75**	**0.0419**	**0.95**	**0.0552**
0.16	0.0261	0.36	0.0313	0.56	0.0361	0.76	0.0423	0.96	0.0569
0.17	0.0264	0.37	0.0315	0.57	0.0364	0.77	0.0427	0.97	0.0590
0.18	0.0267	0.38	0.0317	0.58	0.0366	0.78	0.0431	0.98	0.0620
0.19	0.0270	0.39	0.0320	0.59	0.0369	0.79	0.0435	0.99	0.0670
0.20	**0.0272**	**0.40**	**0.0322**	**0.60**	**0.0372**	**0.80**	**0.0439**		

Figure A.58: Plotted fragility curve and information for glass configuration (24) for the (a) cracking and (b) fallout limit state

Appendix B

Closed-Form Formulation Supplement

This appendix details the development of an $\Phi_{type\text{-}config}$ integrated factor as an alternative to the separate Φ_{type} and Φ_{config} factors. Section B.1 details the development of the $\Phi_{type\text{-}config}$ factor. Section B.2 gives an analysis that investigates whether the first or second term of the base equation (6.6) is more statistically significant, which is needed information for Section B.1.

B.1 Development of: $\Phi_{type\text{-}config}$

As an alternative to separate factors Φ_{type} and Φ_{config}, we can investigate the possibility of using one factor that considers glass type and configuration type in an integrated approach for the closed-form equation. This factor can directly relate the effects that both glass type and configuration type have on the cracking capacity of glass systems when compared with a standard AN-Mono glass configuration. Initially, the factor is defined in Equation **B.1** as follows:

$$\Phi_{type-config} = \frac{\Delta_{crack_{x-y}}}{\Delta_{crack_{AN-Mono}}} \qquad \textbf{B.1}$$

where $\Phi_{type\text{-}config}$ denotes the factor adjustment value as a function of glass type and configuration, $\Delta_{crack\text{-}x\text{-}y}$ is the average cracking drift value from experimental test results for the glass system (x-y) under consideration [x = AN, HS, or FT; y = Mono, sym. IGU, asym. IGU, or Lami], and $\Delta_{crack\text{-}AN\text{-}MONO}$ represents the average cracking drift value from experimental test results for a comparable base AN-Mono glass system.

The definition seen in Equation B.1 is formulated to directly relate the effects that both configuration type and glass type has on the seismic capacity of a glass panel when compared with the capacity of a basic AN-Mono glass system. Data from glass configurations (1-6, 16-21, and 24) in Table 3.1 was input into Equation B.1, and Table **B.1** shows the values for $\Phi_{type\text{-}config}$ that were found. In the table, the value of a given cell is the experimental capacity in relation to the experimental capacity of the base AN-Mono configuration, or cell (a-1). For example, the cracking capacity of a HS-Lami (b-4) glass system is approximately 60% greater than an AN-Mono (a-1) glass system, as represented by the $\Phi_{type\text{-}config}$ factor value of 1.60 for HS-Lami glass panels.

Table B.1: Developed factor values of $\Phi_{type\text{-}config}$ as defined by Equation 5.15

			AN a	HS b	FT c
Mono		1	**1.00**	1.75	1.76
IGU {	Sym.	2	1.71	1.93	
	Asym.	3	1.98	1.98	2.41
Lami		4	1.16	1.60	

Trends that were noted in the development of the separate Φ_{type} and Φ_{config} factors are also seen in this analysis. The integrated $\Phi_{type\text{-}config}$ factor values generally increase from AN to HS to FT glass types with a similar glass configuration. Furthermore, for the most part, the factor values for IGU and Lami configuration types are greater than Mono configuration types with a similar glass type. The only exception is HS-Lami (cell b-4) which has a factor value of 1.60, compared with the HS-Mono (cell b-1) which has a factor value of 1.75.

While the initial definition of $\Phi_{type\text{-}config}$ models the effects that glass type and glass configuration have on the capacity of a glass panel with respect to a standard AN-Mono glass system, the values of the $\Phi_{type\text{-}config}$ factor need to be adjusted so that they appropriately modify the new base closed-form equation for any given glass or configuration type. As an example of this condition, the $\Phi_{type\text{-}config}$ factor currently has a value of 1.0 for AN-Mono glass configuration (1), which had an experiment drift ratio of 0.0138. However, the base Equation 6.6 estimates a cracking drift ratio of 0.0267. Therefore, an applied $\Phi_{type\text{-}config}$ factor value is needed that reduces the predicted drift ratio of the base equation to reflect the experimental capacity, which means the value should be less than 1.0.

It was noted earlier in the section that $\Phi_{type\text{-}config}$ would be applied to the entire equation in the form of a "Y" type factor (see Equation 6.8), but to confirm that this is the best way to employ the factor to the equation an analysis is performed. The analysis finds out which of the following equation components is more statistically critical when

considering differences between predicted and experimental drift ratios; the equation as a whole or only the second term of the equation. To accomplish this task, an overall percent difference was calculated between the predicted drift ratios from the entire base equation and the experimental drift ratios for glass configurations (1-6, 16-21, and 24) in Table 3.1. Then, another percent difference was calculated between the predicted drift ratio of the equation minus the first term ($2c_1$) and the experimental drift ratio minus the first term. Either percent difference represents the critical nature of the entire equation or second term, respectively. The details of this analysis can be seen in Appendix B.2. It was found that the values were close, with an 8.0% difference for the entire equation and 14.8% difference for the second term (with two outlying data points removed). Consequently, the results of the analysis do not signify that either component is more critical than the other.

Therefore, it is determined that $\Phi_{type\text{-}config}$ should take on the form of a type "*Y*" modification factor by justification from other means. The factor should modify the entire base equation because variables glass type and configuration type are present as an affect on a glass panel during both glass responses that lead to cracking failure. Therefore, the factor representing these variables should be applied to both terms of the base equation. Furthermore, if the factor $\Phi_{type\text{-}config}$ was applied to only the second term of the equation, then the factor values would be more affected by the aspect ratio of a glass panel, which is represented by the dimensions *h* and *b* in that term. If the $\Phi_{type\text{-}config}$ factor were to be applied only to the second term, additional studies should be

performed on glass configurations with varying aspect ratios along with varying glass and configuration types. This way the effects that an aspect ratio has on the cracking performance of glass specimens can be further investigated with relation to glass type and configuration.

With the addition of the $\Phi_{type\text{-}config}$ factor, the base closed-form equation is then modified to be defined by Equation **B.2** as follows**:**

$$\Delta_{cracking} = \Phi_{type-config}\left[2c_1 + 2c_2\left(\frac{h}{b}\right)\right] \qquad \textbf{B.2}$$

where all terms were denoted previously.

The $\Phi_{type\text{-}config}$ factor values need to be corrected so that they are appropriately applicable within the context of Equation B.2. In the previous subsection, $\Phi_{type\text{-}config}$ was defined by Equation B.1 which related the capacity of a given glass configuration to the capacity of a basic AN-Mono glass configuration. To correlate these relationships for application to the base equation, the initial definition (Equation B.1) is adjusted such that it is calibrated by applying a multiplier which relates the AN-Mono glass configuration experimental results with the predicted capacity from the base equation. The result is a corrected $\Phi_{type\text{-}config}$ factor that is defined by Equation **B.3**:

$$\Phi_{type-config} = \frac{\Delta_{crack_{x-y}}}{\Delta_{crack_{AN-Mono}}} \times \frac{\Delta_{crack_{AN-Mono}}}{\delta_{crack_{AN-Mono}}} = \frac{\Delta_{crack_{x-y}}}{\delta_{crack_{AN-Mono}}} \qquad \textbf{B.3}$$

where $\Phi_{type\text{-}config}$ denotes the factor adjustment value as a function of glass type and configuration, $\Delta_{crack\text{-}x\text{-}y}$ the average cracking drift value from experimental test results for the glass system (x-y) under consideration, $\Delta_{crack\text{-}AN\text{-}MONO}$ the experimental cracking drift

for the base AN-Mono glass system, $\delta_{crack\text{-}AN\text{-}MONO}$ the drift predicted to cause cracking failure by base Equation 6.6 for the AN-Mono glass system, and c_1, c_2, h, b, x, and y were denoted previously. Applying the experimental data from glass configurations (1-6, 16-21, and 24) of Table 3.1 into Equation B.3, the following values for $\Phi_{type\text{-}config}$ were determined as seen in Table **B.2.** Furthermore, since no experimental data is available to create factor values for cells (b-3) and (d-3) and a user might have a FT-IGU (symmetric) or FT-Lami glass system, it is proposed that these systems adopt the factor values from similar configurations with HS glass types which are highlight in bold in Table B.2. These values are a conservative approach to providing values in these scenarios, because glass strength increases from HS to FT.

Table B.2: Refined factor values of $\Phi_{type\text{-}config}$ as determined by Equation 5.21

			AN 1	HS 2	FT 3
Mono		a	0.52	0.90	0.91
IGU {	Sym.	b	0.88	0.99	**0.99**
	Asym.	c	1.02	1.02	1.24
Lami		d	0.60	0.83	**0.83**

Ultimately, the factor values in Table B.2 allow the closed-form equation to relate the experimental results to the predicted cracking capacity of glass systems accounting for glass and configuration type. For a revised comparison, Table **B.3** summarizes the experimental drift ratios and predicted cracking drift ratio for glass configurations (1-6, 16-21, and 24) of Table 3.1 calculated by Equation B.2 with the refined $\Phi_{type\text{-}config}$ factor values. Column A and Column B show the cracking drift ratios predicted by the first

and second terms, respectively, of the base equation (see Equation 6.6). Column C lists the predicted drift ratio from the original ASCE equation (Column A and B added together) which is also the base for the new closed-form equation. Column D lists the appropriate $\Phi_{type\text{-}config}$ value for each glass configuration. Finally, Column E compares the drift ratio calculated by Equation B.2 with the experimental cracking drift ratio results.

Table B.3: Comparison of current equation and experimental drift ratio values for select glass configurations

	A	B	C	D	E	
	$2c_1{}^*$	$2c_2\left(\frac{h}{b}\right)^*$	$2c_1 + 2c_2\left(\frac{h}{b}\right)^*$	$\Phi_{config\text{-}type}$	**Cracking Failure**	
					$\theta_{predicted}$	$\theta_{experimental}$
1	0.0122	0.0146	**0.0267**	0.52	**0.0138**	**0.0138**
2	0.0122	0.0146	**0.0267**	0.88	**0.0237**	**0.0237**
3	0.0122	0.0146	**0.0267**	1.02	**0.0273**	**0.0279**
4	0.0122	0.0146	**0.0267**	1.02	**0.0273**	**0.0270**
5	0.0122	0.0146	**0.0267**	1.02	**0.0273**	**0.0270**
6	0.0122	0.0146	**0.0267**	0.60	**0.0161**	**0.0161**
16	0.0122	0.0146	**0.0267**	0.90	**0.0241**	**0.0241**
17	0.0122	0.0146	**0.0267**	0.99	**0.0266**	**0.0266**
18	0.0122	0.0146	**0.0267**	0.83	**0.0221**	**0.0221**
19	0.0122	0.0146	**0.0267**	1.02	**0.0273**	**0.0261**
20	0.0122	0.0146	**0.0267**	1.02	**0.0273**	**0.0285**
21	0.0122	0.0146	**0.0267**	0.91	**0.0244**	**0.0244**
24	0.0122	0.0146	**0.0267**	1.24	**0.0332**	**0.0332**

*The results are normalized and given in drift ratios where the predicted drift from the term is divided by the height of the configuration's glass panel

The analysis in Table B.3 shows the predicted drift ratio from the closed-form equation accurately models the experimental cracking results of glass configurations (1-

6, 16-21, and 24). In fact, for some glass configurations the predicted drift ratio value is equivalent to the experimental drift ratio value. While this condition seems improbable, when an integrated approach was adopted for the $\Phi_{type\text{-}config}$ factor, it eliminated any glass type and/or configuration type modeling inaccuracies for some glass configurations. That is because the definition of the $\Phi_{type\text{-}config}$ factor (Equation B.2) essentially relates the magnitude of effect that both glass type and configuration type have with respect to the drift ratio capacity modeled by the geometric parameters underlying the base equation for a given glass system. Overall, the integrated $\Phi_{type\text{-}config}$ factor is an alternative way to model glass type and configuration type.

B.2 Factor Form Analysis

The analysis performed to find out whether the second term is more critical statistically compared with the equation as a whole for selected glass configurations is presented here. The percent difference is the parameter selected to measure the critical nature of either option. For the entire equation, a percent difference between the predicted drift ratios from the entire base equation (see Equation 6.6) and the experimental drift ratios for glass configurations (1-6, 16-21, and 24) in Table 3.1 was found using Equation **B.4**. The equation assumes that either the predicted drift ratio or experimental drift ratio is a correct value, but rather calculates a mutual difference in percent between the two values.

$$\% \, Difference = \frac{\left|\theta_{crack}^{pred} - \theta_{crack}^{exp}\right|}{\left(\frac{\theta_{crack}^{pred} + \theta_{crack}^{exp}}{2}\right)} \times 100 \qquad \textbf{B.4}$$

The results of the analysis for the entire equation are presented in Table **B.4.** In this table, Column A denotes the predicted cracking drift ratio from the base equation, Column B the experimental cracking drift ratio, Column C the difference between Column A and B, Column D the percent difference as calculated by Equation B.3.

Table **B.4**: Percent difference between predicted drift ratio and experimental drift ratio

	A	B	C	D
	θ_{crack}^{pred}	θ_{crack}^{exp}	$\theta_{crack}^{pred} - \theta_{crack}^{exp}$	% Diff
1	0.0267	0.0138	0.0129	63.7%
2	0.0267	0.0237	0.003	11.9%
3	0.0267	0.0279	-0.0012	4.4%
4	0.0267	0.027	-0.0003	1.1%
5	0.0267	0.027	-0.0003	1.1%
6	0.0267	0.0161	0.0106	49.5%
16	0.0267	0.0241	0.0026	10.2%
17	0.0267	0.0266	0.0001	0.4%
18	0.0267	0.0221	0.0046	18.9%
19	0.0267	0.0261	0.0006	2.3%
20	0.0267	0.0285	-0.0018	6.5%
21	0.0267	0.0244	0.0023	9.0%
24	0.0267	0.0332	-0.0065	21.7%
AVG				**15.4%**

For the similar analysis for the second term of the base equation, a percent difference between the predicted drift ratios from the entire base equation minus the first term ($2c_1$) and the experimental drift ratios minus the first term for glass

configurations (1-6, 16-21, and 24) in Table 3.1 was found using Equation **B.5**. The purpose of subtracting the first term from both drift ratio values is to isolate the numeric effects from the predicted drift ratio of the second term in the percent difference computation.

$$\%\ Difference = \frac{\left|\left(\theta_{crack}^{pred} - 2c_1\right) - \left(\theta_{crack}^{exp} - 2c_1\right)\right|}{\left(\frac{\left(\theta_{crack}^{pred} - 2c_1\right) + \left(\theta_{crack}^{exp} - 2c_1\right)}{2}\right)} \times 100 \qquad \textbf{B.5}$$

The results of the analysis for the second equation term are presented in Table **B.5.** In this table, Column A lists the portion of the cracking drift ratio predicted by the first term of the base equation, Column B the portion of the cracking drift ratio predicted by the second term of the base equation, Column C and D the predicted and experimental drift ratios, respectively, Column E the experimental cracking drift ratio minus the first term of the equation (Column A), and Column F the percent difference. The percent difference in Column F is calculated through the use of Equation B.4.

Table **B.5**: Percent difference between predicted drift ratio minus the first term and experimental drift ratio minus the first term

	A	B	C	D	E	F
	$2c_1$ (D.R.)	$2c_2\left(\frac{h}{b}\right)$ (D.R.)	θ_{crack}^{pred}	θ_{crack}^{exp}	$\theta_{crack}^{exp} - 2c_1$	% Diff.
1	0.0122	0.0146	0.0267	0.0138	0.0016	159.4%
2	0.0122	0.0146	0.0267	0.0237	0.0115	23.2%
3	0.0122	0.0146	0.0267	0.0279	0.0157	7.7%
4	0.0122	0.0146	0.0267	0.027	0.0148	1.8%
5	0.0122	0.0146	0.0267	0.027	0.0148	1.8%
6	0.0122	0.0146	0.0267	0.0161	0.0039	114.8%
16	0.0122	0.0146	0.0267	0.0241	0.0119	19.9%
17	0.0122	0.0146	0.0267	0.0266	0.0144	0.9%
18	0.0122	0.0146	0.0267	0.0221	0.0099	37.8%
19	0.0122	0.0146	0.0267	0.0261	0.0139	4.5%
20	0.0122	0.0146	0.0267	0.0285	0.0163	11.4%
21	0.0122	0.0146	0.0267	0.0244	0.0122	17.4%
24	0.0122	0.0146	0.0267	0.0332	0.0210	36.3%
AVG						**33.6%**

The comparison between the average percent difference values between Tables B.4 and B.5 provides insight concerning how the entire equation compares with second term of the equation in terms of influence on the predicted drift ratio, and the difference with the experimental drift ratios. First of all, it can be seen that the average percent difference of 33.6% is greater in Table B.5 (representing the isolated second equation term) than the value of 15.4% in Table B.4. However, this difference is mainly attributed to glass configurations (1) and (6), which had significantly high percent difference values in Table B.4. With these two outlying data points removed, average values become much closer with an 8.0% difference for the entire equation and a 14.8% difference for

the second term. Secondly, a general trend can be seen where glass configurations in Table B.4 which had low percent difference values also had low percent difference values in Table B.5, such as glass configurations (3-5). The same could be stated for glass configurations with moderate percent difference values, such as glass configuration (20), which had a percent difference of 6.5% in Table B.4 and 11.4% in Table B.5. Consequently, these results do not signify that either the entire equation or the second term of the equation is more critical than the other. However, the analysis is useful in gaining an understanding of the statistical significance of the components of the equation for the glass configurations analyzed.